UNIVERSITY OF THESSALY

FACULTY OF ENGINEERING

DEPARTMENT OF MECHANICAL ENGINEERING

PhD Thesis

ACTIVE CONTROL OF WIND TURBINES THROUGH VARYING

BLADE TIP SWEEP

BOULAMATSIS ACHILLEFS

Aircraft Engineer, Hellenic Air Force Academy, 2008

M.Sc., Department of Mechanical Engineering, University of Thessaly, 2011

Submitted for partial fulfillment of the

requirements for acquiring Ph.D.

2017

The approval of the doctoral thesis from the Department of Mechanical Engineering, Faculty of Engineering, University of Thessaly does not imply any endorsement of the author's views (Law. 5343/32 article. 202 par. 2).

ii

Approved by the Members of the examining Commitee:

First Examiner (Supervisor)	Dr. Herricos Stapountzis Associate Professor, Department of Mechanical Engineering, University of Thessaly
Second Examiner	Dr. Tassos Stamatelos Professor, Department of Mechanical Engineering, University of Thessaly
Third Examiner	Dr. Nikos Pelekasis Professor, Department of Mechanical Engineering, University of Thessaly
Fourth Examiner	Dr. Panagiotis Tsiakaras Professor, Department of Mechanical Engineering, University of Thessaly
Fifth Examiner	Dr. Nikolaos Andritsos Professor, Department of Mechanical Engineering, University of Thessaly
Sixth Examiner	Dr. Kostas Papadimitriou Professor, Department of Mechanical Engineering, University of Thessaly
Seventh Examiner	Dr. Athanasios Barlas Researcher, Department of Wind Energy, Technical University of Denmark

Acknowledgements

Firstly, I would like to deeply thank my supervisor Herricos Stapountzis for his guidance, scientific support and inspiration throughout my entire Postgraduate studies in UTH. His expertise in the field of fluid mechanics combined with useful and wise advices let me become an independent researcher.

Special thanks to Thanasis Barlas for introducing me to the theory of wind turbines, for his co-operation and guidance on the algorithms that I developed and computational work that was performed. He stood as a good friend despite the fact that we met only a few years ago.

Thanks to the Committee for reading my work carefully and their suggestions. Thanks also Konstantinos Krommydas and Thanasis Karapatis for their support in the GPU programming part of my codes.

Moving to my personal acknowledgments, I would like to thank my lovely wife Efi Krommyda how supported me throughout this big effort with love, patience, condescension and trust. In addition, the birth of my daughter Maria during the last year of my research, filled me with so much happiness that augmented my performance. I also owe many thanks to my parents and my brother Speeros for their support and encouragement.

Achillefs Boulamatsis

Dedicated to my three girls Efi-Maria-Michaela

iv

ACTIVE CONTROL OF WIND TURBINES THROUGH VARYING BLADE TIP SWEEP

BOULAMATSIS ACHILLEFS

University of Thessaly, Department of Mechanical Engineering, 2017

Supervisor: Dr. Herricos Stapountzis, Associate Professor of Fluid Mechanics

Abstract

In this research work an introduction to an innovative control method, concerning horizontal axis wind turbines, is presented. The concept refers to variable tip swept rotor blades, that have the ability to pivot collectively aft, (in-plane movement) about an axis located at the blade tips. The swept tip can be either part of the main blade with an internal mechanism or an added surface (add-on) to the blades. The idea of this active control feature is to increase power production at specific operating areas and reduce fatigue loads and extreme blade loads during a wind gust passage through small sweep angle variations in the tip area. The investigation is carried out with a modified Blade Element Momentum (BEM) model that takes into account variable tip swept rotor blades and the modifications are based on results from a lifting line theory based model. The latter model was also compared to Computational Fluid Dynamics (CFD) results and speed optimized with the use of CUDA platform before it was used as reference for the modified BEM model. The simulations refer to the 5MW NREL reference wind turbine that incorporates a suitable controller and the first results show beneficial behavior in all of the investigated areas.

Contents

List of Tables

List of Symbols

Latin

A: cross section area – rotor swept area

Amp(x)$_s$: amplitude of a wind turbine parameter due to the harmonic sweeping motion of the blade tip

aif: axial induction factor

B: number of rotor blades

C: closed curve

C$_L$: Lift coefficient

C$_n$: normal force coefficient

C$_P$: power coefficient

C$_T$: thrust coefficient

C$_t$: tangential force coefficient

C$_\theta$: tangential induced velocity

Circ$_{diff}$: bound circulation difference between adjacent blade elements

c: chord length of a blade or a blade section

D: underelaxation factor

D$_{ind}$: induced drag force

D$_{eq}$: damage equivalent load

F: external force

F(r): Prandtl tip loss factor

F$_n$: normal blade force

F$_t$: tangential blade force

f$_g$: glauert correction for axial induction factor greater than 0.3

x

f_s : frequency of blade tip sweeping motion

f_{rot} : rotational frequency of the wind turbine rotor

f: frequency of motion

$f(V_i<V<V_{i+1})$: probability that wind speed lies between V_i and V_{i+1}

G: correction factor (for blade tip sweep)

$G(s)$: transfer function

g_1: correction factor 1 (for blade tip sweep)

g_2: correction factor 2 (for blade tip sweep)

I: turbulence intensity

K: controller gain

k: reduced frequency

L: Lift force

L: vortex filament size

M: rotor torque

$MeanM_x$: average of blade root bending moments

M_x : blade root bending moment

$\dot{m}$: mass flow rate

m: inverse Miner S-N slope

N_{ratio}: non-dimensional variable – amplitude of parameter divided by the same parameter value in stable conditions

n_i: number of cycles for every stress amplitude

P: power

P_{PDF} : probability density function

p: pressure

xi

R: rotor diameter

Re: Reynolds Number

r: distance of a point from a vortex segment – distance of a section from the rotor hub center

s: Laplace operator

T: thrust force – period of motion

t: time

tau: time constant

U: freestream velocity

U_1 **:** signal 1 (used in Matlab function)

U_2 **:** signal 2 (used in Matlab function)

u: flow velocity

u_{rms}**:** root mean square of wind speed fluctuations

V_{cut-in} **:** the minimum wind speed required to start the wind turbine

$V_{cut-out}$ **:** the maximum operating wind speed of a wind turbine

V_0 **:** flow velocity far upstream (from a wind turbine)

V_{ind}**:** induced velocity on a single point

$V_{resultant}$**:** resultant velocity - the sum of induced velocity, freestream velocity and blade section velocity (structure related or otherwise caused)

V_{rot} **:** rotational speed

V_{rated} **:** the designed wind speed of a wind turbine

W: induced velocity

W_0**:** mean induced velocity

w_b**:** induced velocity by bound vorticity

w_i**:** induced velocity by wake vorticity

xii

X_{CpG} : vertical distance travelled in-plane by blade elements according to blade tip sweep angle

X_0 : Parameter value in stable operating conditions

Greek

$\boldsymbol{\alpha}$: axial induction factor

$\boldsymbol{\alpha'}$: tangential induction factor

$\boldsymbol{\alpha}$: angle of attack

$\boldsymbol{\Gamma}$: blade circulation – vortex strength

$\boldsymbol{\gamma}$: vortex strength per unit length

$\boldsymbol{\delta r}$: percentage of vortex filament size

$\boldsymbol{\theta}$: angle between vectors of V and dl

$\boldsymbol{\theta_{blade}}$: azimuthal blade angle

$\boldsymbol{\theta_0}$: azimuthal blade angle when the blade is in the most downstream position (yawed flow)

$\boldsymbol{\Lambda}$: sweep angle

$\boldsymbol{\Lambda_1}$: longitudinal turbulence scale parameter

$\boldsymbol{\lambda}$: tip speed ratio

$\boldsymbol{\lambda_r}$: local speed ratio – rotational velocity of a section divided by wind speed

$\boldsymbol{\mu}$: fluid dynamic viscocity

$\boldsymbol{\rho}$: air density

$\boldsymbol{\sigma}$: blade solidity

$\boldsymbol{\sigma_1}$: turbulence standard deviation

$\boldsymbol{\tau}$: time constant

$\boldsymbol{\Phi}$: rotor yaw angle

φ: inflow angle

χ: wake skew angle

ω: angular velocity of the rotor

Subscripts

avail: available

b: bound

d: drag

i: induced

ind: induced

int: intermediate

l: lift

n: normal

qs: quasi- steady

rms: root mean square

t: tangential

P: power

sw: swept (part)

T: thrust force

trail: trailing

Abbreviations

ADAMS: Automatic Dynamic Analysis for Mechanical Systems

AEP: Annual Energy Production

AIF: Axial induction Factor

BEM: Blade Element Momentum (Theory)

CFD: Computational Fluid Dynamics

CRTEF: Controlled Rubber Trailing Edge Flap

CPSD: Cross Power Spectral Density

CUDA: Compute Unified Device Architecture

DEL: Damage Equivalent Load

DES: Detached Eddy Simulation

DNS: Direct Numerical Simulation

DUSWAMP: Delft University Smart Wind turbine Aeroelastic Modular Processing (model)

EOG: Extreme Operating Gust

FAST: Fatigue Aerodynamics Structures Turbulence (code)

FishBAC: Fish Bone Active Camber

FLEXHAT: Flexible Horizontal Axis Turbines

GENUVP: GENeralized Unsteady Vortex Particle (model)

GPU: Graphic Processor Unit

HAWT: Horizontal Axis Wind Turbine

HPF: High Pass Filter

LES: Large Eddy Simulation

LDV: Laser Doppler Velocimeter

LVDT: Linear Variable Differential Trasnformer

MW: Megawatt

NREL: National Renewable Energy Laboratory

N-S: Navier – Stokes (equations)

NTUA: National Technical University of Athens

PI: Proportional Integral

PID: Proportional Integral Differential

RANS: Reynolds Averaged Navier Stokes

STAR: Swept Twist Adaptive Rotor

TE: Trailing Edge

TU: Technical University (Delft)

TurbSim: Turbulence Simulator

UK: United Kindom

ULL: Unsteady Lifting Line (Theory)

US: United States (of America))

xvii

Chapter 1. Introduction

1.1 Brief Historical Review Of Wind Turbines

Wind energy is one of the most common forms of renewable energies that are still been utilized by man since he managed to tame wind power. At first, (nearly 4000 BC) he put sails on boats in order to travel around the globe and discover new land. Then, at the 1st century AD, the Greek engineer, Heron of Alexandria [1] introduces the earliest known wind-driven wheel that powers his peculiar device called *Pneumatica* [2]. Later, windmills helped man to grind grain, pump water and through that expand the economy of each society. In Netherlands much of today's land was covered with water until it was drained by wind pumps in the 13th century and many arid regions in US and Australia flourished due to them.

It was no earlier than the late 19th century since these windmills and wind pumps were connected to an electric grid in order to provide electric energy to rural areas and thus evolve to the wind turbines as we know them today. In Denmark Poul La Cour was pioneer researcher in this field and one of the first to investigate rotor aerodynamics through experiments in a wind tunnel. However in the early 20th century the interest in wind turbines was not so high as it was supposed to, as engines took over most of the production of electric energy. So, turbines came back in background after the Second World War where fossil – fuel supply was scarce and many countries such as US, Denmark, UK, Germany, France and

1

USSR carried out research in the direction of improving their efficiency. A milestone in this period is the construction of the largest wind turbine in Vermont - US with a full span pitch - regulated rotor of 53m in diameter, power output of 1.25MW and flapped blades. However, in 1945 it ceased its operation because of a catastrophic failure after one blade broke – off.

Another trigger for this effort was the oil crisis in 1973 where large government funds by many countries were approved for research programs concerning wind turbines in order to become less oil-dependent. This of course led to the development of many prototypes including two – bladed horizontal axis turbines, vertical axis turbines ("the Darrieus concept - Canada") and progressively to the three – bladed wind turbine equipped with an asynchronous AC generator, widely known as the "Danish" concept (figure 1.1). So, after 1990 when these concepts became mature enough, along with the global effort for reducing the CO_2 emissions by utilizing renewable energy, led to the large growing pace of the wind turbine industry and the exponential growth of installed global capacity in wind power. It is characteristic that nowadays, Denmark covers more than 40% of its needs in electric energy from the wind [3].
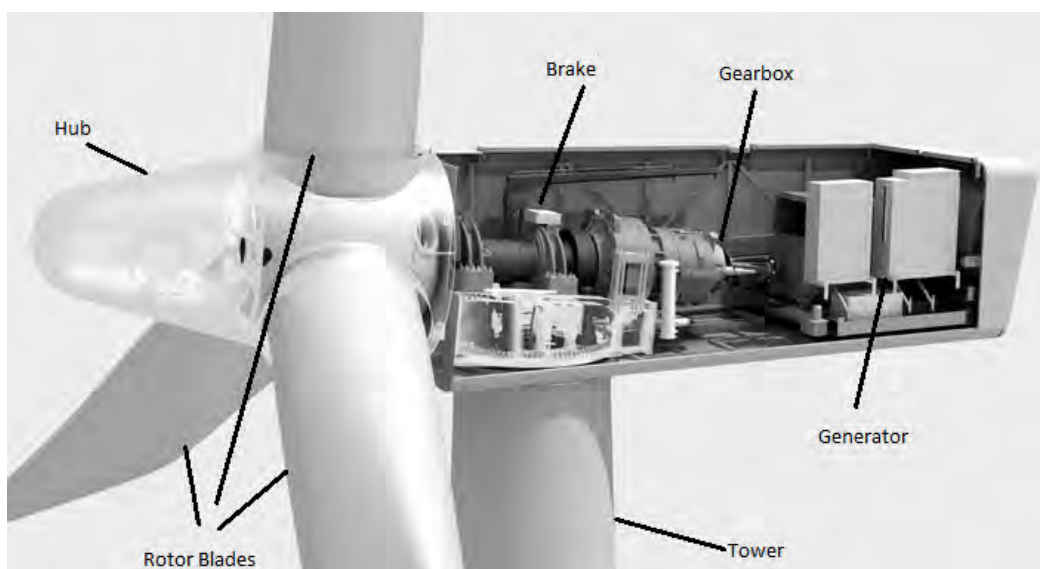

Figure 1.1: Configuration of a modern 3 bladed axial wind turbine, source: [4].

2

1.2 Motivation

After connecting the first wind turbines to the grid the next challenge was to make them produce more power so that they were competitive against the diesel engines. So inevitably they became taller and larger in diameter and thus exposed to harsh weather phenomena which are resulted to high unsteady forces. The aim was to produce the designed electric power for over 20 years without catastrophic failure in a wide range of operating conditions with low cost and also working unattended. For this reason there has been plenty of research in the field of wind turbine control which is basically divided in two categories, passive and active. Passive load control is achieved when changes in wind speed are counteracted through the passively adapting (aerodynamic or aero-elastic) response of the rotor blades. Traditional concepts of passive control are stall control (aerodynamic response) or the use of blade tension–torsion coupling, bend–twist coupling and sweep–twist coupling of the rotor blades (aero-elastic response) [5]. On the other hand, active control (also referred as smart rotor control) refers to an integrated system equipped with sensors, actuators and one or more microprocessors that operate in a feedback loop and control the blade aerodynamic loads. The latter is achieved either by enhancing the flow around the blade with the selective deployment of microtabs and use of boundary layer control methods (like vortex generators and active synthetic jets) or by altering the shape of the airfoil utilizing camber control, active twist or flaps [5].

However, according to the author's knowledge and the current status in the control field of wind turbines that results from the literature review, it seems that the idea of controlling actively the wind turbine parameters such as power production and loads through tip swept rotor blades has not yet been systematically examined. So on one hand, the target of this thesis is to study the effect of tip sweep on wind turbine rotor blades and the impact on

3

the wind turbine itself and on the other hand to develop an active control method that improves its performance and reduces the blade loads. It will also be tried to incorporate this feature in a model which is based on a theory that inherently cannot take it into account.

1.3 Phd Overview

This thesis is structured as follows:

In the next chapter a brief overview in the theory and literature review concerning the subject of the thesis is outlined.

Chapter 3 presents the methodology that was followed in order to achieve the target of the thesis.

In chapter 4 the effect of tip sweep on a fixed wing is investigated and useful conclusions are obtained utilizing two different theoretical backgrounds – Unsteady Lifting Line theory (ULL) and Computational Fluid Dynamics (CFD).

In chapter 5 the investigation of tip sweep effect is extended to a typical wind turbine rotor but only with a ULL theory based model.

In chapter 6 tip sweep feature of rotor blades is incorporated in a Blade Element Momentum (BEM) theory based model which is known for its speed and good predictions compared to more analytical methods (ULL and CFD). This is achieved through an improvement in the calculation of a factor which is critical in the calculation of rotor blade loads.

Chapter 7 presents the application of wind turbine active control through varying tip swept blades in a typical wind turbine and it consists of three parts: improvement in energy production, fatigue blade load reduction and gust load alleviation.

In chapter 8 the conclusions of the thesis are drawn and future work that can follow is proposed.

Chapter 2. Literature Review

In this chapter a review in the theoretical background concerning 3 bladed horizontal axis wind turbines (HAWT) and some of the most common control methods concerning their operation are presented. It starts with the presentation of the models that are currently been used by researchers and industry in order to study and predict the performance of wind turbines, in a decreasing fidelity order. Then, the chapter describes the challenging operating environment of the wind turbines and ends with the discussion for the current state of the art in passive and active control methods with a focus in the geometric feature of sweep.

2.1 Computational Fluid Dynamics (CFD)

In the research field of fluid mechanics, CFD is the most recent and also most promising method from the perspective of detailed analysis of the flow. By this method many parameters can be calculated such as pressure distribution, velocity field or even the transition point from laminar to turbulent flow around an airfoil. A typical problem that is solved with CFD could be the flow around the wing of an aircraft or an entire airplane, the flow of a fluid through a pipeline, the flow field inside a combustion chamber and numerous others. It is classified in the numerical methods that are solved with algorithms and the need in computational resources is usually very high. So, nowadays with the development of super-computers CFD methods are constantly improved and more attractive than ever.

6

CFD is the approach to solve the Navier – Stokes (N-S) equations by numerical methods. They are always solved together with the continuity equation 2.1 which represents the conservation of mass:

$$\frac{\partial \rho}{\partial t} + \nabla \bullet (\rho u) = 0$$

(**2.1**)

where:

- ρ is the density of the fluid

- u is the flow velocity

- ∇ is the del operator

N-S equations describe the viscous flow of fluids based on the 2nd Newton law of motion and thus represent the conservation of momentum. One of the most general forms of the N-S equation (Equation. 2.2) is written for compressible Newtonian fluids. In other words for fluids that their density ρ is not considered constant and their viscous stresses are linearly proportional to the local rate of change of the fluid's deformation or else to the velocity gradient.

$$\rho(\frac{\partial u}{\partial t} + u \bullet \nabla u) = -\nabla p + \nabla \bullet \left(\mu \left(\nabla u + (\nabla u)^T \right) - \frac{2}{3} \mu (\nabla \bullet u) I \right) + F$$

(**2.2**)

where:

- p is the pressure

- μ is the fluid dynamic viscosity

7

- I the identity matrix $I_n = \begin{bmatrix} 1 & 0 & 0 & 0 \\ 0 & 1 & 0 & 0 \\ 0 & 0 & . & 0 \\ 0 & 0 & 0 & 1 \end{bmatrix}$

- F the external force applied to the fluid

Originally derived by Claude-Louis Navier and George Gabriel Stokes in the middle of 19th century it was not until 1960, the T3 group of the Los Alamos National Laboratory made the first steps in the development of numerical techniques that used the N-S equation in order to solve fluid flow problems [6]. Since then, new methods have appeared and along with the evolution of computational power, the application of the N-S equations for solving more complex flows, such as three dimensional (3D) flows, was feasible. However, the N-S equations have no analytical solution for most problems of engineering interest, except for simple flows such as Poiseuille flow or Couette flow [7]. So, in order to use the N-S equations in a wide range of flows (notably turbulent flows) a special formulation was developed which is called Reynolds Averaged Navier Stokes or else RANS.

Depending on the flow characteristics some terms of the N-S equations can be neglected. One characteristic number is the Reynolds number *Re* (Equation.2.3) from which it is determined whether the flow is laminar (low Re number) or turbulent (high Re number). It represents the ratio of the inertial forces to viscous forces. In the N-S equation, the left term of equation 2.2 stands for the inertial forces and the right side consists of the pressure forces plus the viscous forces plus the external forces. So, it is clear that flows of low Re number can be solved easily using a more simplified form of the N-S equation.

$$\mathrm{Re} = \frac{\rho u L}{\mu}$$

(**2.3**)

However most flows are turbulent and the effects of turbulence should be modeled by a suitable model. One of the most common, is the RANS turbulence model by which a different approach is considered with the so called Reynolds decomposition. In particular, variables such as velocity and pressure are decomposed into a time-average motion and a turbulent fluctuation according to equation 2.4 which in turn results in solutions of much lower computational cost.

$$u(x,t) = \overline{u}(x) + u'(x,t)$$

(**2.4**)

where:

- $\overline{u}(x)$ is the time averaged velocity in the x direction

- $u'(x,t)$ is the fluctuating term

Moreover, the RANS turbulent model introduces "new" stresses, also called Reynolds stresses, that model the effects of turbulence fluctuations. Among other models, the ones that are widely used in modern engineering applications are the, Spalart–Allmaras (S–A) [8], k–ε (k–epsilon) [9] and SST k–ω (k–omega) [10]. Yet further analysis about RANS turbulence model and Reynolds viscosity models is beyond the scope of this chapter.

There also other turbulence models worth to mention in the field of CFD with different computational cost depending on the resolution of the turbulence scales – (finer resolution leads to higher computational cost):

- Large Eddy Simulation (LES): In this model only the large and more important eddies are resolved in the N-S equation while the smallest ones with lower contribution to the

9

flow are not taken into account through a suitable filter. This results in lower computational cost.

- Detached Eddy Simulation (DES): In this model the flow is solved with the LES method in areas where the length scale of eddies are larger than the grid dimension and with the RANS equation in the rest areas through a sub-grid, where more resolution is needed. Such areas usually, are the solid boundaries of the emerged body and thus, grid generation is more complex due to this sub-grid model. A good example of this method is described in [11] by Spalart et Al.

- Direct Numerical Simulation (DNS): In this model the N-S equations are solved with all of turbulence scales (spatial and temporal) resolved and so, the computational cost is raised significantly, proportional to Re^3. This method could work as a good substitute for cases where a real experiment is not possible but the computational cost often makes it prohibitive.

In a typical CFD engineering problem the domain is split into a finite number of control volumes, also called mesh or grid, then a number of boundary conditions such as Inlet, Outlet and Walls are defined and finally the N-S equations along with one of the above mentioned turbulence models are solved numerically for every dimension (x, y, z) through a suitable algorithm. The results include fluid velocity and pressure distribution over the geometry of the domain from which many other parameters can be calculated like vorticity and pressure force. However, grid generation is often a difficult task and requires skill in order to create it. One basic requirement for accurate predictions is the careful grid generation, so that the smallest eddies of the used turbulence model are resolved. Moreover, it is proven that increased accuracy is also achieved, by better prediction of the transition area from laminar to turbulent flow and so, several relative models exist in CFD [12].

10

CFD methods have proven their efficiency shortly after their development in applications like flow studies in classical fluid mechanics, aircraft design, vehicle design, etc. For wind turbine applications, CFD became an important tool after 1979 [13], [14] when the first problems of rotating flows were solved numerically. Another major step to this direction was contributed after 1997 through the solution of NS equations for rotor aerodynamics [15], [16]. However, the verification of CFD came after 2000 through the comparison of CFD results with measurements in real operating conditions for the National Renewable Energy Laboratory (NREL) Phase IV wind turbine, following the conduction of corresponding experiments in NASA's Ames wind tunnel [17].

The main difficulties encountered when using CFD methods for rotor applications are grid generation and the strong 3 dimensional (3D) effects of the flow. Grid generation, is usually dealt with, by forming unstructured grids composed of tetrahedral cells, structured grids composed of hexahedral cells and the more complex overlapping grids [18], [19]. With the unstructured grids the domain is divided into cells with a random pattern. The effort required by the user is relatively low and it is highly automated, but it does not perform well in areas near solid boundaries because tetrahedral cells can't fit well in such geometries and so an isotropic image is created. With the second method, the domain is discretized in a more efficient way and the resulting image is usually a streamlined grid near boundaries and a coarse grid in areas which are out of interest. With overlapping grids the domain is divided into areas with different grid structures which overlap in some locations and connect together through interpolation. It is suitable for moving geometries like wind turbines and it is ideal when the whole machine is modeled (rotor – tower – nacelle) because the results are more physically correct. However, it requires far more experience than the other methods and some connectivity problems may appear that are not solved in a straightforward way. Nowadays,

Institutional Repository - Library & Information Centre - University of Thessaly
19/05/2024 19:53:00 EEST - 18.119.112.4

sophisticated software such as **"ANSYS"** [20] includes component systems like *TurboGrid* that are specialized in solving rotor flows or *Fluent* which has the Moving Reference Frame (MRF) capability [20], [21] in which the domain is divided into sub-domains which have the ability to rotate with respect to an inertial frame.

On the other hand, the strong 3-D effects of rotational flows is still under further development and improvement [18]. Prediction of transition in 3D flows is much more difficult than 2D and also, as much important for accurate calculations [22]. New methods exist concerning the derivation of 3D airfoil parameters in rotor CFD applications, like the "reduced axial velocity method" [23]. In fact, 3D yawed flows usually encountered by wind turbines and effects like dynamic stall require different approach in relation to 2D flows and inevitably they are more computationally expensive.

CFD methods have become now a powerful design tool for wind turbine industries after years of development in modeling techniques and evolution of computer power. They are chosen as an experiment substitute for new concepts in rotor blades and in cases where other models of lower order do not perform well. Research is still active and extends to coupled CFD – aeroelastic models that include the whole device (rotor – tower – nacelle).

2.2 Vortex Methods

Over the last 20 years an almost equally effective yet less complex numerical method compared to CFD is widely used to solve problems concerning 3 dimensional separated or non–separated flow areas. This method was proposed by the German scientist Ludwig Prandtl in 1909 in order to calculate more accurately the generated lift from a wing and the corresponding loss due to the flow at the tip area [24]. The demands in computational resources in relation to the detailed analysis of the flow that is achieved with this method are

12

considered low (especially with the current status in computer power) and thus attractive for wind turbine applications. However, there are some configurations of the vortex method which can raise the computational cost as high as CFD methods and so the choice of it is not yet straightforward.

Prandtl's Lifting line theory is fundamental to vortex based models and is usually used with the assumption of incompressible potential flow. According to the theory the wing is divided into small elements (known as horseshoe elements) with all of its bound circulation concentrated to the quarter chord and thus, a refined and physically correct model is introduced having span-wise distribution of bound circulation $\Gamma(y)$ [25] (figure 2.1).

The bound circulation $\Gamma(y)$ is a measure of the fluid rotation (caused by wing's lift) at every element and generally, for a small open element of length dl with a fluid velocity V it applies that:

$$d\Gamma = V \bullet dl = |V||dl|\cos\theta$$

(**2.5**)

where:

- V is the velocity on the open element

- dl is the length of the small element

- θ is the angle between vectors of V and dl

And for a closed curve C (the airfoil in this case) circulation is the line integral of velocity V around that curve (equation (2.6))

13

$$\Gamma = \oint_c V dl$$

(**2.6**)

And it is connected to the vortex strength γ by equation 2.7 :

$$\Gamma = \int_0^c \gamma(x) dx$$

(**2.7**)

where:

- γ is the vortex strength per unit length

This bound vorticity (or else circulation) stems from the lift which is generated by the flow over the wing (or blade) and is concentrated to this single point after the satisfaction of Kutta condition. This condition states that "*The flow leaves the sharp trailing edge of an airfoil smoothly and the velocity is finite there*". So for a typical airfoil the velocity resulting from both sides (upper and lower) would vanish at the trailing edge and the corresponding vortex strength would be zero there, expressed by equation 2.8. In addition, bound circulation is connected to the wing's generated lift, by applying the Kutta – Joukowski theorem [25] and is expressed by equation 2.9 . In particular, the theorem of German mathematician Kutta and Russian physicist Joukowski arose from the observation that in two-dimensional flow lift force is proportional to total circulation and with normal direction to free stream flow.

$$\gamma_{T.E.} = 0$$

(**2.8**)

where:

14

- $\gamma_{T.E.}$ is the vortex strength per unit length at the trailing edge

$$L = \rho U_{\infty} \Gamma$$

(**2.9**)

where:

- L is the generated Lift force by the airfoil

- ρ is the air density

- U_{∞} is the free stream velocity

- Γ is the circulation about the wing

Having in mind [25, 26] from Kelvin Helmholtz theory that a vortex line cannot start or end abruptly in a fluid, when there is a vortex line strength dγ(y)/dy (in this case the bound vortex), a similar vorticity component is introduced in x direction (figure 2.1). This eventually creates the horseshoe elements as mentioned before, with circulation in each side equal to wing's bound circulation Γ, that grows in size according to the direction of flow and retains its strength. So, the discretization of the blade's bound circulation and the wake evolution in time, results in a vortex lattice of figure 2.1 which consists of shed and trailing vortices.
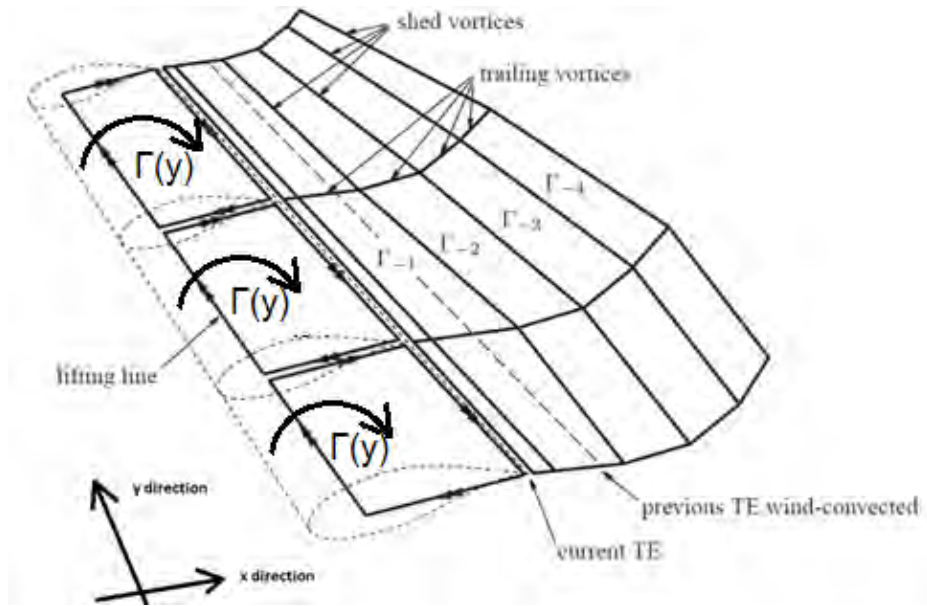
15

Figure 2.1 : Lifting line vortex representation of a wing and its wake, source: [26].

The trailing vortices account for the span-wise bound circulation distribution ($d\Gamma(y)/dy$) whereas the shed vortices account for the time rate of change of bound circulation ($d\Gamma/dt$) (i.e. unsteady lift) and contain the history of the wing's lift force. This implies that in the steady state there are only trailing vortices and no shed - except for the ones that were initially created and are located in the far wake. This vortex lattice in turn, creates a downwash on the blade which is expressed as induced velocity and can be calculated by using the Biot Savart formula.

The Biot Savart law states that a vortex segment of strength γ induces a velocity field around it with tangential components in every single point. A specific formulation of the law for a straight vortex segment, like the ones that constitute the lattice, is widely used and is seen in the following equation.

$$\overline{V_{ind}} = \frac{\Gamma}{4\pi} \frac{\left(r_1 + r_2\right)\left(\overline{r_1} \times \overline{r_2}\right)}{r_1 r_2 \left(r_1 r_2 + \overline{r_1} \cdot \overline{r_2}\right)}$$

(**2.10**)

16

where:

- $\overline{V_{ind}}$ is the induced velocity in a single point (by nearby vortex segments)

- Γ is the circulation of the straight segment

- r1, r2 the distances of the vortex edges from the point where induced velocity is calculated as depicted in figure 2.2
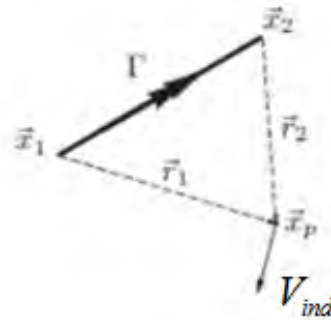

Figure 2.2 : Lifting line vortex representation of a wing and its wake source: [26].

The induced velocities are calculated with the above formula at the so called, control points, which are located in the middle of every horseshoe element over the quarter chord. By superimposing induced velocities with free stream and blade section velocities (structure related or otherwise caused) results in a resultant velocity V for every section, which can be used directly in the three-dimensional form of Kutta-Joukowski equation (2.11) or for the determination of an effective angle of attack and finally extract lift, drag and moment coefficients by 2-D steady state aerodynamic data. Of course, viscous effects can be taken into account by using each time the suitable tabular data depending on Reynolds number. So, it is concluded that total wing forces and distributions of them are calculated straight from the vortex lattice.

$$d\vec{F} = \rho \Gamma \vec{V} \times d\vec{l}$$

(**2.11**)

Two approaches for the vortex lattice exist when using the lifting line method, the prescribed wake and the free wake evolution. With the prescribed method awareness of the wake development is needed a priori. This can be achieved only if corresponding experiments have preceded for the examined case and so makes this approach restrictive. However, it is orders of magnitude faster than the free wake approach when simulations are ran on computer based on corresponding algorithms. On the contrary, free wake approach lets the wake to develop physically as a result of interactions between shed and trailing vortices of the vortex lattice. In particular, induced velocities are calculated from every vortex segment on every point of the lattice and after the addition of free stream velocity the convection of them is determined. The advantage with this method is that effects like wake distortion, vortex roll - up at the wingtip area and wake expansion are modeled which consequently leads to better predictions. So, it is suitable for wind turbine applications where yawed flows are usually met and also, for cases where transient cases are examined (such as change in wind direction or wind turbine orientation or in blade geometry). The disadvantage on the other side is the high computational cost because of the large number of calculations needed for every lattice point that constantly grows in size as the wake unreels. In addition, stability problems on free wake algorithms can arise when wake points get close together due to singularities in the calculation of induced velocities.

One important issue is that the free wake approach does not take into account viscous effects in the wake which is another facet of physics. Typically, because of them, vortex cores of all filaments should increase in time and the tangential velocities should decrease correspondingly. Several models exist to model viscous effects on vortex cores like the Lamb

18

– Ossen model [27], the Ramasamy and Leishman model [28], the Squire model [29], the modified Lamb – Ossen model by Bhagwat & Leishman [30] and also coupled viscous - inviscid models by Sorensen [31].

One common use of lifting line theory is when unsteady flows or generally unsteady operating conditions are encountered. In this case the span-wise bound circulation distribution of the wing changes continuously in time and an iterative process is applied based on equation 2.11 which matches the bound circulation distribution with lift. Firstly the wing is divided into i=1:N small elements as depicted in figure 2.1 and simulation time into m time steps where a guess is made about the wing's bound circulation distribution. Usually every time step starts with the distribution of the previous one. The trailing and shed vortices in turn are determined in accordance with equations 2.12 and 2.13 . Since the vortex strength of all segments both from the wing and the wake is known (the wing vorticity derives from the initial guess and the wake vorticity has already been calculated from the previous time steps) the induced velocity, the resultant velocity and the effective angle of attack of every element are calculated. So, lift coefficient is acquired from tabular data and lifting force is exerted from equation 2.14 and a new bound circulation is determined from equation 2.11 . Now, the bound circulation of the next step is given by equation 2.15 where an underelaxation factor is applied in order to prevent solution from diverging. This process is repeated until a user defined convergence criterion expressed with equation 2.16 has been obtained.

$$(\Gamma_{Trail})_{i,m} = (\Gamma_{Bound})_{i,m} - (\Gamma_{Bound})_{i+1,m}$$

$$(\textbf{2.12})$$

$$(\Gamma_{Shed})_{i,m} = (\Gamma_{Bound})_{i,m-1} - (\Gamma_{Bound})_{i,m}$$

$$(\textbf{2.13})$$

19

$$Lift = \frac{1}{2} \rho_\infty V_{resultant}{}^2 C_L c$$

(**2.14**)

where:

- C_L is the Lift coefficient

- $V_{resultant}$ is the sum of induced velocity, freestream velocity and blade section velocity (structure related or otherwise caused)

- c is the chord of the wing element

- ρ_∞ is the air density

$$\Gamma_{input} = \Gamma_{old} + D(\Gamma_{new} - \Gamma_{old})$$

(**2.15**)

$$\text{while} \quad \max[(\Gamma_{input} - \Gamma_{old})/\Gamma_{old}] > convergence\_criterion \quad \text{repeat}$$

(**2.16**)

Besides the well known lifting line theory it is also worth to be mentioned that a more analytical vortex method exists, called vortex-lattice model [25], in which the wing and the wake is divided into small panels (Figure 2.3). According to Green's Theorem the potential flow in which a lifting surface is submerged can be represented by distribution of sources σ and doublets μ placed on the wing's boundary [25]. Sources σ determine the solid boundaries of the body by displacing the flow whereas doublets μ provide lifting force through the circulation that they introduce. The solution of the flow is achieved after the discretization of the body and the wake into panels of constant vortex strengths μ and the application of the

20

non-entry boundary condition to the so called collocation points placed either at the center of the panels (Neumann boundary condition) or inside the body (or wing) (Dirichlet boundary condition). So, after the calculation of μ distribution on the wing, induced velocities and the wing's angle of attack (AoA) are determined and finally loads are acquired from tabular data as happens with the lifting line model. The major difference of vortex lattice model compared to lifting line is that a more detailed distribution of the wing flow or loading - span wise and chordwise - is obtained and the thickness of the wing is taken into account thus leading to better predictions yet it is more computationally expensive. Further development of the vortex lattice method was implemented by Hess [32] who introduced a piecewise source distribution to the body in order to model accurately the body geometry and Chorin [33] who used vorticity particles instead of segments that are able to convect freely into the wake and thus resulting in a smoother induction velocity field, also known as vortex blob method.
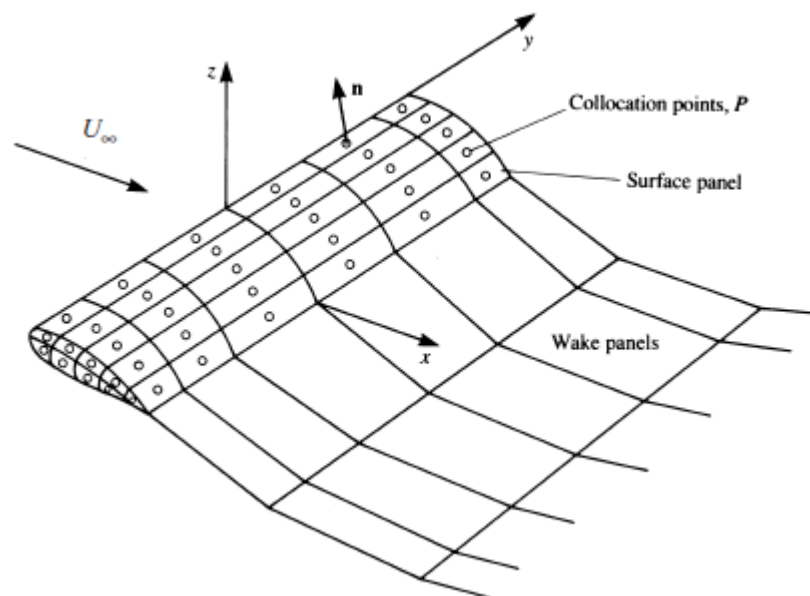

Figure 2.3 Representation of the discretized wing and wake according to vortex lattice model source: [25]

21

Prescribed vortex methods were used to study rotor aerodynamics in the late 60's starting with helicopter applications [34]. At first hovering flight was investigated by Landgrebe [35], then Gilmore and Gartshore, Kocureck, Tangler and Berkowitz. In particular Landgrebe conducted experiments for over seventy rotor configurations and developed equations which describe the tip vortices from both ends of the rotor (inner and outer) whereas the intermediate ones are determined through interpolation [36]. Later in 1985, Beddoes developed another generalized prescribed wake model and achieved good agreement in vertical velocities of tip vortices in forward flight, between his simplified prescribed model and a free wake vortex model [36]. Then, investigations extended to free wake modeling of helicopter rotors with Miller (1982) [37], Bliss (1983) [38] and Bagai & Leishman (1995) [39]. Inevitably their work continued in the direction of reducing the computational cost of free wake models ([40] and [41]) either by new approaches in calculation of the wake or with the use of adaptive grids and also velocity field interpolation schemes.

So, the experience obtained from helicopter applications was utilized on axial wind turbines with the development of prescribed vortex methods [42] and free wake methods [43]. GENUVP [44] is a characteristic high fidelity aerodynamic model developed by Voutsinas et al based on free moving vortex particles to model the wake and it is validated against full scale tests of pitch steps and extreme yawed operation for the TJAEREBORG 2MW wind turbine. It can also be combined with a beam elastic model and stand as a complete aeroelastic model.

Currently vortex methods play an important role to wind energy field and they are commonly preferred for detailed wake analysis of wind turbines. These methods perform well in dynamic changes such as pitch steps, in safety stops and yawed operation of the turbine.

22

The main drawbacks are the high computational cost and the convergence issues in inboard sections where stalled flow is encountered.

In this thesis both CFD and vortex methods (outlined in paragraphs 2.1 and 2.2) are used in order to study the effect of the geometric feature of blade tip sweep on wing aerodynamics and subsequently on wind turbine parameters. The reason is that both methods are capable of modeling such geometric features, yet the extend of their application is determined by the available computer power from the researcher.

2.3   Blade Element Momentum Method – BEM

The two preceding methods that were presented are used for a variety of applications where aerodynamics are to be studied including of course, wind turbines. However, Blade Element Momentum (BEM) method was developed only for HAWT (rotational axis parallel to flow). In fact this type of turbine has prevailed over years of evolution and currently represents 95% of all installed wind turbines [45]. HAWTs (Figure 1.1) rotate due to the tangential component of the lifting force that is generated by the blades (usually 3) which has proven to be the most efficient way to extract power from the wind. This type is amendable to a lot of control features for optimizing blade loads and high power gain of the order of 10MW [46]. The main drawback is the need of a yaw mechanism that should perform the alignment of the rotor axis to the prevailing wind direction (sensed by anemometers).

On the other hand, the vertical axis wind turbine concept is met in two versions (figure 2.4) the one which rotates based on drag force of the rotor blades (Savonius rotor) and the well known Darrieus concept (common to H – rotor design) which has two curved blades connected to the vertical axis and rotate due to the combination of lift and drag blade forces. Despite the fact that they do not need a yaw mechanism to align them with the flow they have

23

other design disadvantages such as low rotational speed, inherently low power coefficient, unsteady loads and that they need an external power source to make them start. For this type of turbine a different theory exists which is based on the streamtube model, originally introduced by Templin [47] using one streamtube for the turbine and after modifications took its final form by Paraschivoiu [48] and Read and Sharpe [49] with the development of double multiple streamtube models.
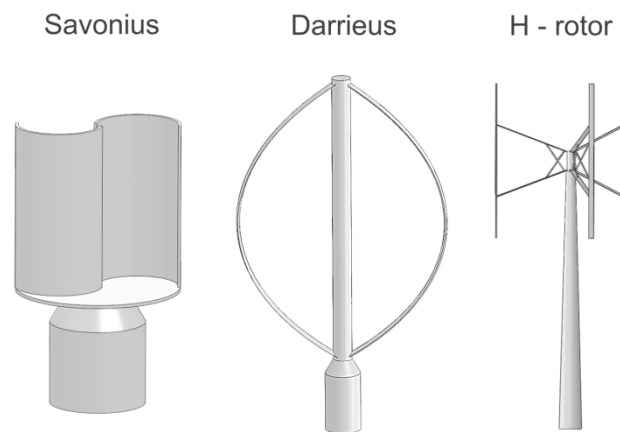

Figure 2.4 Versions of vertical axis wind turbines source: [50]

BEM is the most widely used method to study the aerodynamics of HAWTs and is preferred for its high speed, low computational needs and good quality of the results. It is based on many assumptions and so has equivalent limitations. Many additions have been made through empirical corrections over the years in order to improve the results, extend its applicability and thus it is still the first tool that is used by industries to investigate new designs. It was originally developed by Glauert in 1932 [51] and combines the 1-D momentum theory developed by Froude in 1878 with a 2-D blade element analysis. In principle this method divides the flow over the actuator disk considered by momentum theory into annular streamtubes, solves the momentum equation by which induced velocity is determined and matches it with the rotor's torque and thrust (figure 2.5).
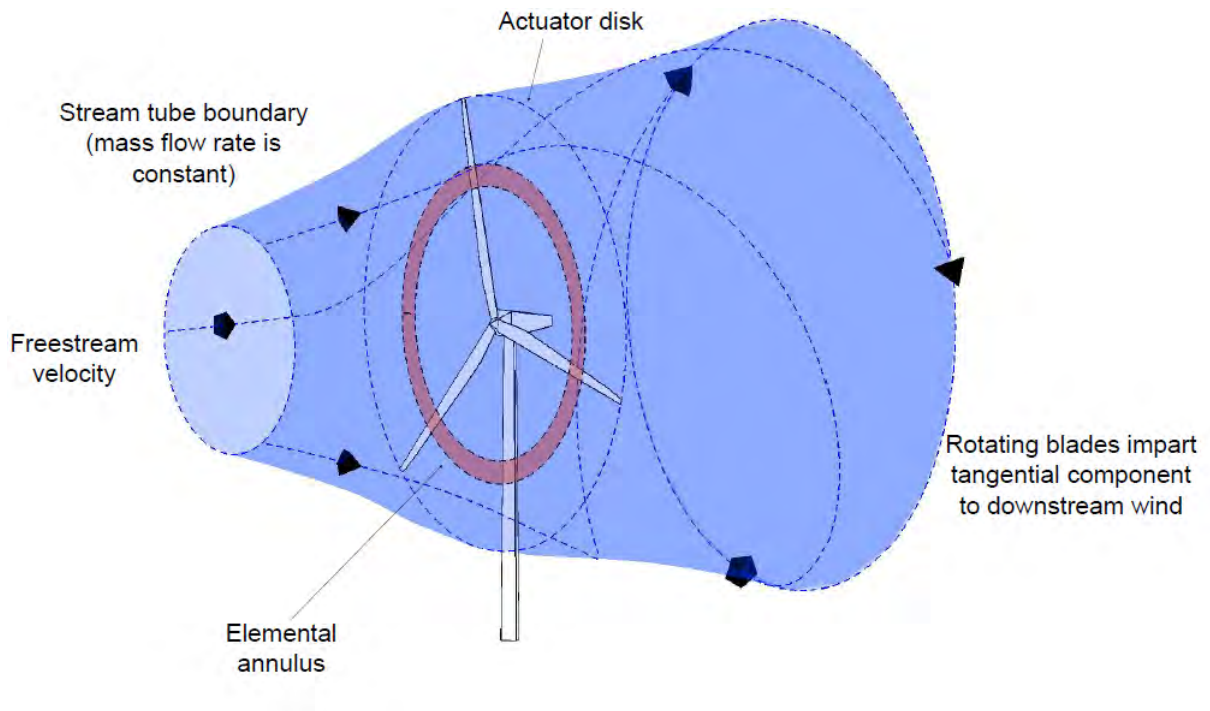
24

Figure 2.5 BEM model representation source: [52]

The basic assumptions of BEM method include incompressible, inviscid, axisymmetric, unyawed and steady-state flow. In addition, the aerodynamics of blade sections are determined from 2-D steady state loading data and there is no interaction between radial sections of the actuator disk. Therefore, BEM would be unsuitable for unsteady loading conditions. One other limitation which is explained later is the break down of the theory for axial induction factor (equation 2.19) over 0.5 - in other words operating conditions of high thrust or loading.

The actuator disk in 1-D Momentum theory is an idealized thin surface that extracts energy from the mean flow, assuming infinite number of blades, resulting in the streamtube of figure 2.6 . The streamtube starts from the undisturbed flow upstream and ends far downstream with a characteristic slow down and expansion of the flow. In figure 2.7 the corresponding streamlines and velocity – pressure spatial variation is depicted.

25
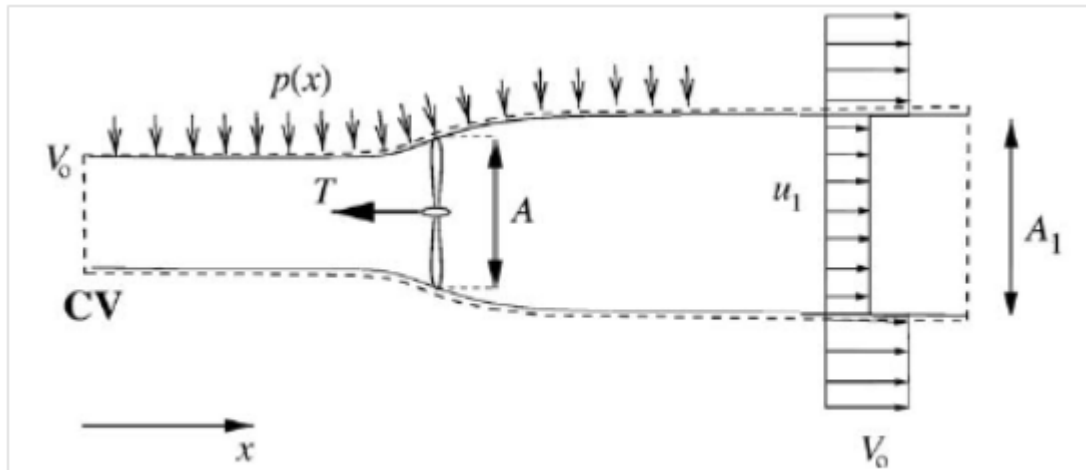
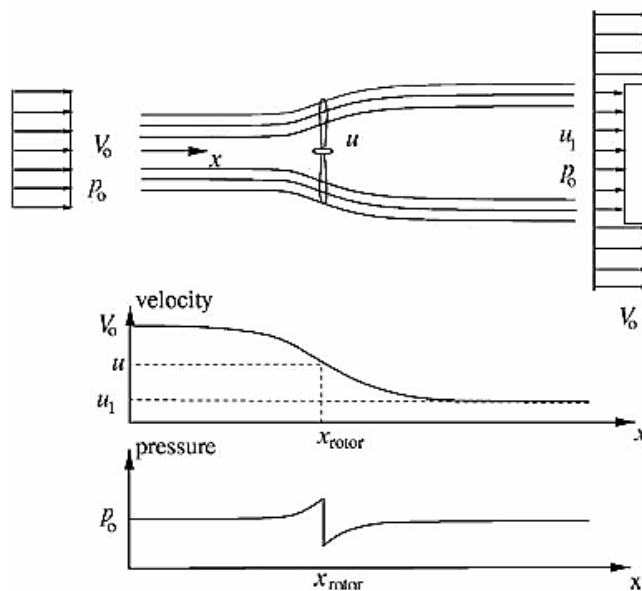Figure 2.6 1-D Momentum theory representation source: [4]

Figure 2.7 1-D Momentum theory velocity and pressure source: [4]

From the conservation of mass it is implied that the mass flow rate is equal everywhere in the streamtube so:

$$\dot{m}_0 = \dot{m} = \dot{m}_1 \quad \text{or} \quad \rho A_0 V_0 = \rho A\, u = \rho A_1 u_1$$

(**2.17**)

26

where:

- A_0 and V_0 are the cross section area and velocity far upstream

- A and u are the cross section area and velocity at the actuator disk

- A_1 and u_1 are the cross section area and velocity far downstream

It is seen from figures 2.6 and 2.7 that as the actuator disk extracts energy from the wind stream there is a pressure rise right before the rotor disk, a discontinuous pressure drop over it and then a gradual recovery to the atmospheric value p_0. This variation in pressure is translated in gradual velocity drop across the streamtube and a corresponding rise in the cross sectional area. So, an axial force T acts on the fluid control volume due to this pressure difference. Moreover, according to 3rd Newton's law an equal axial force acts on the actuator disk which is called thrust T and is calculated from the following equation:

$$T = \Delta p \mathrm{A}$$

(**2.18**)

where:

- Δp is the pressure drop over the actuator disk

- A the cross sectional area of the rotor equal to πR^2

The velocity deceleration is expressed through the axial induction factor a and it is defined according to the following equation and depicted in figure 2.11 .

$$u = (1-a)V_0$$

(**2.19**)

27

According to 2nd Newton's law thrust force is also equal to rate of change of momentum across the streamtube or else thrust equals to:

$$T = \Delta p A = (p^d - p^u)A = \dot{m}(V_0 - u_1) = \rho A u (V_0 - u_1) = \rho A (V_0 - u_1)V_0(1-a)$$

(**2.20**)

Pressure difference can be also found from Bernoulli's equation by applying it to both sides of the rotor.

$$\frac{1}{2}\rho V_0^2 + p_0 = \frac{1}{2}\rho u^2 + p^u$$

(**2.21**)

$$\frac{1}{2}\rho u_1^2 + p_0 = \frac{1}{2}\rho u^2 + p^d$$

(**2.22**)

And the pressure difference derives from:

$$p^d - p^u = \frac{1}{2}\rho(V_0^2 - u_1^2)$$

(**2.23**)

So, after combining equation 2.23 with equation 2.20 :

$$\frac{1}{2}\rho(V_0^2 - u_1^2)A = \rho A(V_0 - u_1)V_0(1-a)$$

(**2.24**)

Which then results in:

28

$$u_1 = (1 - 2a)V_0$$

(**2.25**)

Which means that the velocity deficit in the far wake is twice as much that of the corresponding velocity deficit in the actuator disk as it is seen in figure 2.7 . After combining equation 2.20 with 2.25 yields a different expression for thrust:

$$T = 2\rho A V_0^2 a(1-a)$$

(**2.26**)

Having in mind that:

$$P = Tu$$

(**2.27**)

After combining equations (2.19), (2.26) and (2.27) power is expressed by:

$$P = 2\rho A V_0^3 a(1-a)^2$$

(**2.28**)

The available power for the cross section of the actuator disk is determined by the equation below:

$$P_{avail} = \frac{1}{2}\rho A V_0^3$$

(**2.29**)

So, the power coefficient is defined as the fraction of the produced power divided by the available power:

29

$$C_P = \frac{P}{\frac{1}{2}\rho A V_0^3}$$

(**2.30**)

Thrust coefficient is defined as the ratio of the thrust force on the actuator disk divided by the maximum thrust that can be felt by the disk:

$$C_T = \frac{T}{\frac{1}{2}\rho A V_0^2}$$

(**2.31**)

Substituting in equation (2.30), equation (2.28) and in equation (2.31), equation (2.26) results in the following expressions for C_P and C_T as a function of the axial induction factor a :

$$C_P = 4a(1-a)^2$$

(**2.32**)

$$C_T = 4a(1-a)$$

(**2.33**)

Equation 2.32 is very important because from this, the upper limit of the power coefficient is determined after differentiating:

$$\frac{dC_P}{da} = 4(1-a)(1-3a) = 0$$

(**2.34**)

30

Thus, $C_{P\max}$ is 16/27 = 0.593 for axial induction factor $a = \dfrac{1}{3}$ which corresponds to an ideal wind turbine rotor with all of the assumptions mentioned earlier for the BEM method and it is called Betz limit [53]. The plot that results from equations (2.32) and (2.33) is seen in figure 2.8 .
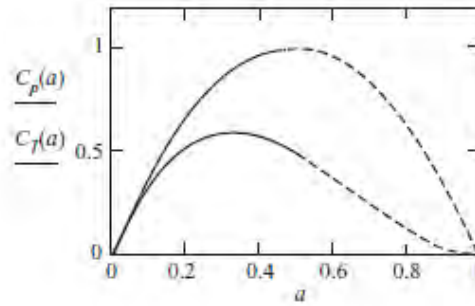
Figure 2.8 Plot of C_P and C_T VS axial induction factor a according to ideal 1-D momentum

theory. source: [54]

This limit though can be exceed with the introduction of a shrouded rotor – in other words a diffuser outside the rotor with the shape of an airfoil which will push more flow through it (figure 2.9). The bound vorticity created at the airfoils of the shroud resulting from the incoming flow will induce a beneficial velocity through the disk thus increasing the flow. However the benefits of this solution have to be evaluated as a whole by taking into account all of the additional weight, loads and cost of the turbine.
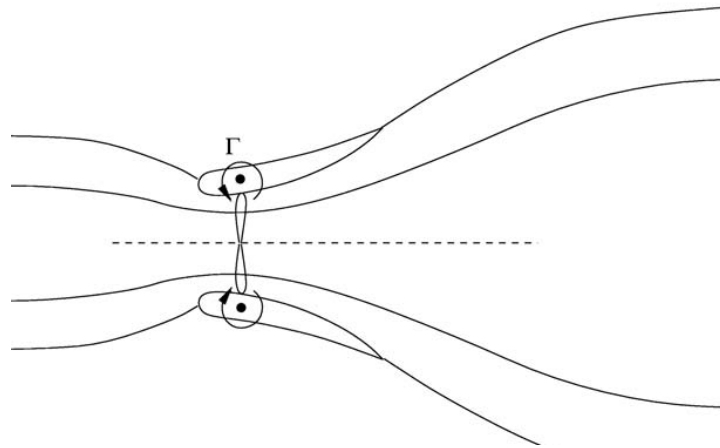
Figure 2.9 Shrouded rotor. source: [4]

In a real wind turbine, the rotation of the blades due to torque would induce a rotational speed to the wake due to the equal and opposite torque acting to the flow. Thus a corresponding induction factor α′ (referred as tangential) is introduced and defined by equation 2.35 . This additional kinetic energy to the wake is translated into power losses for the wind turbine so it is desirable to keep the tangential induction factor low. This is generally achieved with high rotational speed of the turbine rotor and it is explained in figure 2.10 - as rotational speed V_{rot} increases, tangential induced velocity C_θ (or else v) decreases

$$v = (1 + a')\omega\, r$$

(**2.35**)

where:

- ω is the angular velocity of the rotor

- r is the radial distance of the section from the rotor hub

32
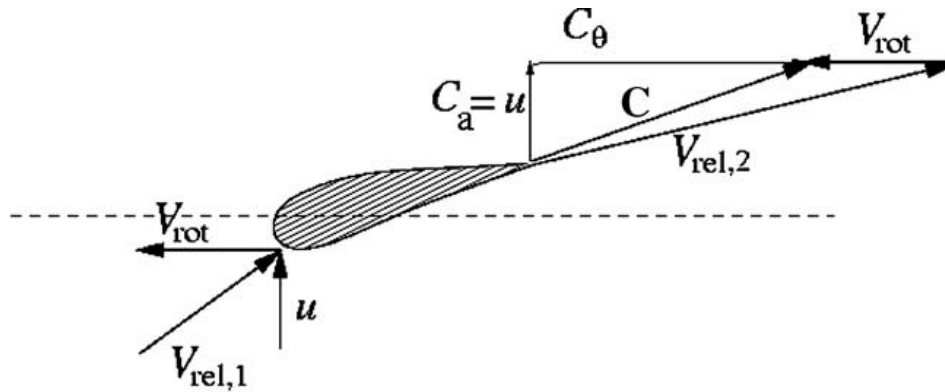
Figure 2.10 Velocity triangle in the wake of a rotor section. source: [4]

The induction factors of equations 2.19 and 2.35 calculated from 1-D momentum theory are used for the determination of the resultant velocity $V_{resultant}$ seen locally by the airfoil sections and thus the corresponding angle of attack α (Figure 2.11). Angle β refers to the blade's twist at that point, whereas φ stands for the inflow angle. After combining the generated lift (equation 2.36) and drag forces (equation 2.37) according to the inflow angle the two resulting forces are the normal force Fn (or out of plane force) expressed by equation 2.38 and the tangential force Ft (or in plane force) expressed by equation 2.39 . The normal force Fn is responsible for the thrust force T experienced by the rotor whereas Ft is responsible for the rotor torque M.

$$L = \frac{1}{2} \rho V_{resul\tan t}{}^2 c C_l$$

(**2.36**)

$$D = \frac{1}{2} \rho V_{resul\tan t}{}^2 c C_d$$

(**2.37**)

33

$$F_n = L\cos\phi + D\sin\phi$$

(**2.38**)

$$F_t = L\sin\phi - D\cos\phi$$

(**2.39**)

Where lift and drag coefficients (Cl and Cd) are acquired from 2-D tabular data and thus it is suitable to define a corresponding coefficient for the normal and tangential forces with the form of:

$$C_n = C_l\cos\phi + C_d\sin\phi$$

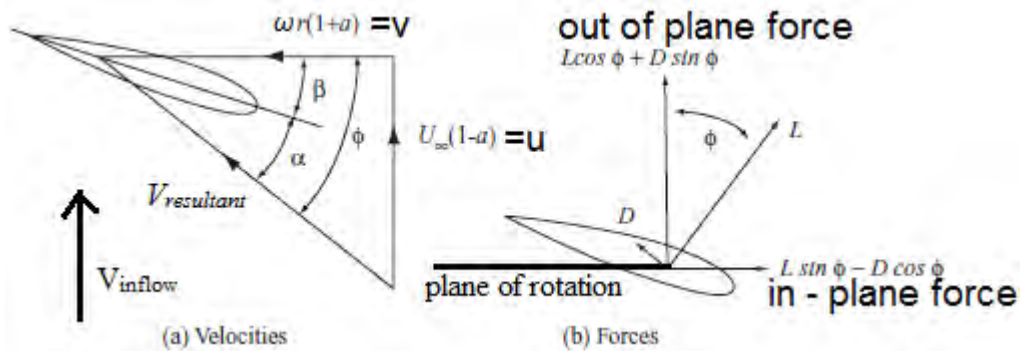(**2.40**)

$$C_t = C_l\sin\phi - C_d\cos\phi$$

(**2.41**)

Figure 2.11 Velocity triangle and forces of a rotor section. Source: [54]

The basic rule of the BEM theory is that only the forces acting on every radial section of the rotor are responsible for the momentum change in every annular streamtube. According to this concept equation 2.18 can be used in combination with equations 2.19 and 2.25 in order to calculate the thrust in every annuli of the streamtube:

34

$$dT = \dot{m}(V_0 - u_1) = \rho(dA)u(V_0 - u_1) = 4\pi r \rho V_0^2 a(1-a)dr$$

(**2.42**)

In addition, the torque M in every annuli is calculated by an equivalent to equation 2.42 expression with the assumption of irrotational flow before the rotor ($V_{rot0}=0$) and rotational velocity in the far wake equal to C_θ :

$$dM = d\dot{m}(V_{rot0} - V_{rot1}) = rC_\theta d\dot{m} = 2\pi r^2 dr \rho u C_\theta$$

(**2.43**)

C_θ is defined as α´ωr from equation 2.35 and combining it with equation 2.19 for u the former expression becomes:

$$dM = 4\pi r^3 \rho V_0 \omega (1-a)a'dr$$

(**2.44**)

Moreover, thrust dT and torque dM of every annuli may be written alternatively as a sum of thrust and torque of every blade element from every individual blade according to:

$$dT = F_n dr B$$

(**2.45**)

$$dM = F_t r dr B$$

(**2.46**)

where B is the number of rotor blades.

35

Now after substituting in equations 2.45 and 2.46 Fn - Ft from equations 2.38 and 2.39 and dT - dM from equations 2.42 and 2.43 correspondingly the expressions of the two induction factors are acquired:

$$a = \frac{1}{\dfrac{4\sin^2\phi}{\sigma C_n} + 1}$$

$$(\ 2.47 \ )$$

$$a' = \frac{1}{\dfrac{4\sin\phi\cos\phi}{\sigma C_t} - 1}$$

$$(\ 2.48 \ )$$

Where σ is the fraction of the chord length of B blades divided by the circumference length in a specific annuli (equation 2.49). This is an important parameter for the determination of the rotor performance [54].

$$\sigma_r = \frac{c_r B}{2\pi r}$$

$$(\ 2.49 \ )$$

As was already stated the forces on the rotor require the calculation of the two induction factors. This is not accomplished in a straightforward way from equations 2.47 and 2.48 because the two parts of the equations are interdependent. The procedure that is followed is an iterative process in which initial values for the two induction factors are guessed in the beginning (usually zero), then the value of inflow angle φ, angle of attack and normal – tangential forces are calculated resulting in a new value for the α and α′ . The process stops when convergence is achieved or else when the parameters have changed less than a preset

tolerance and so the final values are acquired. So total thrust and torque are provided through the summation of dT and dM for every blade multiplied by the number of blades.

The concept of 1-D momentum theory assumes one uniform axial induction factor for the whole disk or rotor. This is rarely true for a spinning wind turbine ($\alpha' \neq 0$) but it can be proven that this assumption does not do much harm in the load calculations, yet with a limitation. Glauert [51] has shown (figure 2.12) that the Betz limit is practically achieved for tip speed ratios (equation 2.50) over 6. From the reference figure it is also deduced that the assumption of 1-D momentum theory is valid for tip speed ratios over 3 where C_P equals over 90% of the optimum value (0.593).
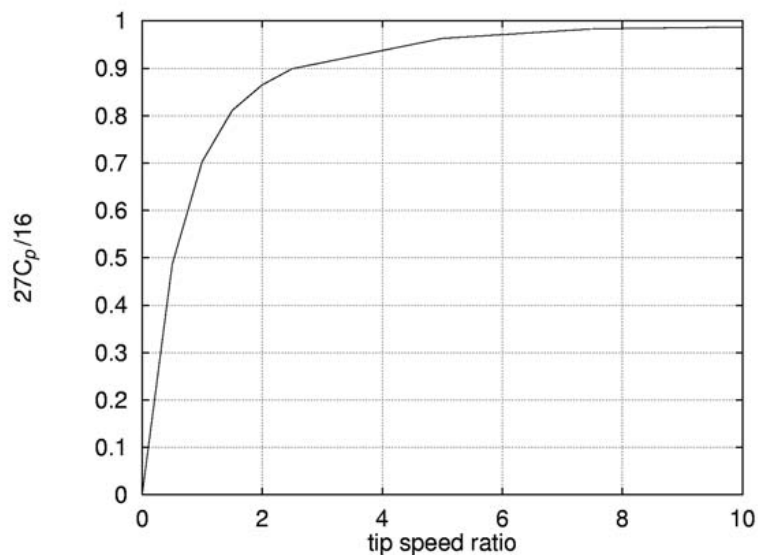
Figure 2.12 Power coefficient in relation to Betz limit for increasing tip speed ratio λ of a spinning wind turbine. Source: [4]

$$\lambda = \omega R / V_0$$

(**2.50**)

The reason that the assumption of uniform axial induction factor for a spinning wind turbine cannot hold is explained by the simplified vortex cylinder theory. As it is seen in

37

figure 2.13 the rotating blades produce lift which is expressed as bound circulation of radially constant vortex strength $\Delta\Gamma$. In this simplified model, a vortex of this strength escapes from the tip of every blade and convects downstream. This is also the case for the blade root area where the vortices form a line vortex of strength $\Delta\Gamma$ that also convects downstream. Thus the vortex tube is defined by the outer vortices, the bound vortices of the blades and the line vortex which lies down the axis of rotation. Everywhere else the flow is considered irrotational and with the use of Biot Savart law (equation 2.10) it is possible to calculate the induced velocity in every point as was already explained in the previous section. The approximation for no expansion of the vortex tube as flow slows down in the wake is also used in the simplified model. So, this vortex field alters the induction factor of the blades by means of lowering the angle of attack at the blade sections in relation to the actuator disk of the 1-D momentum theory model. This phenomenon also occurs for wings of finite span and expressed as tip losses. Prandtl investigated them for both wings and propeller blades in the early 20th century.
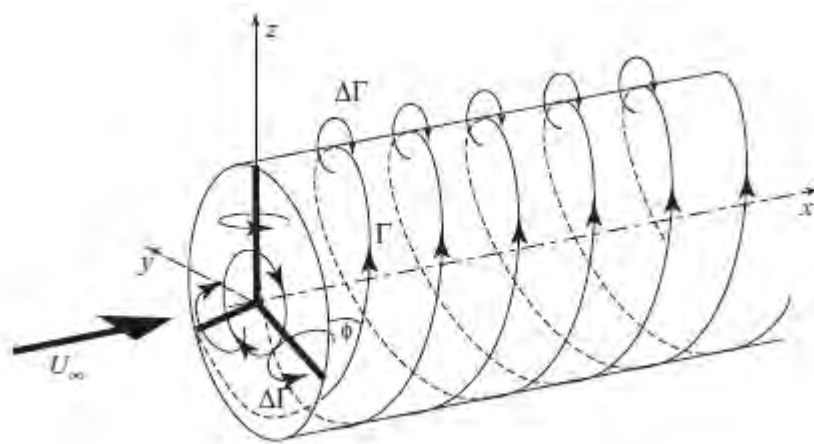
Figure 2.13 Simplified Vortex Cylinder Theory. Source [54]

In order to correct BEM theory concerning tip losses (which is a characteristic of rotors with finite number of blades), Prandtl developed a factor which is a function of radial

38

distance r - $F(r)$. Instead of using a vortex cylinder model he introduced successive discs in the wake that move with velocity $(1-a)V_0$ (equation 2.19) and separated by the same distance of the tip vortices described in the cylindrical model (figure 2.14). This lets part of the undisturbed fast moving air to enter in the wake, thus altering the induction of the rotor. Of course, for small radial distances – near the root area – the penetration is small and so is the induction difference which is translated to tip loss factor equal to one $(F(r)=1)$. For any other radial distance the tip loss factor is between the values of one and zero $(0 < F(r) < 1)$. The final expression that is used in BEM codes nowadays is a modification to the Prandtl's tip-loss factor and suggested by Glauert [51]. This factor, F(r), is applied to both the axial induction factor and the tangential induction factor and equals to zero, at the rotor tip.

$$F(r) = \frac{2}{\pi} \cos^{-1}[e^{-\frac{B}{2}(\frac{\lambda}{\lambda_r}-1)\frac{1}{\sin\phi}}]$$

(**2.51**)
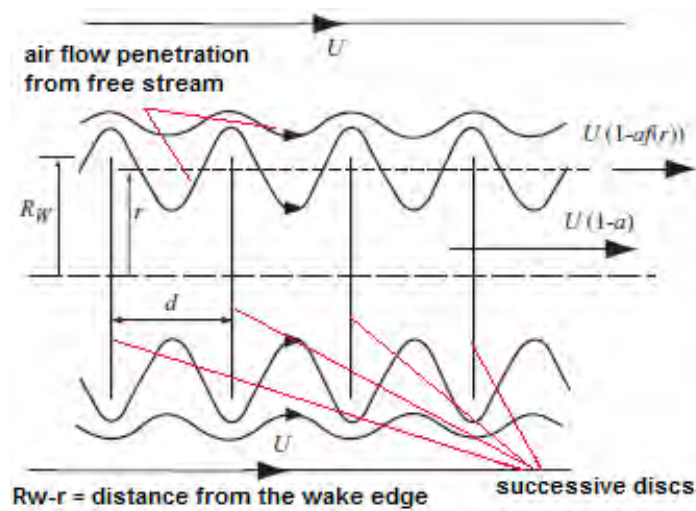
Figure 2.14 Prandtl's consideration for the development of tip loss factor. Source [54]

39

Goldstein [55] in 1929 has also studied tip losses of propellers and obtained a solution in terms of Besssel functions for the helical screw flow, yet it cannot be implemented in the BEM theory. Over the last years research still continues to the direction of improving the tip-loss factor through the use of vortex methods in conjunction with the BEM method [56]. The benefit is important and leads to more accurate predictions of the wind turbine Annual Energy Production (AEP) because the largest part of total rotor torque consists of the sum of the tip section torque values. Of course, a similar factor can be obtained to account for the root losses and thus create a complete tip/root loss factor [54] but it is of lower importance in contrast to the tip loss factor as the root area produces small amount of torque.

The streamtube consideration and thus the flow field as depicted in figure 2.5 is not valid. BEM theory breaks down for high rotor loading or else high thrust operating conditions and predicts reversal flow. In reality this happens when the tip speed ratio (equation 2.50) λ becomes too large (high rotational speed in contrast to inflow wind velocity) and so the rotor tends to be an impermeable disk. In this case the slow moving air behind the rotor creates an area of very low pressure and the flow around the rotor disk tries to fill the gap creating a recirculating flow pattern in the wake, also referred as turbulent wake state (TWS). Glauert [57] has introduced a modification to the calculation of thrust coefficient based on empirical corrections and extended accordingly the C_T-α curve (figure 2.15) for axial induction factor greater than 0.3. So, equation 2.33 with the correction for tip losses and high induction factor cases, becomes:

$$C_T = 4aF(1 - f_g a)$$

(**2.52**)

where:

40

- F is the Prandtl tip loss factor

- f_g is the glauert correction for α>0.3 and equals to $\frac{1}{4}(5-3a)$ [18]
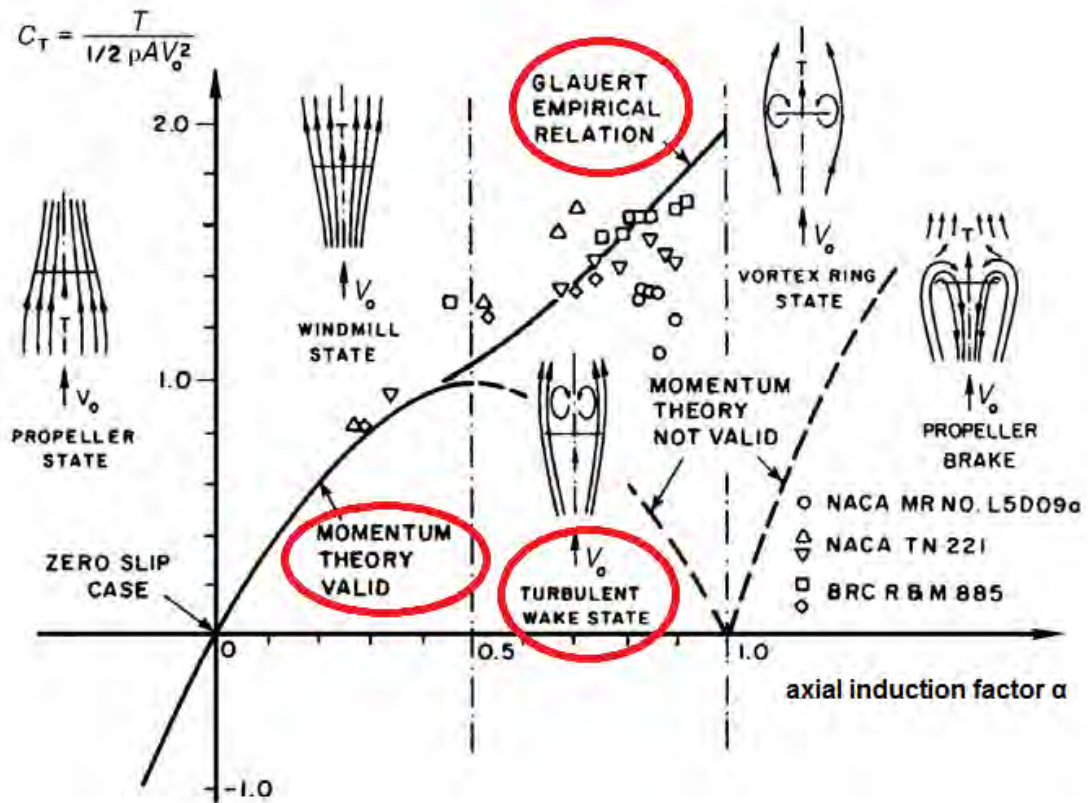

Figure 2.15 Glauert correction to C_T-α curve and the corresponding rotor states. Source [4]

Another issue concerning BEM theory is the assumption for non-yawed flow which is also rarely met in real operating conditions but continuously pursued through a yaw mechanism installed in the tower of the modern wind turbines. In yawed flows, when the incoming flow is not perfectly aligned to the rotor axis, there is an azimuthal (θ_{blade}) (figure 2.16) variation in the induction field of the rotor. In particular, the downstream side has higher induction than the upstream side and thus, the downstream side sees lower wind speed than the upstream side. This eventually leads to higher loads in the upstream side that tends to re-align the rotor axis with the flow. In figure 2.16 V' denotes the velocity in the wake which

41

is deflected by the wake skew angle χ. W is the induced velocity and its calculation is accomplished by the following equation proposed by Glauert in his autogyro theory [58] where he predicted that the induction of the rotor would not be uniform in yawed flow.

$$W = W_0 (1 + \frac{r}{R} \tan(\frac{\chi}{2}) \cos(\theta_{blade} - \theta_0))$$

(**2.53**)

where:

- W_0 is the mean induced velocity of all blades in radial position

- θ_{blade} is the azimuthal blade position

- θ_0 is the position of the blade when it is in the most downstream position

- χ is the wake skew angle

Rotor plane seen from above

42
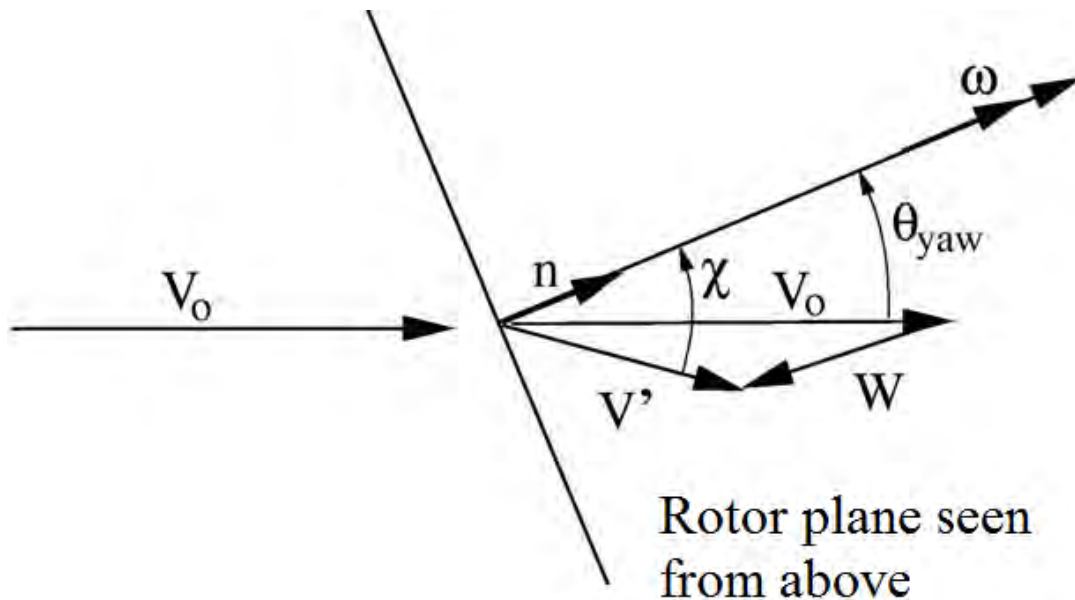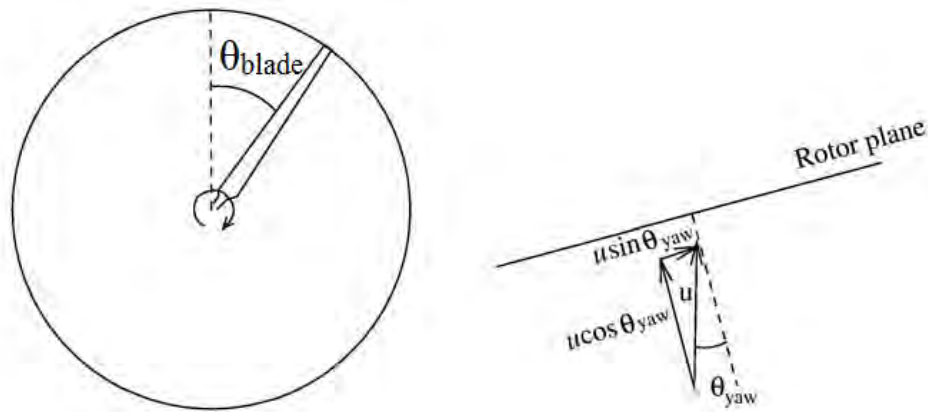
Figure 2.16 Wake velocity (V') and induced velocity (W) in the wake of a yawed rotor (up)

Definition of blade azimuth angle (θ_{blade}) and the yawed rotor plane seen from above

(bottom): Source [4]

The corrections described above concern only cases of steady inflow and apply generally to preliminary design calculations of wind turbines. "Preliminary" refers to design parameters such as power, blade loads, tower loads, efficiency and blade geometry. The next step in the design is the consideration of unsteadiness in the incoming flow field or the unsteady effects induced by blade features such as variable pitch or deployment of aerodynamic devices. If simple BEM is used and it is assumed that the wake is always in equilibrium as if the wind is steady at any instant a quasi – steady approach is considered. However, it is expected that the wake will not adapt immediately to rapid changes in blade loads and time will be needed in order for a new equilibrium to be achieved.

Therefore, dynamic models were developed in order to overcome this issue and one of the most popular was presented by Pitt and Peters [59] in which a system of ordinary differential equations was incorporated to calculate blade loads and moments as a sum of steady and unsteady part. In addition, Oye in 1986 [60] introduced a different dynamic inflow model based on a filtering scheme for the induced velocities consisting of two first order

43

differential equations (2.54) and (2.55). At first, the quasi steady value of the induced velocity is determined and then an intermediate value is calculated by applying a first order filter for the whole rotor. Eventually the induced velocity W is calculated by applying successively a second (first order) filter, which is a function of radial distance r and ensures that the tip elements react faster than the root elements. The time constants τ_1 and τ_2 are calibrated with a simple vortex method [4] [equations (2.56) and (2.57)].

$$W_{int} + \tau_1 \frac{dW_{int}}{dt} = W_{qs} + k\tau_1 \frac{dW_s}{dt}$$

(**2.54**)

$$W + \tau_2 \frac{dW}{dt} = W_{int}$$

(**2.55**)

where:

- W is the calculated induced velocity

- W_{int} is an intermediate value of the induced velocity

- W_{qs} is the quasi steady value of the induced velocity

- k is a constant and equals 0.6

- τ_1 and τ_2 are time constants

$$\tau_1 = \frac{1.1}{(1-1.3\alpha)} \frac{R}{V_0}$$

(**2.56**)

44

$$\tau_2 = (0.39 - 0.26(\frac{r}{R})^2)\tau_1$$

(**2.57**)

This model has been validated with measurements for the 2WM Tjaereborg wind turbine showing very good agreement (figure 2.17). The changes in torque is a result of sudden changes in blade pitch whereas firstly the pitch is increased and so the angle of attack of the blade sections decrease and after 30 seconds blades revert to the zero pitch state. The basic conclusion is that every sudden change results in an abrupt surge or overshoot of the blade parameters and after significant time they recover in accordance with the new equilibrium state.
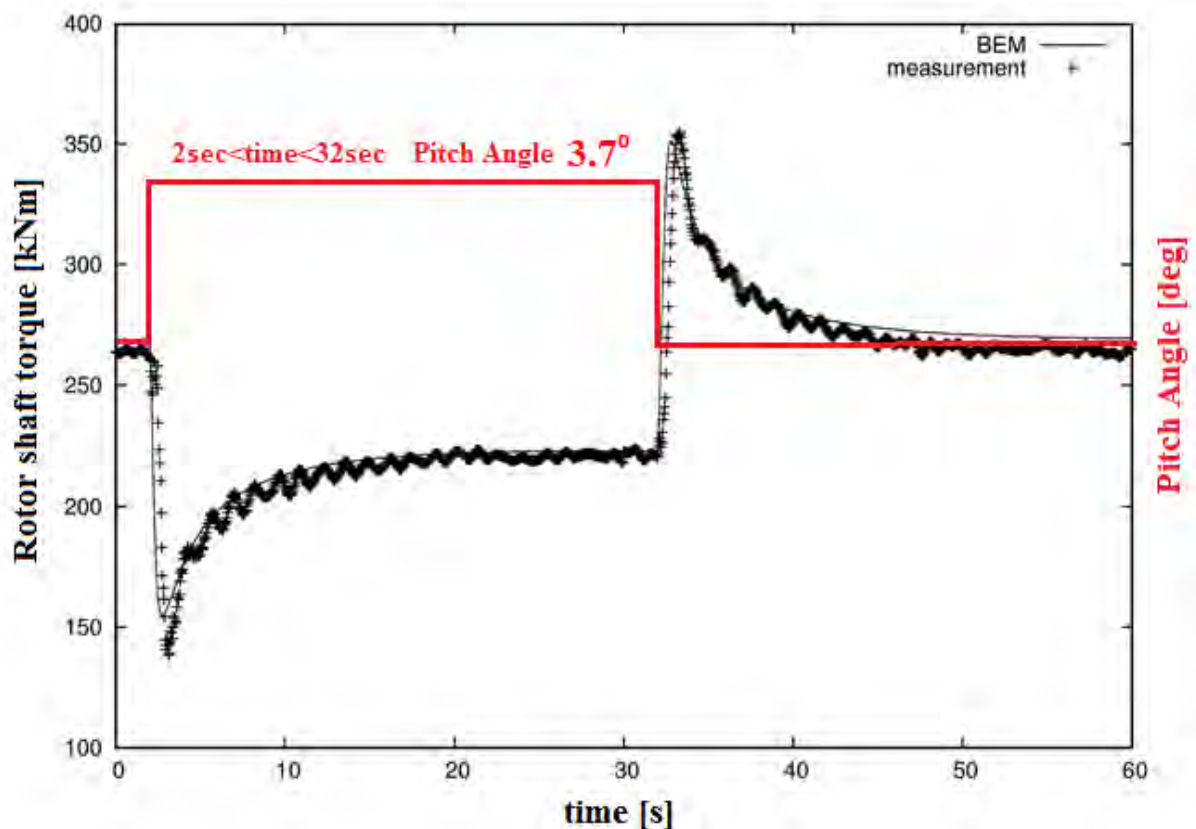
Figure 2.17 BEM method with Oye dynamic inflow model validated with measurements for 2WM Tjaereborg wind turbine after sudden pitch changes: Source [4]

45

Unsteady conditions are not only met in large scales (such as the inflow field of a wind turbine) but also in the blade level due to various reasons. The angle of attack seen by the blade segments is changing continuously because of the tower effect, the wind shear, the atmospheric turbulence and the yawed flow. In many cases the changes are cyclic due to the inherent rotating motion of the rotor and the angle of attack changes according to a sinusoidal function.

McCroskey [61] and Carr[62] focused on the unsteady aerodynamic loading of wings (buffeting) and on the dynamic stall effect by utilizing numerical methods and experimental data. Tolouei et al [63] studied experimentally the unsteady pressure distribution of the pitching airfoil EPPLER 361. In brief they discovered that there is a close relationship between Reynolds Number (equation 2.3) and the reduced frequency k (equation 2.58– the non-dimensional number that relates the wave length of the disturbance to the chord length and describes how severe it is or not) in the wake formation and the wing loads.

$$k = \frac{\omega c}{2U_\infty}$$

(**2.58**)

where:

- ω is the rotational frequency of the disturbance or sinusoidal load

- c is the chord of the airfoil

- U_∞ is the freestream velocity

46

They also considered that the "bubble that is formed in the leading edge of a pitching airfoil beyond static stall angles, convects downstream, reenergizes the boundary layer and allows greater lift coefficients to be achieved before dynamic stall occurs". In cases when the flow remains attached and the wing is oscillating, the lift coefficient still is not a linear function of angle of attack (figure 2.18) but it is determined according to Theodersen theory [64] who derived an exact solution for a harmonically oscillating thin airfoil with flap. Similar work was conducted by Von Karman and Sears [65] who examined the case of a sinusoidal vertical gust inflow field. In addition, Wagner and Kussner [66], [67] studied the response of a thin airfoil to indicial (step or impulsive) changes in angle of attack.
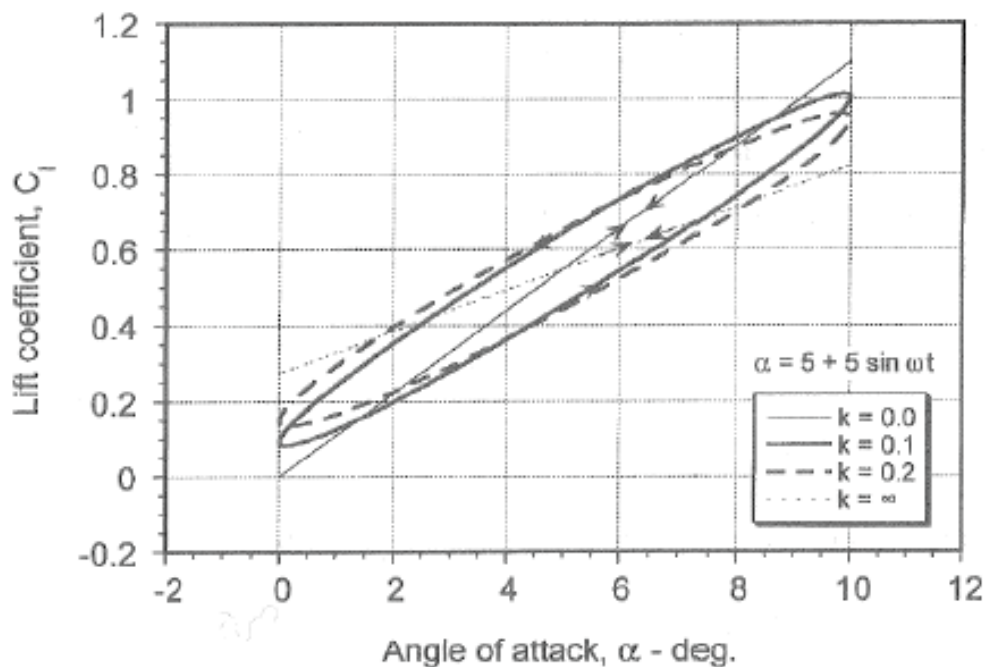
Figure 2.18 Lift coefficient Vs angle of attack for various reduced frequencies k calculated with Theodorsen theory – no static stall region: Source [36]

One of the most widely known models concerning unsteady aerodynamics is the Beddoes-Leishman model [68] which includes compressibility effects (which the aforementioned models do not) and uses relatively few empirical coefficients. It was

47

originally developed to determine and predict the unsteady loads encountered in helicopter aerodynamics [36] and is also suitable for wind turbine applications. It consists of an unsteady attached flow module, a non-linear trailing edge separation module, a leading edge flow separation module and a dynamic stall module for the shedded vortices that induce loads.

Despite the numerous assumptions and simplicity of the BEM theory, it is undoubtedly an efficient tool for industries and research. It is suitable for preliminary calculations of adequate accuracy concerning power output and loads due to the aforementioned corrections that were implemented after years of evolution. Nowadays, sophisticated software for wind turbine applications such as FAST [69], BLADED [70], HAWC2 [71] and DUSWAMP [72] use unsteady BEM theory as a basis for their aerodynamic module. Then, combined with a structural (elastic) model – or a multi body dynamics model, full aeroelastic simulations can be executed.

Research still goes on with new methods that couple BEM theory with Lifting Line Theory [56] that lead to more accurate tip loss factor calculations and thus correct the Annual Energy Production (AEP) value. In another research work [73] a near wake model, originally developed by Beddoes [74] , is further developed and coupled with a far wake model based on BEM. The near wake model calculates accurately the induction in the root and tip areas of the blades by taking into account the first 90 degrees of their rotation and it is based on Lifting Line theory. Then, it is coupled with the far wake model based on BEM theory in order to take into account and the rest of the wake. The results which are compared to CFD and GENUVP, show improved results in relation to steady and unsteady BEM modeling. In addition, the influence of trailed vorticity on flutter speed estimations, is determined.

2.4 The Challenging Operating Environment of Horizontal Axis Wind Turbines

HAWT appears as a simple device to the eye of someone not familiar with it. However, the design of each part of a wind turbine is a result of extensive research so that it will be able to operate without faults for a period of 20 years (which is the typical design life). Power is produced from the wind and in fact, wind is a highly unstable parameter and in addition difficult to predict. According to equation 2.29 the available power from the wind is proportional to the cube of its velocity and thus, it is obvious that it plays a significant role in the designed rated power. Another facet of the wind's unsteadiness is the unsteady fatigue loads that are encountered by the components. Figure 2.19 shows the wind speed spectrum after measurements at Brookhaven, New York from Van Der Hoven [54], [75] which indicates that the wind is never steady.
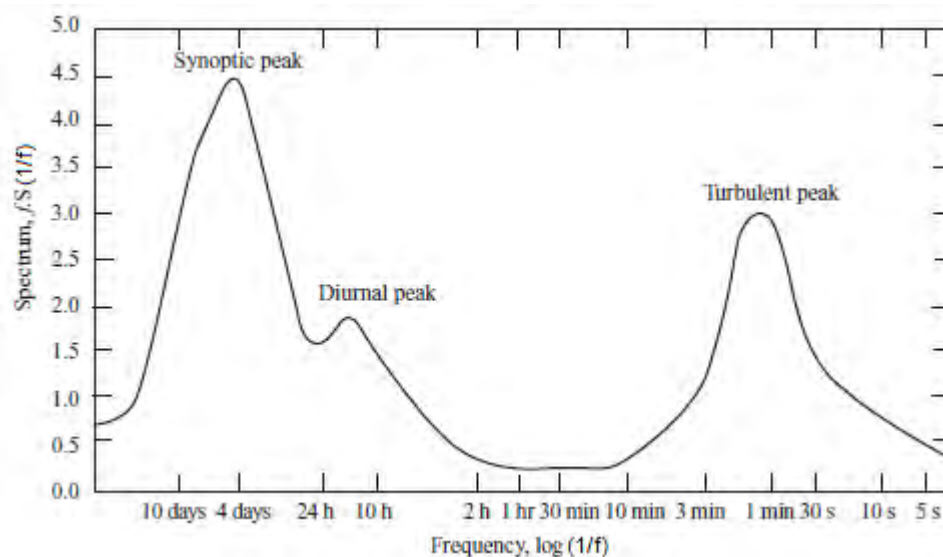
Figure 2.19 Wind Speed spectrum measured by Van der Hoven at Brookhaven. source: [54]

Synoptic peaks are of high time-scale and refer to meteorological systems that affect the wind flow in a region. Weather is a result of many parameters – it starts from the non-

49

uniform solar heating of regions near and far from the equator, the earth's rotation and the corresponding Coriolis force effects that create a global wind scheme. The angled orientation of the earth axis (24° degrees) plays also a major role in the formation of meteorological systems. In fact the four seasons that are met in regions of temperate climate are due to this earth's angle shift. In local level the weather systems are also affected by parameters such as altitude and the morphology of the terrain (high mountains – hills – lakes - valleys – proximity to the sea). Regions near the sea include diurnal peaks (24h frequency) usually caused by temperature differences between land and sea which creates the well known land and sea breezes. Regions near high mountains face strong downstreams resulting from the temperature differences between high and low altitude areas in a daily basis. Turbulent peaks refer to speed variations of small time-scales about the wind speed average and is met in all directions. Equation 2.59 gives the definition of turbulence intensity *I* which is used to quantify the turbulence of a flow field and is responsible for energy peaks introduced into the grid or load peaks sensed by the blades. Turbulence is a "chaotic" phenomenon described in terms of statistics, yet it obeys the rules of conservation of energy and mass. It is caused mainly by fluid viscosity and also thermal variations in the flow field which leads to energy exchange between different regions and thus flow mixing.

$$I = \frac{u_{rms}}{\overline{U}}$$

(**2.59**)

where:

- u_{rms} is the root mean square of wind speed fluctuations

- $\overline{U}$ is the average wind speed

50

Unsteady flow phenomena could also be caused by gusts, rotor yaw misalignment and wind shear. The first refers to abrupt changes in wind speed that happen in a relatively short period of time (few seconds). They are categorized according to the frequency that occur in a region (once a year or once in 50 years) and wind turbines are tested for such cases [76] in order to prove that they are capable of withstanding the extreme loads that are developed because of gusts. The second refers to the orientation of the wind which is rarely steady and sometimes changes suddenly too. The angle between the direction of the wind and the rotor axis is referred as $\boldsymbol{\Phi}$ and it is easily proven that the produced power is proportional to Φ^3. In addition, yaw misalignment is responsible for asymmetric rotor loading as it was already discussed in paragraph 2.3. Lastly, wind shear is associated with the ground boundary layer which is expressed as a gradual velocity rise starting from zero (at the surface) and reaching the freestream velocity in a specific height. Wind shear depends on the earth's roughness (dense forests result in high boundary layer height whereas seas and open fields result in lower height), geostrophic wind strength, Coriolis effects from earth's rotation and thermal effects. Except for the turbulence that is introduced because of ground boundary layer it also leads to asymmetric rotor loading. In particular the lower half of the rotor experiences lower wind speeds in contrast to the higher half.

Apart from physical influences, wind inflow unsteadiness is also caused by structural design known as, tower shadow effects or by the arrangement of a wind farm, known as wake array effects. For rotors that have their blades in the upstream side (which is the most common) there is a flow deceleration right in front of the tower which in turn is translated to small changes in blade loads as they pass by this position. For downstream rotors the phenomenon is more severe, as the blades pass through Von Karman vortices [77] that are formed behind the cylindrical tower. This situation poses risk for blade excitations near their

natural frequencies and eventually structural failures may be caused. Moreover, the wake array effects refer to the case in which a turbine operates (partially or fully) in the wake of another wind turbine. It was already mentioned that the flow behind the rotor of a HAWT expands, rotates and decelerates. In addition, turbulence intensity increases, mainly due to the tip vortices that are shed from the blades and convect downstream and due to the flow mixing between the wake and the external undisturbed flow. This situation is met in wind farms consisting of many wind turbines and leads to power losses, increased fatigue loading and generally inefficient operation for a number of devices.

Figure 2.20 is a descriptive presentation of the challenging - unsteady operating environment of HAWTs. It separates the unsteady loading caused by unsteady wind inflow in two main categories : cyclic loading (occurs in every revolution of the blades) and non – cyclic loading.

52
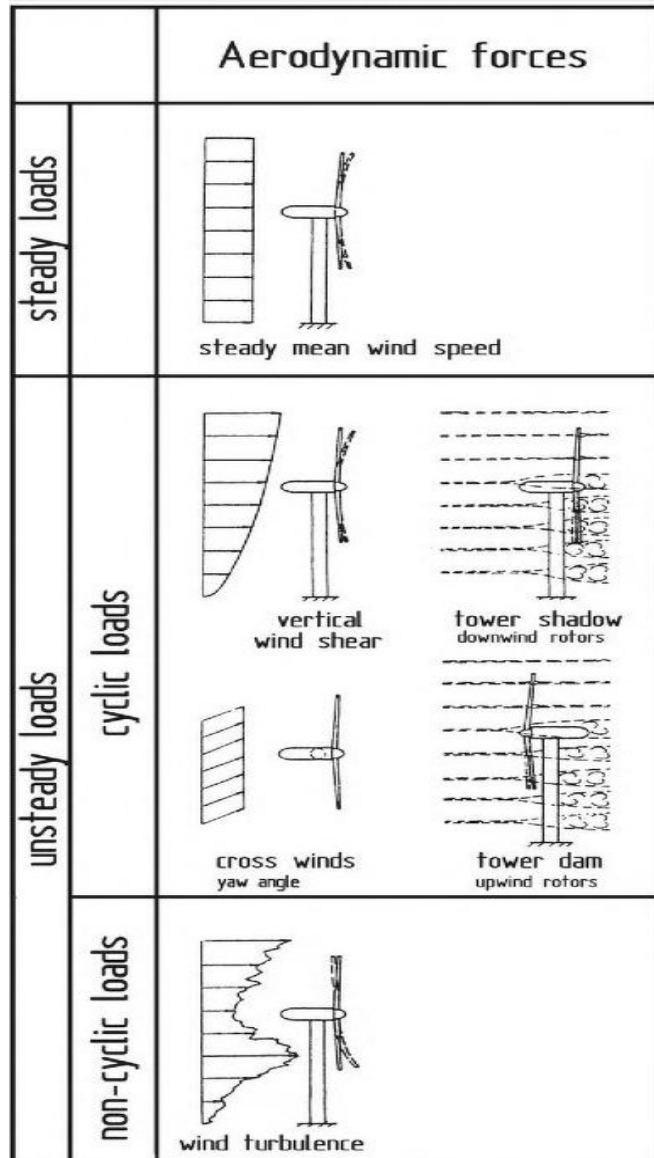
Figure 2.20 The challenging operating environment of HAWTs. source: [78]

2.5 Control Methods for Horizontal Axis Wind Turbines

A wind turbine is designed for operation in the rated speed, in order to deal with the continuously changing wind speed velocity and simultaneously extract as much energy from the wind as possible without jeopardizing its structural integrity. Figure 2.21 shows the power curve of a typical wind turbine according to the wind inflow. Cut – in speed is defined as the lowest operating speed of the wind turbine which is essential to start. Beyond this wind

53

velocity the torque produced by the blades overcomes friction and rotational inertia of the device including rotor, rotor axis, gearbox and generator. As wind speed increases the power output increases accordingly, till it reaches the rated speed (or else the speed that is designed to operate). Beyond the rated speed, power output could increase further but this would result in higher loads than the upper threshold set by the designer in order to ensure safe lifetime operation. So, wind turbine is controlled through suitable mechanisms that maintain power output and loads to the desired value. For even higher wind speeds (> Vcut-out), loads cannot be moderated and the wind turbine ceases its operation and locks in the parked position to prevent structural failures.
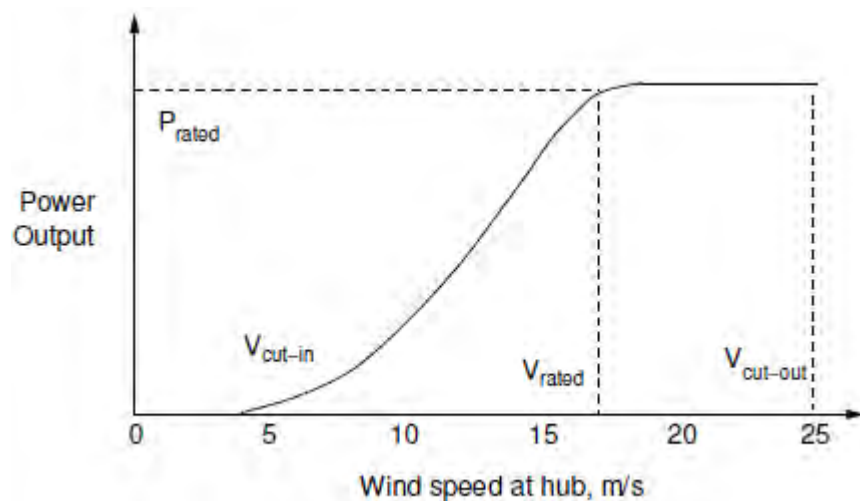
Figure 2.21 Typical wind turbine power output in respect to wind speed at the hub.

source: [54]

The challenging operating environment of wind turbines described in the previous paragraph causes severe fatigue loading on the blades and structure. Moreover, wind turbine blades have already surpassed 60m of length in the name of higher power production (5MW NREL reference wind turbine has 63m blades) and along with the evolution of materials, they weigh less and thus they are more flexible. This increased elasticity leads to shape changes

54

that in turn alter the blade aerodynamic loads and again the shape and so on. So, this aeroelastic coupling is another facet of the challenge faced by the wind turbine designer. Controlling the device with a variety of systems is a solution that ensures efficient operation on one hand and low fatigue / extreme loads. It also provides stable operation and thus better quality of power output due to the absence of sharp peaks. Controlling of wind turbines is divided into traditional and modern methods depending on the period they were introduced into the industry. The most common traditional control methods utilize blade stall, blade pitch, yaw misalignment and speed regulation.

Stall regulation is usually met on small wind turbines and the major characteristic is that they have their blades in a fixed pitch angle. As wind speed increases, the angle of attack of the blade sections increase accordingly until stall occurs, therefore leading to lower lift – lower torque (figure 2.11). So, the rotational speed is kept within a specified range and correspondingly to non-optimal tip speed ratios values (equation 2.50). Pitch regulation is widely used in large wind turbines whereas a mechanism mounted on the hub turns the blades about their spanwise axis and adjusts the blade aerodynamic loads and thus the wind turbine parameters through the adjustment of the inflow angle φ (figure 2.11). So, in cases when the power production is about to overcome the rated value the blades pitch in the direction of reducing the inflow angle and thus the angle of attack, the produced lift and torque. Blade pitch can also be used to stall the blades in an emergency situation (severe weather conditions) by pitching them to the opposite direction and park the turbine – this is called active stall control through blade feathering. The blade pitch mechanism can be either collective (acting concurrently on every blade) or selective (acting individually), full span or partial span (applied only at the blade tip area). Apart from power regulation, this control strategy is also useful for load reduction during wind gusts. Yet, the pitch change rate of the

mechanism has to be over 5deg/sec as it is stated in [54] in order to deal with the majority of them. With pitch regulation a wind turbine generally operates very close to the optimal value of power coefficient (equation 2.34). The yaw misalignment correction of the turbine relatively to the wind direction can be achieved by the same mechanism that constantly monitors for zero yaw error during normal operation. This method can easily reduce power production (as was already mentioned in paragraph 2.3) when needed but it introduces additional unsteady aerodynamic loads and has lower reaction time due to the high inertia of the rotating rotor.

Finally, the variable speed wind turbines are allowed to run at different rotational speeds other than the rated, in order to achieve the optimal tip speed ratio for each wind inflow velocity. This is aerodynamically efficient on one hand but it requires the use of a frequency converter connected to the generator and so increases complexity and introduces electrical related losses that could be higher than those caused by the sub-optimal operation of a constant speed turbine (with wind speeds that lead to non optimal tip speed ratios).

The research field of wind turbine control is still active and concepts already applied to aircrafts and rotorcrafts are questioned for their effectivity in wind turbines. These ideas refer mainly to aerodynamic surfaces or devices that affect the flow field over the blades and thus the aerodynamic forces. The activation of these features is performed by an integrated system equipped with actuators and sensors that operate in a closed – loop and constantly monitor the wind turbine parameters. These systems define the "smart rotor" control concept and an extensive overview is found in [72] and [79]. However, the benefits of such concepts have to be carefully weighted along with the drawbacks that they introduce. Typical disadvantages are additional weight to the turbine and blades, increased complexity, added maintenance requirements, increased cost of energy, possible failures and the need of

56

developing fail-safe mechanisms. On the other hand, typical advantages are the high potential of changing total loads or the distribution of loads while occupying relatively low space or area of the blades (usually placed at the blade tip area).

Smart rotor concepts are on the foreground due to the evolution of new materials like the shape memory alloys, piezopolymers or piezoceramics and the development of new sensors like accelerometers, strain sensors and LVDT sensors. Shape memory alloys can recover to their original shape after up to 10% deformation [72] while piezo – materials induce displacements or deformations when electric energy is applied to them. Accelerometers are used to measure vibrations on different parts of the structure, strain sensors to measure the strain of blades due to loads and Laser Doppler Velocimeter (LDV) sensors to measure the velocity field of the incoming wind. The major challenge is to create a control system that is capable of counteracting the unsteady loads. To do so the actuators of the control system have to react at least with double frequency of that of the unsteady loads [72]. The operation of all components of the control system are under the authority of the controller which could follow a classic closed loop feedback design such as Proportional – Integral (PI) and Proportional – Integral – Differential (PID) [80] or a feed forward design combined with the use of an LDV sensor. In brief the most common PI and PID controllers are algorithms that provide a control signal which is the sum of a proportional to the error term and a proportional to the integral of the error term. The error is the difference of the desired value from the real value. The PID controller includes an additional term proportional to the error rate of change. More advanced active control methods like (LQR, LQG, H_2, H_∞), focused on oscillatory disturbances are reviewed in [81]. Modern design control methods utilize the following features in order to change on demand the aerodynamic loads on the

57

blades as a response to power output disturbances or off-limit states and to increased fatigue loads or load exceedances.

Flaps are the most common aerodynamic devices used in aircraft wings and act by means of shifting the Cl-α curve up (deployment towards pressure side) or down (deployment towards suction side). Concerning wind turbine blades it is more feasible to consider trailing edge flaps either as a separate surface supported by a hinge or a deformable surface as part of the main blade structure. The latter resembles to camber morphing which is a separate concept. Flaps can be distributed in the spanwise direction at strategic points and improve the distribution of loads or decrease fatigue loads by small individual changes in the deflection of the flaps during operation. The major advantage of this concept is that small deflections of flaps lead to large alterations in loads especially when installed at the tip area which produces the highest percent of the overall rotor torque and is subjected to the largest deflections compared to the rest of the blade. The flap configuration is a big issue for the designer who has to choose between adding weight with a separate surface and a mechanism to move it or compromise with a change in the structural rigidity of the blade by adding flexible trailing edge surfaces on some points across the blade and additional equipment to deflect them. In [82] the implementation of flap concept on the 5MW NREL reference wind turbine has been investigated with the use of DU-SWAMP engineering model. In [83] the potential for fatigue load reduction of a turbine with variable trailing edge geometry at yaw conditions was sought, including wind tunnel experiments on a small wind turbine in TU Delft and showed that large dynamic load reduction is attainable. Full scale experiments were also conducted on a Vestas V27 wind turbine, for a modified rotor equipped with one trailing edge flap covering 5% of the total blade span and significant blade root bending moment reduction was measured [84]. Figure 2.22 shows an application of the flap concept with the introduction of a prototype

58

deflectable flap consisting of small chambers that give the desired deformation by applying pressurized air or fluid in the upper or lower side.
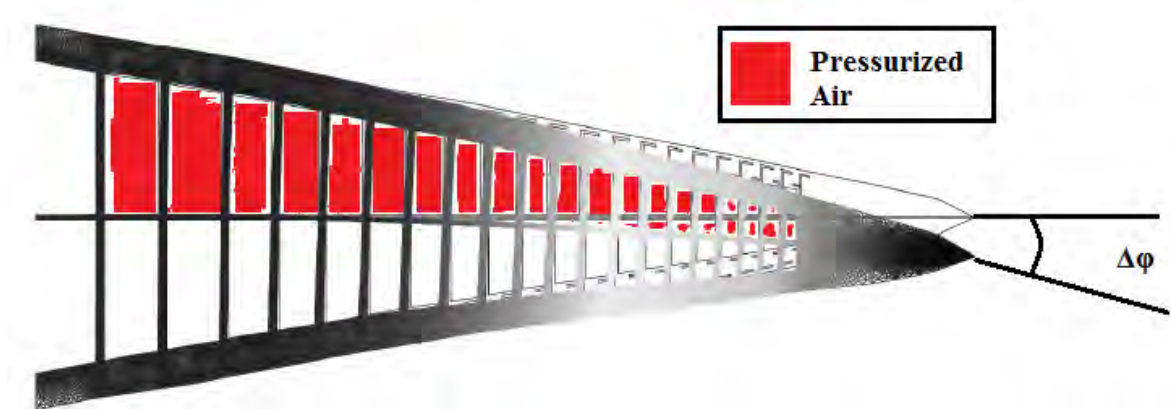
Figure 2.22 Controlled Rubber Trailing Edge Flap or CRTEF: [85]

The use of microtabs is another concept of aerodynamic control on wind turbines and has been investigated by Van Dam [86] & [87]. It refers to small surfaces (with length in the order of boundary layer thickness) that can be deployed vertically to the wing's surface and change the lift characteristics of the blade in accordance to the spanwise position that they are placed. If they are deployed near the trailing edge, on the pressure side, the Kutta condition (equation 2.9) point is translated, the effective camber of the airfoil is changed and lift is increased. If they are deployed in the suction side and near the boundary layer transition point they can cause flow separation and thus lift reduction. The advantages of these devices is that they induce large aerodynamic changes in relation to their size, they are light and easily deployed with an electro-mechanism. On the other hand, they are usually used in "on-off" mode (not mid positions) which limits the control authority and efficiency.

The idea of camber morphing through smart materials which are embedded in the skin of the blade or adapted in its structural box is a promising concept as it poses changes to the airfoil section shape and thus its aerodynamic characteristics. One facet of this concept is the

59

use of a deformable trailing edge. However, as it was already mentioned the added weight of the mechanism or the reduced rigidity of the blade design in order to cause or allow the desired camber change is an important issue. Recently, research in the field of active morphing of airfoils the Fish Bone Active Camber (FishBAC) morphing structure has been proposed, with promising results in terms of aerodynamic efficiency increase [88]. In addition, research has been conducted concerning optimization of camber controlled rotor airfoils for vibration reduction in helicopters [89]. Similar to this concept in terms of not adding aerodynamic devices is the active twist control. Control is achieved through torsion of the blade which in turn changes the blades' design twist angles (figure 2.11). So, it energizes bending – torsion or tension – torsion coupling in order to control the loads. It does not change the shape of the airfoil but it does change the torsion characteristics of the blades which poses questions for development of aeroelastic phenomena. The twist control is possible with smart materials (like piezoelectric fiber composite actuators) and has been investigated on helicopter rotors for noise – vibration reduction and extends to improvement of performance and rotor stability [90]. Yet the application in wind turbines of large size and thus inertia is still a big challenge.

Finally another form of active rotor control can be considered with boundary layer control strategies. This concept was adopted in the early wing designs of aircrafts and consists of suction/blowing jets, synthetic jets and vortex generators that control the wing's boundary layer. Suction of air through small orifices in the suction side near the trailing edge of the airfoil leads to reattachment of the boundary layer whereas blowing of air in specific points of the suction side reenergizes the boundary layer and retards the separation. Synthetic jets are produced from the same fluid that runs past the airfoil through small membranes that vibrate inside a cavity and add momentum to the flow thus reenergizing the boundary layer. Vortex

60

generators are small surfaces that protrude from the airfoil's surface, placed in specific points and introduce vortices into the boundary layer in order to make it more resistant to separation. The obvious drawback is that they increase drag forces of blades. Vortex generators are usually met in fixed configuration but there has also been research for active control of them in [91].

Apart from the aforementioned active control methods which are essentially considered modern there have also been investigated passive control methods in the late years. Stall regulation was already analyzed before and belongs to the traditional control methods. Newer passive methods utilize the coupling of usually two degrees of freedom whereas changes in loads are counteracted by the aeroelastic response of the blades. Typical cases of aeroelastic adaptation are tension-torsion coupling, bending-twist coupling and sweep-twist coupling. In the first case, under the effect of tension forces that occur at increased rotational speeds the tip is twisted towards feather or a spring – loaded mechanism turns a part of the blade towards feather resulting in load reduction (figure 2.23). This passive concept is met in the Dutch FLEXHAT programme [92] and an improvement was proposed by Joose and Kraan with "Tentortube" [93]. In the second case the blade twists towards feather when it bends under the influence of high aerodynamic loads. This is feasible in the construction phase by orientating off the pitch axis the composite fibers and was investigated by Lobitz Veers et al [94].

In the third case the blade is sweptback (or else curved) so, the aerodynamic point is placed behind the elastic point, causing a moment about the pitch axis to develop and reduce the aerodynamic loads (figure 2.24). This concept was originally proposed by Liebst [95] and showed promising results in the direction of reducing bending moment and tip deflections

61

during gusts. Finally, another way of passive control of wind turbines is through addition of flexibility to blade root which was also considered in the FLEXHAT program [92] leading to noteworthy load reductions.
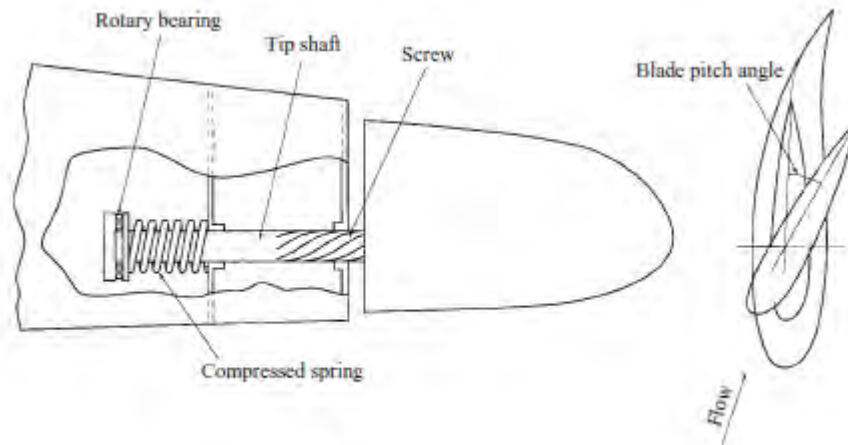
Figure 2.23 Tension-torsion coupling through a spring loaded mechanism source [54]
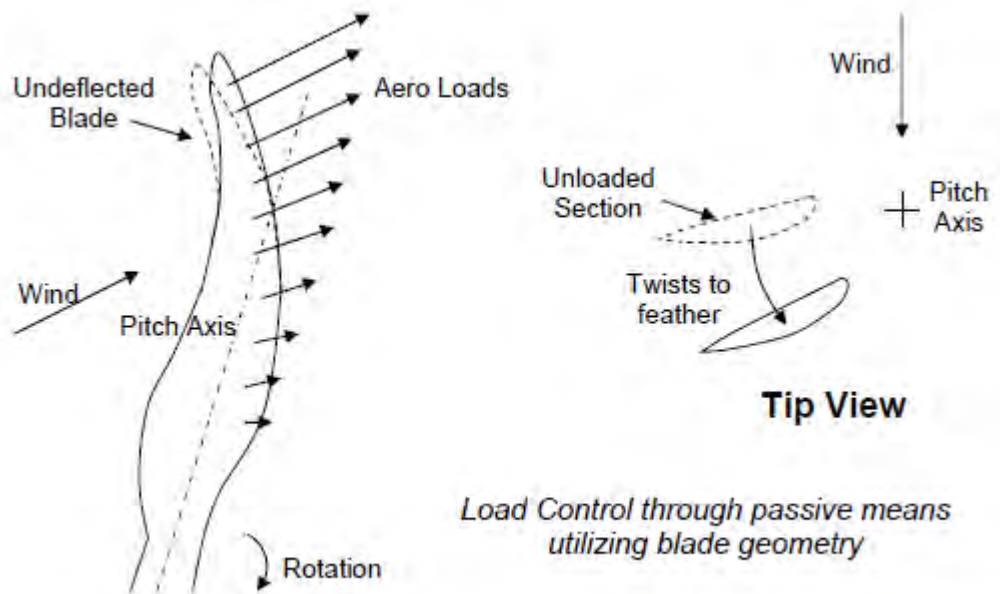
Figure 2.24 Sweep-twist coupling: source [96]

62

Passive control concepts are usually more simple in the design and construction phase, more light and also less expensive to maintain and manufacture in contrast to the active control concepts. However, they are inherently open-loop and thus designed to work efficiently for a specified operating envelope (wind inflow, fatigue load spectrum) whereas some cases may not have been taken into account. In particular the operation of HAWTs in the unsteady and also challenging environment, which was presented in paragraph 2.4, cannot be controlled in the best possible way by passive means – steady devices [81].

2.6 Sweeping of blades as a rotor control concept

The term "swept wing" is used to describe the angled direction of wing root to wingtip beyond the spanwise axis [97]. Sweep angle is commonly referred as «Λ» (figure 2.25). Aft-sweeping of wings was introduced in aircrafts, in order to improve their aeroelastic behavior (flutter, buffeting), stability and also to let them break the speed of sound barrier by reducing the occurrence of shock waves. Fore-sweeping was also considered and improved low-speed handling as stall started from the wing root and not the tip (where ailerons are placed), in contrast to aft swept wings. However, this design was prone to aeroelastic phenomena and led to heavy constructions in order to ensure higher wing stiffness. Moreover, variable swept aircraft wings (such as F-14 Tomcat) were used in order to expand the flight performance envelope and lately the "raked" tips (tips which are swept beyond the sweep angle of the wing) which are used in modern passenger aircrafts such as Boeing 787, have been proven to improve fuel efficiency. As far as rotorcrafts are concerned, mainly aft sweeping was utilized at the blade tip area with many different configurations (figure 2.26). Among others, the Westland BERP rotor blade (figure 2.27) is a characteristic design of tip-modified rotors for improved aerodynamic efficiency. The tip area of rotor blades plays a crucial role to rotor

63

performance as it is subject to high Mach Numbers and dynamic pressure due to shock waves [36]. Sweeping of rotors not only reduces the Mach number seen by the tips but also affects the formation of tip vortices in the direction of reducing induced drag. The sweeping angle of rotors however, does not exceed 20 degrees in order to avoid the influence of sweep - twist aeroelastic coupling [36].

Figure 2.25 Swept wing design in aircrafts: source [97], [98], [99], [100]
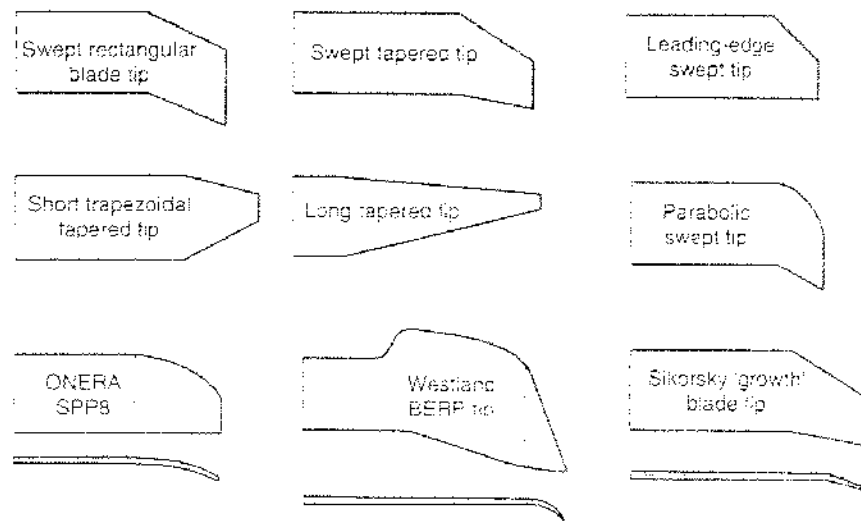
Figure 2.26 Different designs of tip swept rotor blades: source [36]
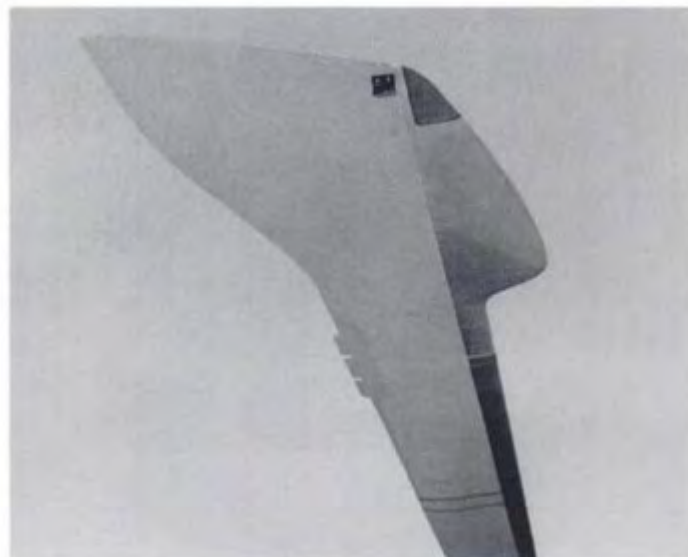
Figure 2.27 Westland BERP tip: source [36]

Due to its proven ability to improve the aerodynamic and aeroelastic performance of aircrafts and helicopter rotors the tip sweeping concept, was adapted in wind turbine blades, too. With the current size of rotors compressibility effects are not encountered at the tip area as happens to helicopter rotors but it is not unlikely to see in the near future larger rotors installed at offshore wind turbines that will face tip speed velocities near 0.3Mach (after

65

which compressibility effects are considerable). So, tip – sweeping was investigated as a passive load control strategy, tip deflection reduction mechanism and also tip vortex formation improvement feature.

Sweep – twist adaptive blade rotor (STAR) development program is the most representative implementation of the geometric feature of sweep in wind turbines. This project began in 2004 and after 4 years of research and bench testing, the prototype blades were fabricated figure (2.29) and field tests on a Zond 750 KW - 50m diameter wind turbine took place in the Tehachapi Mountain area of California (from April 2008 to June 2008) [101]. For evaluation, 4 different blade planforms with different characteristics were initially prepared and after detailed design led to the STAR 6 blade. The goal was to increase Annual Energy Production AEP by 5% -10% without exceeding the design loads. In order to achieve that, the curved blades were increased in length from 25m to 28m for the Z-50 turbine, so that the below rated energy capture would be increased accordingly. In [102] there is a comparison between the STAR 6 rotor (aft – swept blades 56m diameter), the BASE 6 rotor (straight blades 56m diameter) and the Z-50 (straight blades 50m diameter) turbine rotor. It is seen that the average power capture is increased in the order of 5%-10% for the STAR6 blade in contrast to the Z-50 blade, though it is slightly lower than the energy capture of the BASE6. STAR6 and baseline rotor tip deflections were on the same level. Moreover, STAR6 peak flap bending loads were 20% lower than that of the BASE6 but slightly higher than the baseline Z-50. In [96] advanced engineering models (such as FAST) are used to analyze swept rotor concepts and up-scaling this idea to rotors of higher diameter than the Z-50 is sought. In this work there is also a parametric study of sweep in terms of torsional stiffness, the exponent of sweep curve and the amount of sweep at the tip. It is concluded that higher sweep reduces fatigue loads without meaning that it also reduces tip deflections. In addition it is of high

66

importance to reduce the torsional stiffness of the blades in order to reduce fatigue loads and deflection. As far as the up-scaling idea is concerned, the author used as baseline the WindPACT [103] models of 1.5MW and 3.0 MW wind turbines and concluded that without changing the torsional stiffness of the blades and with relatively lower tip sweep, flap bending loads were reduced, yet there is no relief for the edge bending loads which are significant for large wind turbines [96].

Figure 2.29 Field testing of STAR rotor (left). STAR blade construction phase (right): source [101]

Similar investigations have also been conducted for even larger wind turbines by Riso utilizing its aeroelastic simulator known as "HAWC2". In [104] the effects of sweeping (aft and fore) the rotor blades of the reference 5MW NREL pitch controlled wind turbine, are studied. In particular 120 different swept blade configurations for a wide wind speed range (4-26 m/s) and 2 different control pitch controllers (the original one by NREL and one

67

implemented by Riso). For the aft swept blades it is concluded that flap-wise fatigue load reduction up to 10% and extreme load reduction up to 15% can be achieved. In addition, there is a significant reduction for the tower base and shaft yaw tilt fatigue loads. However, power output is lower in below rated conditions and edge-wise blade root fatigue loading is increased as was also concluded in [96]. Blade root torsion fatigue was significantly affected and led to a maximum of 400% increase for both controllers. Back swept blades reduced the NREL pitch controller activity despite the fact that the pitch angle travel was increased. For Riso's controller generally the activity was reduced along with the pitch angle travel. Conversely, fore sweeping of blades led to increased fatigue loads, extreme loads and also pitch angle travel. In some cases though fore swept blades caused instabilities in controller's operation.

Another interesting investigation concerning aft swept blades was conducted by NTUA for various configurations as seen in figure 2.30 utilizing the GENUVP free wake code. Once again it was proven that load reduction is achieved accompanied by a reduction in power output which varies according to blade curvature (b value) or tip offset (a value) [105]. The other interesting conclusion is that BEM codes compared to free wake codes lack the ability of taking into account correctly the effects of blade sweeping.

68

$$z_e = a \cdot \left(\frac{r - r_0}{r_{tip} - r_0} \right)^b$$
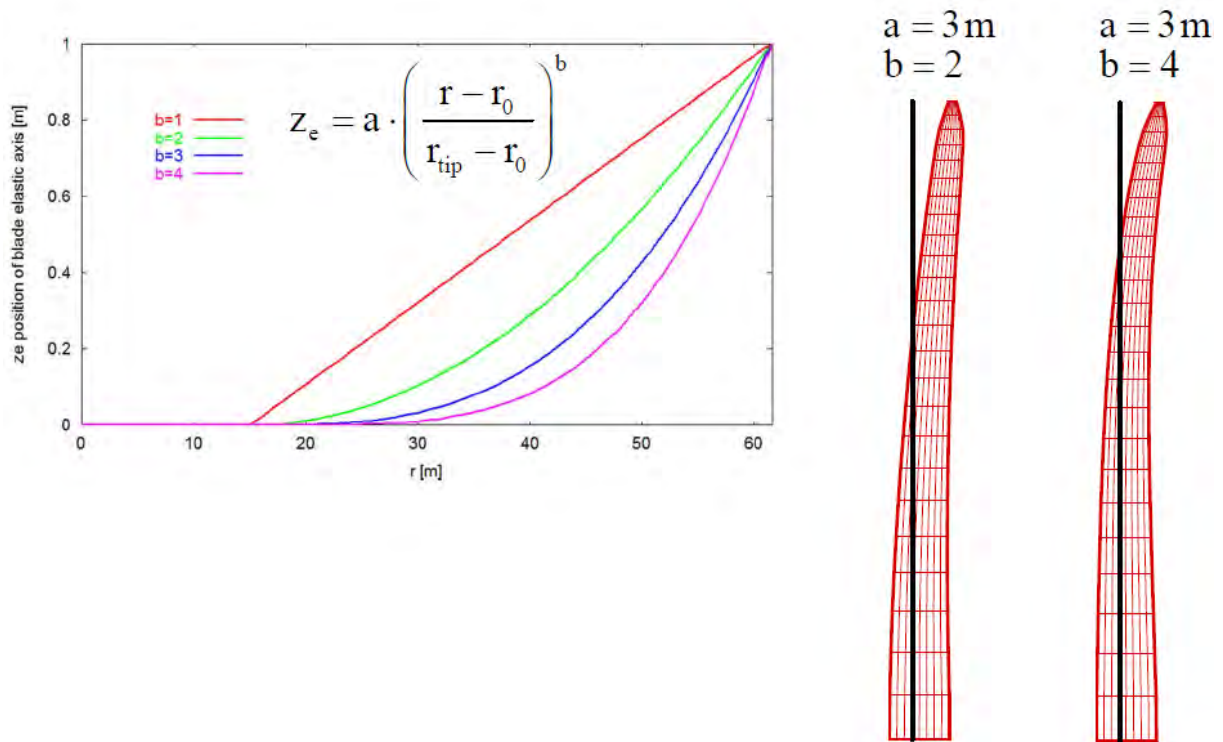
Figure 2.30 Parametric study for various swept blades. source [105]

The goal of this thesis is to fill in the gap of active wind turbine control methods through the investigation of varying blade tip swept rotor blades that has not yet been considered, according to the author's knowledge and current literature. The accomplishment of this goal with the use of a model based on a simple theoretical background (like BEM) is a challenge but, it will be shown that it is feasible with the implementation of suitable modifications.

69

Chapter 3. Methodology

In this chapter, the methodology used in this research work is outlined first and then a schematic diagram is presented which explains the intermediate steps of the study that led to the results.

3.1 Computational Methods

In this research work neither experiments were conducted, nor results from other experiments were used. So, in order to obtain an as much as possible clear picture, for the effect of tip sweeping on rotor blades, the use of different methods was essential. Computational methods were utilized first, in the form of Computational Fluid Dynamics (CFD) simulations. The CFX module of ANSYS software [20] provided the platform and the logic sequence (figure 3.1) in order to calculate the aerodynamic loads on fixed swept wings. However, the geometric design for the parametric study of various sweep configurations was performed at Solidworks software [106] because of its higher capabilities and the author's familiarization with the program. Simulations referred not only to steady cases but also to moving geometries, namely the variable swept tip. CFD simulations provided analytical solutions for the examined cases, consistent with the corresponding results derived later from numerical methods and intended to fill in the gap of the absence of experiments. Nevertheless, the high computational needs which characterize those CFD simulations, render the method practical only for simple cases concerning fixed wings with variable tip sweep geometry. In

specific, typical simulations for the moving geometry cases took approximately 3 days each, despite the fact that a powerful desktop was available (Intel i7 3,2 GHz / 16GB RAM / SSD Hard Drive). If investigation is to be extended to rotating blades and wind turbine applications the use of a cluster is mandatory. Thus, CFD simulations for wind turbine applications were not conducted.
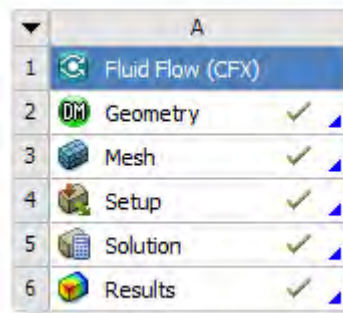
Figure 3.1 The simulation sequence in ANSYS CFX module for aerodynamic calculations

3.2 Numerical Methods – Numerical algorithms

Numerical methods refer to mathematical tools designed to provide solutions to a variety of problems and the subject of this research work is a typical example. The prescribed and free wake codes written in Matlab [107] for this thesis, are numerical algorithms based on steady and unsteady lifting line theory. They were used to calculate aerodynamic forces through an iterative process and a suitable convergence criterion. In particular, free wake models are also capable of calculating the wake formation behind rotating blades with the geometric feature of tip sweep and thus a more physically correct solution is obtained. The results of these algorithms were compared initially with the corresponding results of CFD simulations for the fixed wing and then these algorithms were modified in order to be used for wind turbines. The prescribed configuration of the codes needed few computational resources and it was proven that they perform as well as the free wake codes for the examined cases. On

71

the other side, free wake codes had much higher demands in computational resources comparable with those of CFD simulations for the moving tip of a tip swept wing. Yet, in line with the present trend for fast computations free wake codes were further modified to run on Graphic Processor Unit (GPU) utilizing CUDA platform [108] (Appendix A.3) and its integrated support in Matlab and the process was accelerated up to 60 times. The results of these numerical models are of high importance as they were used as baseline in order to understand the influence of tip sweep in wind turbine performance and aerodynamic blade loads. In addition, they were considered for the development of the correction (for sweep) that was later incorporated into the engineering model based on BEM theory.

3.3 Engineering models

Engineering models were also used in this thesis. They refer to applied theory models which are developed for specific engineering problems. In the beginning of this research work, the aeroelastic simulation tool FAST [69] was used, so that the author could obtain a general idea about wind turbine loads and performance in turbulent environments. The turbulent wind inflow was determined by TurbSim simulator [109]. However, one of the major goals of this thesis was to incorporate variable tip sweep capability into the most common (to the field of wind turbine applications) engineering model of BEM. BEM model is based on simple theory as was already outlined in paragraph 2.3 and after the implementation of suitable empirical and semi – empirical corrections has become a useful engineering tool with the desirable accuracy. Nevertheless, the time varying trailed vorticity encountered in tip swept rotor blades is computed with a tip loss model which leads to inaccurate results due to the assumption of radial independence in the BEM model [110]. Thus, it was modified accordingly utilizing the lifting line theory based codes for swept rotor

blades as a guideline. The BEM model of this thesis was based on the aerodynamic part of DUSWAMP [72] developed in the Simulink module of Matlab and the major corrections are found in the tip loss factor calculation module. The demands in computer power are low for BEM and simulations took only minutes to complete. As for the sweep controller, which is analyzed in Chapter 7 a low order engineering model was developed and optimized using Simulink.

3.4 Intermediate steps of the research work

The steps that led to the results of this thesis are presented in figure 3.2 :
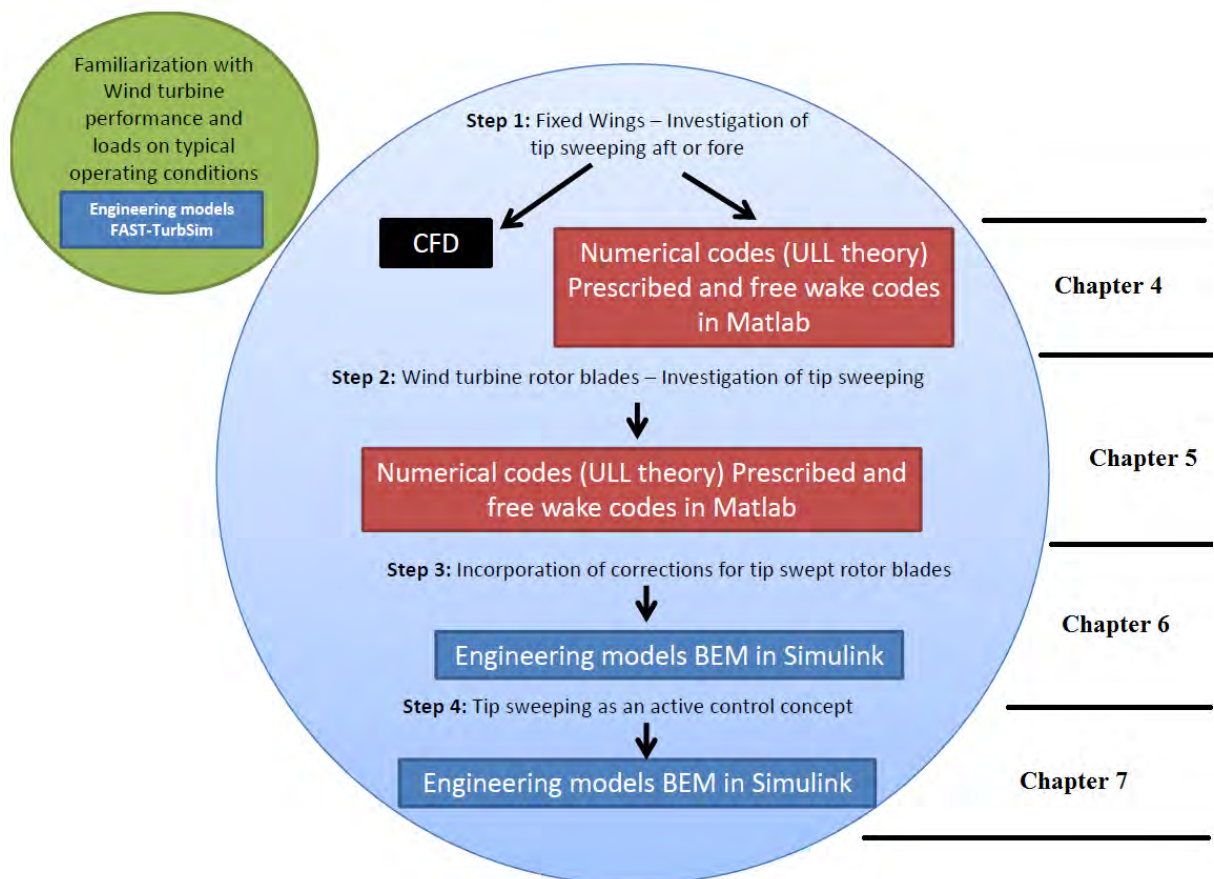
Figure 3.2 Schematic diagram of the thesis intermediate steps

Chapter 4. Investigation On The Fixed Wing Case With Tip Sweep Capability

In this chapter the unsteady aerodynamic effects of a variable swept wing tip, on a wing, are investigated through the utilization of a numerical model based on Lifting Line Theory and 2D steady state airfoil data. Firstly, the simplest case is modeled, with steady flow and wing characteristics, in order to examine the effect of tip sweep. In addition, the terms "tip sheared" and "tip swept" are clarified. Thereafter, an unsteady lifting line vortex model is developed and it is used for cases where the sweep angle of the tip changes sinusoidally. The results of the above method are compared to results from CFD simulations, referring to the same cases and contribute to the understanding of the unsteady flow features. The theory of the two used methods (Computational and Vortex) were previously analyzed in chapter 2.

4.1   Discretization of Sheared and Swept wings

Since, the main characteristic of the problem is the modification of the blade tip in terms of sweeping it back or forward, it has to be a clarification between two similar cases that exist. Generally, the term "swept wing" is used to describe the angled direction of wing root to wingtip beyond the spanwise axis as was already mentioned in paragraph 2.6.

However, sheared wing is the wing that is produced from the parallel movement of the airfoils, namely chordwise [111] and thus there is no change in their aerodynamic characteristics, no matter what is the angle. Of course, this isn't necessarily valid for the

aerodynamics of the whole wing. On the contrary, swept wings are pivoted around an axis which results in a change of the airfoil shape according to freestream direction that depends on the sweep angle "Λ" as it is seen in figure 4.1.
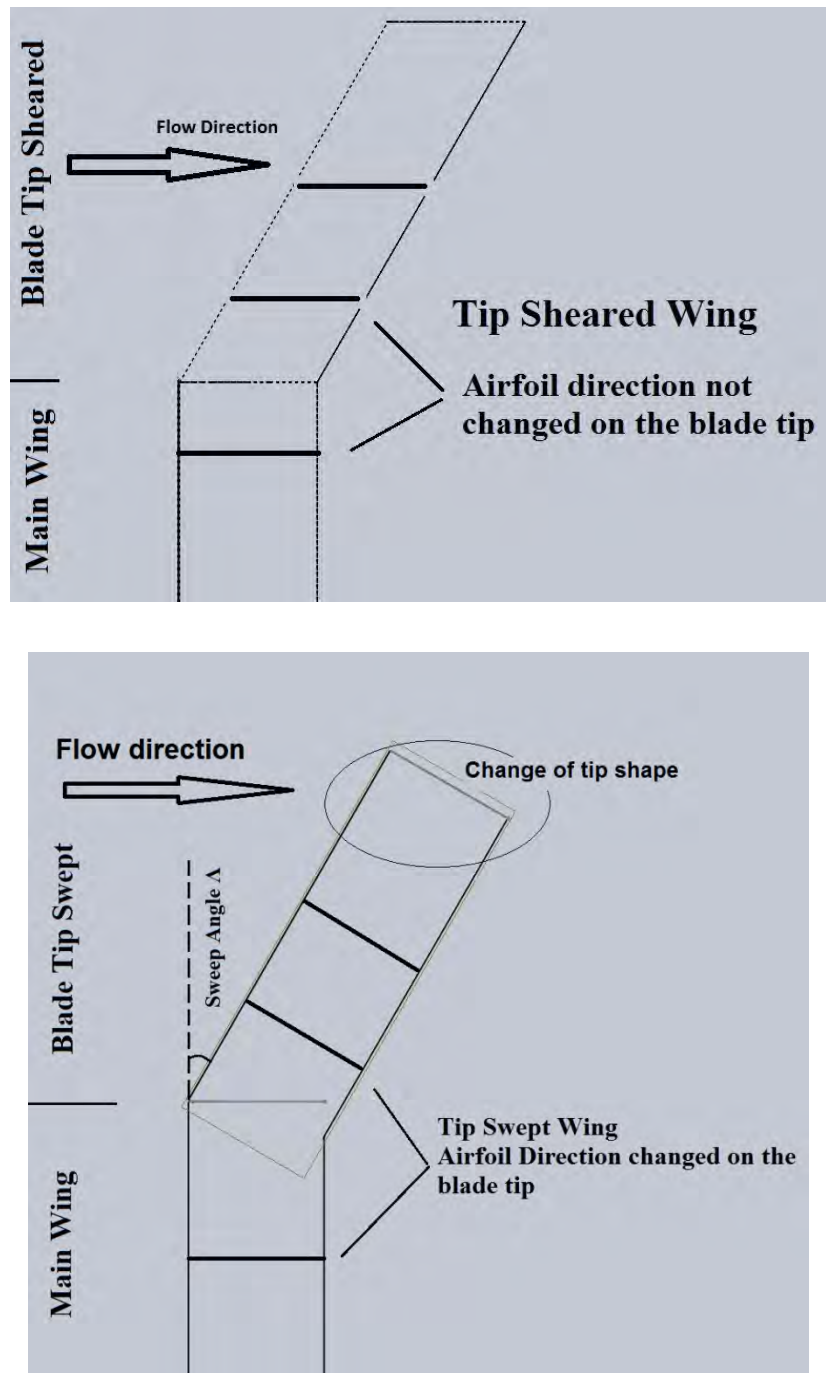
Figure 4.1 : Clarification between tip sheared and tip swept wing

Specifically for the swept wings, flow velocity Vo, can be analyzed into two velocity components (figure 4.2) - one normal to the wing's leading edge Vn which equals Vo*cos(Λ) and the other parallel to it. Assuming that only Vn corresponds to wing's lift, simple mathematic calculations lead to the following equation [102]:

$$(CL_{sw} = CL_o \cos^2(\Lambda))$$

(**4.1**)

where:

- CL_{sw} is the Lift coefficient of the swept wing
- CL_o is the Lift coefficient of the unswept wing
- Λ is the wing's sweep angle
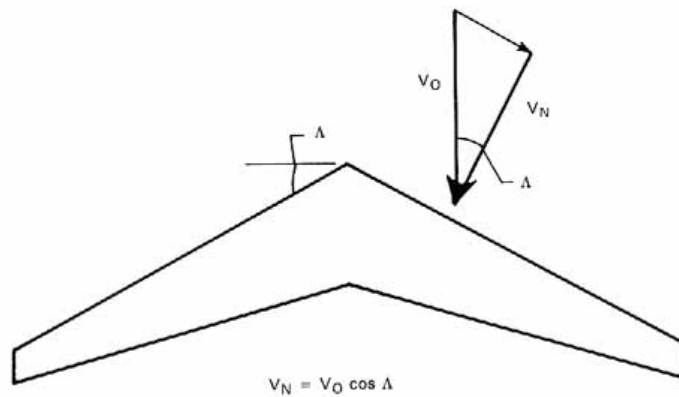
Figure 4.2 : Flow analysis over a swept wing. source: [112].

Certainly the spanwise velocity component is also of great importance, because it is the source of 3-D phenomena that alter the stagnation point, by moving it further beneath the leading edge, and causing the tip segments - in the sweptback case - to stall early [97].

4.2 Modeling the steady case of a tip swept wing

4.2.1 Steady 2-D Lifting Line Vortex Model (Matlab code)

The investigation of the effect of tip sweep angle on wing's lift, starts by developing a steady 2-D lifting line vortex model concerning a thin lifting surface for small angles of

76

incidences and a corresponding code was made using *Matlab* software. In this case, where the airfoil thickness is negligible and thus is not modeled, the sheared and swept cases coincide. Therefore, only the wing configuration - i.e. the percentage of tip sweep and magnitude of sweep angle - define the fluid dynamic loads which makes it a relative good, first approach of the problem.

The method used [25], divides the wing planform in smaller elements, as depicted in figure 4.3 , which consist of the bound vortex element BC located at the quarter chord, two trailing vortices AB and CD and the far wake starting vortex AD. Additionally there is the collocation point, which is the point where induced velocities of the wing are calculated and is placed at the 3/4 of the chord and in the middle distance of BC segment. This location is the result of the implementation of the 2-D Kutta Condition on the trailing edge of a lifting flat plate that is represented by only one vortex Γ (or else lumped vortex element) [25].
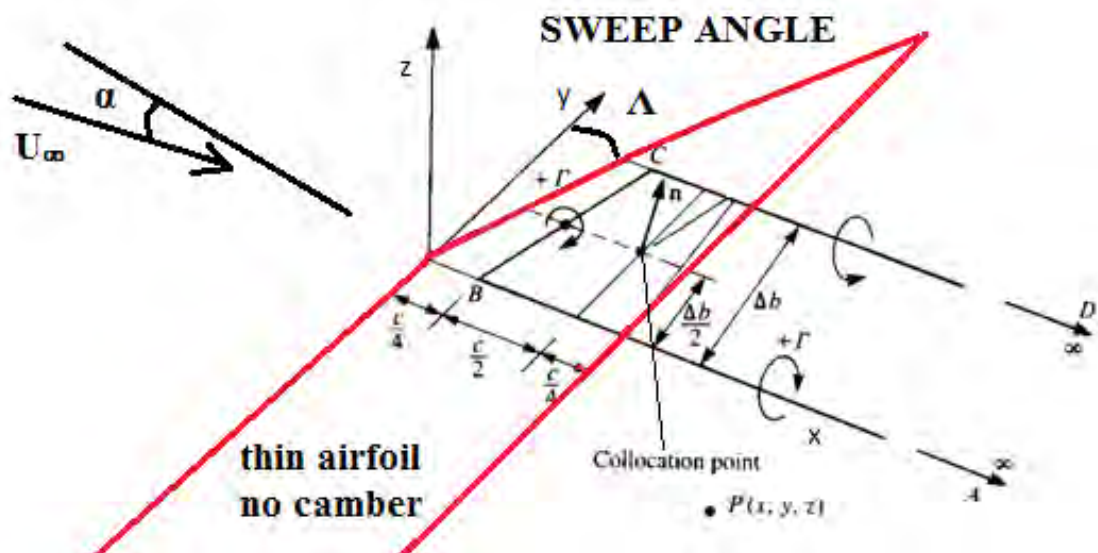
Figure 4.3 : A spanwise horseshoe vortex element of a swept wing. Source: [25].

Although, BC doesn't need to be parallel to y axis, at the tips of the element the shed vortex must be parallel to free stream, so that no force acts on the trailing vortices. Thus, the

77

vortex segment AD is placed in the far wake having negligible effect and parallel to local flow as shown in figure 4.3 .
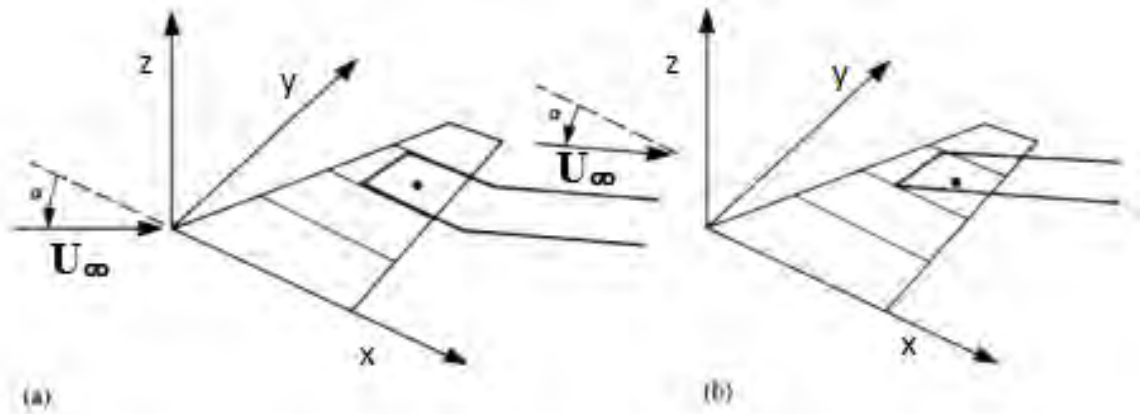
Figure 4.4 : Modeling the far wake. source[25].

Figure 4.4 a shows the bent that has to be made in order to meet the above requirement and 4.4 b a simpler way to model the wake. Since in the current model only small angles of attack are concerned, the second case was applied.

Therefore, the implementation of the aforementioned method to a thin wing planform including tip sweep leads to the following representation of the vortex model in figure 4.5 . Moreover in this figure, the way the induced velocity on every collocation point (defined as *) is calculated from the developed wake, is shown.

78
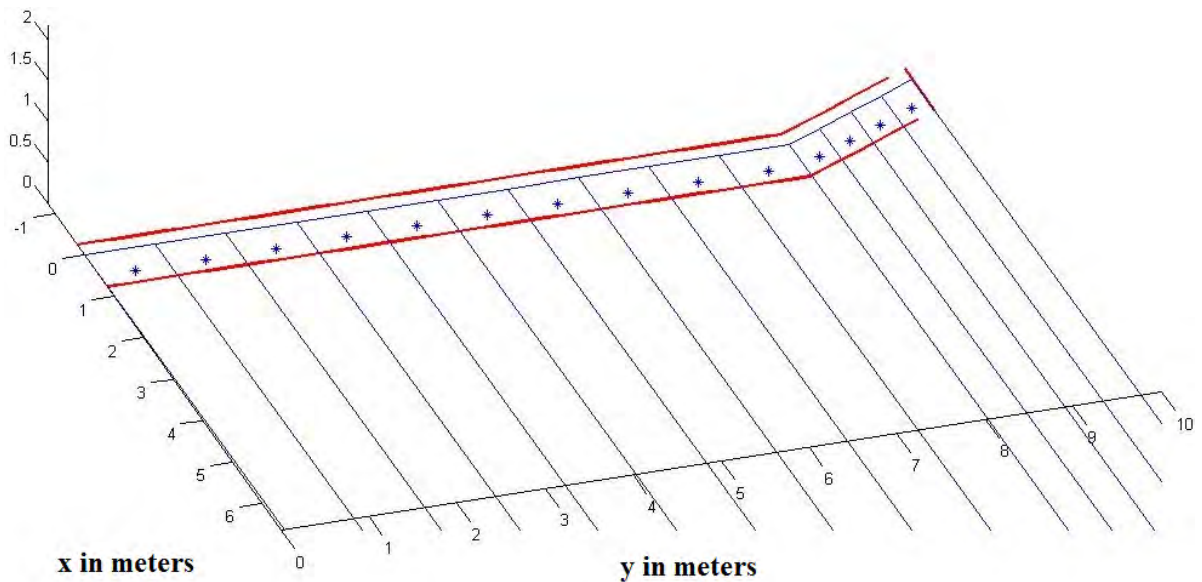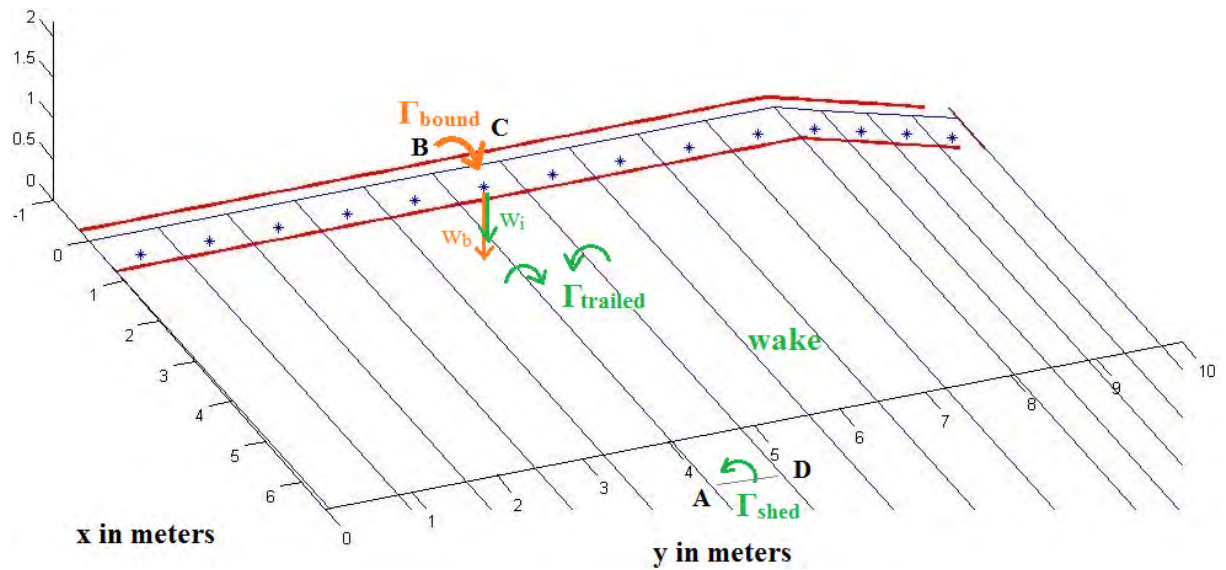
Figure 4.5 : Steady Lifting Line Vortex Model for a tip swept wing (Backswept and

Forwardswept)

After the separation of the wing into horseshoe elements the next step is to calculate
the bound vortex strength Γ dustribution. For this reason an initial assumption is made for the
vortex strength Γ of every horseshoe element which is set to 1. Then two influence
coefficients 'a' and 'b', are calculated for every collocation point. The first influence

79

coefficient 'a' is calculated by taking into account all vortex segments (of strength 1) and practically represents the induced velocity caused by the segments.

So, by applying the zero normal flow condition described in equation 4.2 on every collocation point, the vortex strength distribution Γ is computed. Accordingly lift force distribution is estimated by applying equation 2.9 and total wing lift results from the summation of individual lift of every horseshoe element.

$$w_b + w_i + U_\infty a = 0$$

$$(\mathbf{4.2})$$

where:

- w_b is the normal velocity component induced by bound vortices

- w_i is the normal velocity component induced by the wake (trailed vortices and shed vortices – shed vortices neglected when placed in the far wake)

- $U_\infty a$ is the normal velocity component induced by the free stream (α is the angle of attack and for small angles $\sin\alpha \sim \alpha$)

Accordingly, influence coefficients 'b' are calculated by taking into account only the trailing segments (AB & CD) of vortex strength 1 and when multiplied with Γ distribution give the wake induced velocity w_{ind} on collocation points. Subsequently, equation 4.3 is applied and the value of induced drag force is specified:

$$D_{ind} = \Sigma \ (\rho * w_{ind} * \Gamma_j * \Delta y_j)$$

$$(\mathbf{4.3})$$

where:

80

- ρ is the air density

- w_{ind} is the wake – induced downwash on the wing

- Γ_j is vortex strength of every segment

- Δy_j is the segment bound vortex bound vortex projection normal to the free stream

The induced velocities mentioned before, are calculated from the application of Biot Savart law on collocation points concerning only straight vortex filaments (figure 2.2), which is valid for all segments ABCD of the current model. The equation that describes the Biot Savart law was mentioned on chapter 2 as equation 2.10.

In order to avoid induced velocities of infinite value and simultaneously acquire a smooth decrease to zero, for those collocation points that are located close to vortex filaments, a cut-off radius is introduced to the filament and equation 2.10 is modified to equation 4.4 . It is suggested by Van Garrel though, that for bound vortex calculations the cut off radius value should be about 0.01% of the vortex filament size [26] & [113].

$$\overline{V_{ind}} = \frac{\Gamma}{4\pi} \frac{\left(r_1 + r_2\right)\left(\overline{r_1} \times \overline{r_2}\right)}{r_1 r_2 \left(r_1 r_2 + \overline{r_1} \cdot \overline{r_2}\right) + \left(\delta_r L\right)^2}$$

(**4.4**)

where: δr is percentage of vortex filament size *L*

Thus, induced velocity near vortex filament with increasing cut-off radius takes the following form in figure 4.6 .

81

Induced velocity against distance from vortex core with and without cut-off

No cut-off radius

1% Cut-off radius

2% Cut-off radius

Induced Velocity in m/s

Distance from vortex core in meters
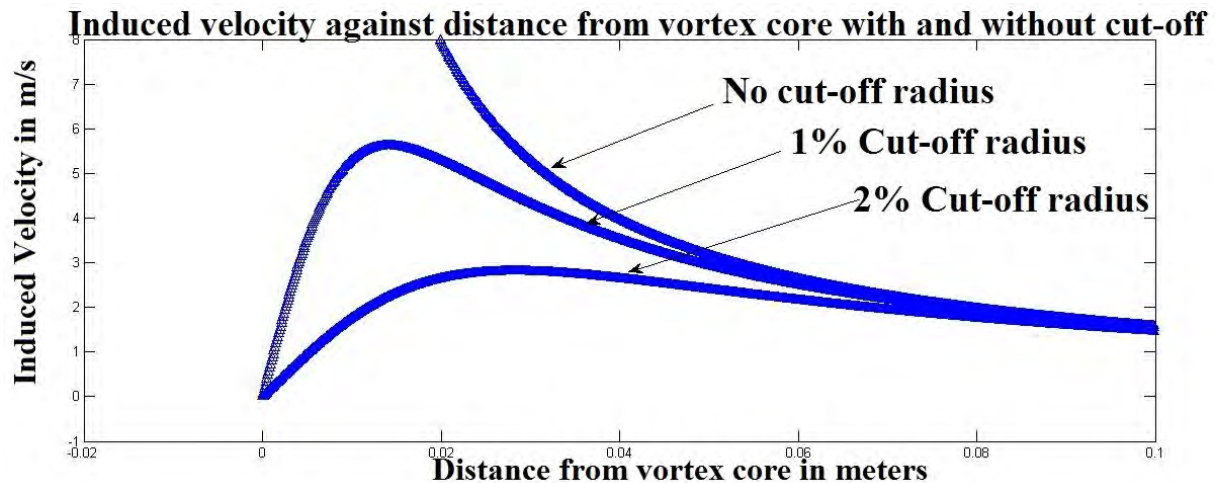
Figure 4.6 : Incorporation of Cut-off radius to a vortex filament

4.2.2 Results of the steady cases

The case examined with the aforementioned model concerns a 10m x 1m flat (no camber) wing, at 5 degrees angle of attack, 30m/s of freestream velocity. The variables are:

- Number of elements for swept and unswept part

- Percentage of tip sweep

- Sweep angle

Number of elements are examined first, in terms of code sensitivity to element distribution and it is essential in defining the more efficient one. Figure 4.7 shows that convergence is achieved in the increasing direction of elements on both parts. Of course, it is desirable that unswept and swept elements have the same length for uniformity reasons. Consequently, for a 30% tip swept wing with the above dimensions, a choice of 35 elements for the unswept part and 15 for the swept part is quite efficient in terms of uniform distribution and lift convergence. Accordingly, for 20% tip sweep percentage a good choice is 40 and 10.

82
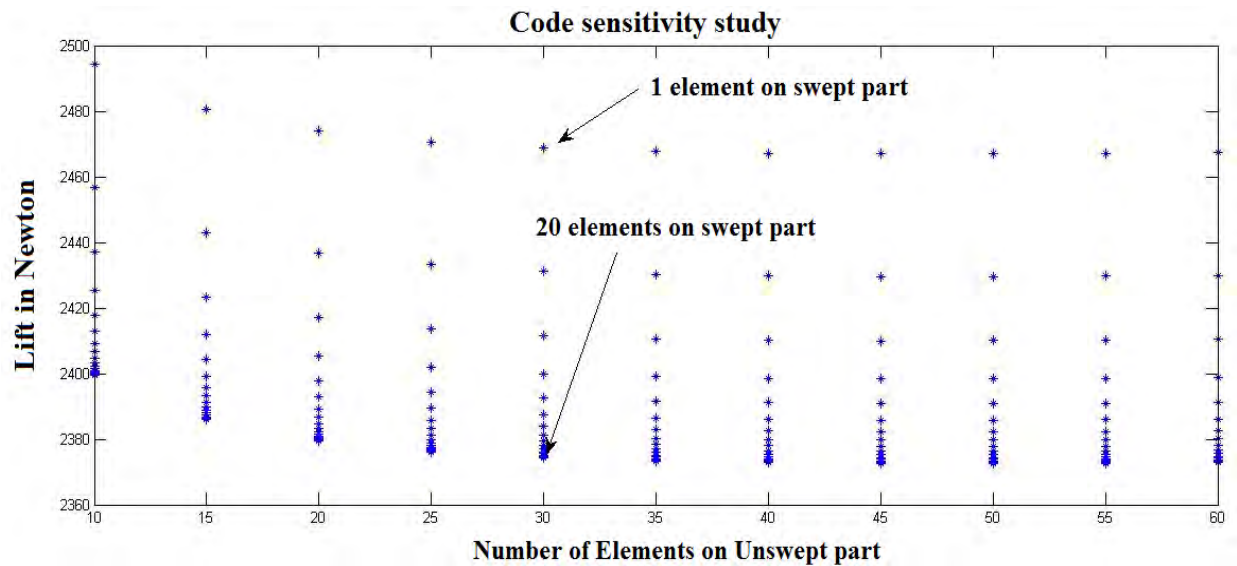
Figure 4.7 : Code sensitivity in element distribution for a 10m x 1m flat wing at 5 degrees
angle of attack and 30m/s flow velocity

Since the distribution of elements is determined, the influence of the other two variables can be examined. For practical reasons the values of tip sweep percentage and sweep angle where chosen to be feasible for applications concerning blades - wind turbines blades for instance.

So, the tip sweep percentage was ranged from 5% to 30% of wing span and sweep angle from 40deg forward-swept to 40 degrees backswept. The effect of those variables on lifting force is presented on the following figures 4.8 & 4.9 , in terms of percentage to the lifting force of the unswept wing.

Figure 4.8 shows that increasing tip sweep percentage causes lift force to decrease and even linearly, for all angles of sweep. In addition, the strength of the effect (in other words the slope) is higher for higher angles of sweep and the symmetry observed seems to be inherited from the symmetry of the geometry of the problem.

83
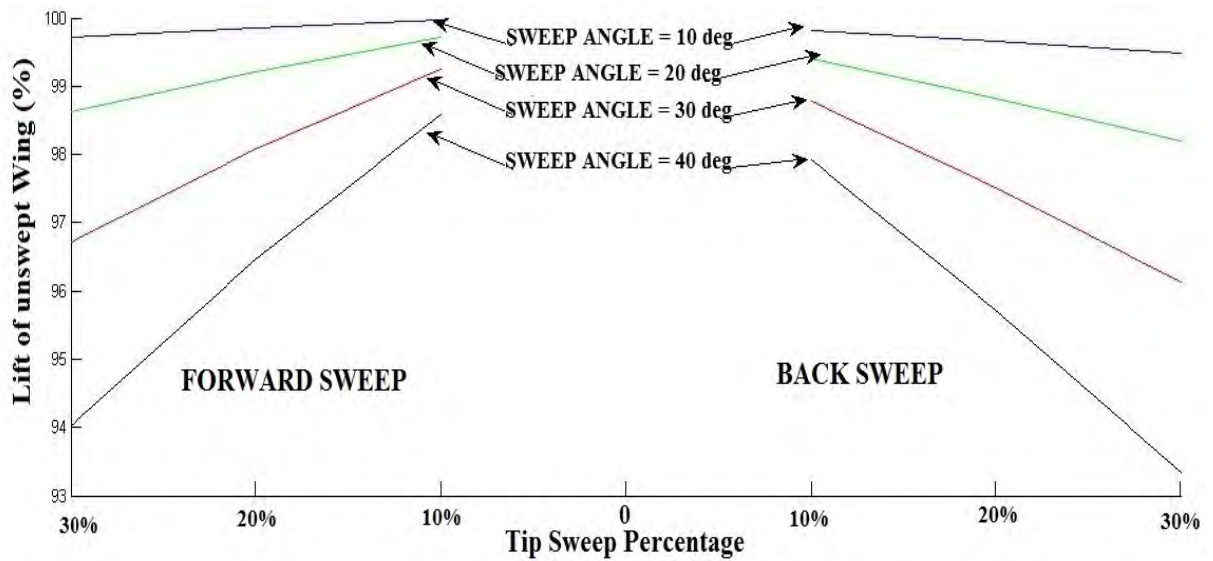
Figure 4.8 : Effect of tip sweep percentage on lift (expressed as percentage of unswept lift)

The effect of sweep angle is displayed in figure 4.9 and the results are similar with those of figure 4.8 . Lift is proportional to $\cos^2(\Lambda)$ and thus, it has the form of $y = \cos^2 x$ .Symmetry is obvious again and the effect is stronger for higher percentages of tip sweep.
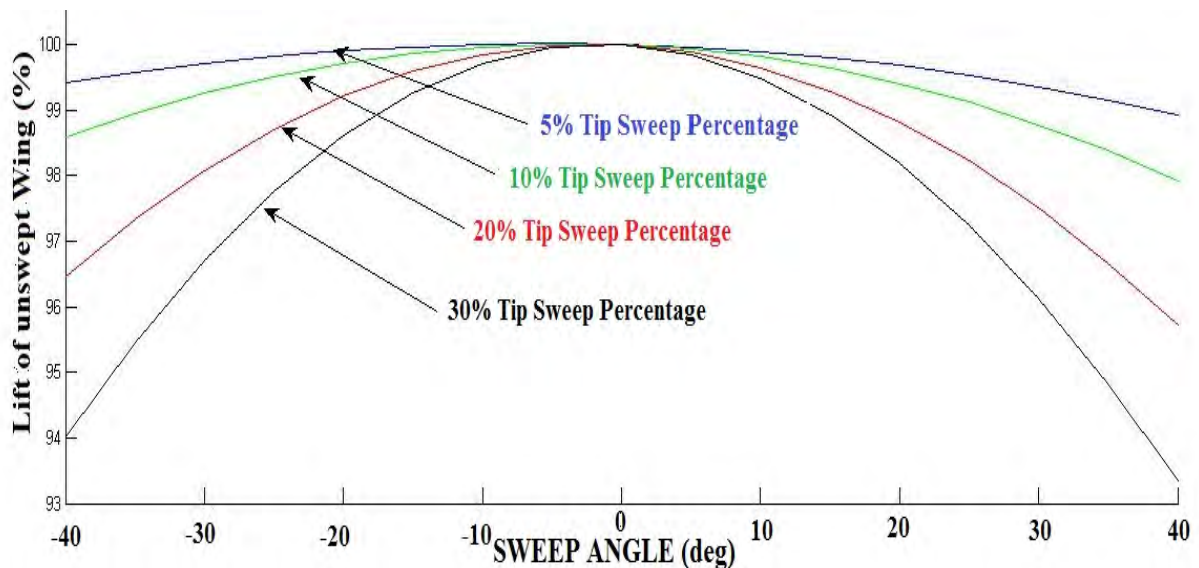
Figure 4.9 : Effect of sweep angle on lift (expressed as percentage of unswept lift)

Moreover, it has to be mentioned that the lift loss for the cases examined does not surpass 7% of the unswept lift which is a suitable value, for small corrections of wing forces.

84

However, lift distribution is of even more importance when practical applications are concerned such as helicopter blades or wind turbine blades. Subsequently, typical charts of Γ distributions for representative cases of tip sweep percentage and angle are presented in figure 4.10 . This distribution of course, is analogous to lift distribution from equation 2.9 and can be used as a qualitative approach.
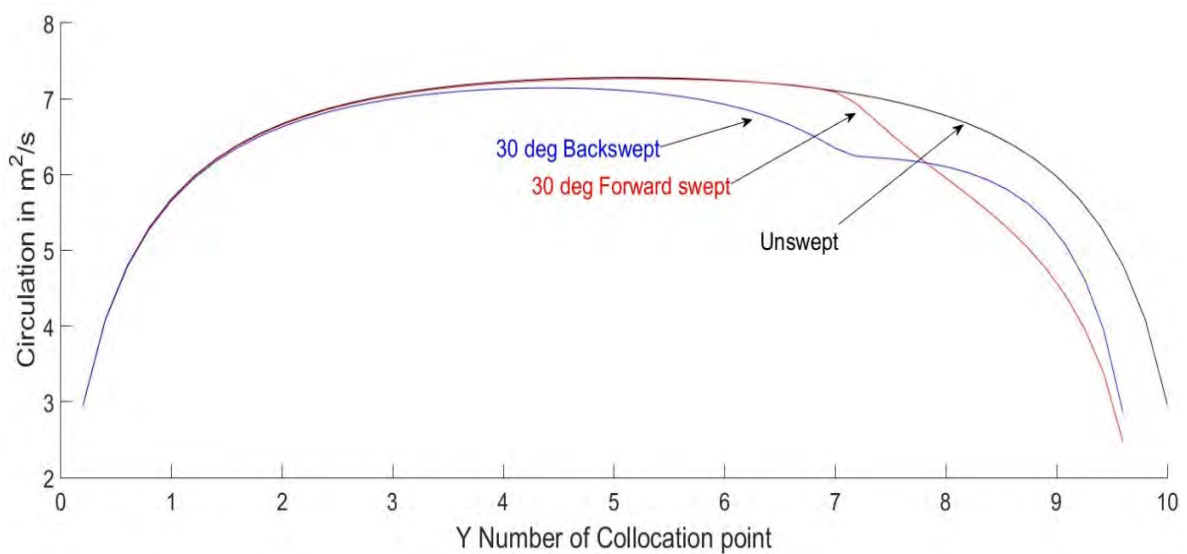
Figure 4.10 : Distribution of vortex strength Γ per unit length for a 30% - 30degrees tip swept wing

It is obvious that for both cases of sweep, the area under the curve is reduced but with a different way. The reduction of course occurs mostly at the swept part and it is smoother for the backswept case.

Finally, another useful result obtained from this model is the wake induced velocities on collocation points (at 3c/4) which are used to calculate the third component of drag force - the induced drag from equation 4.3 (friction drag and pressure drag are the other two components). Figure 4.11 displays the corresponding downwash created by the Γ distribution and clearly shows that near wingtips, where $|d\Gamma(y)/dy|$ is the largest, that two concentrated

85

trailing vortices can be formed and force the wake to roll up. Likewise, the sweep cases show a similar but opposite behavior at the beginning of the swept region, introducing a kink to the downwash.
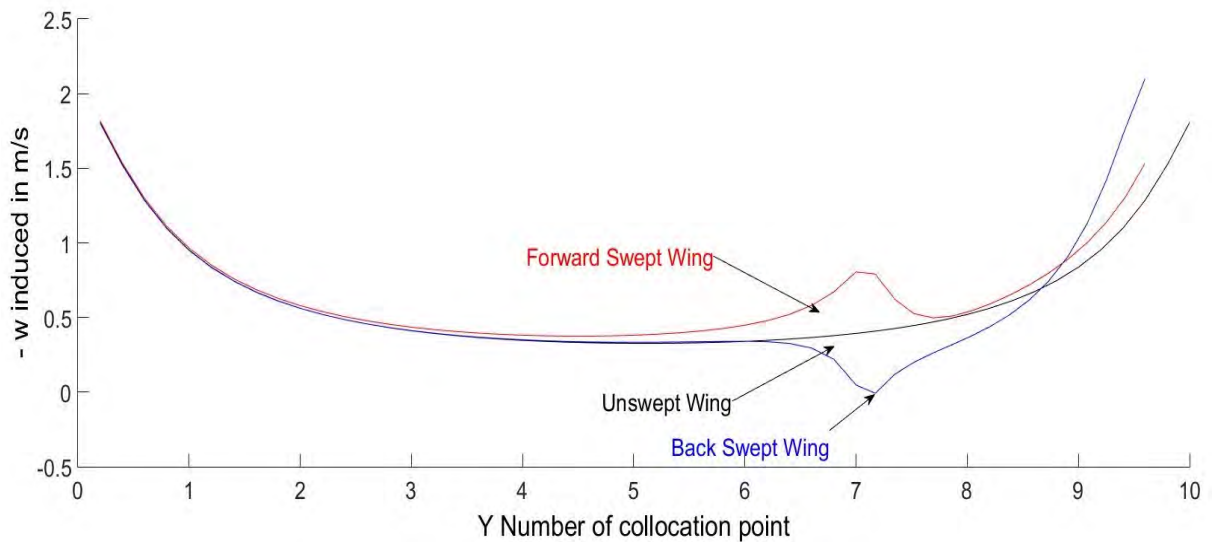
Figure 4.11 : Distribution of -wake induced velocity for a 30% - 30degrees tip swept wing
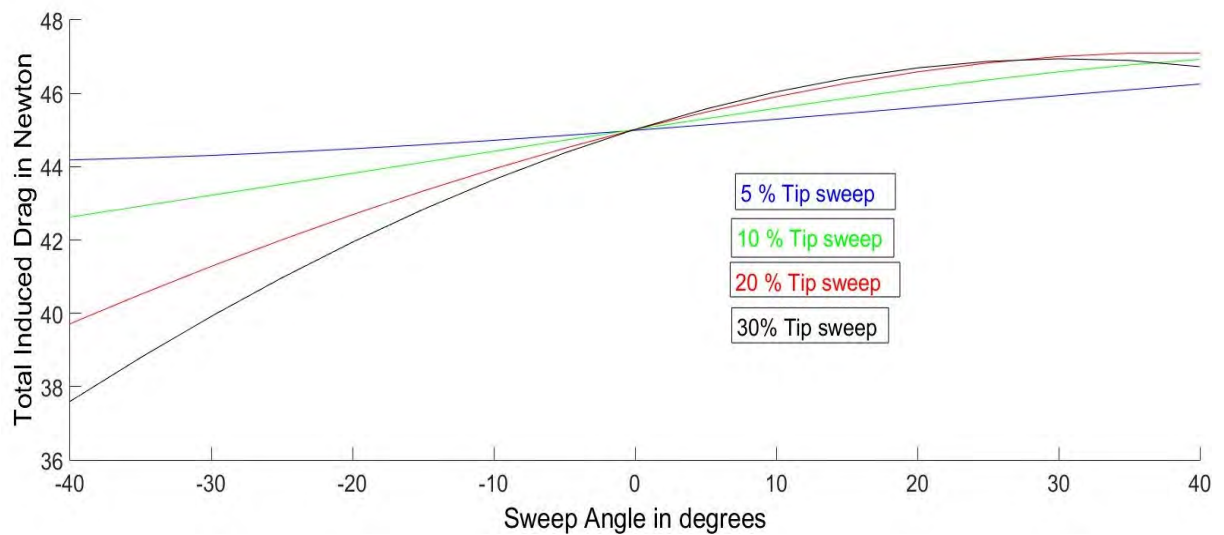
Figure 4.12 : Effect of sweep angle on Total induced drag force

Accordingly, figure 4.12 displays the effect of sweep angle on total induced drag for different percentages of sweep. As it is seen, induced drag force is higher for backswept and

86

lower for the forward-swept wings compared to the unswept case. This can be explained by the rise of induced velocities ($-w_{ind}$) that is observed for the ones in figure 4.11 .

4.3   Modeling the steady case on ANSYS CFX

Although the results of the numerical approach seemed to be reasonable, a comparison with a CFD approach is thought to be useful. For this reason, a different approach of the problem was attempted by setting up CFD simulations for the aforementioned cases of tip sweep , using the *ANSYS CFX* software. It is true that CFD computations provide a better picture of the problem as they include boundary layer and 3-D effects which play an important role on swept wings and were not included at all previously. So, an assessment of the influence of the effects can be used for further assessment of the steady Lifting line vortex model.

CFX is based on the finite volume technique, in which the area of interest is divided into small sub-regions, called control volumes and the Navier - Stokes equations are solved iteratively for each of them in order to evaluate variables such as velocity and pressure in specific points. Thus, a full picture of the flow behavior is acquired and fluid dynamic loads on the wing are determined [20]. The sequence followed for the solution was presented earlier on figure 3.1 . The first two modules - geometry and meshing - can be generated separately with use of different software and the other three software modules (Setup – Solution - Results) define the physics of the problem, solve the equations and provide post processing tools to analyze and visualize the simulation results.

The geometry of the problem was defined with the use of *Solidworks* software and the corresponding files were imported to ANSYS CFX. Wing span, chord and hinge point (c/4) were kept the same and a NACA 0012 airfoil was chosen as being more suitable to model the

87

thin airfoil of the lifting line model. Modification at regions of swept part rotation, such as small fairings, were necessary in order to eliminate gaps. The control volume was designed in such a way, that allows the development of a high quality mesh by the CFX mesh module, minimizes wall effects and lets a reasonable distance for the wake to form. Thus, the inlet surface was made circular, the walls were placed 10 chords away from the wing edges and 20 chords from the trailing edge as it is seen in figure 4.13 .
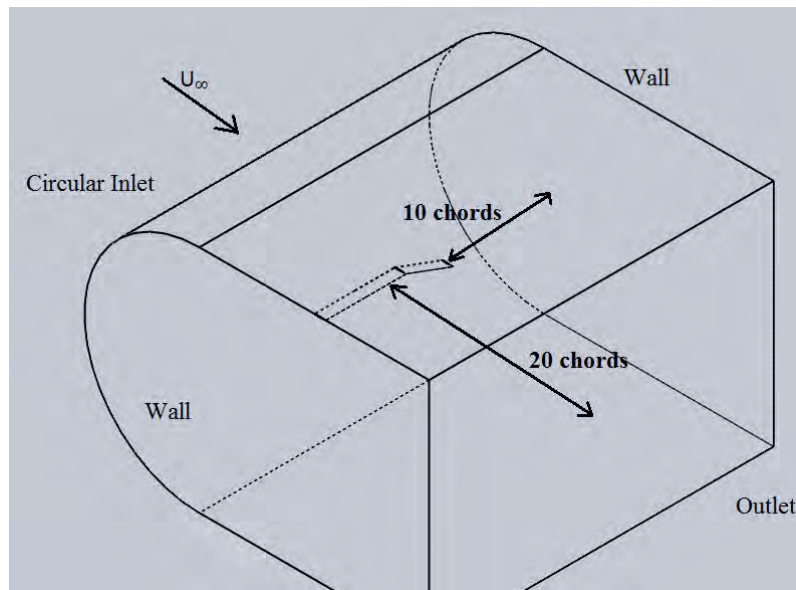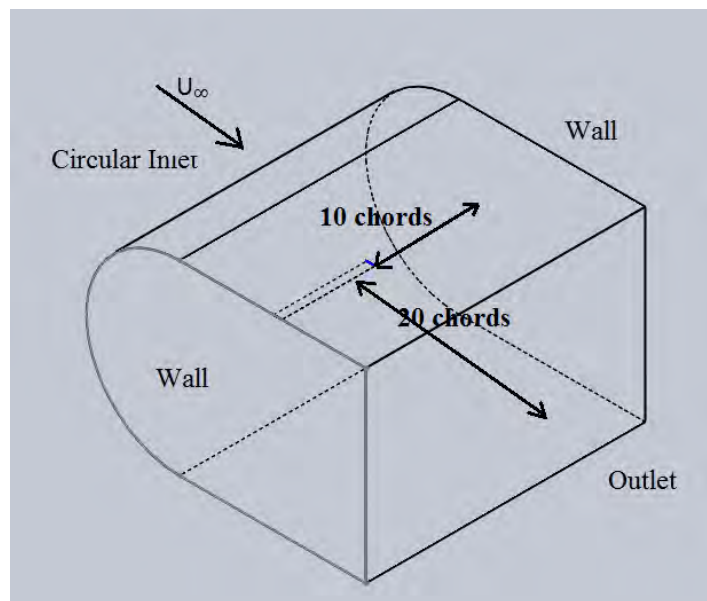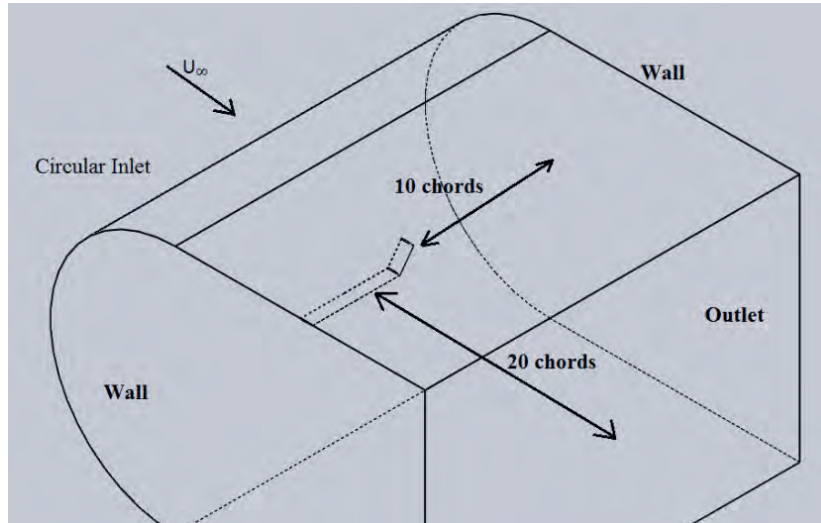
Figure 4.13 : Geometry of the wing (NACA 0012) created on Solidworks (Typical examples

Back sheared - Forward swept - Unswept wing)

Thereafter, an unstructured mesh with boundary layer inflation was created for the domain and the following settings were incorporated. A face sizing of 1.6m was chosen for the wall faces (excluding the side walls) and 1.8cm "mapped face meshing" for the wing. The mapped face sizing setting was determined in accordance with the wing's trailing edge face size, which is the smallest. In addition, inflation of elements for the control volume was

89

adopted, with the airfoil face being the boundary. The transition ratio was set to 0.2 and determines the growth rate of adjacent elements. Growth rate was set to 1.2 and determines the relative thickness of adjacent inflation layers and maximum layers was set to 10. The inflation algorithm was selected to Pre and thus the surface mesh was inflated first and then the rest of the volume [20]. Care was taken, in order to ensure that mesh shape is maintained through the wing's "rotation" region and up to the wingtip. A typical view of the resulting mesh is displayed in figure 4.14 .
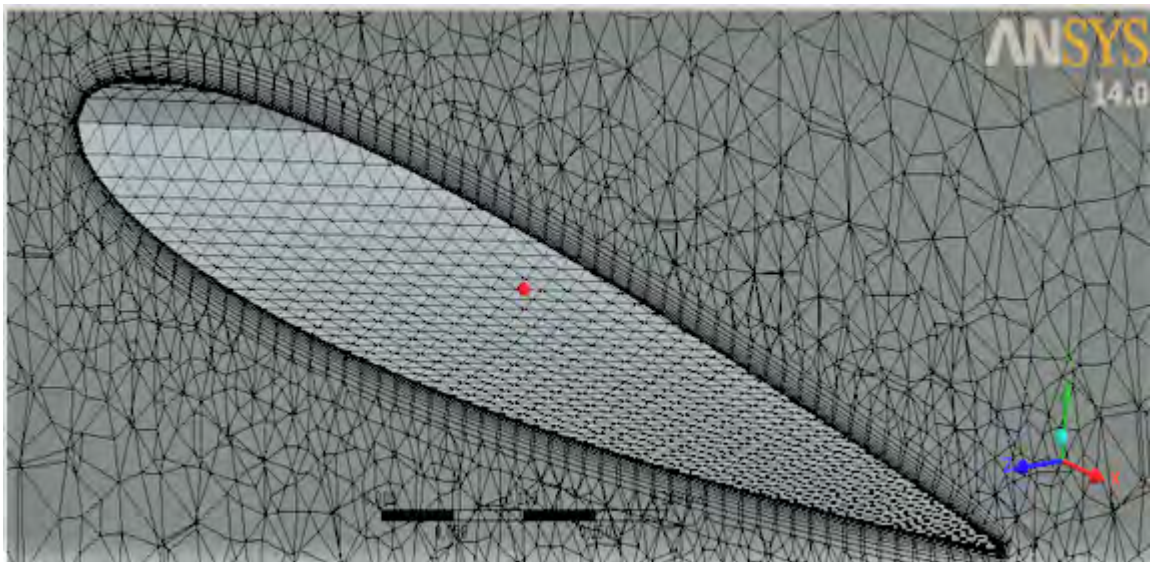
Figure 4.14 : Geometry of the wing (NACA 0012) created on Solidworks

As far as physics of the problem are concerned, a K-epsilon turbulence model was chosen at low turbulence intensity (~1%), for two freestream velocity magnitudes - 20m/s and 30m/s. In particular, two velocity vectors in X and Y direction were introduced so that by summation a vector of 5 degrees angle with the required magnitude (20 or 30) is created. Of course this angle coincides with the airfoil's AOA because its chord lies in the X axis.

90

4.3.1 Results of the steady cases - Sheared wings

In paragraph 4.1 two different cases of tip modifications were mentioned – tip sheared and tip swept. In the sheared case, tip movement happens parallel to freestream velocity (chordwise) and thus the airfoil aerodynamic characteristics are not altered.

Figure 4.15 shows the lift force produced from wings of the same configuration as in paragraph 4.2.2 (excluding the 5% tip sweep and -40 / 40 deg of sweep angle cases) at 30m/s freestream velocity. For each wing configuration a corresponding geometry file was developed in *Solidworks* software.
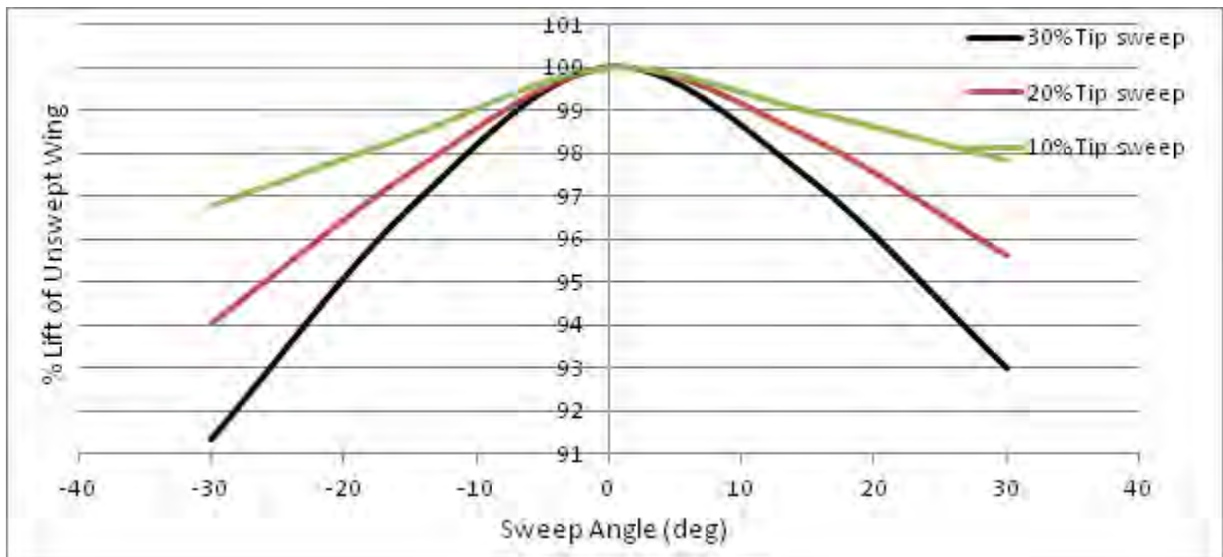
Figure 4.15 : Sheared Wing CFX - Effect of sweep angle on lift (expressed as percentage of unswept lift)

It is observed that both shear angle and tip shear percentage cause lifting force to drop with increasing effect when those values increase. For constant values of tip percentage and opposite values of angle, symmetry is observed. However, reduction doesn't surpass 9% of the unswept's wing lifting force and are higher for "forward" angles.

4.3.2 Results of the steady cases - Swept wings

The swept cases are of even greater interest because they incorporate a change in the geometry of the airfoil relative to flow direction, while the sweep angle changes. In addition, sweeping causes the tip to change in shape, as it was depicted earlier in this Chapter (figure 4.1) and potentially impose important changes on the wing's aerodynamic features. Therefore, CFD simulations will reveal the significance of those changes and thus the weaknesses of Lifting Line theory. Nevertheless, a different approach to the swept problem was chosen for reasons explained in paragraph 4.6.

Figure 4.16 refers to the produced lifting force for sweep angles of -17deg to 23deg, freestream velocity of 20m/s and tip sweep percentage of 10% to 30%.
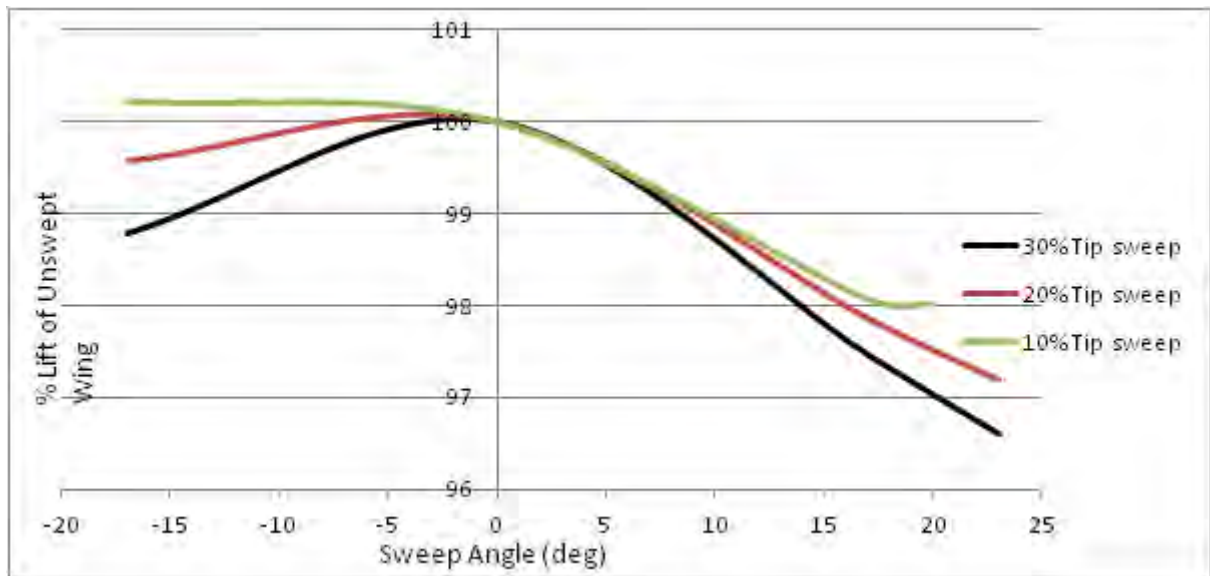
Figure 4.16 : Swept Wing CFX - Effect of sweep angle on lift (expressed as percentage of unswept lift)

The above results indicate a slightly different but still similar behavior compared to the corresponding ones of sheared wings. More specifically, lift drop is higher on back sweep angles compared to their opposites and for 10% of tip sweep percentage lift is even higher

92

than the unswept's wing lift. Of course, the effect of sweep is still stronger as tip percentage increases.

4.4 Discussion of results from CFD to results from Lifting Line theory Based Model

Having in mind that Steady Lifting Line model and CFD for sheared wings results refer to the same tip shape, tip configuration (angles - percentage) and freestream velocity render them comparable. Figure 4.17 displays the results in the same diagram for comparison:
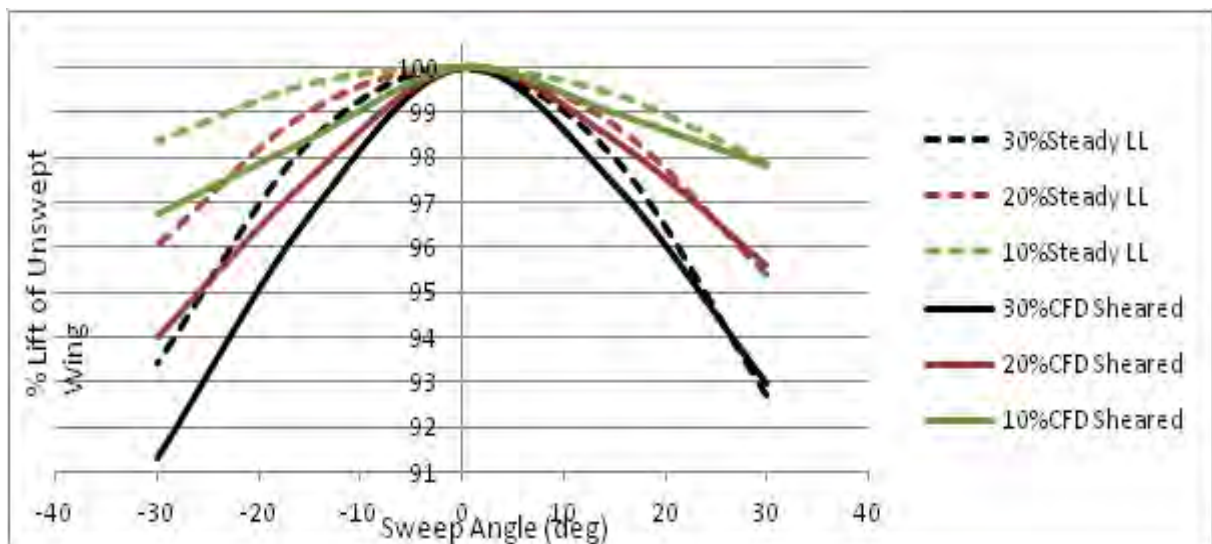
Figure 4.17 : Comparative diagram of Steady Lifting Line and CFD for Sheared wings results

First of all, it has to be mentioned that lifting force is shown in percentage of the absolute lift for both approaches. In CFD approach, lift of unswept wing was 8.5% lower of that calculated by Steady Lifting line model and so, in every case lift is divided by the corresponding value. The diagram indicates that results of back sheared angles are in very good agreement between both approaches although more steep on CFD. However, for opposite angles the behavior is slightly different with the Steady Lifting Line Model predicting higher lift than CFD. In addition, results from the model show that lifting force is

93

also higher for forward angles than for their opposites which happens to agree with CFD results on swept wings (figure 4.16), although they refer to different wind speeds and tip configurations.

4.5   Modeling the unsteady case

4.5.1   Unsteady Lifting Line Theory (Matlab code)

After having a sense of physics that are met on thin airfoil wings with tip sweep (or tip shear), the next step is to examine them on unsteady conditions. From the previous results it seems that the governing factor is geometry, whereas in the following approach an additional factor will play active role and this is the unsteady wake formation induced by variations of the wing's geometry.

The method used in the steady case and described in paragraph 4.2.1, was a direct method and the bound vortex was calculated by imposing the zero normal flow condition (equation 4.2) on the wing's collocation points (3c/4). However, for the unsteady case a different method will be used which matches the lift force calculated with Kutta - Joukowski theorem (equation 2.8) to the lift associated with the local flow direction through an iterative process as described in paragraph 2.2. With the unsteady approach the wing is separated as before (paragraph 4.2.1) but a new point is introduced, called control point. The control point is placed in the middle of BC section at c/4 (or else c/2 ahead of collocation point – figure 4.2) and stands for the point where the induction and the angle of attack is calculated [26] & [113].

94

4.5.2 Discretization of the wake

It was earlier mentioned in paragraph 2.2, that the wake can be either prescribed or free to develop according to bound vortex distribution of every time step. In the first case which is the simplest, the wake geometry is divided in fixed nodes and quick calculations can be derived. Every time step, the first nodes are released at 25% of the distance traveled with the free-stream velocity [26] & [113] and consequently have the wing's geometry of the previous step and the rest travel with the current free stream velocity.

On the other hand, free wake approach is more accurate and reflects the shed vorticity transportation which in turn affects the unsteady aerodynamic response of the wing. First wake nodes are released with the same way but the rest of the nodes travel with the vectorial sum of free stream velocity and calculated induced velocities on them from the wake vortex lattice. This leads to a more physically correct result that is displayed below in comparison to the prescribed wake. With this method roll up of the trailing vortices is successfully represented.
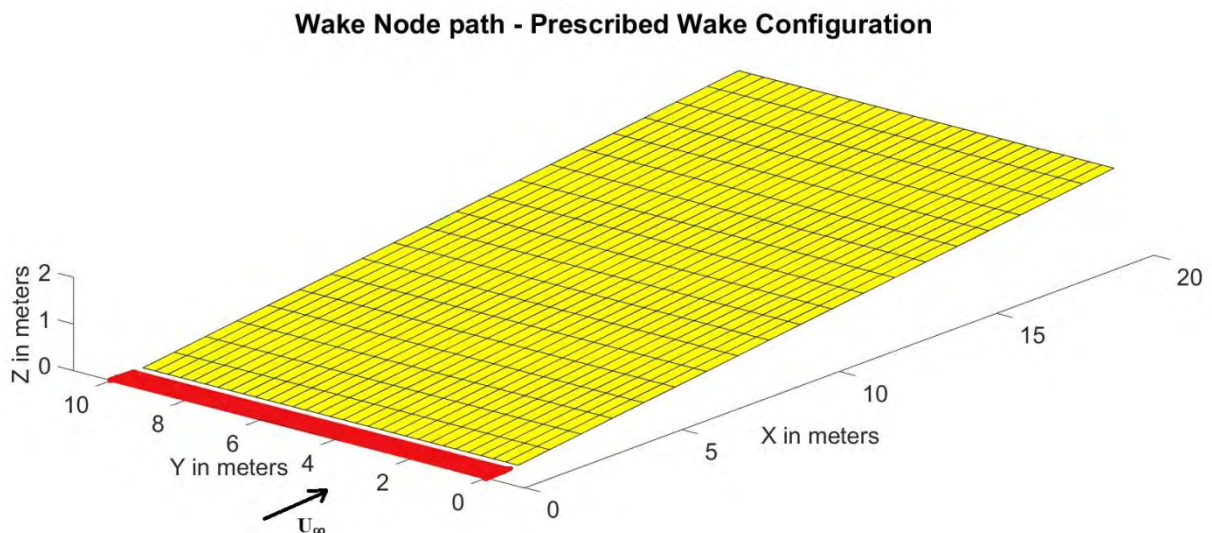
Figure 4.18: Prescribed wake geometry
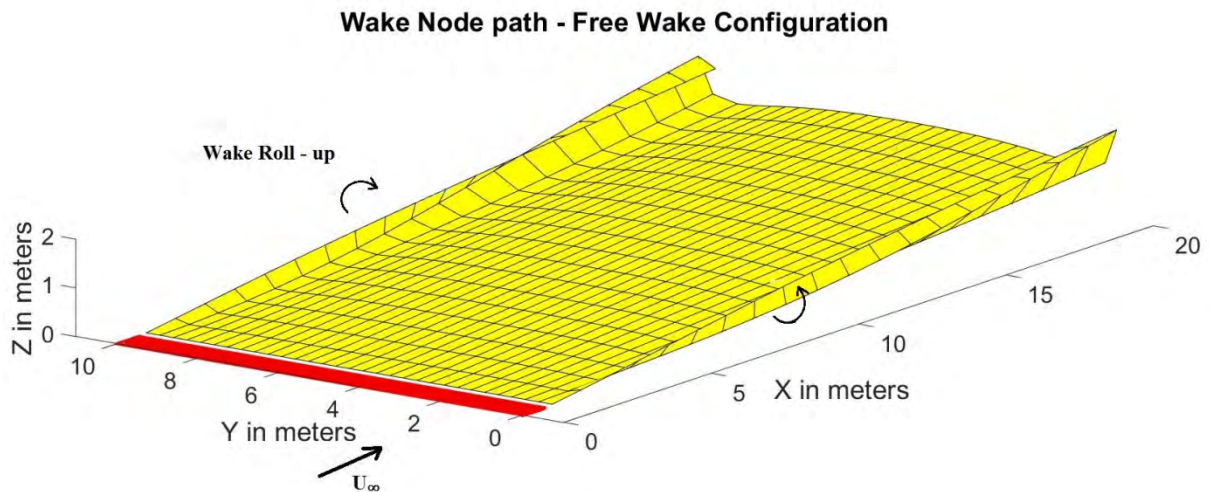
Figure 4.19: Free wake development

The main boundary condition for the solution of the entire system of the wing and the wake is Kelvin Helmoltz theorem which states that total circulation within the domain, defined by the wing and its wake, remains constant in time [113].

$$\frac{D\Gamma}{Dt} = 0$$

(**4.5**)

The strength of the trailing and shed vortex filaments that are released during each time step depend on the span-wise distribution of the bound vorticity (Γ_B) at the current and previous time-step. Bearing in mind that the total circulation in the domain should remain constant, equations 2.12 and 2.13 are derived for the shed and trailing vortex strengths [113].

4.5.3 Modeling specific aspects of the swept case

There are four points in the swept case that need special consideration:

- Wing tip should change shape more realistically in contrast to the simplified consideration of steady Lifting Line model of paragraph 4.2.1 (figure 4.5). Therefore,

96

a transformation matrix which rotates all points of swept part around the selected hinge point (c/4) was utilized rather than a lone rearrangement of swept elements, ignoring the wing tip shape.

- Lift calculated for the swept elements only, should be in accordance to the physics of swept wings, so equation 4.1 was taken into account and equation 2.14 was modified to read:

$$\rho_\infty V_{Blade} \Gamma = \frac{1}{2} \rho_\infty V_{Blade}{}^2 C_L \cos^2 \Lambda c$$

(**4.6**)

- During the rotation of the swept part about the hinge point (c/4) horseshoe elements are rearranged in such a way that the last wake node doesn't leave from the correct point. Therefore, corrections were applied as it is seen on the following figures. More specifically, in the first case the last element is stretched so that the outboard node leaves from the tip where in the other case the node is forced to leave from the intersection of the last element (CD section) and wing tip segment.

97
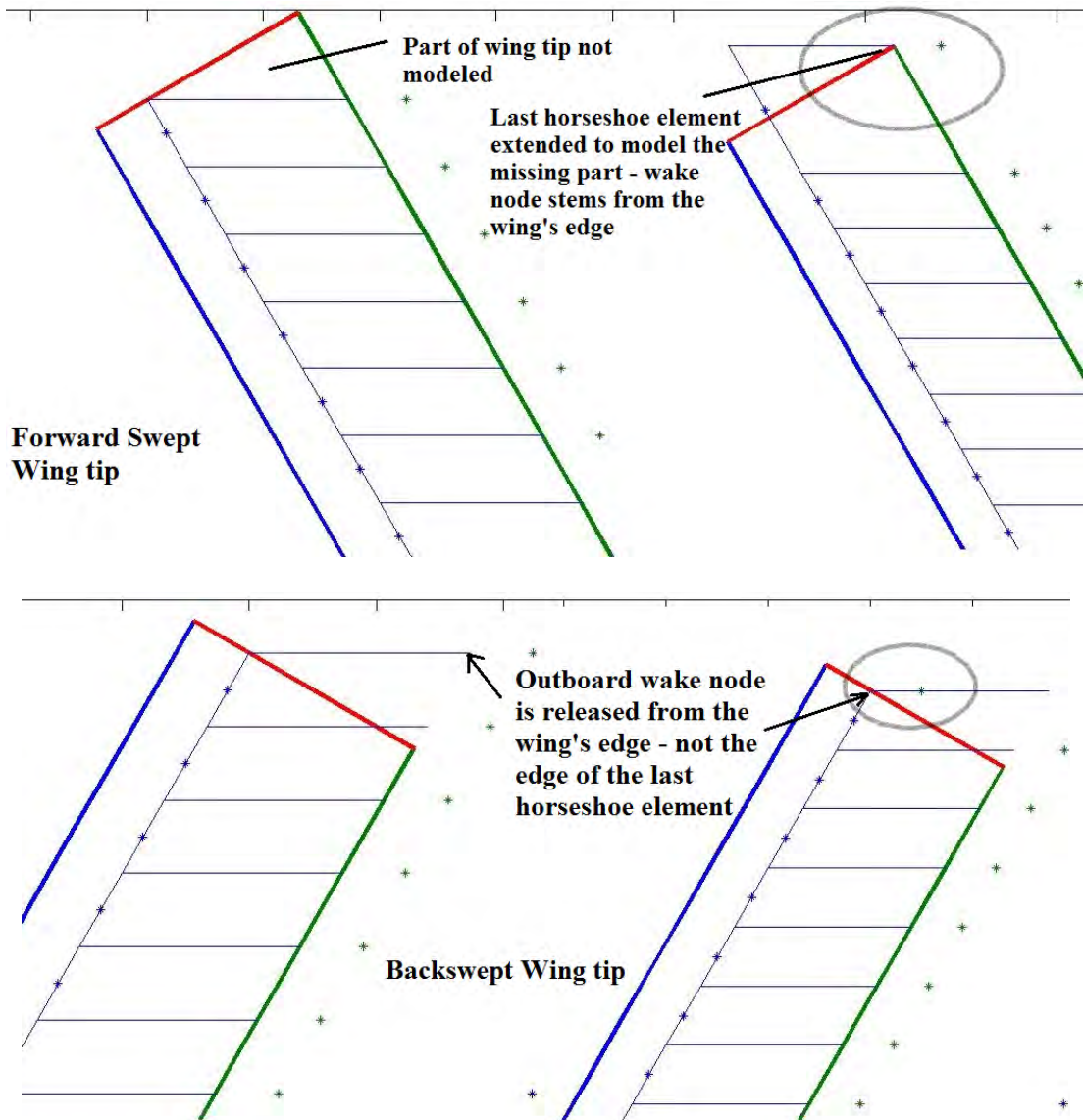
Figure 4.20 : Corrected release of last wake node for Forwardsweep (left) and Backsweep cases (right)

- However, the above modifications lead always to overestimation of last element's lift because every time larger surface than that of the tip's surface is covered. Therefore, the correction applied into the Matlab code takes into account only part of the last element's lift by calculating an approximate "effective chord" for that element. Of course, lift produced from a forward half of an airfoil (backswept cases) is intuitively more than the aft's half (forward - swept cases), but this is not modeled separately.

98

4.5.4 Configuration of Unsteady Lifting Line Code & Sensitivity investigation

The development of a ULL model after the utilization of the aforementioned theory and implementation of useful modifications, requires sensitivity investigation to the incorporated parameters. Suitable values should provide fast and stable calculations that expose in the best way possible, the physics of the problem.

- The discretization of the wing was more scattered compared to the steady model for reasons of time efficiency. The dividing distance value was chosen at 0.33m against 0.2m of the steady case and the behavior was not considerably altered. This distance is translated into a total of 30 elements against 50 of the steady case.

- The cut-off radius δ of equation 4.4 , for the bound vortex filaments was 0.01% of their length as mentioned in paragraph 4.2.1 and 10% for the rest filaments, without considerable differences for lower values of the latter, up to 1%.

- The damping / underelaxation factor D of equation 2.15 was set to 0.3 for all elements, because higher values render the solution divergent where lower values in the order 0.05 lag notably the convergence.

- The convergence criterion (equation 2.16) for the solution was set to 1% and tested for 0.5% without considerable differences.

- The time step was set to 0.05sec where higher value of 0.1sec gave similar results and lower values close to 0.01sec showed "unstable" behavior.

- Tip corrections introduced before on paragraph 4.5.3 seem to improve the results without changing the code's behavior.

- In terms of time efficiency, a cutoff distance was introduced in order to consider only the wake nodes that induce measurable velocities to the control points. Thus, a

suitable distance for the cases studied and described in the next paragraph was 50 chords away from the wing's trailing edge.

- The code ran for the two types of wake discretization free wake and prescribed wake. Additionally, the free wake case was parted into two sub-cases where in the first, initial nodes emanated from the wing's trailing edge with 25% of freestream velocity (paragraph 4.5.2) and in the other with the calculated induced velocity from all vortex filaments. Simulations showed that free wake - first sub case - and prescribed wake results have very good correlation, which is of great importance because prescribed wake code runs much faster than the free wake code. However, the second sub - case of the free wake code produced unstable results but still, maintained an equivalent response.

4.5.5 Results of ULL Model on steady conditions – Comparison with CFD

Although the model was developed for unsteady conditions, it was useful to set a few simulations on steady conditions in order to validate the results with the corresponding ones on CFD (figure 4.16). However, the wing tip was not initially swept but was chosen to reach the required sweep angle, gradually. This was also the scenario of the CFD steady cases due to reasons explained later at paragraph 4.6 The results in figure 4.21 refer to freestream velocity of 20m/s (zero turbulence) and equal values of sweep angles.
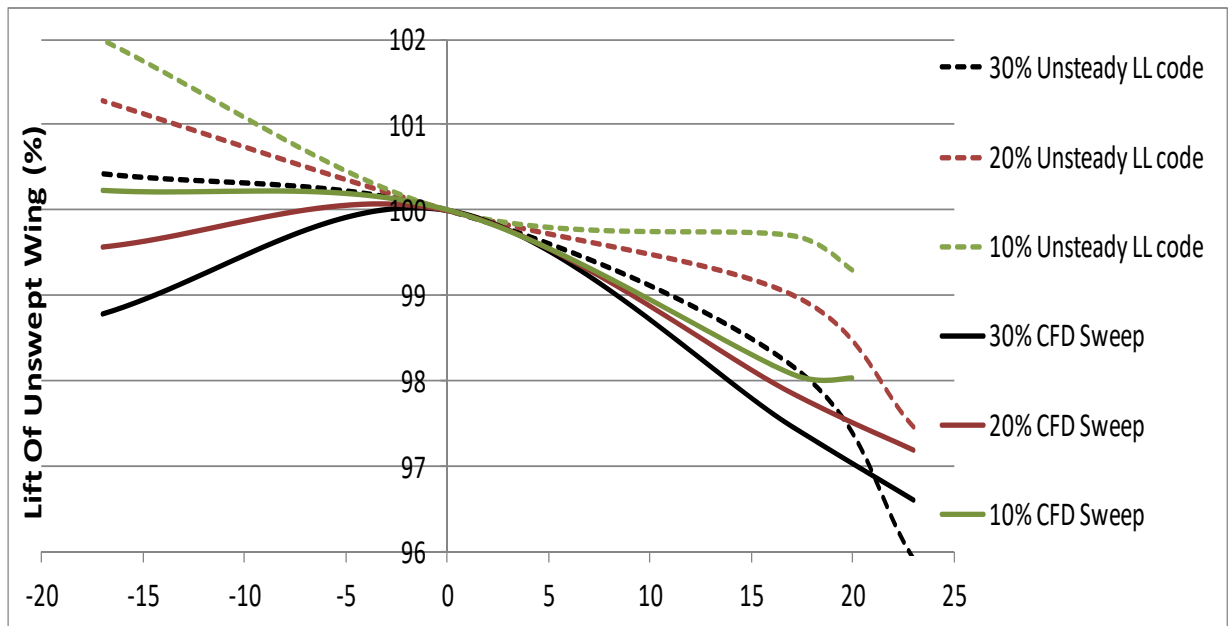
Figure 4.21 : Comparative diagram of Unsteady Lifting Line and CFD for Swept wings results

Figure 4.21 shows that there is a qualitative agreement between ULL model and CFD model. The fact that lift drops more on backsweep cases is possibly because the hinge is placed at c/4 causing greater surface overlap during movement of tip. In addition, tip sweep percentage seems to have stronger effect on ULL model for backsweep angles and in contrast to CFD after the value of 17deg, lifting force drops with higher rate. Nevertheless, taking into account the differences that exist between the two approaches on geometry (thickness not modeled on ULL), discretization (horseshoe elements VS mesh), physics (lifting line theory VS Navier - Stokes equations) and the fact that results are in the same order of magnitude, it can be stated that ULL is in good agreement with CFD for steady cases.

4.5.6 Results of ULL Model on unsteady conditions - Sinusoidal tip movement

In order to obtain a qualitative sense of the physics that govern the unsteady case, a sinusoidal movement of the wing tip was chosen for reference. The wing planform had the same geometric characteristics of the steady cases, the freestream velocity was set to 20m/s,

101

the angular frequency was set to π rad (or 2 seconds for a complete cycle), sweep angle amplitude to 17deg and sweep percentage to 30% of the overall wing span. It has to be mentioned though, that freestream velocity and angular frequency values were chosen so that unsteady effects can be highlighted - in other words velocity of tip movement has to be in the order of freestream velocity.

The following figure depicts lift variation as a response to tip movement. The wing is initially unswept for adequate time (0.7sec) so as to develop lift and its wake becomes stabilized. Then, tip is suddenly excited to a sinusoidal movement with the specified characteristics (frequency and amplitude). Sweep angle curve and lift curve are shown together, for clarity reasons. Moreover, the doted curves stand for the produced lift by the wing in steady conditions and configuration i.e. 0 degrees / Amplitude / - Amplitude.
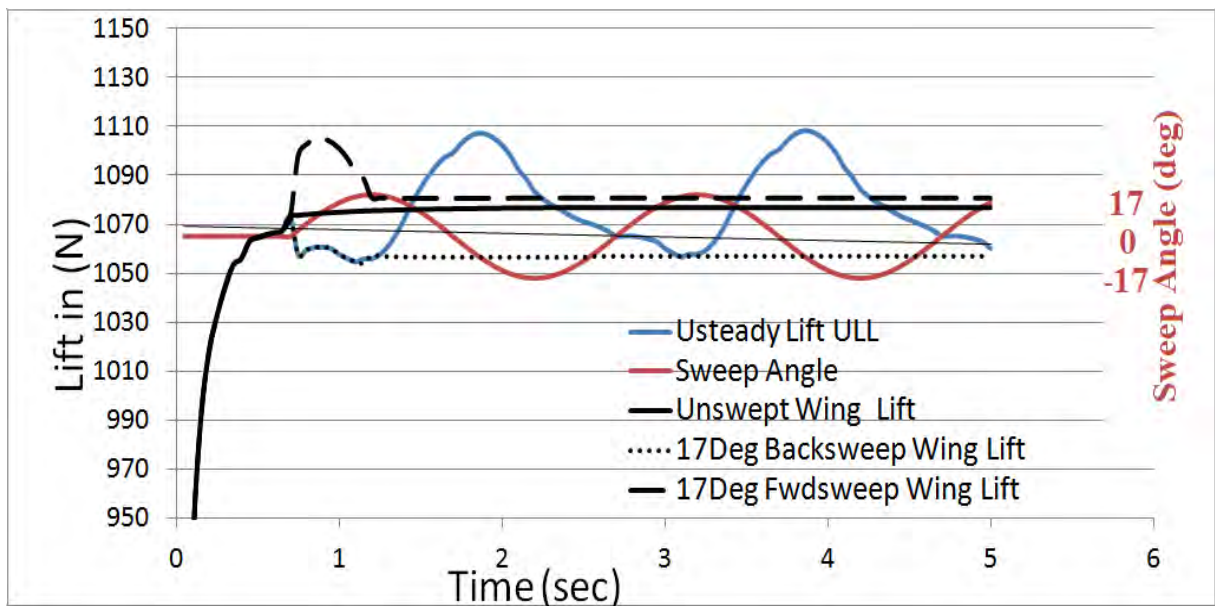
Figure 4.22: Unsteady lift predicted from ULL (30% tip sweep, 17deg Amp & π radial Frq)

It is obvious that there is a phase lag between sweep angle and lift response. It seems that maximum lift is achieved when tip moves toward forward angles and falls to minimum when it stops for an instant at maximum backsweep angle. Both statements are rational and

102

indicate that lift is strongly dependent to velocity of the wingtip and secondarily to wing's geometry. In addition, a lift overshoot is observed when tip passes from neutral position (0 degrees) moving towards forward angles which is in the order of 2.82% compared to the unswept wing's produced lift. On the other hand, minimum lift is observed short after the tip passes from neutral position but with the opposite direction. Its value though, is equal to the value of the 17deg backsweep steady case.

Of course, it is useful to calculate whether lift leads or lags tip sweep angle variation and how much. For this, embedded *Matlab* functions were utilized to calculate cross power spectral density, coherence function and phase lag from the two "signals" - sweep angle and Lift response. It has to be noted though, that the number of values for both signals deriving from ULL, where multiplied manually in order to amplify their coherence. The function CPSD (Cross Power Spectral Density) that was used in Matlab calculates the value of angular frequency ω that the two signals have the best coherence. The following figures show the results:

Figures 4.23 and 4.24 show that sweep angle and lift signal have the best coherence at angular frequency of 0.1565(rad/sec). This implies that they are best correlated for sampling Period of Ts = 2*π/0,1565 =40.148 samples (~40) or 40 * timestep(0.05s) = 2seconds. This of course is the period of the sinusoidal tip movement. However, phase lag is acquired from Figure 4.25 which shows that Lift - Sweep Angle equals -2.208 rad i.e. Lift lags **126.5 degrees**
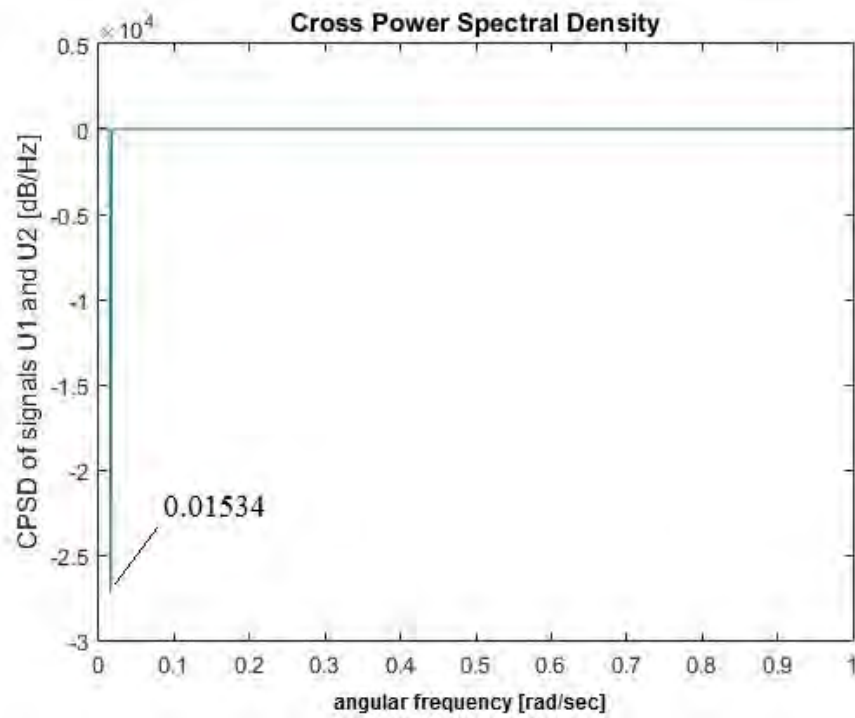
103
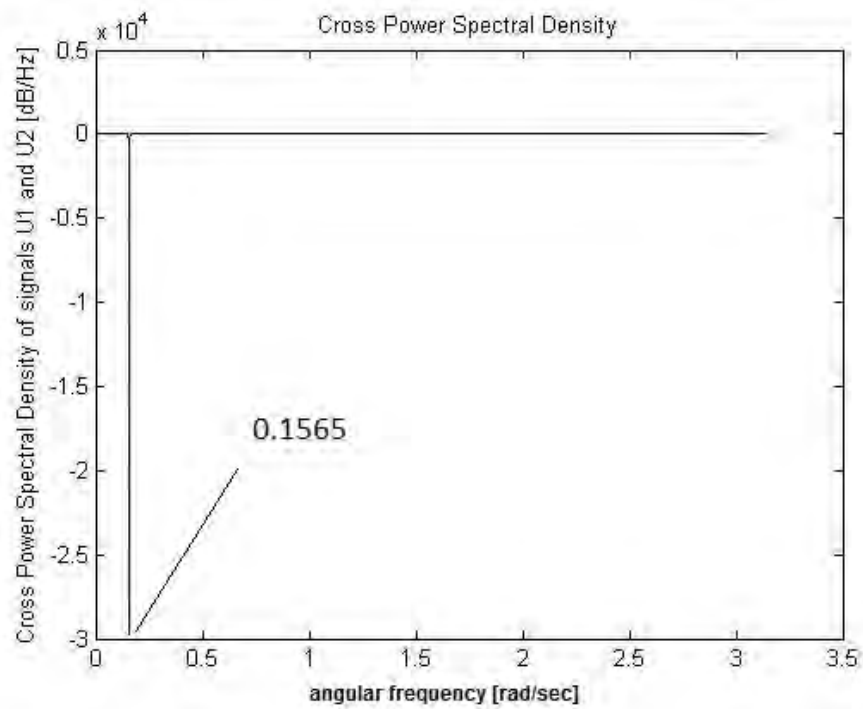
Figure 4.23: Cross Power Spectral Density VS Angular Frequency (max at 0.1565 rad/sec) - ULL
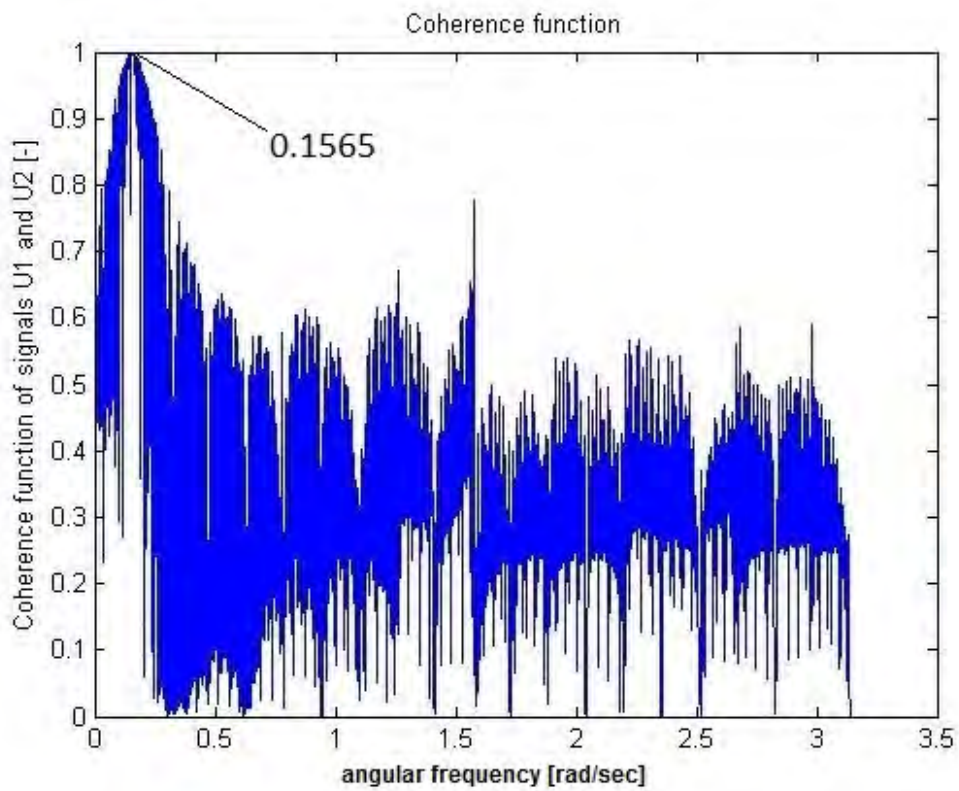
Figure 4.24: Coherence Function VS Angular Frequency (max: at 0.1565 rad/sec)

104
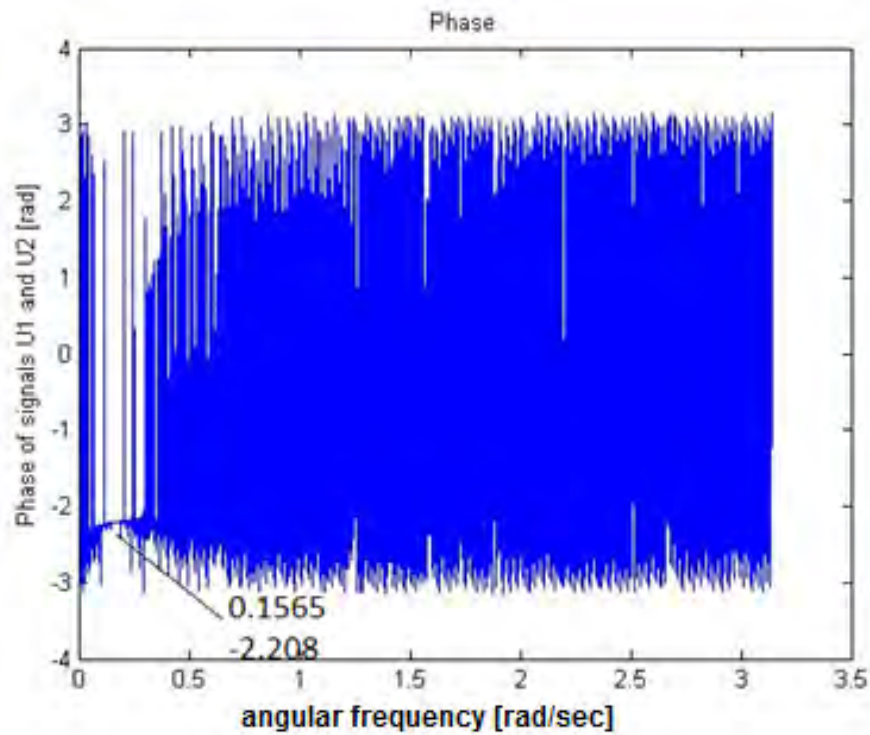
Figure 4.25: Phase Lag of Lift - Sweep Angle (-2.208rad at 0.1565 rad/sec)

Another useful result for many applications such as wind turbines, is the calculation of the induced velocity field behind the wing. In figure 4.26 , the calculated induced velocity field refers to the wing's control points (c/4) for the outmost sweep angles during the wing tip motion.

105
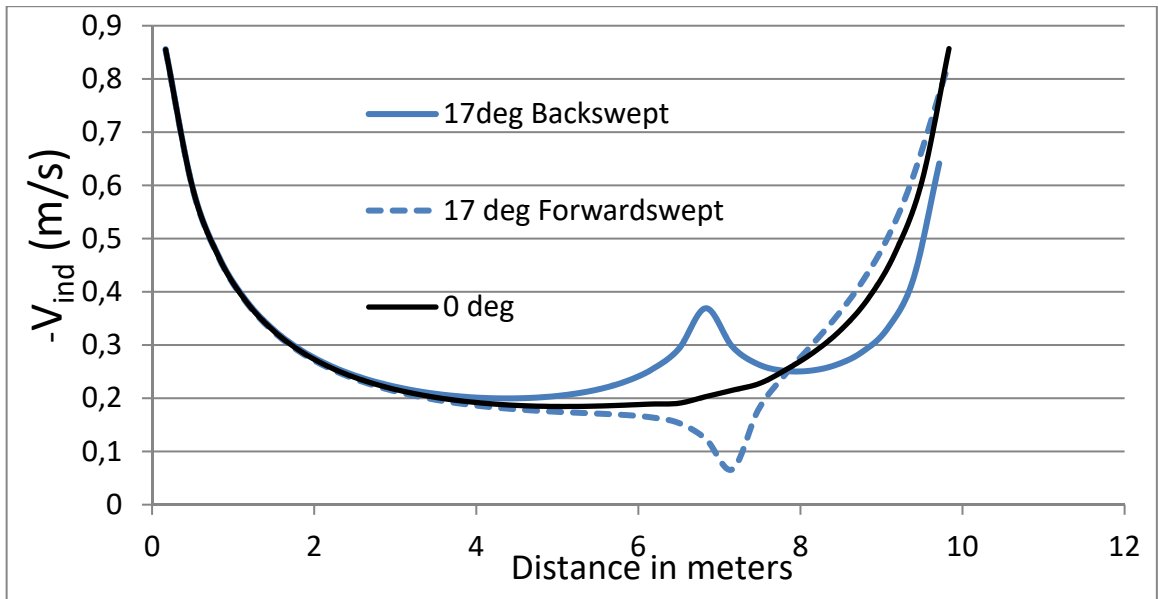
Figure 4.26 : Induced velocity field calculated at control points - ULL

It is seen that only in the wing tip area the velocity field is notably altered and a kink is formed at the hinge point (7m) with opposite direction for opposite angles.

In terms of flow visualization the next figure displays how tip movement affects wake formation:
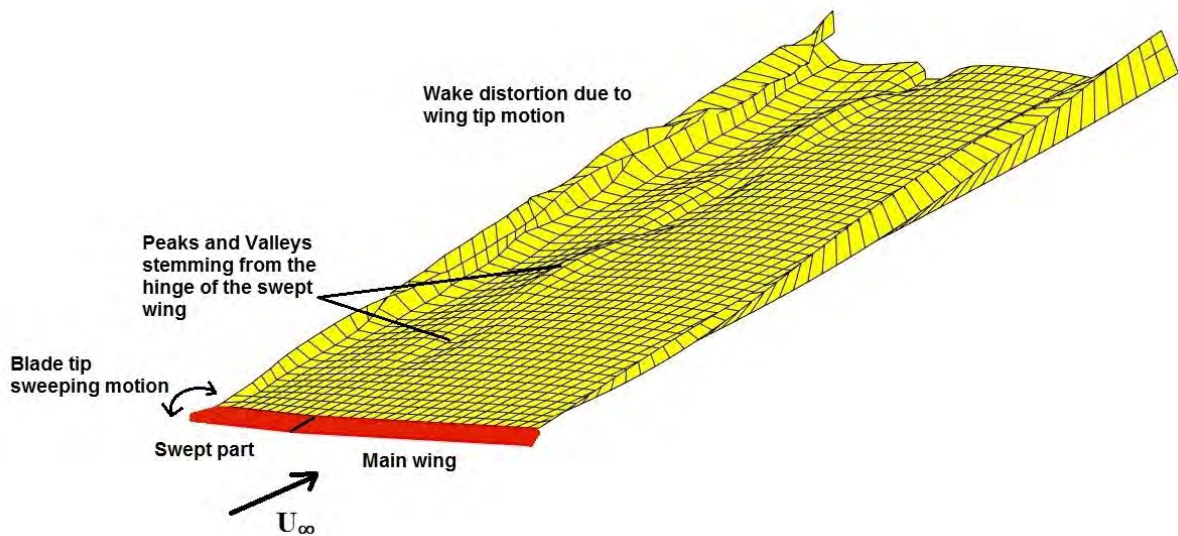
Figure 4.27: Wake formation due to variable sinusoidal tip sweep angle variation

106

As before, it is seen that only in the vicinity of the moving tip the wake is notably disturbed. In addition, a wave seems to be formed behind the hinge which is strongly related to the sinusoidal tip sweep angle variation.

4.6 Modeling the unsteady case on ANSYS CFX

The methodology applied for the unsteady case on CFX was basically the same with the one described in paragraph 4.3 except for the movement requirement of the wingtip. This implies that an equivalent function should take over remeshing of the domain as the wingtip rotates about the hinge point. A script from reference [114] was utilized which in principle deforms the mesh until the value of orthogonally-based quality will trigger remeshing of the domain. Of course, the initial mesh settings were identical to the settings of paragraph 4.3. Moreover, the remeshing script was also utilized on steady conditions with the wing initially unswept and gradually moved to the required sweep angle and let to stabilize. By this, comparison of unsteady and steady conditions can be made on exactly the same basis because every time the results refer to exactly the same geometry and mesh. However, sweep angle can not take values higher than approximately 23 degrees, because this leads to problems concerning mesh quality and a solution is not achieved. In addition, time step had to be reduced to the extent that cause the smallest possible deformations on the mesh and simultaneously produce stable solutions for the N-S equations at every step. Thus, time step value for CFX was chosen to be 0.005sec (10 times smaller than the ULL's approach).

4.6.1 Results of CFX on unsteady conditions - Swept Wing

In terms of validating the ULL model on unsteady conditions a same scenario was run on CFX with the methodology and settings described on paragraphs 4.3 and 4.6.

107
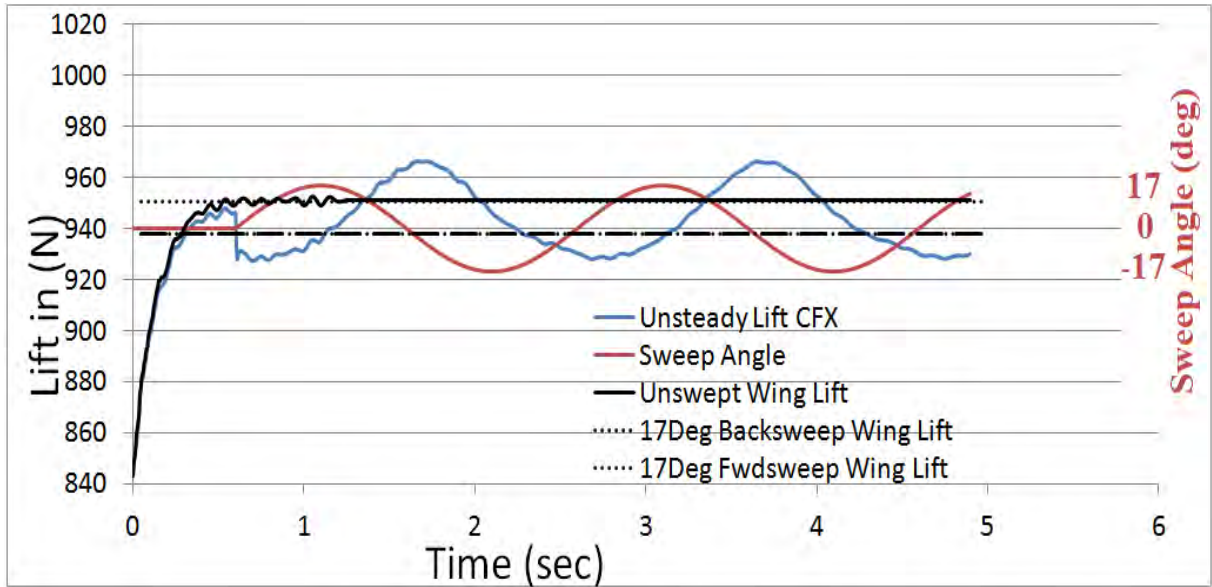
Figure 4.28: Unsteady lift predicted from CFX (30% tip sweep, 17deg Amp & π radial Frq)

The CFX results - similarly to ULL results - indicate a phase lag between Lift and sweep angle. Unsteady lift introduces an overshoot of 1.55% compared to the unswept wing's produced lift and a "downward" overshoot of 1.09% compared to the 17deg backswept steady case.

The phase lag value was recovered with the methodology of the previous paragraph and the corresponding figures are introduced:

108

Figure 4.29: Cross Power Spectral Density VS Angular Frequency (max at 0.01534Hz) –

CFX
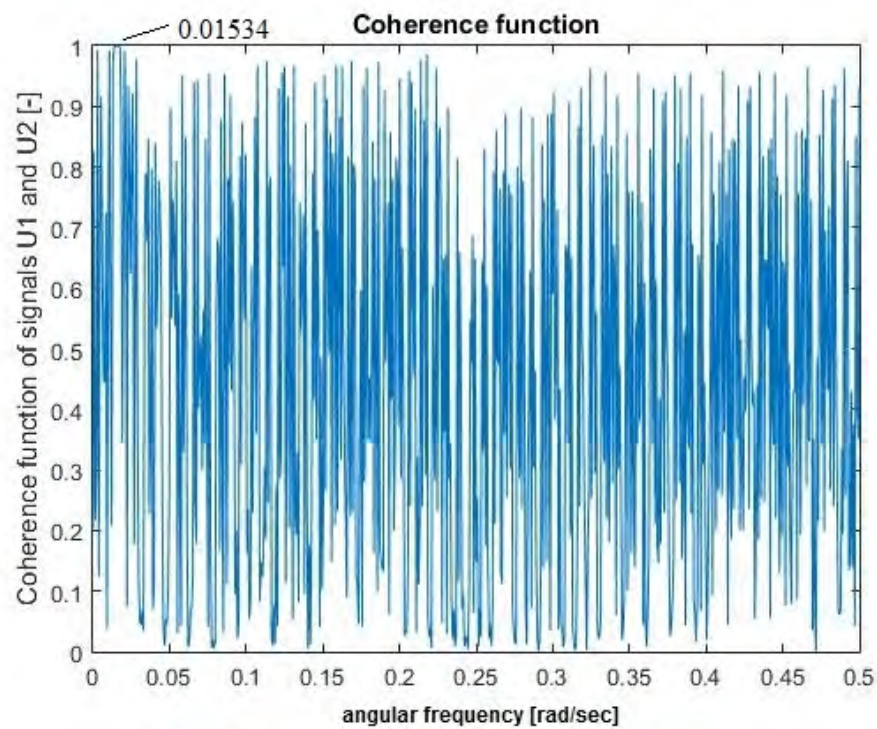
Figure 4.30: Coherence Function VS Angular Frequency (max:1 at 0.01534Hz)

109
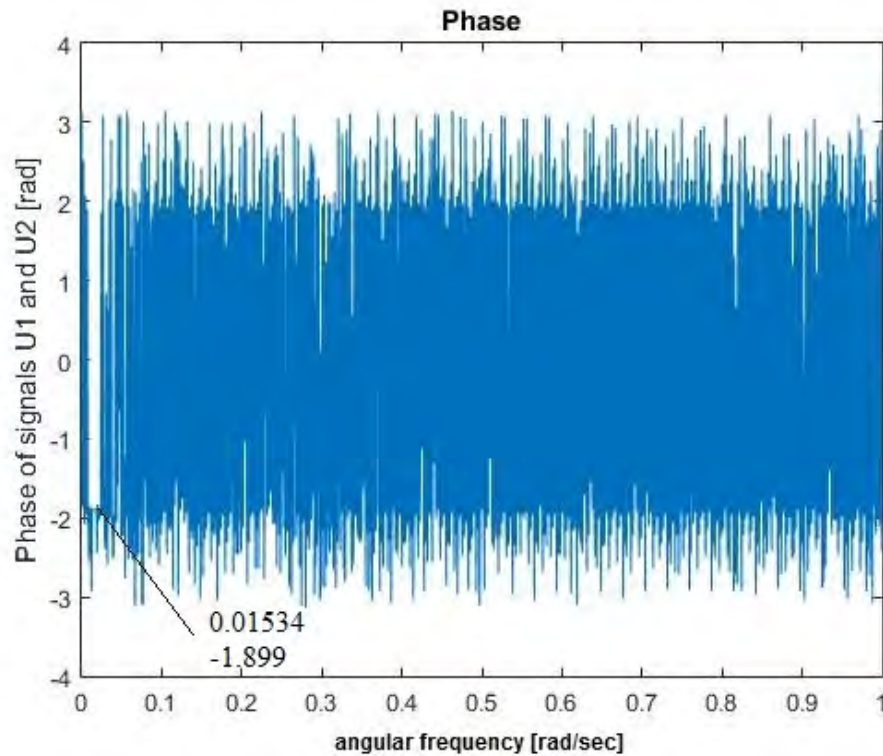
Figure 4.31 : Phase Lag of Lift - Sweep Angle (-1.899 rad at 0.01534Hz)

Similarly to the ULL phase lag analysis, lift response and sweep angle variation are best correlated at angular frequency of 0.01534 (rad/sec) or for sampling Period of Ts = $2*\pi/0,01534$ =409.6 samples (~400) or 400 * timestep (0.005s) = 2seconds. Thus, from figure 4.31 phase lag magnitude is calculated at -1.899 rad or **108.8 degrees.**

As far as the induced velocity field is concerned, a direct calculation at the points of the ULL cases was not possible due to the thickness of the airfoil on CFX simulations and the corresponding inability to define a line inside the wing to calculate those velocities. So, the field was calculated at points of the same spanwise distance and short behind the trailing edge. More specifically, the points were placed 10% of the airfoil chord away from the trailing edge in order to be far enough from the Kutta condition point (zero circulation) but still close enough to the model the flow disturbances. In addition, contours of the velocity field were made in CFX post to assist in the previous decision (figure 4.32).

110
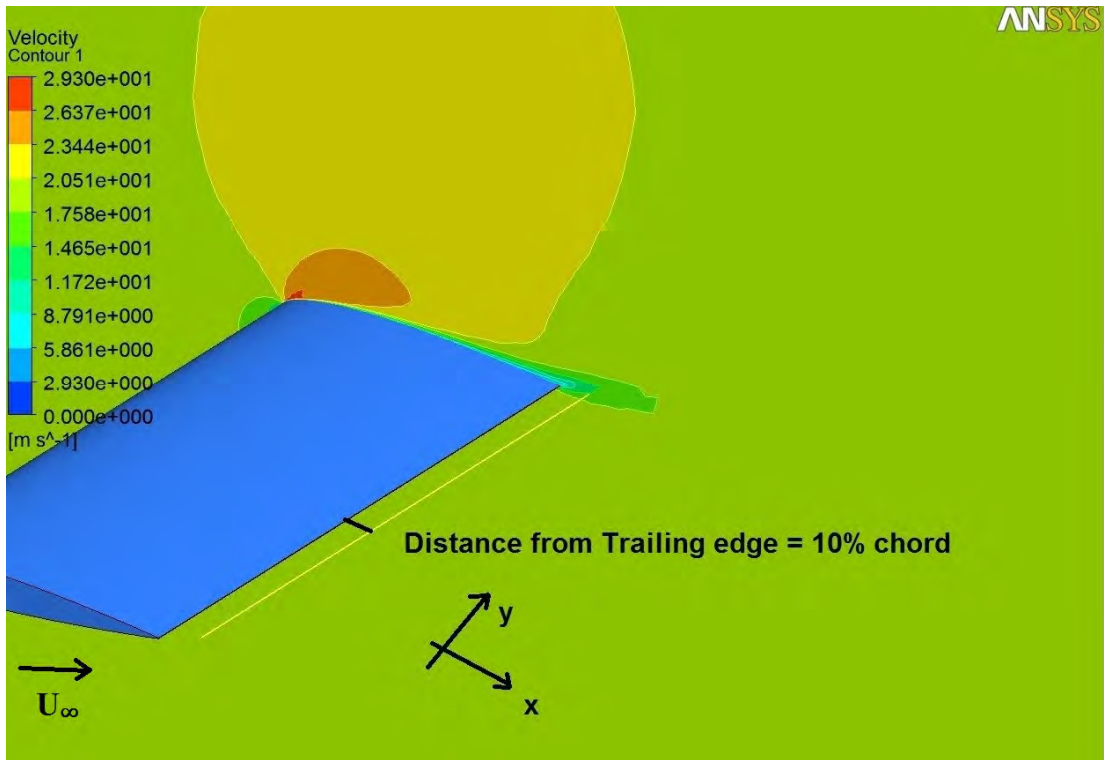
Figure 4.32: Contours of the velocity field in a wing section and the "induction" line
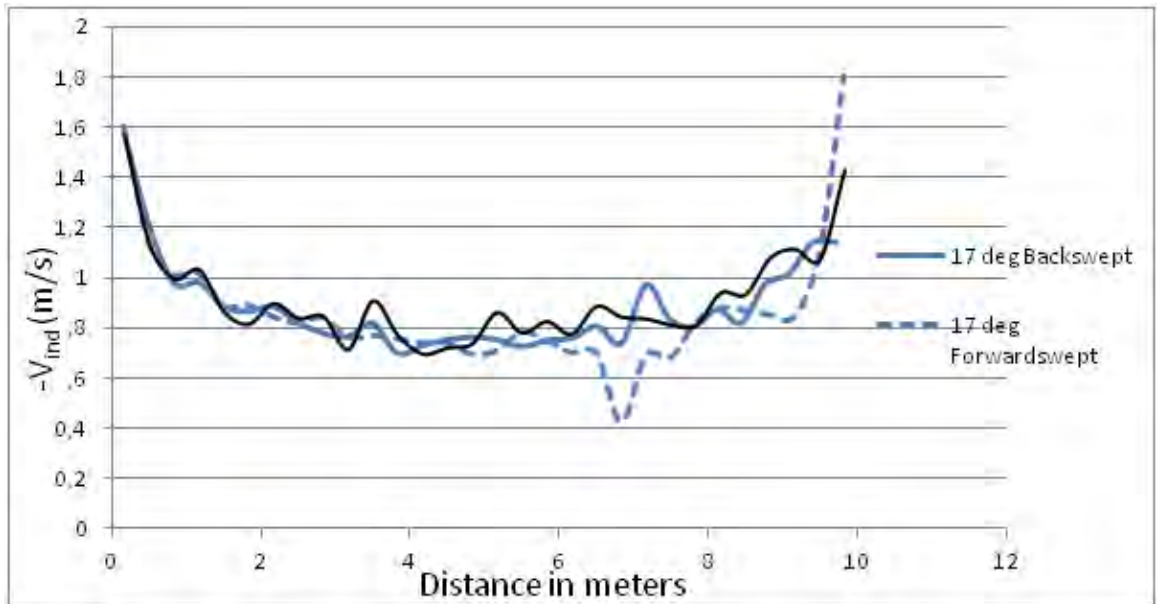
Figure 4.33: Induced velocities calculated at the "induction" line (10%c behind T.E.)

111

It is seen that there is a kink in the hinge region with opposite direction for opposite sweep angles. However, the not so smooth line across the span is caused probably by turbulence behind the wing's trailing edge.

4.6.2 Discussion and comparison of ULL and CFX results for unsteady conditions

Figures 4.22 and 4.28 indicate that the two different approaches produce quite similar results for the wing's lift. Both of them predict:

- Similar behavior in unsteady lift.

- Similar behavior in wing induction.

- Lift maximum or minimum for approximately the same sweep angle values.

- Phase lag between lift and sweep angle variation.

- Lift overshoot.

But, on the other hand:

- Absolute values of lift predicted by ULL are approximately 10% higher than of the CFX values.

- Absolute values of induced velocities differ.

- Lift overshoot is calculated 1.27% higher in the ULL approach.

- ULL does not predict a "downward" overshoot as CFX.

- Phase lag in ULL is by 16% higher of the CFX value.

A figure that shows the results of both approaches normalized (by subtracting their mean value) follows:

112
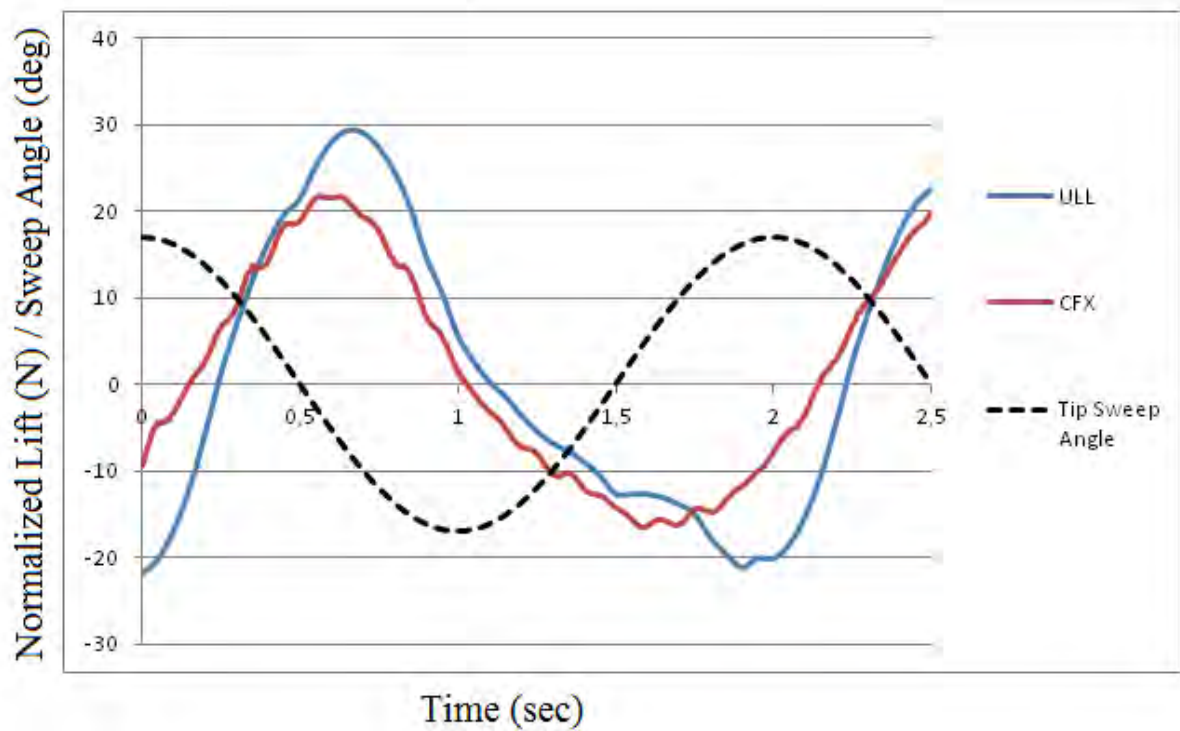
Figure 4.34: Comparative diagram of normalized lift ULL Vs CFX

Also, the induced velocities fields from ULL and CFX are shown together for comparison:
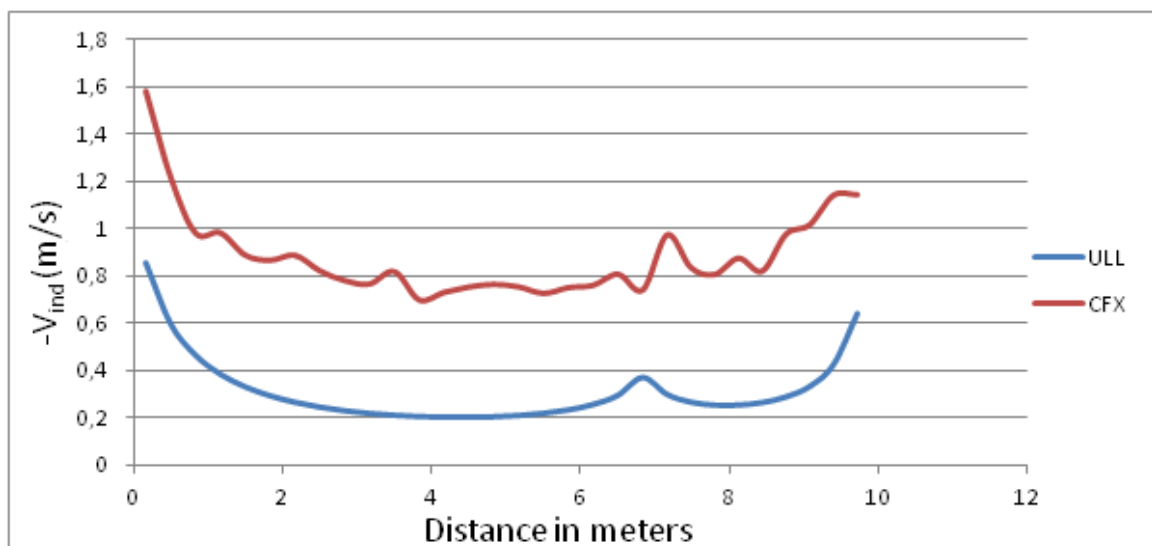
Figure 4.35: Comparative diagram of Induced Velocities for 17deg Backswept angle ULL Vs CFX

113
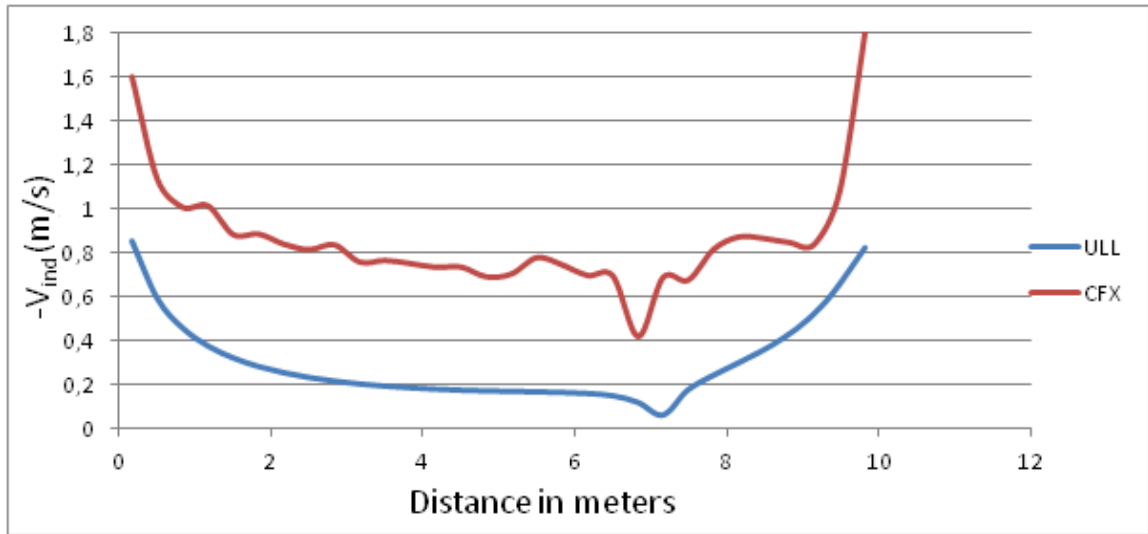
Figure 4.36: Comparative diagram of Induced Velocities for 17deg Forwardswept angle ULL

Vs CFX

The differences in absolute values is explained by the different points on which velocity is calculated. It is observed that in the near wake (10%chord behind the trailing edge) velocities are higher than in the c/4 points, which seems to be rational because of the corresponding smaller distances (equation 2.10).

Taking into account the differences that exist by definition between ULL and CFD, it can be stated that the approaches are in a quite good agreement. As far as program run time is concerned, the comparison of ULL model and CFD simulations showed that for 5 seconds of real time simulation the former ran for approximately 28 minutes where the latter for over 7 hours. Of course, time step on CFD was set 10 times smaller than the that of the ULL, but it was the structure of the problem (remeshing requirement) that didn't allow a bigger one. The available computer was equipped with an Intel Core i7 2600K at3.4GHz processor and 8Gb of RAM.

114

4.7 Summary and Conclusions

In this chapter a first attempt to model the aerodynamics of a tip swept wing on steady and unsteady flow conditions, has been tried. At first, the relatively simple case of a tip sheared thin airfoil wing was modeled, by utilizing Lifting Line Theory and a code was written using *Matlab* software. The term sheared was mainly used to point out that all airfoils of the tip section were kept parallel to their initial orientation. The results showed that wing lift is reduced from 1% to 7% (for the specific cases examined), with increasing tip sweep percentage and sweep angle magnitude and also that lift loss was equal for opposite sweep angles. Moreover, diagrams of vortex strength and induced velocity on collocation points were made and the effect of tip sweep on induced drag force was determined.

In terms of comparing the previous results with a more analytical model than the developed ULL theory based model, CFD simulations were carried out with the use of ANSYS CFX. The various wing cases were designed at Solidworks, and NACA 0012 was used to model the thin airfoil. The flexibility provided by Solidworks allowed the modeling not only of the sheared but also of the swept tip. As for the sheared tip configuration, the results of wing lift showed very good agreement and as for the swept tip configuration, the results were used to verify ULL Model.

ULL is a method that models the unsteady effects of variable sweep by implementing wing tip rotation around a specified hinge point and also, the swept lift coefficient according to equation 4.1 . The methodology applied in order to calculate the unsteady lift is based on [26] and [113] and modified accordingly to fit the problem. However, its results were verified firstly at steady conditions with the corresponding CFD simulations and showed that a good agreement is achieved better on qualitative basis.

115

As far as unsteady conditions are concerned, a sinusoidal sweep angle variation scheme was chosen and showed qualitative agreement between ULL model and CFD simulations. Both of them, simulate wing's lift phase lag and the overshoot when the tip passes from zero angle at maximum speed. Of course, there are also slight differences which are described in paragraph 4.6.2. Additionally, the induced velocity field behavior on control points predicted from ULL matches with that of the near wake calculated from CFX.

Concluding, the ULL model seems to be a suitable tool for producing robust and even fast results for tip swept wings on unsteady conditions. Its main weakness though, appears to be in the wing geometry discretization. The key is to model in the best way possible the moving wing tip geometry, define its horseshoe element and thus the points from which the wake nodes stem into the flow.

The originality that this chapter incorporates is the conduction of CFD simulations for a tip swept wing with variable sweep angle capability and the corresponding development of a robust ULL model which models this geometry feature for a thin airfoil wing and produces similar results.

116

Chapter 5. Investigation On The Rotor Case With Tip Swept Blades

In this chapter, the investigation of the effect of variable tip sweep is extended to a three bladed HAWT with the use of an ULL theory based model, due to its proven good agreement with CFD simulations concerning the fixed wing case and its feasibility within the capabilities of a typical powerful desktop. Firstly, the implementation of the theory and the specific aspects of the problem are described. Thereafter, an investigation and discussion about the differences of Free wake and Prescribed wake code configuration takes place. In addition, results of representative cases such as step changes of sweep angle and harmonic motion of the tip are presented. In the end, a parametric study concerning the effect of the harmonic tip motion for blade configurations of smaller tip sweep percentage is shown and useful conclusions are addressed.

5.1 Implementation of Lifting Line Theory on a HAWT

For this thesis the generic NREL 5 MW, 3 bladed upwind HAWT was chosen for the investigation of variable tip sweep capability on HAWTs. This is also the reference wind turbine for plenty of research works such as [105], [115], [116] and all necessary data are available from [117]. Table 5.1 shows its basic characteristics. Yet in terms of simplicity, it was considered that the blades had only one airfoil section (that of NACA 64618) across their entire span and the controller was set to off. The problem was built in two coordinate systems

117

- the inertial and the blade system which is continuously moving (figure 5.1). So, every term which was defined easier in the moving system, such as the rotating velocities of the blade elements ($\omega*r$) or the position of them, later they were analyzed to the inertial frame by using the corresponding transformation matrix.

Rotor Orientation	Clockwise rotation - Upwind
Control	Variable Speed - Collective Pitch
Cut in wind speed (m/s)	4
Cut out wind speed (m/s)	25
Rated power (MW)	5
Number of blades	3
Rotor Diameter (m)	126,0
Hub Diameter (m)	3,0
Hub Height (m)	90,0
Rated Rotor Speed (rpm)	12,1
Rated Generator Speed (rpm)	1.173,7
Maximum Tip Speed (m/s)	80,0

Table 5.1: Main characteristics of 5MW NREL reference wind turbine
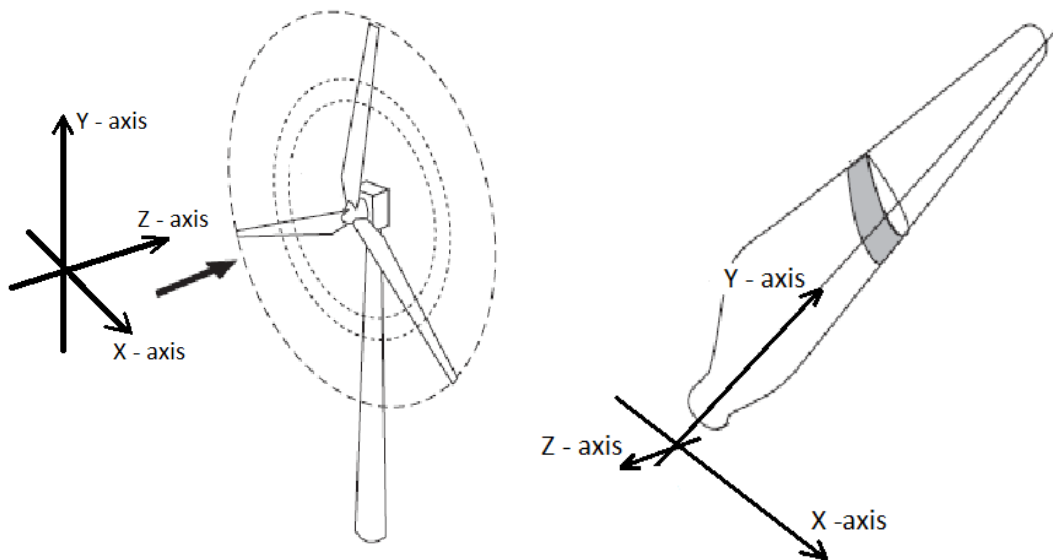
Figure 5.1 : Inertial and moving coordinate systems. Source: [54]

118

According to the theory all of the blades are divided into horseshoes elements and their corresponding control points. The dicretization is done on the basis of creating a high speed code that produces good and stable results for this specific problem. For this reason the earlier investigation on a similar problem concerning fixed wing (chapter 4) was taken into account and the blades were divided into 30 equal length elements. Of course, a distribution with denser elements near the tips of the blade and near the junction of the swept part with the un-swept part would be more preferable as it would model better the large gradients in bound vorticity there. However, it was proven from test runs of the code with this denser distribution, that the problem could not always converge to a solution especially when tip sweep was introduced.

As the wake develops behind the three blades, a triple vortex lattice is formed and induced velocities on every control point are calculated from this wake scheme. The effective angles of attack that result from the vectorial summation of induced and free-stream velocities are used in a table that contains values of steady state lift and drag coefficients for a range of angles, concerning NACA 64618 (Appendix A.1). Corresponding lift and drag coefficient are determined through interpolation. Then, the iteration process described above is repeated until the convergence criterion is achieved on every blade. Suitable values for the damping factor and the convergence criterion were defined from the implementation of this code on the fixed wing case and thus were set to 0.3 and 1% correspondingly.

In the case of tip-sweeping, the elements of the corresponding blade portion are reordered to their new positions according to the sweep angle. Now, this change in blade geometry and of course the rate of it, will have a direct effect on the wake development and will establish a new state on the blades which in turn will affect the performance of the turbine and its loads. In other words, time dependent wake related phenomena will show up.

119

The choice of the time step value is of great importance in order to uncover this dynamic behavior and 0.05 sec was proven to be convenient from previous tests on this code and the investigated cases of this chapter. In particular, it will be seen that in the cases where dynamic phenomena are introduced through the motion of the blade tip, with an angular frequency in the order of pi (or 0.5Hz), every complete motion is modeled with 80 steps by the model.

5.2   Specific aspects of the variable tip swept rotor blades

The application of tip sweep at the blades has to be modeled properly in order to achieve good predictions. Lifting line theory allows geometric modifications to the blades as there is no restriction for the bound vortex to be parallel to the span-wise direction. In this model the blades have 30% of their span linearly swept (aft or fore) with the "hinge" located at the quarter chord.
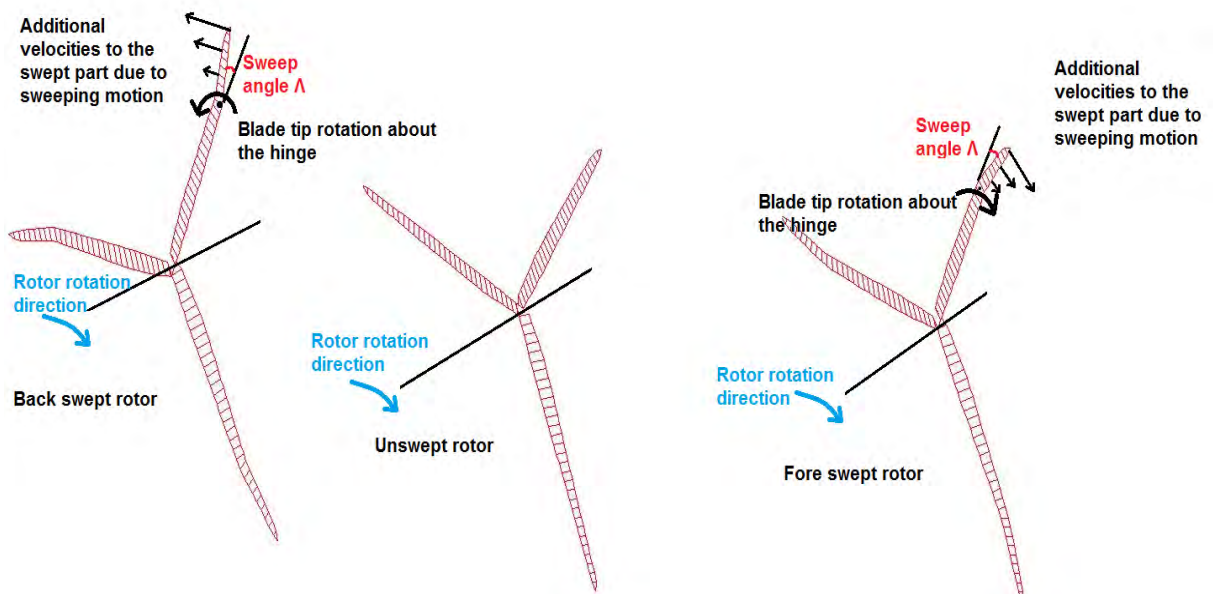
Figure 5.2 : Aft tip-swept blades 12deg / Un-swept blades / Fore tip-swept blades 12 deg

Three are the basic issues of a wind turbine with tip swept blades that play critical role in the prediction of its performance and loads. These are, modification of the lift coefficient of

120

the swept section, consideration of the in-plane blade velocity due to tip sweep and in addition rotor diameter reduction. The first issue is dealt with equation 4.1 $(CL_{sw} = CL_o \cos^2(\Lambda))$, based on [102].

The second issue deals with the calculation of the resultant velocity on the blades. As sweep angle changes in time, every element of the swept section gains an additional in-plane velocity relative to the flow. This portion is superimposed to the induced and free-stream velocities and the effective angle of attack on every element is determined. The following equation is used for the calculation of the in-plane velocity:

$$\overline{V}_{sweep} = -\frac{\overline{X}_{(t+1)} - \overline{X}_t}{\Delta t}$$

(**5.1**)

where:

- $\overline{V}_{sweep}$ is the additional velocity of the blade sections due to sweep (figure 5.2)

- $\overline{X}_{(t+1)}$ is position on the x axis of the blade section in the next time step

- $\overline{X}_t$ is the current position on the x axis of the blade section

The third issue is more simple because the rotor diameter reduction is easily calculated geometrically and taken into account in the calculation of torque and root bending moments. Those issues are of great importance as they refer to sections near the tip where small modifications there, can create large errors in crucial terms like AEP or fatigue loads.

121

5.3 Prescribed wake Vs Free wake code configuration

Two configurations of the wake can be considered with either one having its own advantages and drawbacks. Generally it was already mentioned that free wake configuration creates a more physical result as it allows the wake to develop freely but makes the model much slower than with the alternative configuration.

5.3.1 Prescribed wake configuration

In this configuration wake nodes stem from the blades' trailing edge with velocity equal to 25% of the vectorial sum of free-stream and blade section velocity ($\omega*r$) [26] & [113]. The rest of the nodes travel with 2/3 of the free-stream velocity which is an assumption that defines optimal operating conditions for the wind turbine by using the optimal axial induction factor derived from momentum theory [113]. Figure 5.3 depicts the wake formed from the NREL 5MW wind turbine that operated for a time period of 12 seconds from start up. As it seen the wake structure is determined only by the rotational velocity of the rotor and the convection speed of the nodes.

122
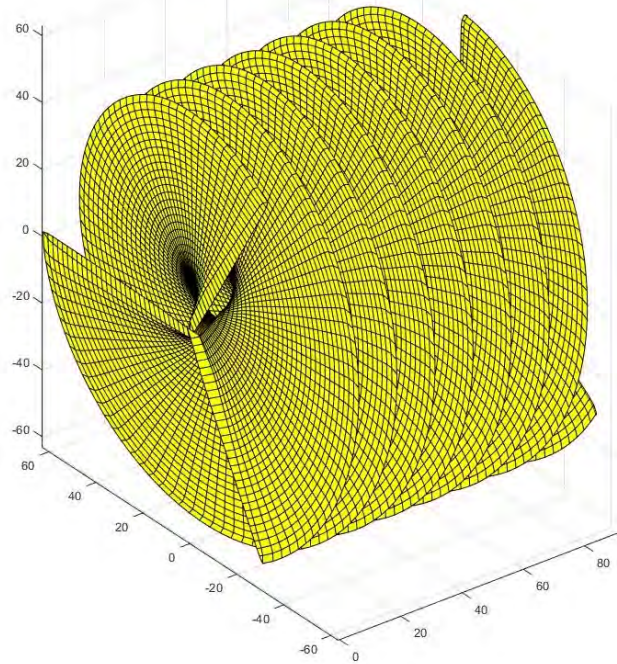
No wake expansion

Profile View
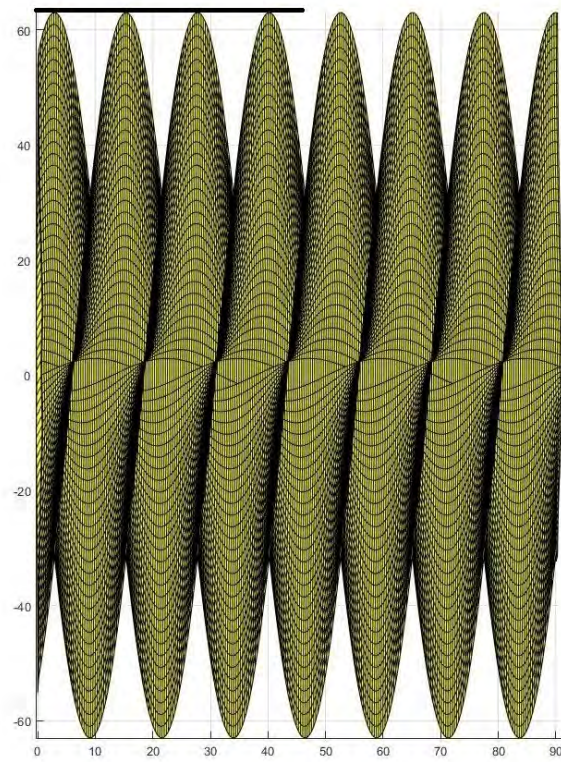
Figure 5.3 : Prescribed wake development after 12 sec simulation run, from start-up

123

5.3.2 Free wake configuration

In free wake configuration a large number of additional calculations take place as every wake node is moved with the velocity induced from the triple vortex lattice. So, main effects like expansion, distortion and roll-up of the wake are modeled and more valid results are derived. Figure 5.4 depicts the development of the near wake for the NREL 5MW wind turbine after 12 seconds of simulation with all of the aforementioned effects included. It is worth to be noted that in the beginning of the simulation the wake doesn't expand as expected because the problem hasn't converged yet.

124
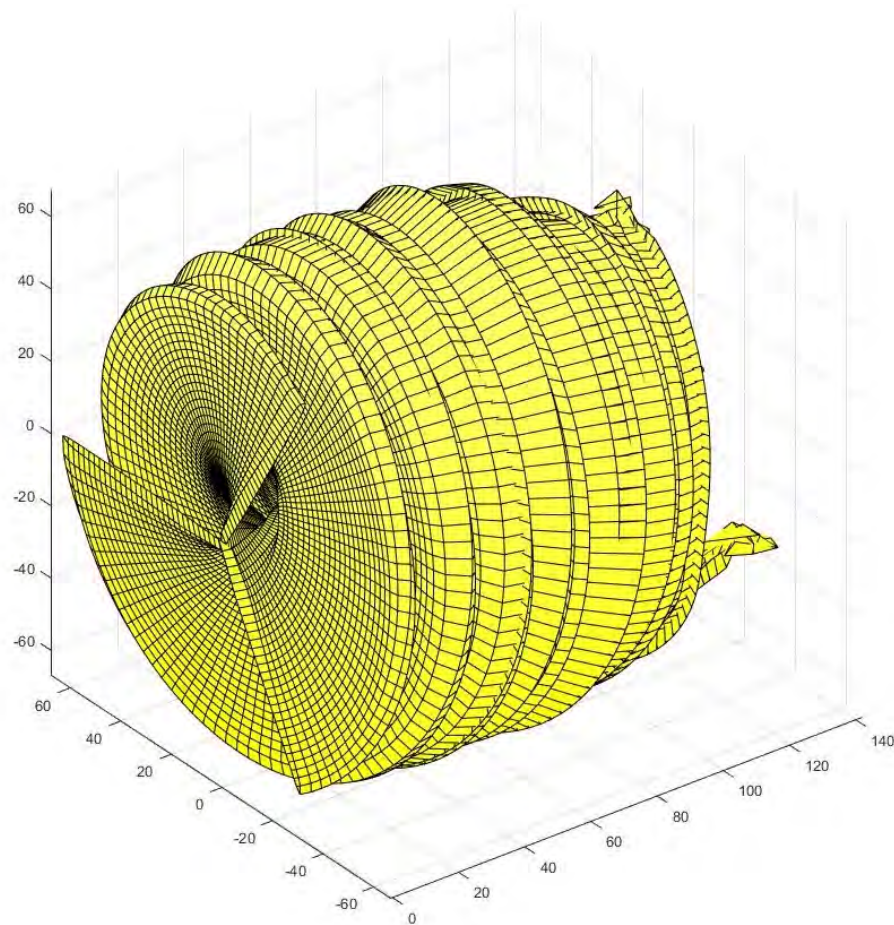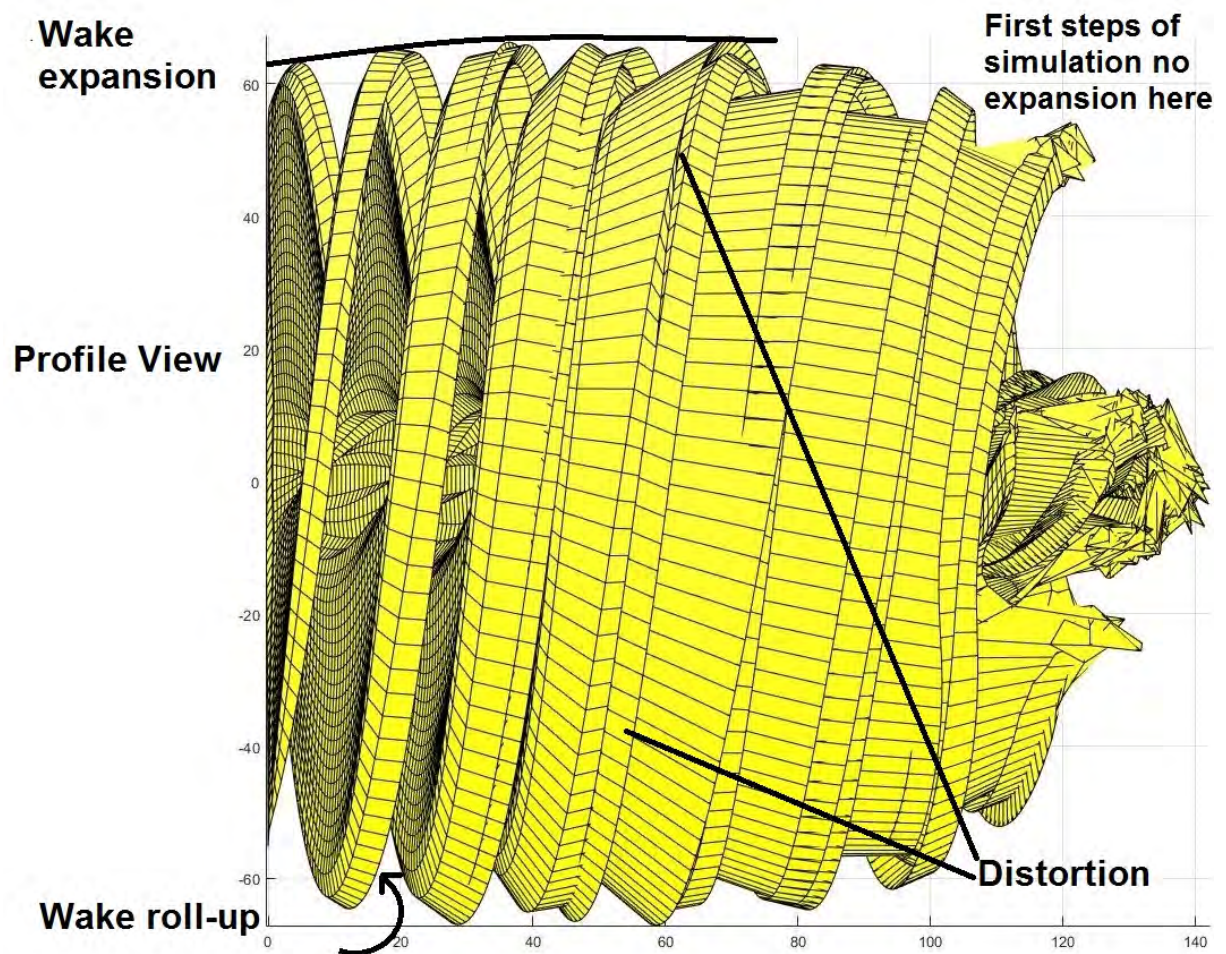
Figure 5.4 : Free development after 12 sec simulation run, from start up

However, this free wake configuration does not take into account viscous effects in the wake which is another important part of the physics. Typically, because of them, vortex cores of all filaments should increase in time and the tangential velocities should decrease correspondingly. Furthermore, mixing of the turbine helical wake with the external flow should lead to a dramatic change of its shape somewhere in the far wake. Of course, there are plenty of theories to model viscous effects (mentioned in paragraph 2.2) but in this thesis the basic subject of study is the effect of tip sweep and the near wake phenomena that arise.

125

5.3.3 Results and Discussion

As happens when seeking the most suitable theory to study the effect of sweep, between BEM theory, Lifting Line theory and Navier stokes equations (CFD) the same issue arises when seeking the proper configuration of the unsteady lifting line model. There is always a trade-off between computational resources and accuracy of the predictions which has to be balanced and adjusted by the researcher.

The prescribed wake configuration code clearly loses in physics but it is much faster than free wake configuration. In specific, the real time needed to simulate the 12 first seconds of wind turbine operation is below 20 minutes while for the other configuration is 4 days (for the available desktop for the this thesis). In terms of this investigation, a fast and reduced order engineering model was needed to account for the sweep effect on the turbine and model the near wake phenomena. However, before using the fast configuration in order to study the effect of tip swept blades, a comparison with the free wake code was necessary. An agreement on blade lift and induced velocity distributions would be a very good indication of the validity of the prescribed wake results. In addition, more coarse values shall be compared as well, such as wind turbine power, thrust and root bending moments of the blades.

The following figures depict the distributions of the z-axis (inertial frame) induced velocity, effective angle of attack, circulation and thrust on every control point of blade 1 for both configurations of the code. The blade choice is random as the problem is axisymmetric. The results refer to the reference NREL 5MW wind turbine of table 5.1 with un-swept blades, operating at the rated speed of 12.1rpm and wind velocity of 11.4 m/s for 12 seconds from start up (or 2.5 revolutions) [117].

126
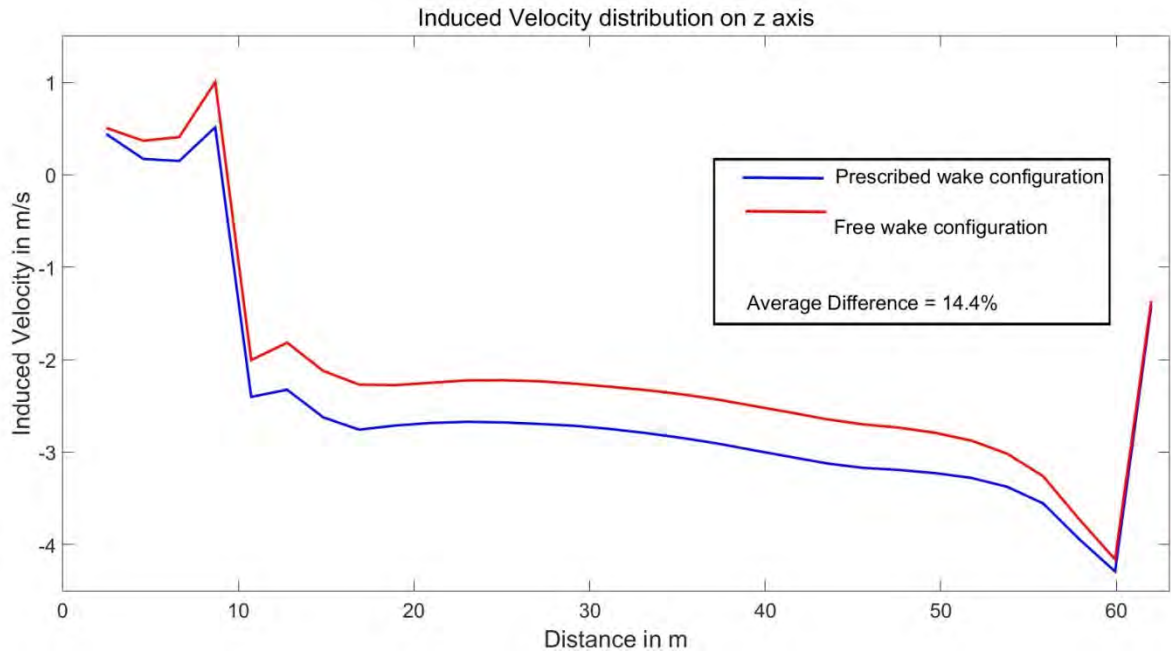
Figure 5.5 : Induced z- axis Velocity distribution on control points of Blade 1
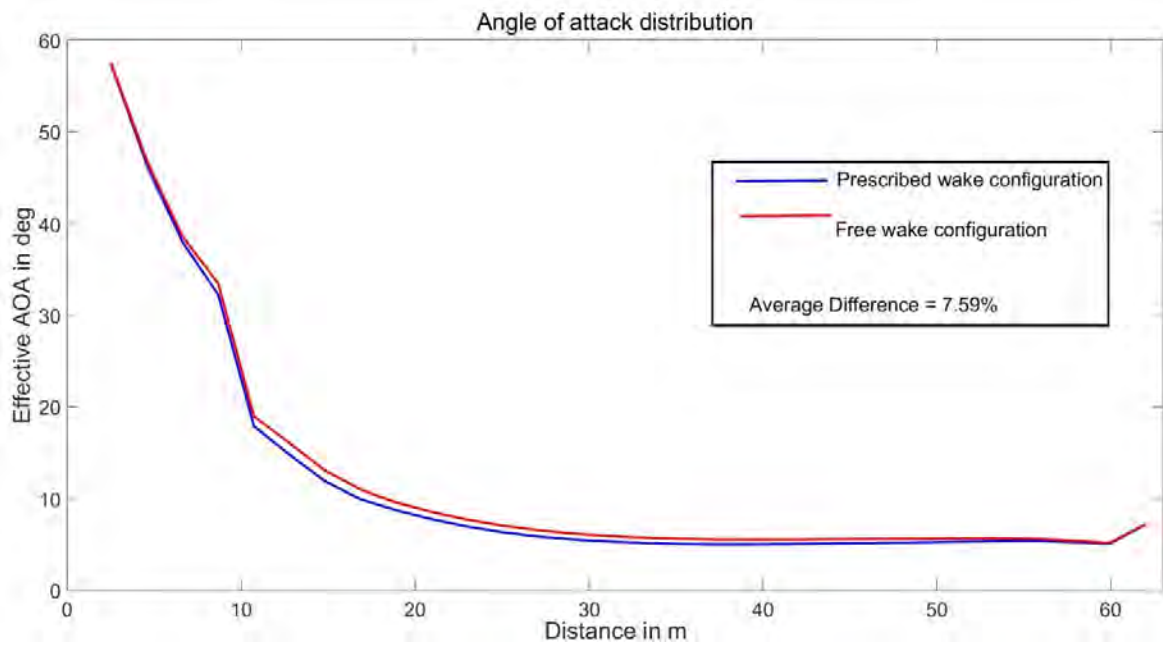
Figure 5.6. : Effective angle of attack distribution on control points of Blade 1

127
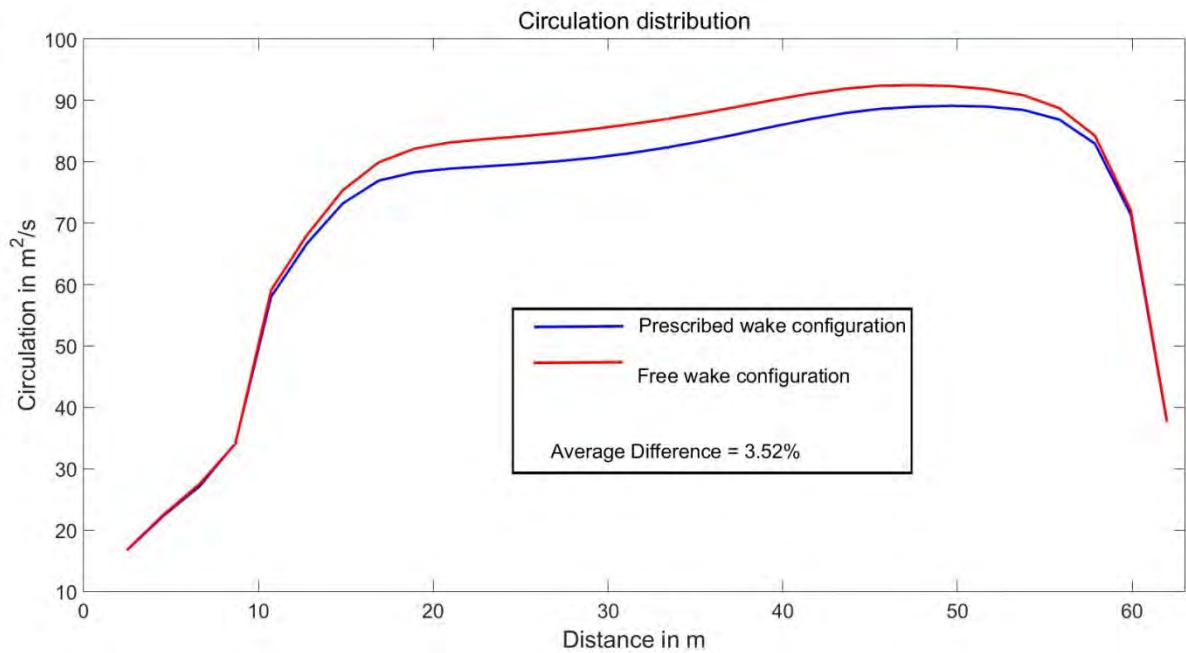
Figure 5.7 : Circulation distribution on control points of Blade 1
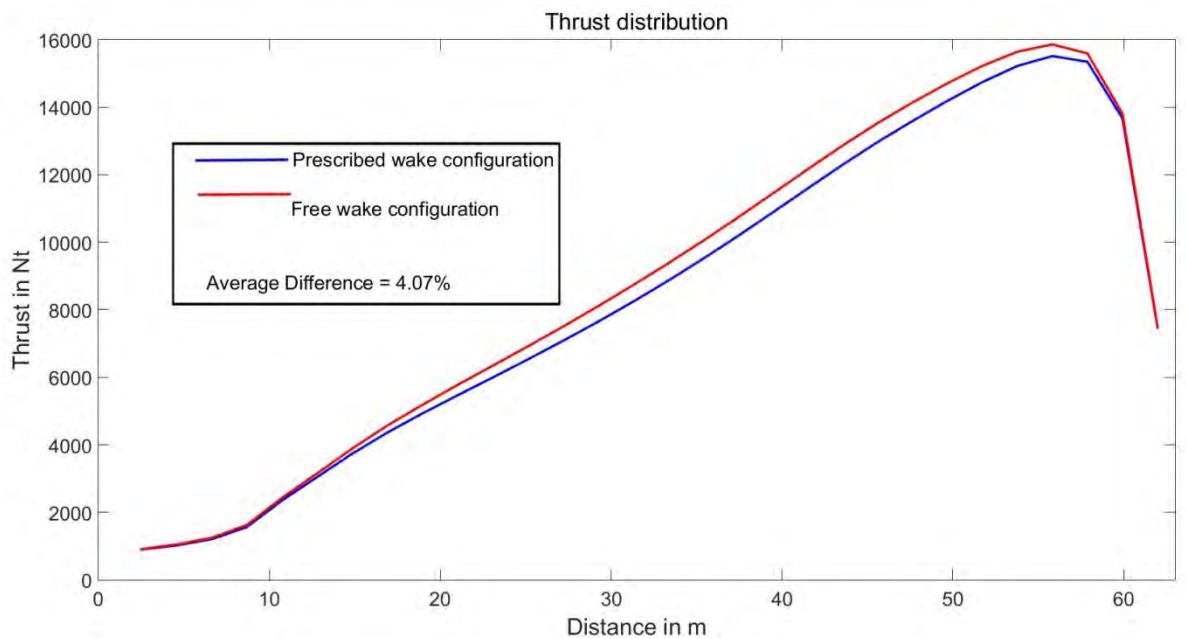
Figure 5.8 : Thrust distribution on control points of Blade 1

It is seen that there is a very good agreement between the two configurations of the code as far as the shape of the distribution is concerned. Clearly, the prescribed wake code models at least the basic physics of the wind turbine with the main part of numerical

128

differences located at the middle of the blade. Indeed, the average values of the relative differences lies between 3-8% except for the z-axis induced velocities which is 14.4% (higher values for the free wake code) . This means that the latter parameter is mostly affected by the wake formation and the speed that is convected downstream. The difference in the shape is shown in figure 5.5 and the average speed of the wake nodes of the free wake configuration is calculated at 77% of the free-stream velocity in contradiction with the prescribed configuration which was set to 66% - ideal induction factor assumption (0.3). Furthermore, it should be mentioned that the differences between the two code configurations in qualitative basis are also found in another code based on the lifting line theory and a possible explanation is that: " *the first shed vortices possibly remain a bit closer to the blade in the free wake code, which causes locally higher induced velocities"* [113].

It is obvious that the wake plays a key role to the predictions of the lifting line model. In addition, the presentation of the above figures is in line with the sequence of the calculations within the code. Starting from the z-axis induced velocity on the blade control points, it is seen that the setting of the wake convection velocity to 66% of the free-stream results in, lower values than the free wake configuration. This in turn produces in average 8% lower effective angles of attack on the blade for the prescribed wake configuration, as the previous parameter plays an important role in these calculations (see also figure 2.11). Eventually, the loads of the blade are underestimated with respect to the free wake configuration and so does the thrust distribution (Figure 5.8).

Figures 5.9 and 5.10 depict the development of the wind turbine's performance and loads for 12 seconds from start up and wind speed at 11.4 m/s:

Institutional Repository - Library & Information Centre - University of Thessaly
19/05/2024 19:53:00 EEST - 18.119.112.4
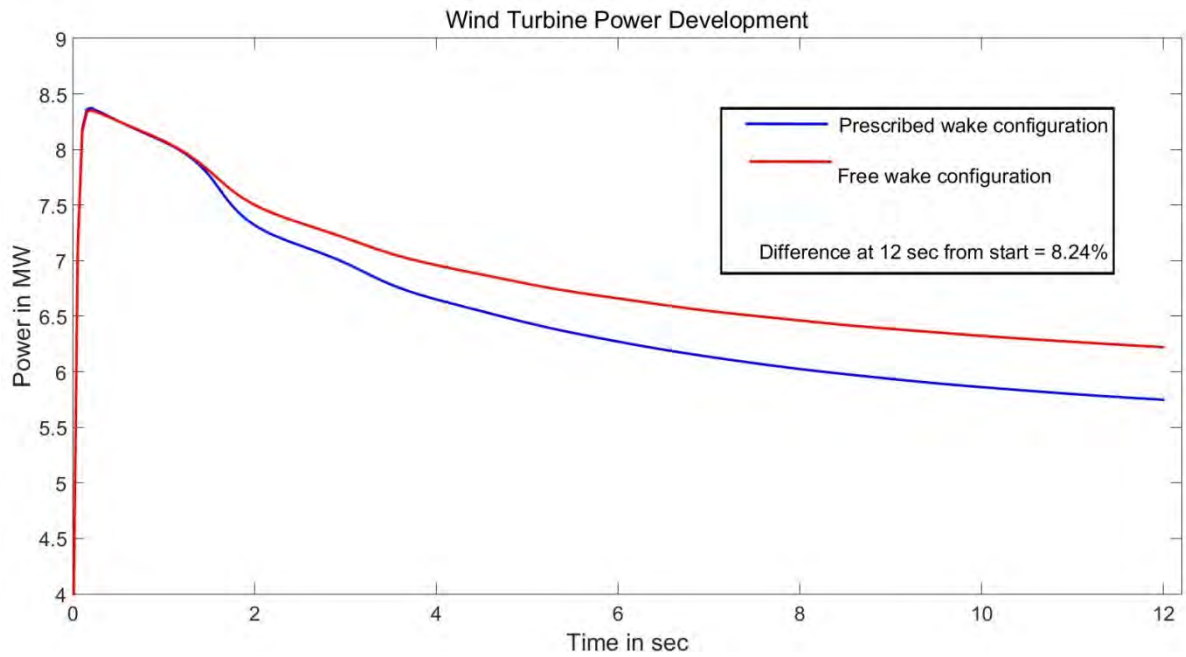
Figure 5.9 : Wind Turbine Power Development for a time period of 12 sec from start up
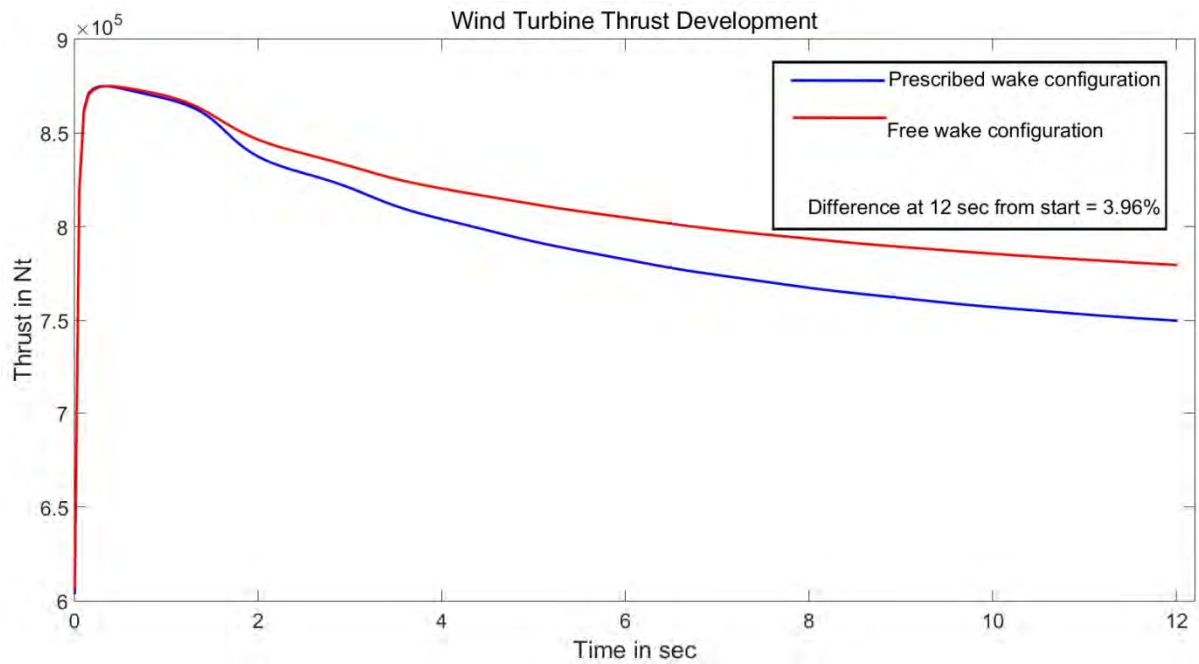
Figure 5.10 : Wind Turbine Total Thrust Development for a time period of 12 sec from start
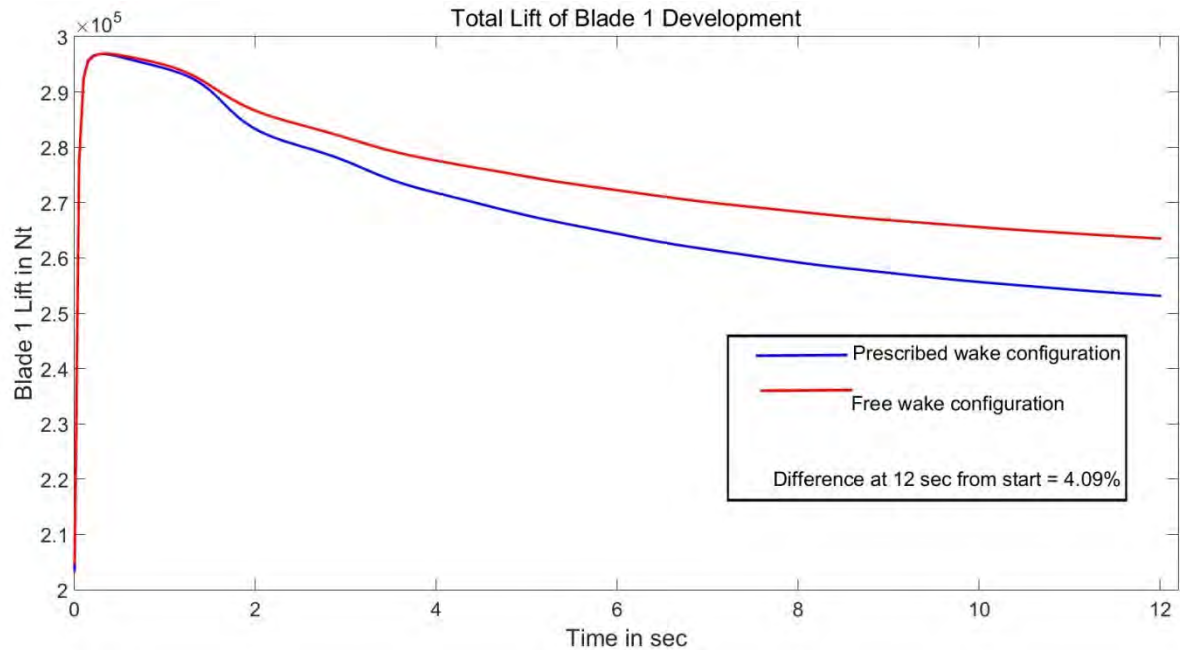
up

130

Figure 5.11. : Wind Turbine Total Lift of Blade 1 for a time period of 12 sec from start up

The similarity in shape between the prescribed and free wake code for these coarse parameters is obvious again and as the wake is developed a constant difference is obtained. The large peak during the early steps is due to the abrupt start of the wind turbine. As mentioned before, the prediction of lower angles of attack results in lower loads which affects of course and the above magnitudes. At this point though, a paradox is observed : Despite the fact the wake is moving slower in the prescribed wake code than the free wake code the power and total thrust of the wind turbine are lower. According to the 1-D momentum theory a slower moving wake means that a larger amount of energy from the actuator disc of the wind turbine is captured. In this case this was explained earlier and is related to the calculation of the wake z- axis induced velocities.

At last, it is worth to be mentioned that the power calculated from the model is close to the rated power of 5MW of the NREL Wind Turbine (14% higher for the prescribed and 24% for the free wake configuration). In specific, the codes ran only for 12 seconds of

131

simulation, at the rated rpm and wind speed in ideal conditions without wind shear, yaw misalignment, tower shadow effects and vortex decay phenomena which should further lower the power output.

5.4   Results of step and harmonic motion with prescribed wake

The basic subject of this chapter is to examine the effect of tip swept blades on wind turbine performance and loads by utilizing a model based on Lifting Line Theory. Previously, the presentation of the methodology took place, the specific aspects of the problem were defined and a choice concerning the configuration of the wake was to be made. Plainly, the prescribed wake is the most suitable choice because it is orders of magnitude faster and gives very similar results to the free wake which incorporates "more physics". This choice is supported by previous studies which showed that the effect of wake roll-up (one of the most basic features of the free wake) on the unsteady response was found to be minimal [115] & [118].

The results presented below refer to the wind turbine of paragraph 5.1 and are separated into two parts: step and harmonic variation of the blades' tip sweep angle. In all cases the turbine operates at rated conditions (speed and wind inflow) and before the introduction of variations, a period of 20 seconds from start-up, for convergence is allowed. As it is seen from figure 5.9 , convergence is already visible from the 12th second. The examined parameters are power output, total thrust, Lift of blade 1, root bending moment of blade 1 and distributions of z- axis induced velocity and circulation Γ (only for the step responses).

132

5.4.1 Step response scenario

The turbine response in a step change of sweep angle suggests a good first insight into the dynamics of the problem. This scenario is presented in figure 5.12 where the tip sections obtain an initial velocity $\overline{V}_{sweep}$ at time step "0" and at time t+dt the blades are swept $\Lambda=\Lambda_1$ and the section velocities due to sweep fall to zero ($\overline{V}_{sweep}=0$). But, in order to actively support the choice of the prescribed wake configuration a special comparative test to the free wake code is presented concerning the first moments of the response. Then, two step cases (only in prescribed wake configuration) are examined - a small step of 5 degrees and a larger step of 12 degrees both for Aft and Fore - sweep.
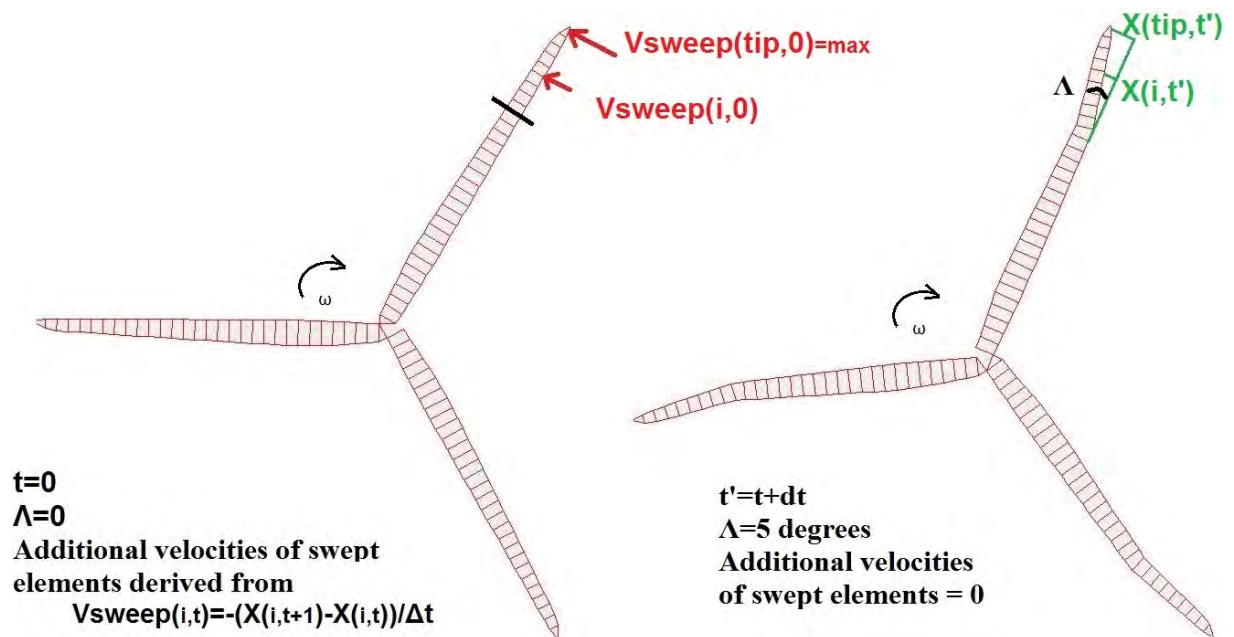
Figure 5.12 : Step change of tip sweep angle scenario

5.4.2 Step response - Prescribed wake VS Free wake code

The special comparative case, refers to the turbine described in this chapter, and a step of 5 degrees aft sweep for every blade is experienced after 12 seconds (not 20) of

133

convergence, because of the large computational needs with respect to the available computer power.
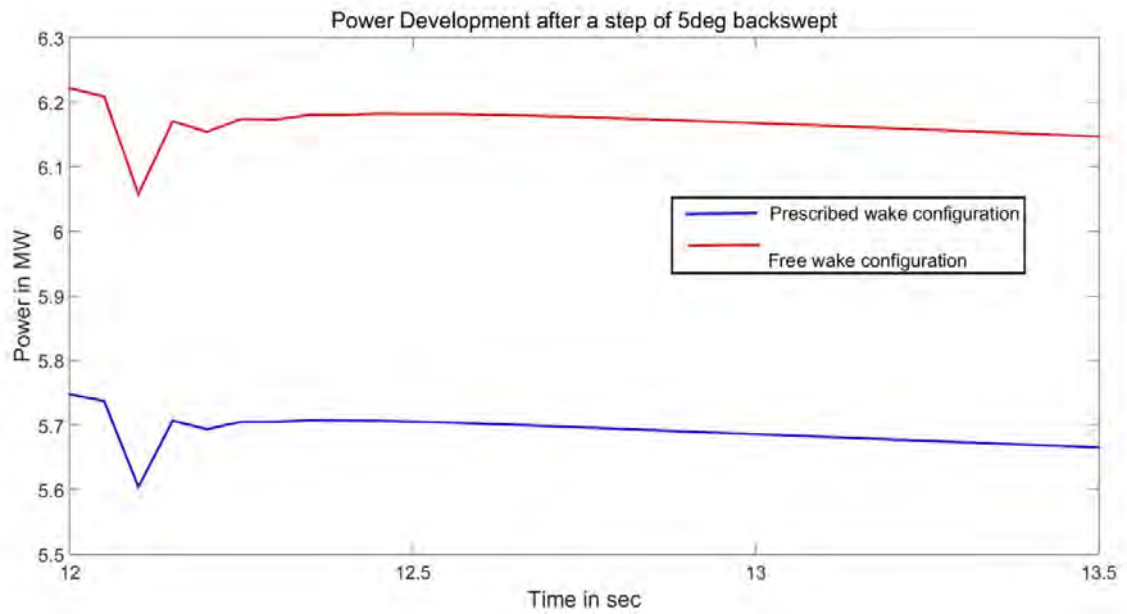
Figure 5.13 : Power Response of PW and FW code after a 5 deg aft sweep step (12 sec convergence)
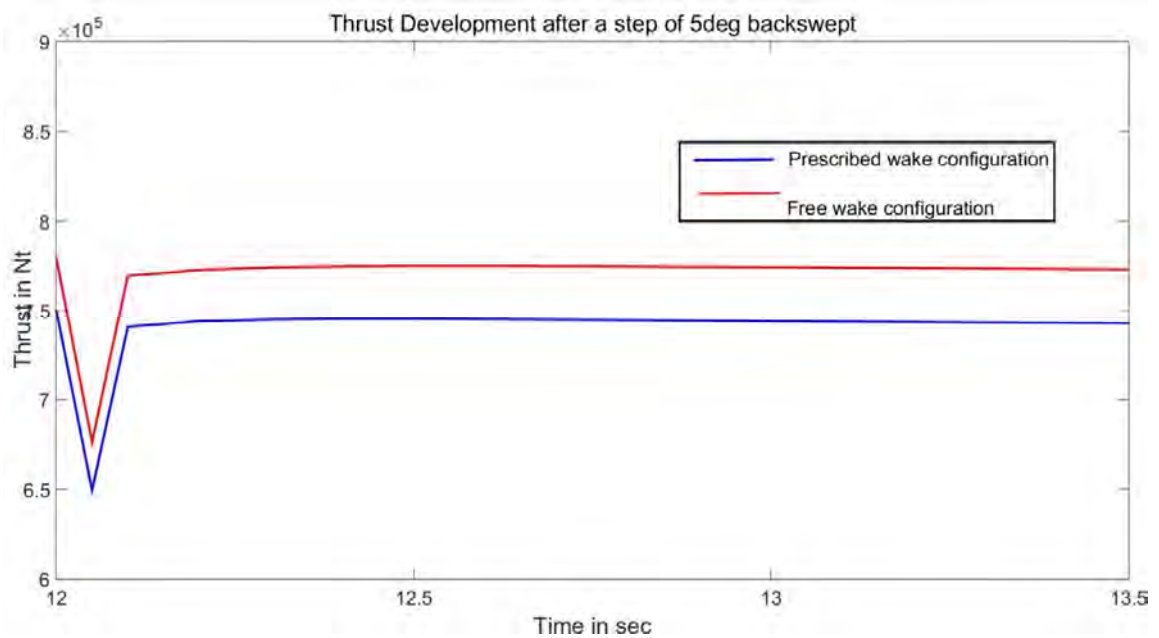
Figure 5.14 : Total Thrust Response of PW and FW code after a 5 deg aft sweep step (12 sec convergence)

134
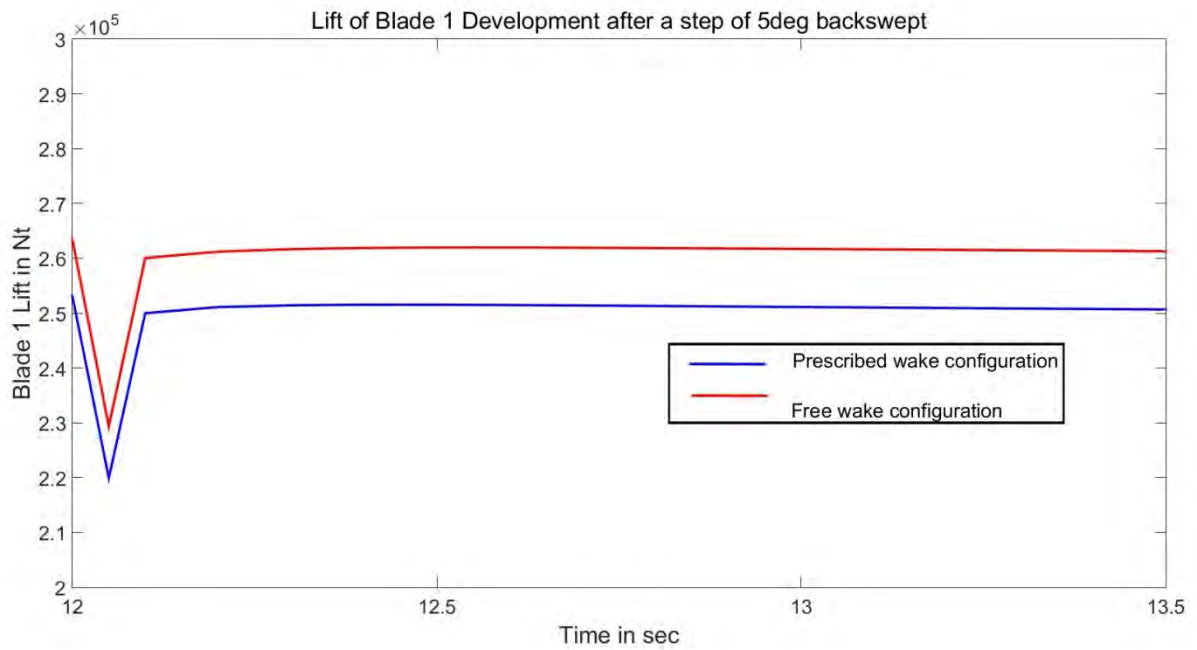
Figure 5.15 : Blade No1 Lift Response of PW and FW code after a 5 deg backsweep step (12 sec convergence)

Figure 5.16 : Blade No1 Root Bending Moment Response of PW and FW code after a 5 deg backsweep step (12 sec convergence)

135

From the above figures it is obvious that the differences between the codes are negligible. The dynamic behavior of all parameters is practically the same. In fact, only the power curve of the free wake code has more visible oscillations than the prescribed, but still not significant. The calculated drop, for the prescribed code, in percentage to the value just before the step-change is -0.183%, -13.4%, -13.1% and -18.1% respectively, whereas for the free wake is -0.197%, -13.26%, -12.96% and -18%. This means that the initial velocity of the tip sections due to sweep, causes considerable alterations in the effective angles of attack (in this case they rise) and in the effective resultant velocity which lowers. Of course, these alterations affect total lift of the blades and in turn, root bending moments of the blades and total thrust of the turbine. However, power seems to drop more, in the second time step compared to the reduction of the first time step, after the step change in sweep angle, having values of -2.31% and -2.44% which means that rotor diameter reduction due to sweep plays a more important role on this parameter by reducing the torque.

Moreover, it is also useful to compare the span-wise distributions of circulation and z-axis induced velocity at the end of the simulation - in this case 1.5 seconds after the step.

136
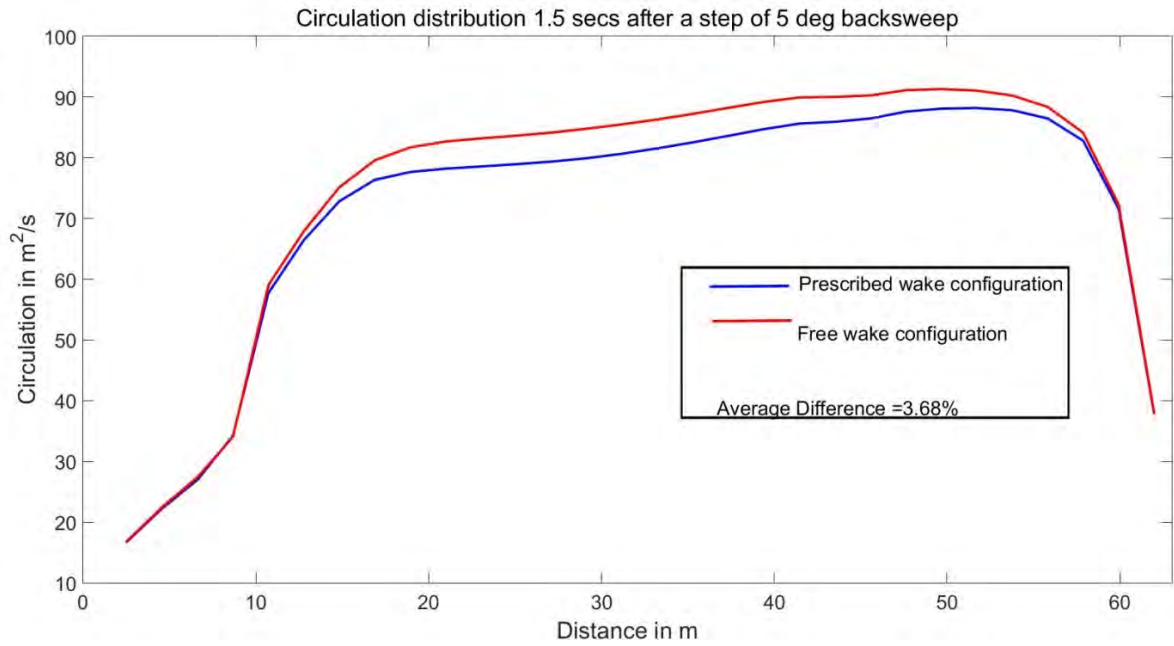
Figure 5.17 : Circulation Distribution of PW and FW code 1.5 seconds after a step of 5 deg aft
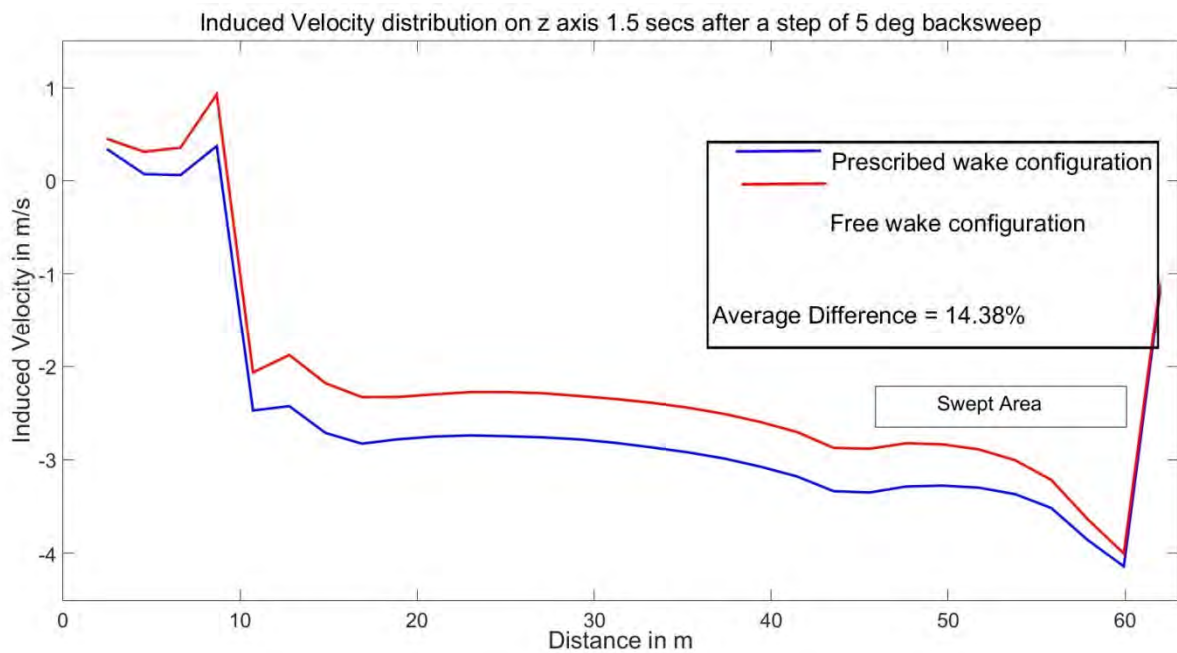
sweep

Figure 5.18 : Z-axis Induced Velocity Distribution of PW and FW code 1.5 seconds after a

step of 5 deg aft sweep

These distributions validate the statement that the prescribed wake code "catches" all

the physics concerning dynamic phenomena. Still, the differences are expressed only as an

137

offset in the middle blade area and have practically the same offset values of the steady case (paragraph 5.3.3). Furthermore, the effect of the aft-swept blade tip is visible in both induction distributions and is uttered as a "bump" in the swept area. So, it can be said that the prescribed wake code is a suitable tool for prediction of the performance and loads of a HAWT which experiences sweep variations in the blade tips.

5.4.3 Step response in Aft and Fore Sweep - Prescribed wake code

In this paragraph the changes in wind turbine's parameters concerning a step of sweep angle in the blade tip area, are examined by utilizing the prescribed wake code. The parameters are allowed to converge for 20 seconds from start-up and another 20 seconds after the introduction of the step. Two cases are presented: 5 degrees and a large step of 12 degrees. The target is to show the influence of sweep direction and the influence of the step magnitude to the turbine.
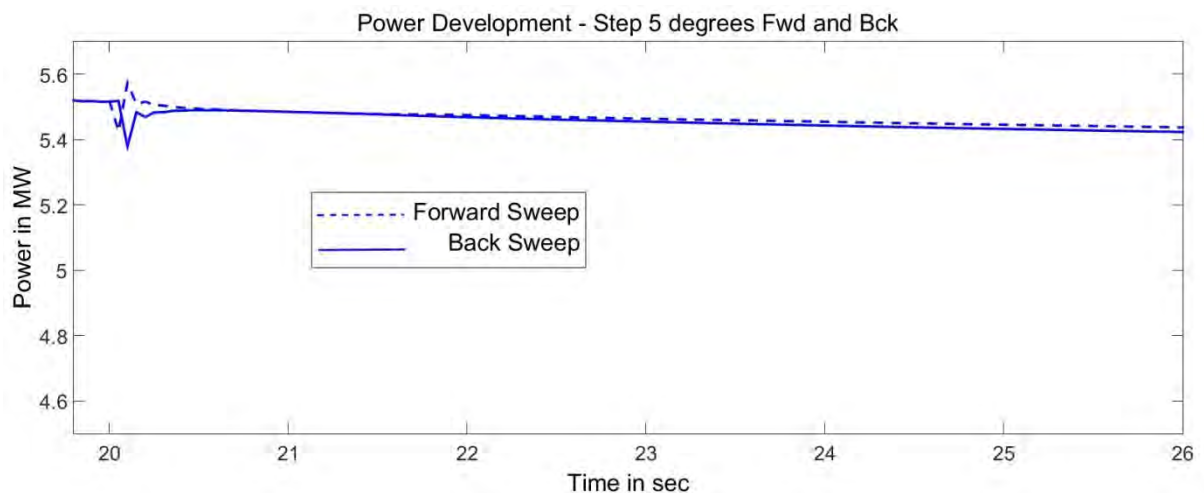
Figure 5.19 : Power Response after a sweep angle step of 5 deg aft and fore with prescribed wake code

138
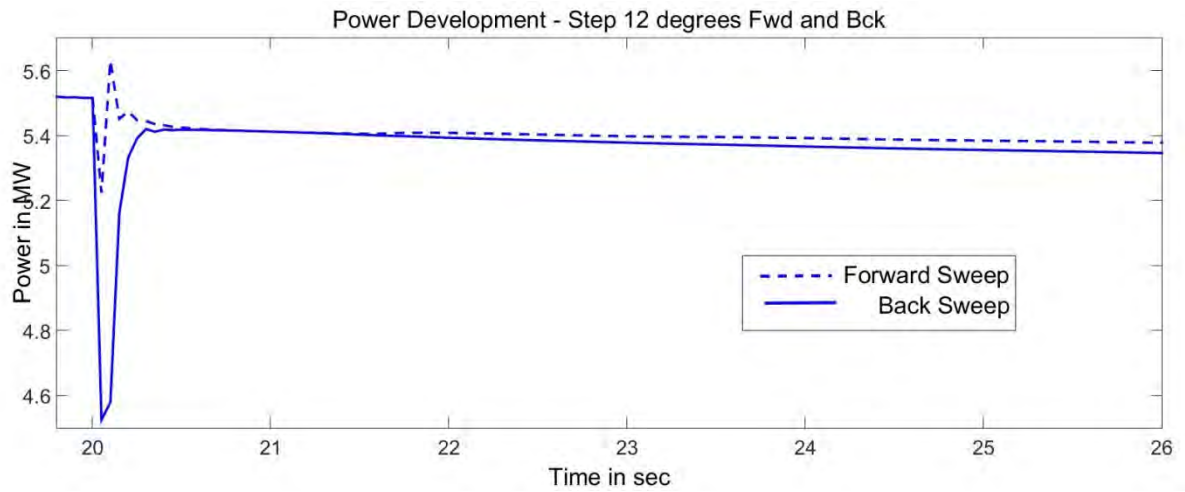
Figure 5.20 : Power Response after a sweep angle step of 12 deg aft and fore with prescribed
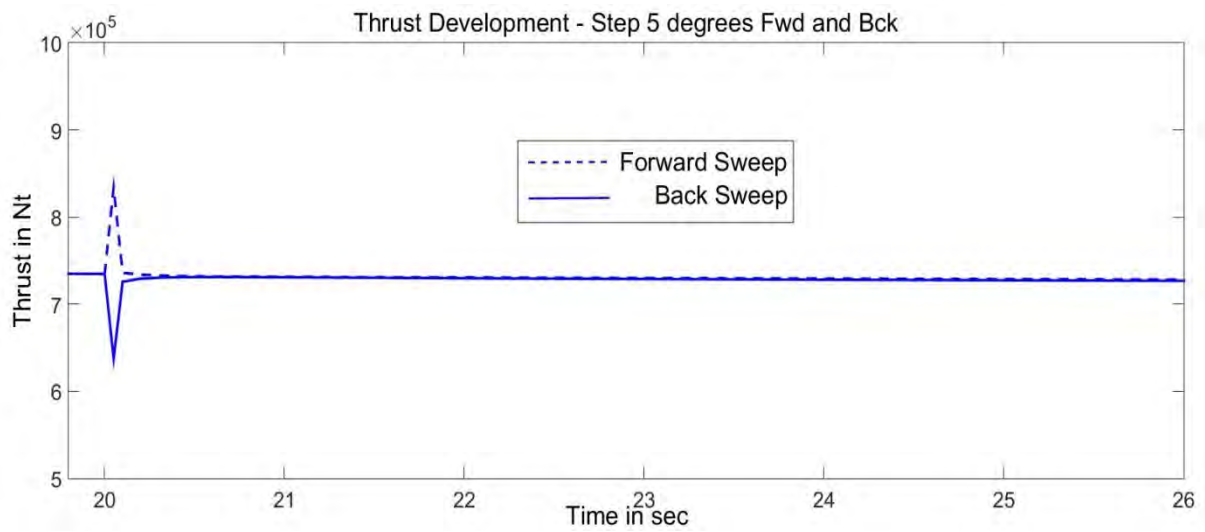
wake code

Figure 5.21 : Total Thrust Response after a sweep angle step of 5 deg aft and fore with
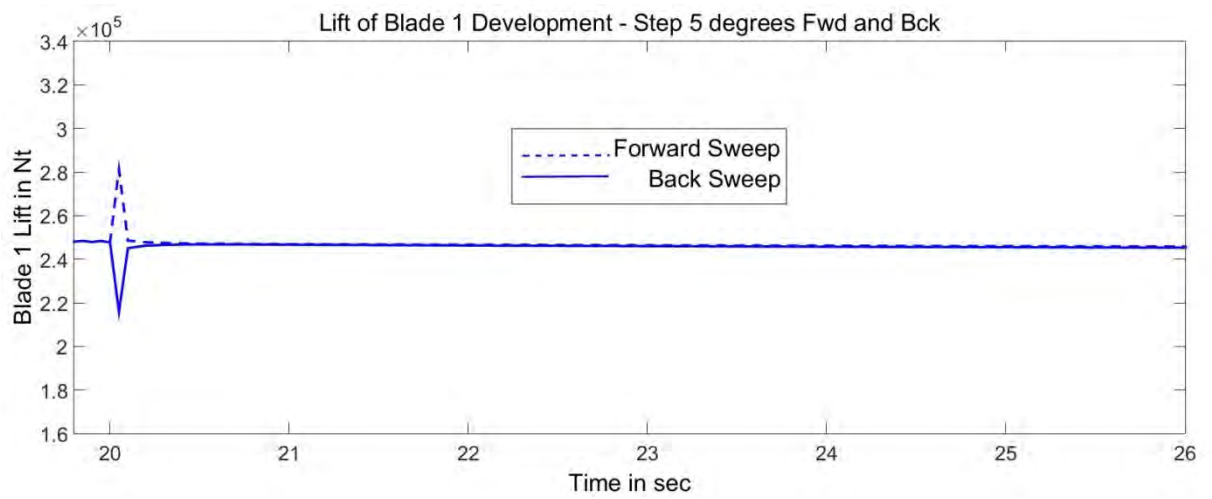
prescribed wake code

139
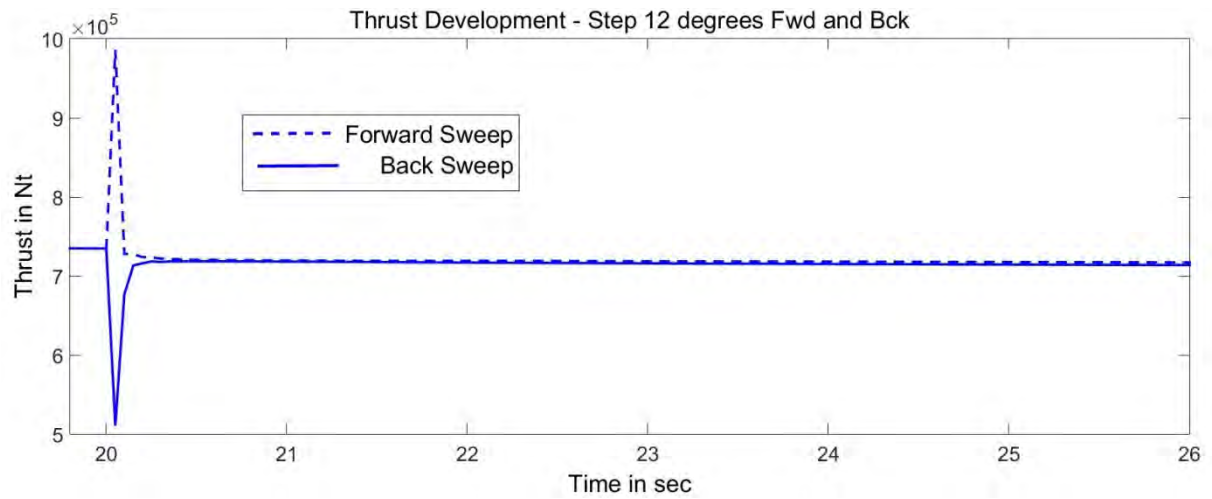
Figure 5.22 : Total Thrust Response after a sweep angle step of 12 deg aft and fore with

prescribed wake code

Figure 5.23 : Blade No 1 Lift Response after a sweep angle step of 5 deg aft and fore with
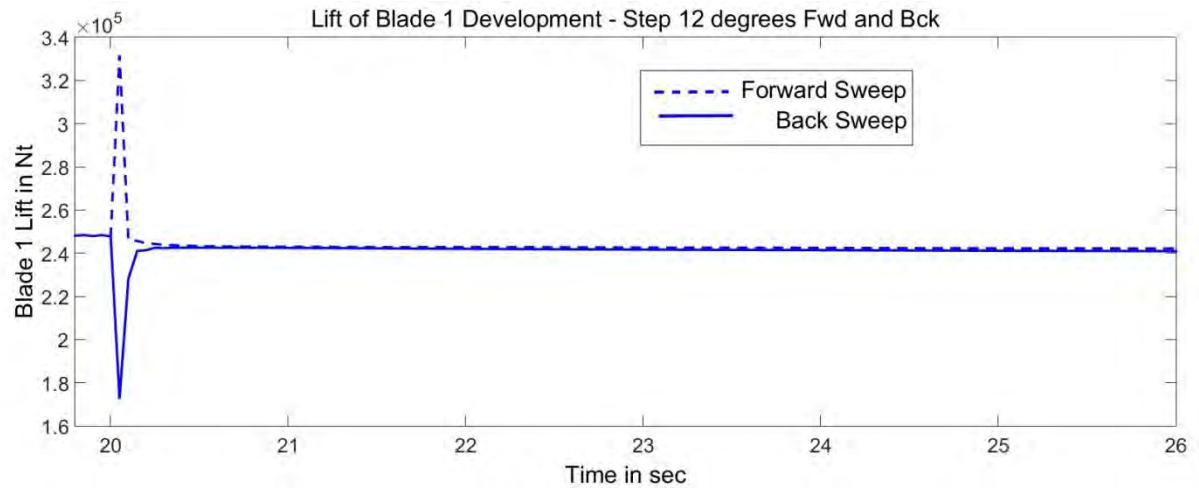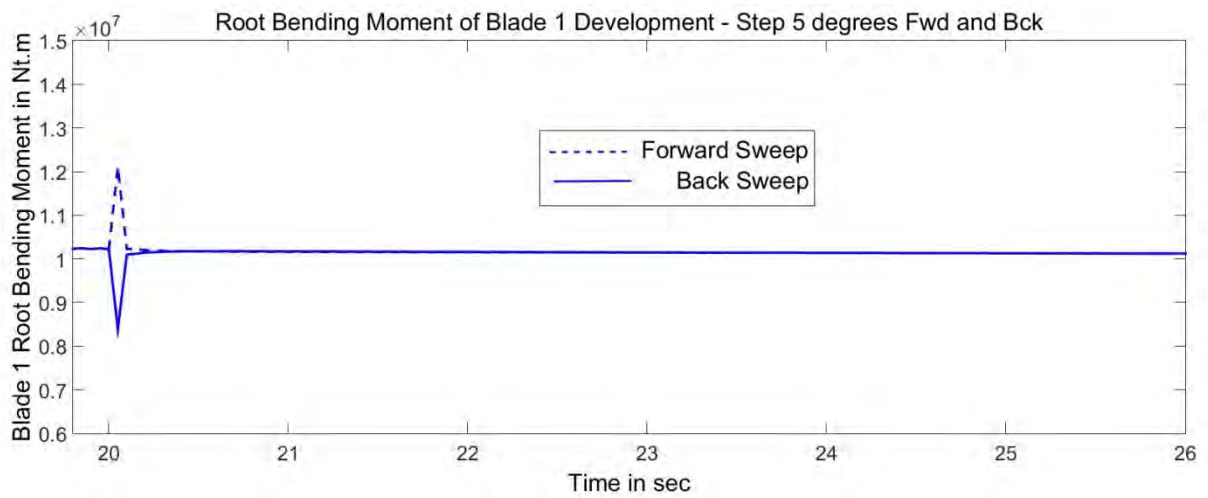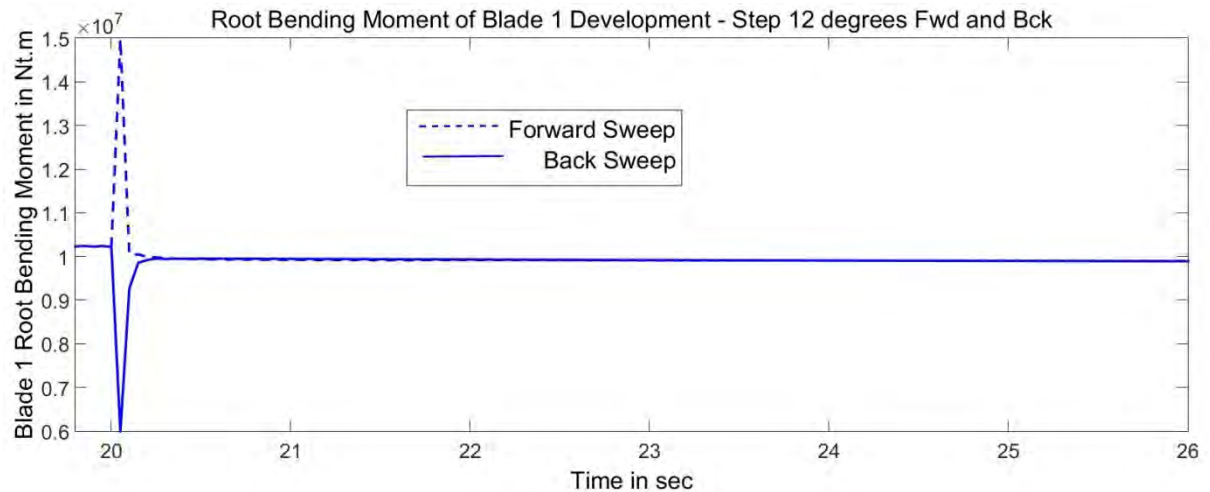
prescribed wake code

140

Figure 5.24 : Blade No 1 Lift Response after a sweep angle step of 12 deg aft and fore with

prescribed wake code

Figure 5.25 : Blade No 1 Root Bending Moment Response after a sweep angle step of 5 deg

aft and fore with prescribed wake code

141

Figure 5.26 : Blade No 1 Root Bending Moment Response after a sweep angle step of 12 deg aft and fore with prescribed wake code

It is seen that the direction of sweep plays an important role mainly at the moment of sweep angle change, where the additional velocity (figure 5.2) is maximum. Starting from the power curve a double peak response is observed in the fore sweep case where in the aft sweep only one. This fact can be explained as follows: At the time when the swept part of the blade obtains a forward velocity (relative to the movement of the blade), a reduction in their effective angles of attack and a rise in their resultant velocities is induced. According to figure 2.11 , torque is proportional to the sinus of the angle of attack and so it is largely affected by its reduction and drops accordingly. In the next step, when the tip has moved to its new position and the angles have recovered, power rises again and then starts to converge in a new value which is slightly lower to that before the step. This happens because of the swept tip and the reduction in the distances of the swept sections relative to the axis of the turbine. In the aft-swept case the backward velocity of the tip, leads to a rise in the angles of attack and fall to the resultant velocities. So, power drops accordingly at this stage and when the tip sweeps back to its new position power rises again and converges to a lower value of that before the step due to the same reasons of the forward case.

142

It is concluded that the direction of sweep affects the dynamic response of power in a different way. In both cases power initially falls but for different reason - in the first case due to angle of attack reduction and in the second case due to resultant velocity reduction. The strength of the resultant velocity is higher and explains the large drop in the aft - sweep case and the absence of a second peak during the recovery. Of course, the higher the sweep angle step the higher the effect and it seems to behave in a non - linear way. In particular, the percentage of reduction for the forward cases of 5deg and 12 deg are respectively -1.62% and -5.29% and for the backward cases -2.48% and - 17.97%. However, it has to be mentioned that in the 12 deg aft-sweep case (with this specific configuration of the wind turbine) the angle of attack of the most far blade section reaches a value of 79.9 deg during the step - deep into the stall area. In this area this model cannot take into account dynamic stall phenomena and so needs to be modified accordingly. Finally, as for the converged power value the different direction of sweep - which allocates accordingly the swept elements - and the fact that the "hinge" is set to the quarter chord (1/4c) leads to a slight difference in the order of 0.33% and 0.75% respectively.

Taking a look to the other figures it is seen that lift, thrust and blade root bending moment respond in an opposite way for opposite sweep directions. According to figure 2.11 thrust is largely connected to blade Lift and so does the root bending moment which is equal to the thrust of every section multiplied by its distance from the turbine axis. So, same dynamic behavior is met for these three parameters. In specific, when the tip sweeps forward the angles of attack reduce and the resultant velocity increases and vice versa. The percentage of rise for the 5 degrees forward step is 13.53%, 13.49% and 18.52% where for the 12 degrees step is 34.2%, 33.85% and 46.65% respectively. In addition, the percentage of drop for the 5

degrees backward step is -13.3%, -12.8% and -17.95% where for the 12 degrees step -30.5%, -30.37 and -41.58% respectively.

Therefore, it is seen that the percentage of change for every parameter is larger with a larger step and root bending moment is the most affected parameter. Also, every of them converges quickly to its new value with minor differences between forward and backward steps (in the order of 0.5%). Although these results suppose a linear behavior of the problem, large steps must be treated according to dynamic stall theory and define the limits of this linearity.
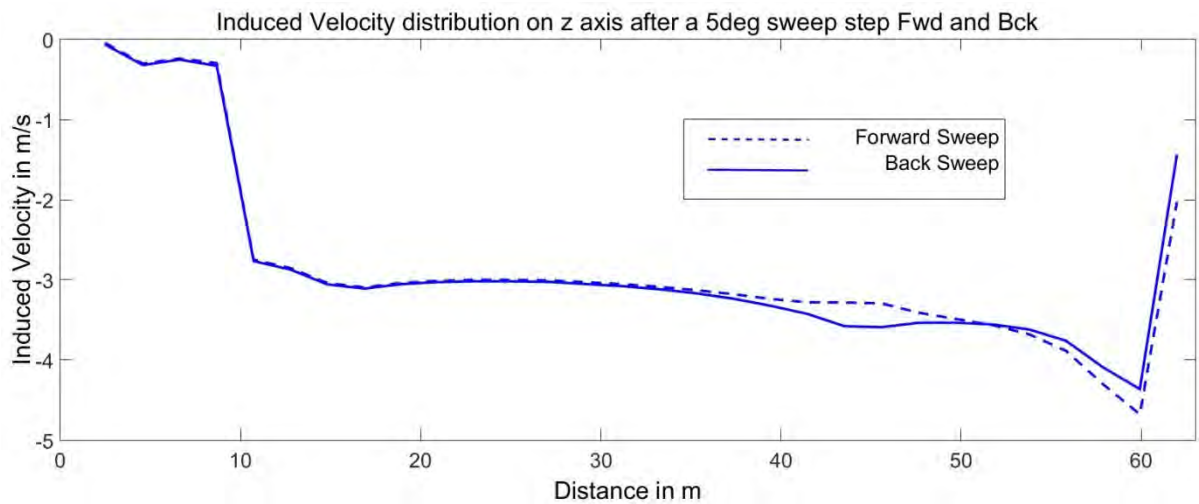
Figure 5.27 : Z-axis Induced Velocity Distribution 20 secs after a sweep angle step of 5deg

Fore and Aft

144
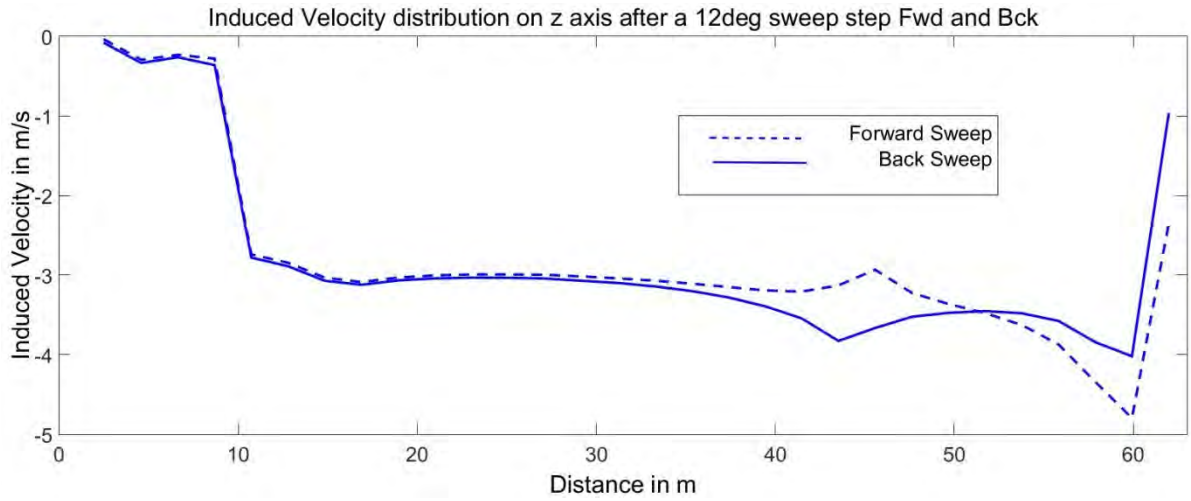
Figure 5.28 : Z-axis Induced Velocity Distribution 20 secs after a sweep angle step of 12deg
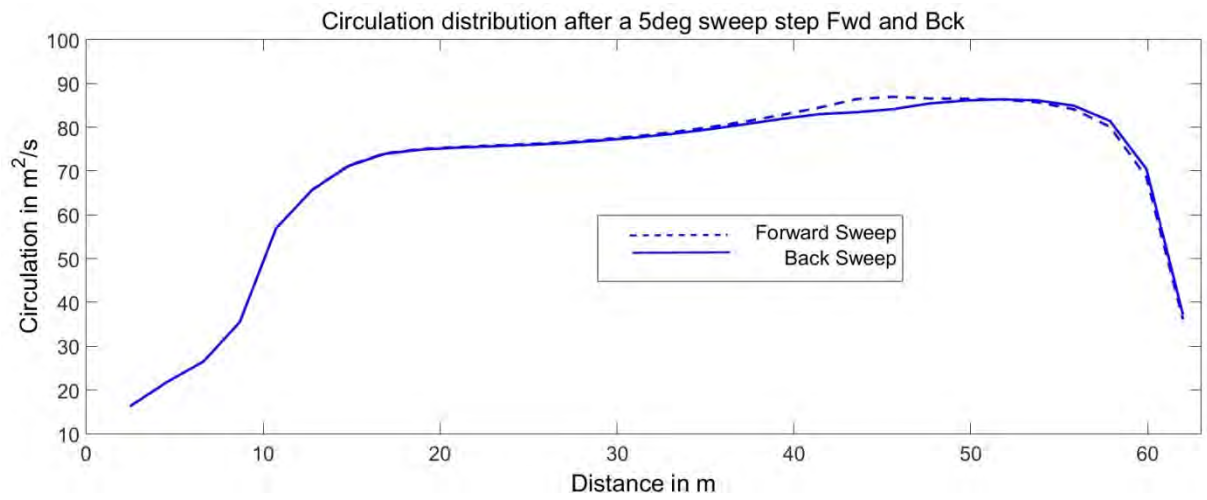
Fore and Aft

Figure 5.29 : Circulation Distribution 20 secs after a sweep angle step of 5deg Fore and Aft
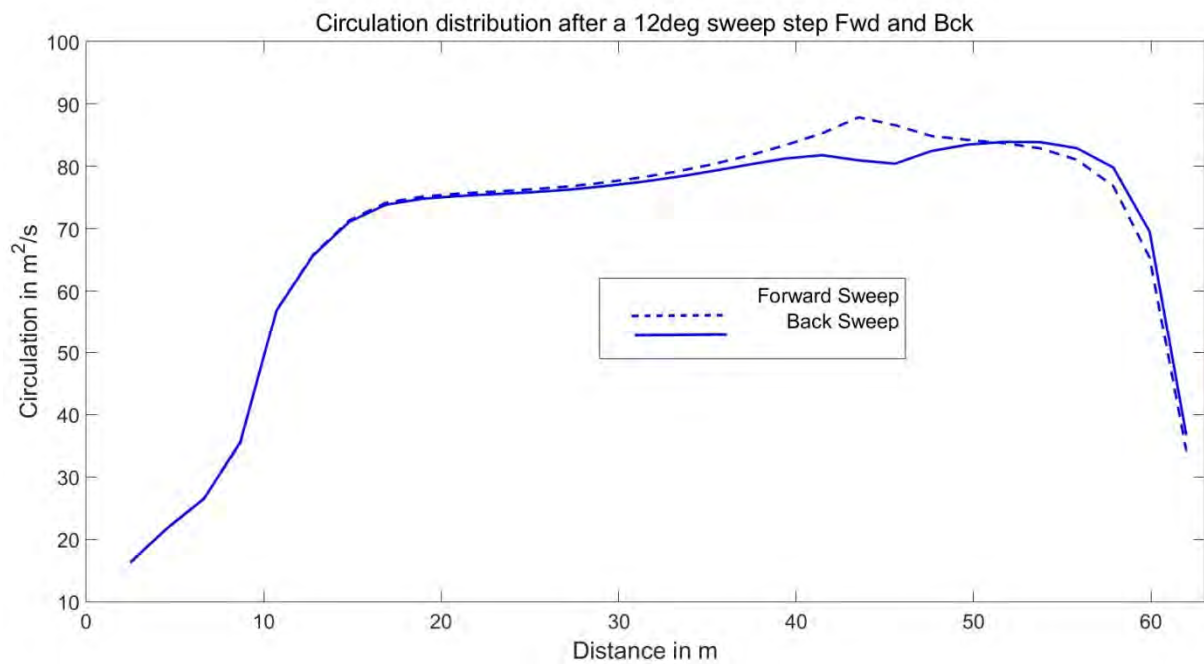
145

Figure 5.30 : Circulation Distribution 20 secs after a sweep angle step of 12deg Fore and Aft

The above figures clearly show the effect of tip sweep on z-axis induced velocity and in turn on circulation distributions 20 seconds after a step in tip sweep. This effect is obvious mainly in the swept part area and a few meters before the "hinge" and is stronger for larger steps. It has opposite results for opposite directions with the forward case introducing higher loads in the hinge area and the backward case introducing higher loads in the tip area. Still, the overall loads lie below that of the un-swept case and as shown earlier the differences between the two cases is minimal yet, the distribution of them is always of higher importance in such applications.

5.4.4 Harmonic response - Prescribed wake code

A more analytical picture about the dynamic response of a wind turbine concerning blades with variable tip sweep can be gained through a harmonic motion of this part of the

146

blade, in this case 30% of the overall span. Equation 5.2 is the equation of the examined harmonic motion:

$$\Lambda = \Lambda_0 \sin \omega t$$

(**5.2**)

where:

- Λ is the sweep angle of the swept tip (positive for backsweep and negative for forward sweep)

- Λ_0 is the amplitude of the harmonic motion

- ω is the angular velocity of the swept part

In the following cases the amplitude of oscillations was set to 5 degrees and the angular velocity ω, to pi/4, pi/2 and pi in accordance with the requirement for absent dynamic stall phenomena. The parameters depicted with this variation scheme on the blade tips are power and thrust of the turbine and lift - root bending moments of blade No1. The figures are sorted by increasing frequency and a snapshot of a complete motion is shown 8 seconds after its start. Also, positive sign of sweep angles stands for backward sweep and vice versa.
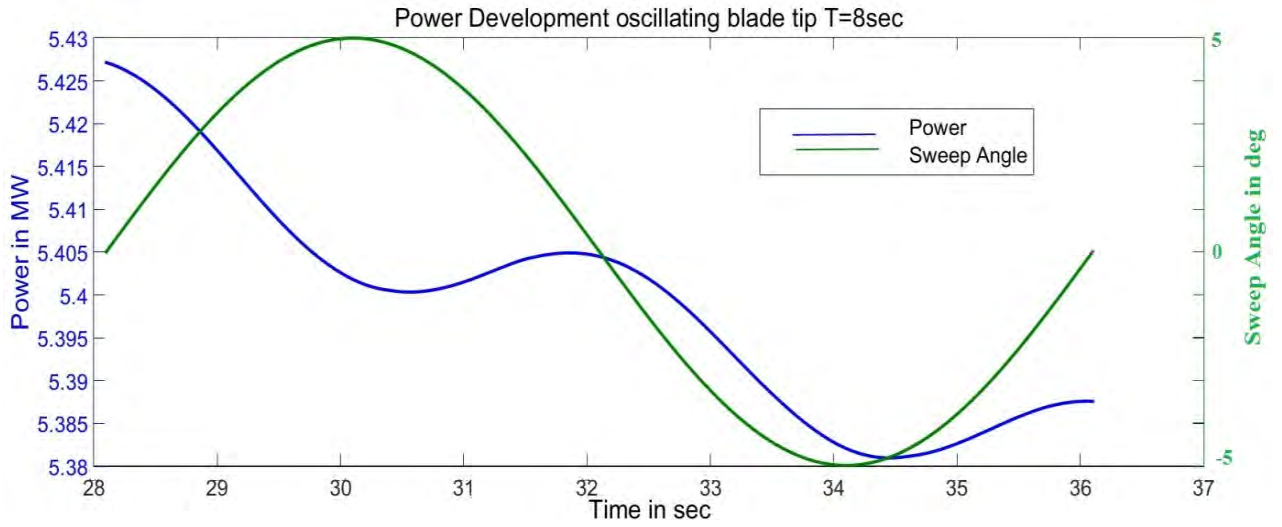
Figure 5.31 : Power Development for one complete harmonic tip sweep angle variation with
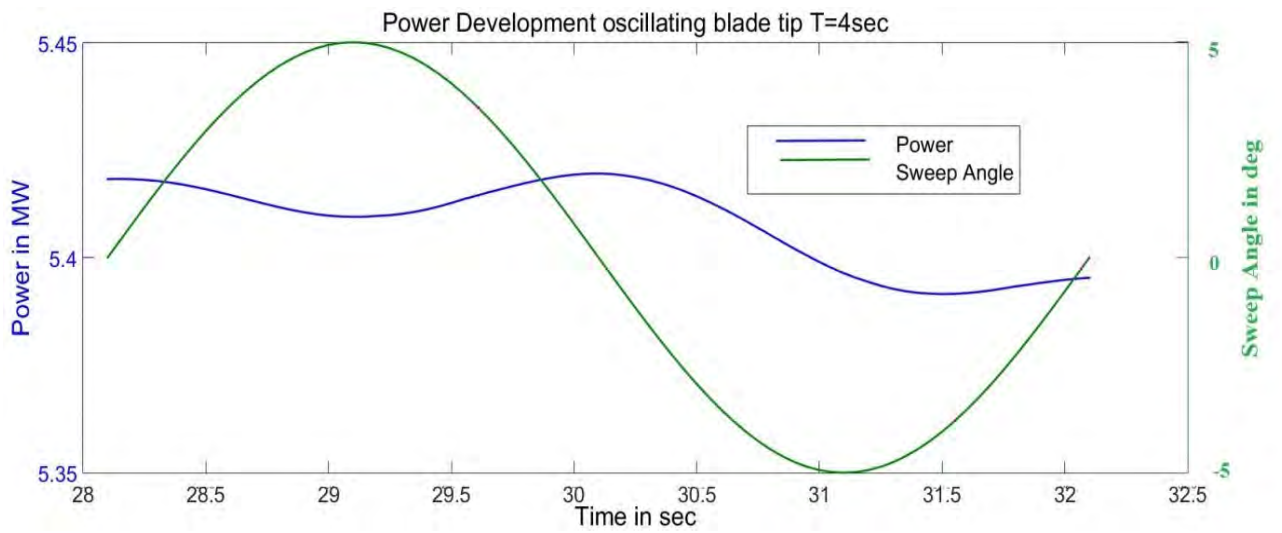
5deg Amplitude and Period T=8sec

Figure 5.32 : Power Development for one complete harmonic tip sweep angle variation with
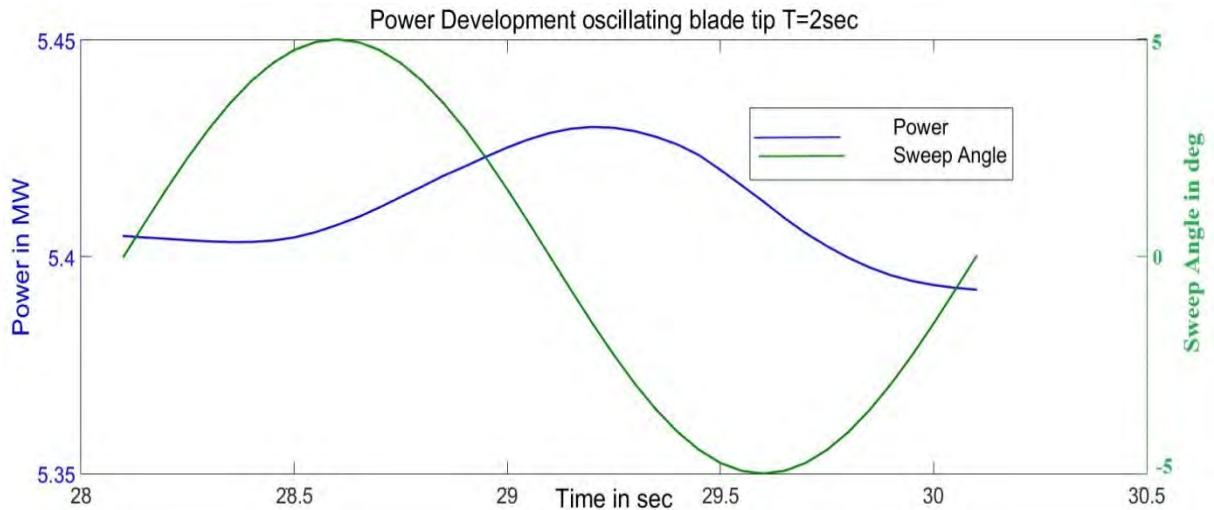
5deg Amplitude and Period T=4sec

148

Figure 5.33 : Power Development for one complete harmonic tip sweep angle variation with

5deg Amplitude and Period T=2sec

The power curve seems to change dramatically with the tip's sweeping frequency. When the motion is slow, the additional tip velocities are small and the rotor is allowed to follow the changes. Thus, the power is continuously dropping to achieve a new equilibrium governed mainly by the blade tip position (not the additional velocity) and a characteristic phase lag is observed during all phases of motion. When the tip oscillates faster, lead - lag phenomenon starts to show up. In particular, during the backward movement power seems to lead and during the forward movement to lag. In the faster case though, (T=2secs) the governing factor is the additional velocities and the shape of the curve has changed a lot. Local peaks are only seen when the tip passes the un-swept position with forward direction (i.e. with the maximum additional velocity) which results in equivalent blade's lift raise. On the other hand, valleys are observed when the tip passes the un-swept position but with the opposite direction.
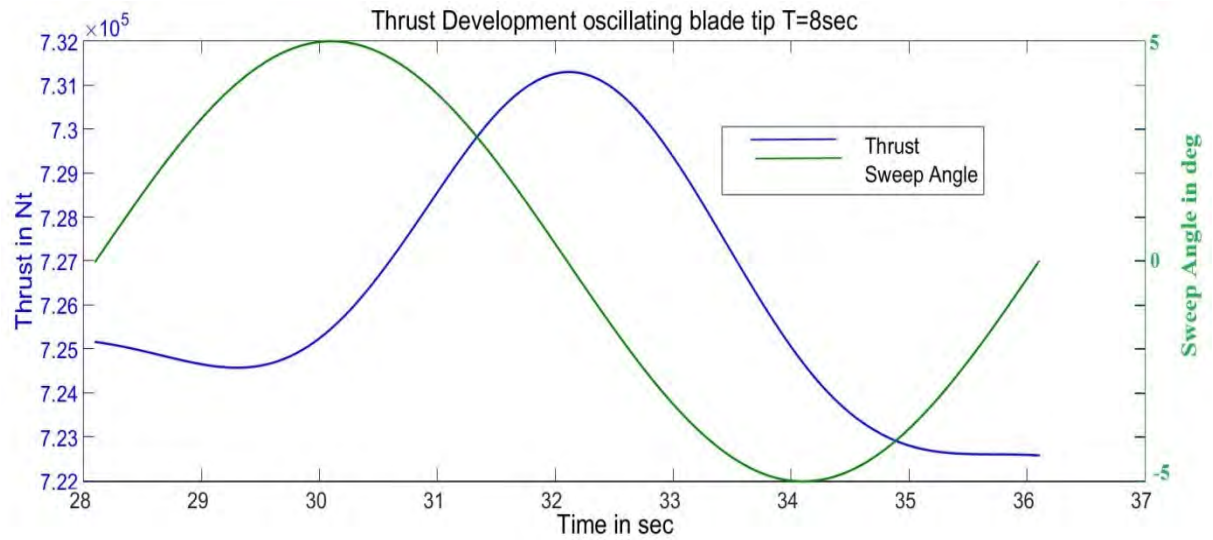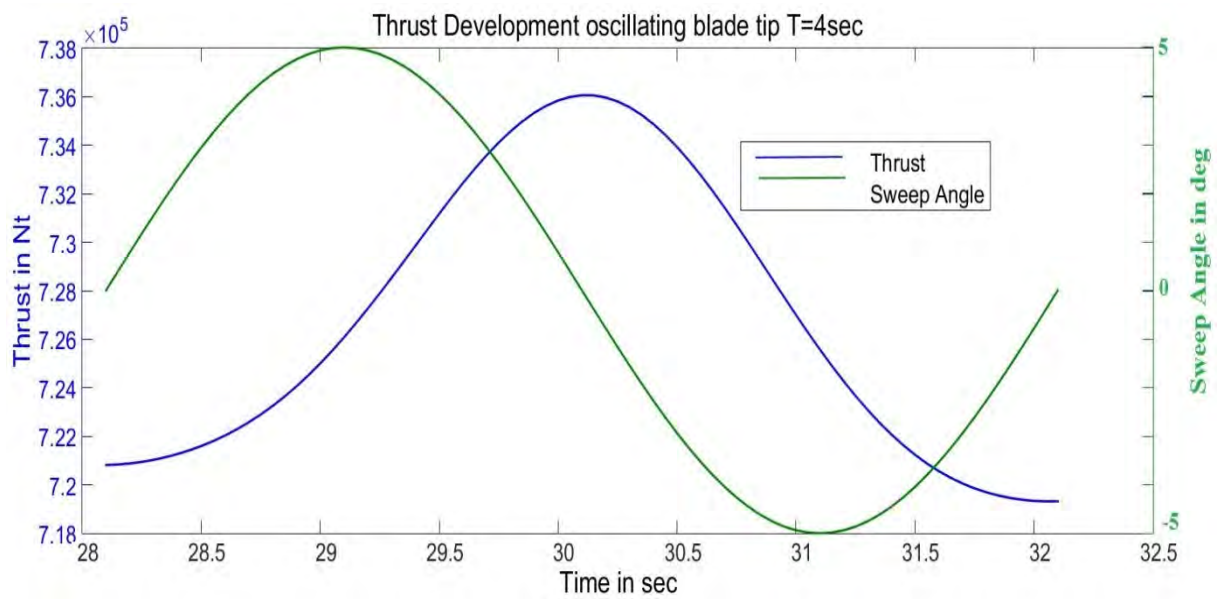
149

Figure 5.34 : Thrust Development for one complete harmonic tip sweep angle variation with

5deg Amplitude and Period T=8sec

Figure 5.35 : Thrust Development for one complete harmonic tip sweep angle variation with
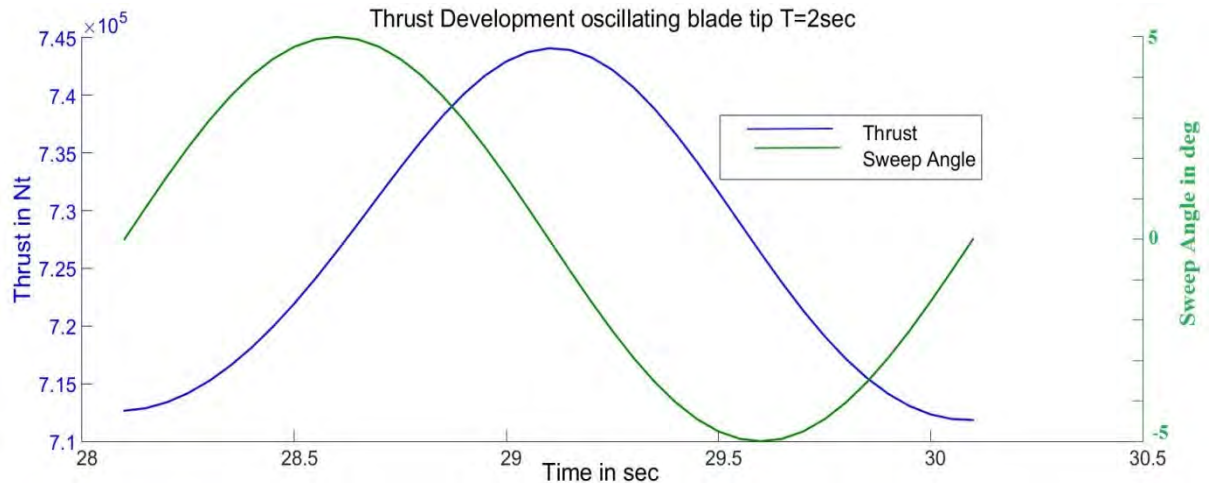
5deg Amplitude and Period T=4sec

150

Figure 5.36 : Thrust Development for one complete harmonic tip sweep angle variation with

5deg Amplitude and Period T=2sec

The Total thrust diagrams uncover a more definite picture about the behavior of this parameter in respect to the sweep angle variation frequency. As mentioned before, when step response was examined, this parameter is highly depended upon lift which converges faster than power. In specific, local peak occurs at the un-swept position of the blade with forward direction of movement and local valley at the same position with opposite direction. In the two cases of T=4sec and T=2secs were additional velocity is the predominant factor a phase lag is clearly seen. However, in the slow case T=8sec were the position (i.e. the tip sweep angle) plays also an important role, the local valley doesn't occur at the un-swept position but a few time steps later.

Of course, it is useful to calculate how much is this phase lag. So, embedded *Matlab* functions were utilized to calculate cross power spectral density, coherence function and phase lag from the two "signals" - sweep angle and Total Thrust response. It has to be noted though, that the number of values for both signals deriving from ULL, where multiplied manually in order to amplify their coherence. The following figures show the implementation of this methodology to calculate the phase lag for the T=2sec case:
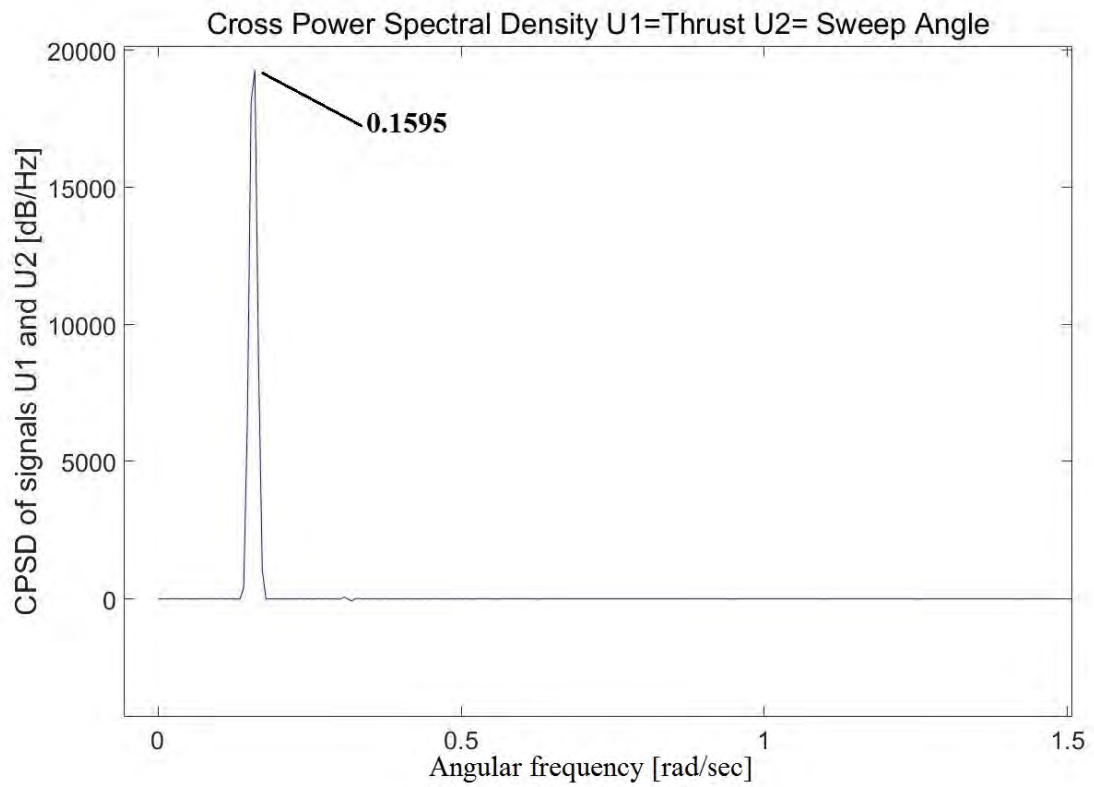
151

Figure 5.37 : Cross Power Spectral Density Thrust VS Sweep angle for the T=2sec case
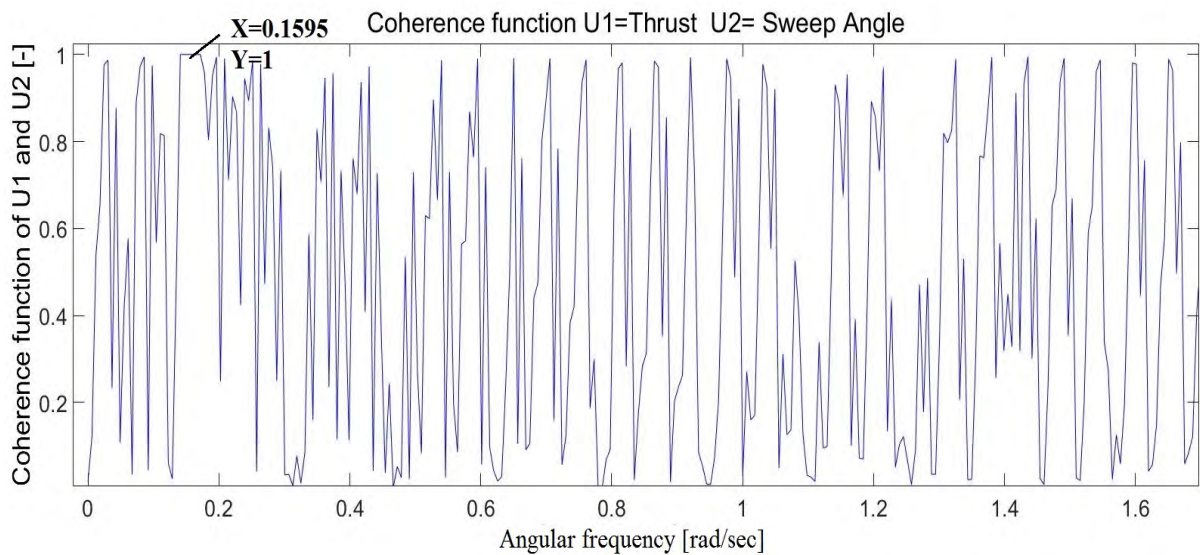

Figure 5.38 : Coherence Function of Thrust VS Sweep angle for the T=2sec case
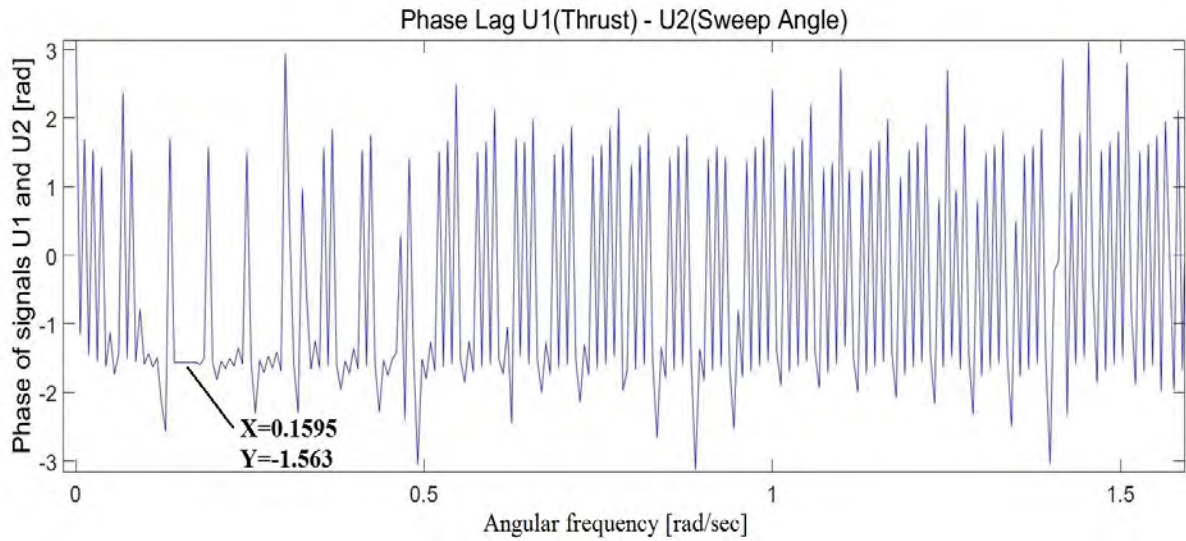
152

Figure 5.39 : Phase Difference between Thrust and Sweep angle for the T=2sec case

It is seen that these signals have the best coherence at angular frequency 0.1595Hz(rad/sec). This implies that they are best correlated (i.e. coherence function equals unity) for sampling Period of Ts = 2*π/0,1595 =39.39 samples (~40) or 40 * timestep(0.05s) = 2seconds. This of course is the period of the sinusoidal tip movement. However, phase lag is acquired from figure 5.39 which shows that Thrust - Sweep Angle equals -1.563 rad i.e. Thrust lags **89.55 degrees**. Accordingly, in the T=4sec case Thrust lags **87.49 degrees** and in the T=8sec case phase lag is **81.3 degrees.**
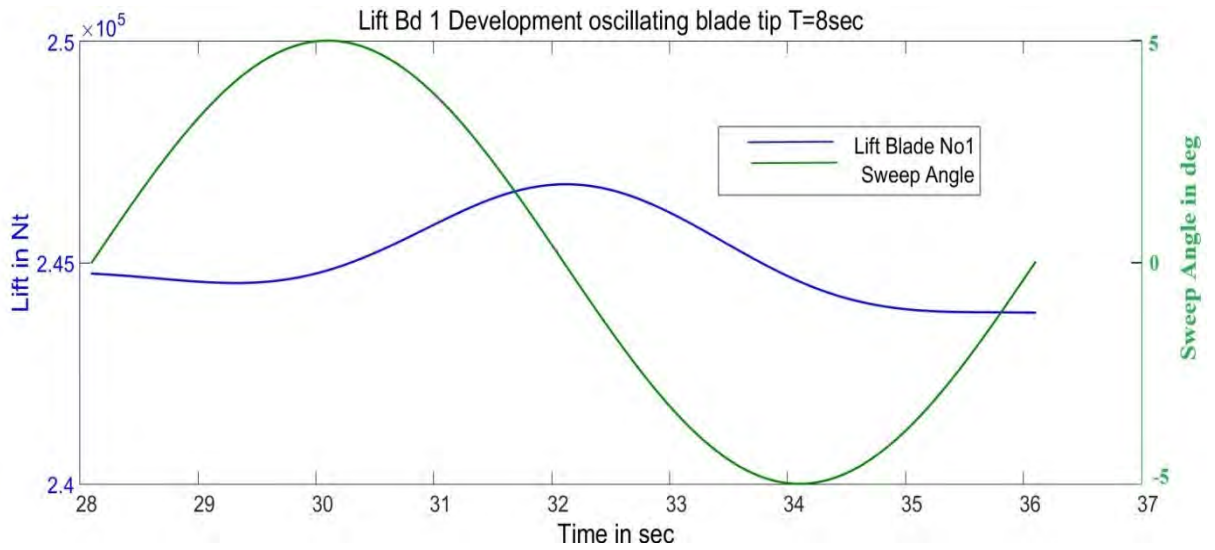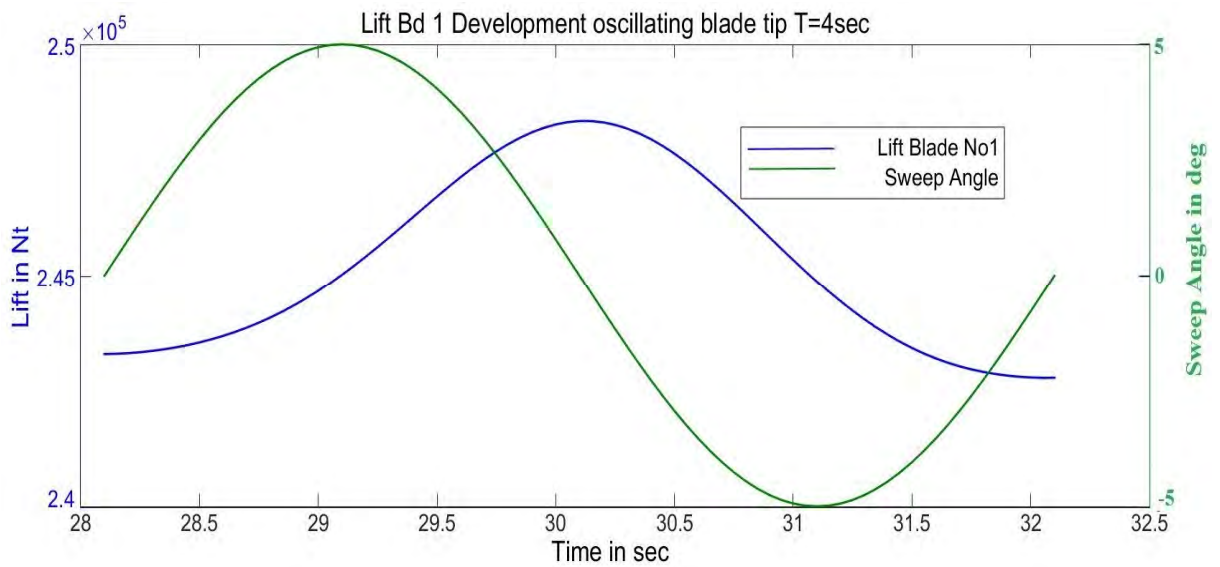
153

Figure 5.40 : Blade No1 Lift Development for one complete harmonic tip sweep angle

variation with 5deg Amplitude and Period T=8sec

Figure 5.41 : Blade No1 Lift Development for one complete harmonic tip sweep angle

variation with 5deg Amplitude and Period T=4sec

154
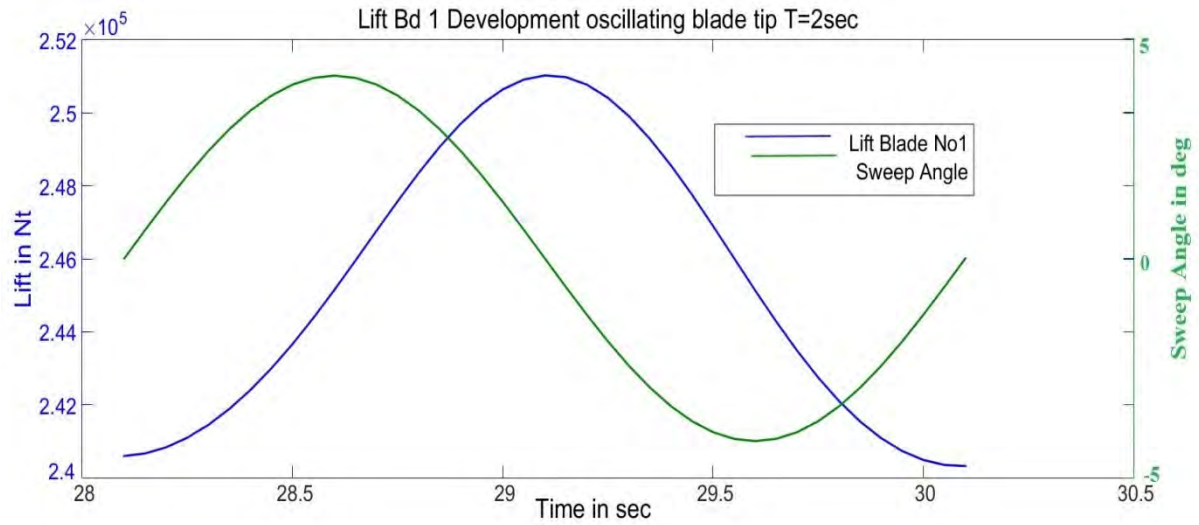
Figure 5.42 : Blade No1 Lift Development for one complete harmonic tip sweep angle

variation with 5deg Amplitude and Period T=2sec

As expected, it is seen that Blade Lift has the same behavior as Wind Turbine Thrust.
The phase lag for the cases of T=2sec, T=4sec and T=8sec are calculated at **89.66 degrees,
87.6 degrees** and **81.36 degrees** respectively.
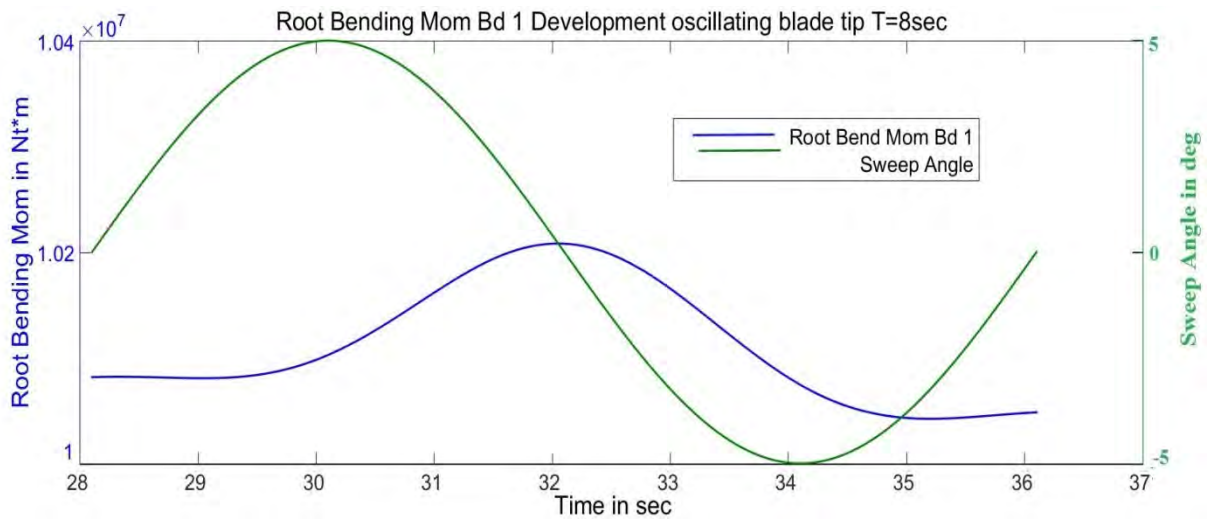
Figure 5.43 : Blade No1 out-of-plane Root Bending Moment Development for one

complete harmonic tip sweep angle variation with 5deg Amplitude and Period T=8sec

155

Figure 5.44 : Blade No1 out-of-plane Root Bending Moment Development for one complete

harmonic tip sweep angle variation with 5deg Amplitude and Period T=4sec

Figure 5.45 : Blade No1 out-of-plane Root Bending Moment Development for one complete

harmonic tip sweep angle variation with 5deg Amplitude and Period T=2sec

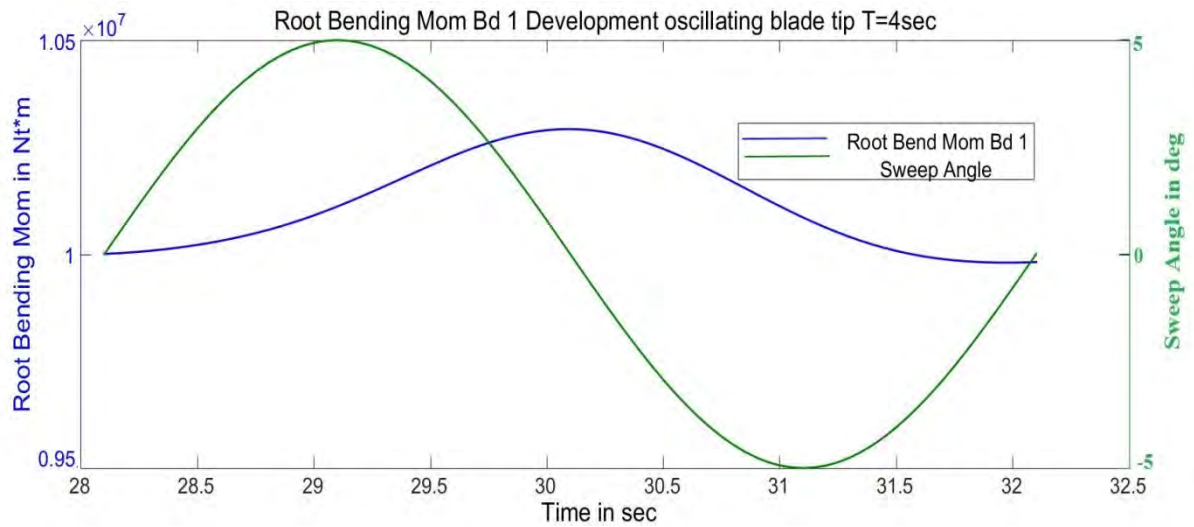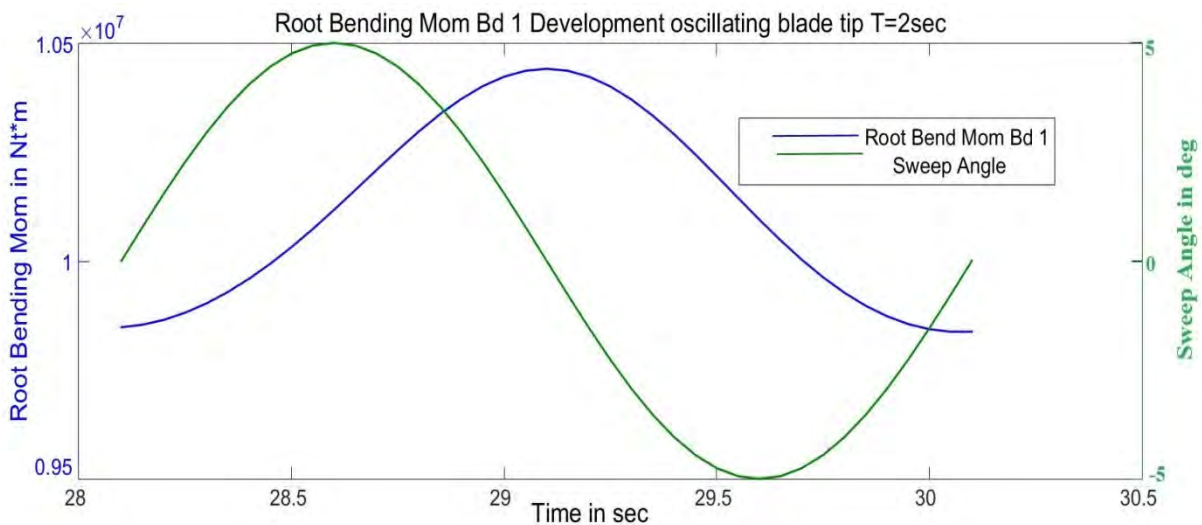Of course, neither the root bending moment of the blades can have different response

from Blade Lift, because they are highly depended upon it. In other words it equals lift

multiplied by the arm of the sections. Phase lag is calculated at **87.72 degrees, 84.62 degrees**

156

and **77 degrees** respectively. The minor differences of these values, compared to Lift phase lag values, are due to alterations to the length of the section arms during this motion scheme (paragraph 5.2 third issue).

A diagram presenting the phase lag versus the period of the oscillatory motion for Total thrust would be useful:
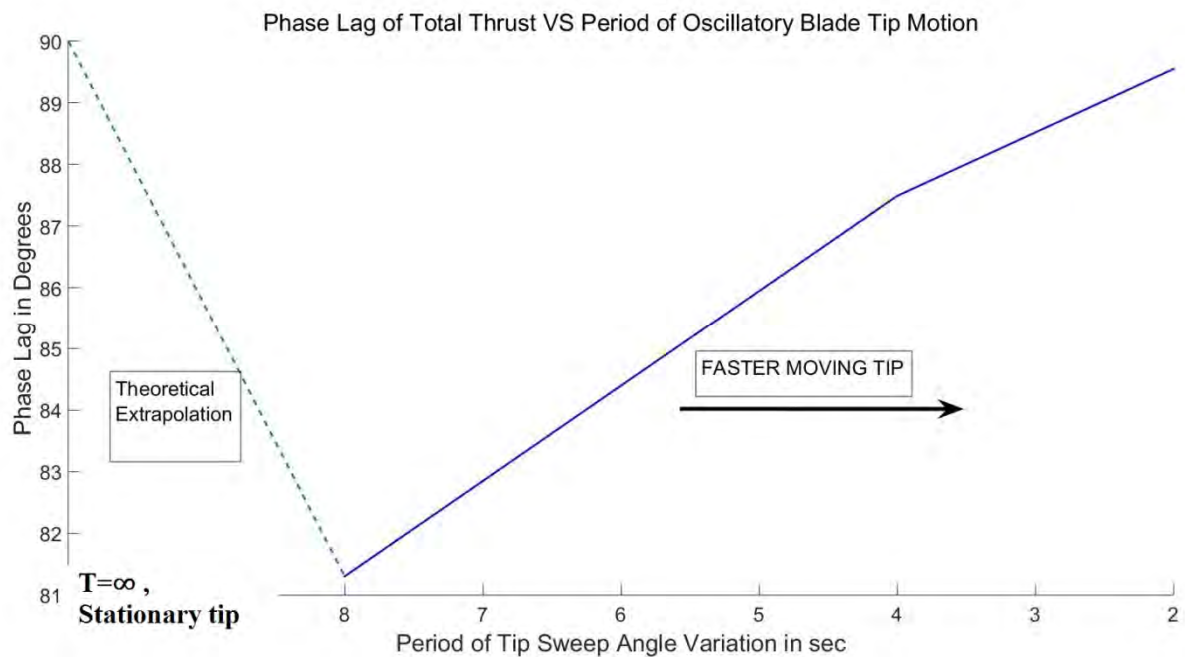
Figure 5.46 Period of oscillatory motion VS Phase lag of Thrust - Sweep Angle

The thick line represents the results from the examined cases where the dotted line is an extrapolation that corresponds to the stationary blade tip (T = ∞ and frequency =0) where the phase lag equals 90 degrees. This is presumed from figures 5.21 and 5.22 that show a reduction in Total thrust for either sweep angle direction (positive or negative). So, total thrust is maximum when sweep angle is zero (Λ=0) and thus phase lag between them equals 90 degrees. It is also seen in figure 5.46 that as the frequency of the moving tip is increased, the phase lag value initially drops and then tends to reach 90 degrees for a second time. This supports the statement that for low frequencies, tip sweep angle (i.e. the position) is the

157

predominant factor of the Wind Turbine performance and as it gets higher, lead lag effects start to show up until the additional velocities to the swept blade tips (due to their motion) create an obvious phase lag scheme.

5.5 Parametric study concerning the harmonic tip motion

In terms of obtaining an even better picture about the effect of tip sweep in a three bladed HAWT (in this case the 5MW reference wind turbine), the research extends to blade configurations of smaller tip sweep percentage, such as 10% and 20%. The simulations are performed on the same ULL model modified for the aforementioned configurations and focus on the harmonic tip motion (equation 5.2). In particular the amplitude of sweep angle Λ_0 is set to 10 degrees and the angular velocities are set to pi/4, pi/2 and pi. The effect of sweeping motion on three basic wind turbine parameters, Power, Thrust and Blade No1 Root Bending moment, is addressed through the non-dimensional variable N_{ratio} against the non-dimensional variable of f_{ratio} defined by equations (5.3) and (5.4).

$$ N_{ratio} = \frac{Amp(x)_s}{X_0} $$

(**5.3**)

where:

- $Amp(x)_s$ is the amplitude of the examined x parameter (power, total thrust or root bending moment of blade No1) that results from the harmonic tip motion.

- X_0 is the value of the same parameter in stable conditions (11.4m/s wind speed in this case) and un swept blade configuration (Λ=0).

158

$$f_{ratio} = \frac{f_{sw}}{f_{rot}}$$

<div align="right">(5.4)</div>

where:

- f_{sw} is frequency of the sweeping motion of the blade tip.

- f_{rot} is rotational frequency of the rotor.

Figure 5.47 presents the effect of harmonic sweeping motion of the blade tip on three basic wind turbine parameters and figures 5.48 , 5.49 and 5.50 show the same effect individually.

Figure 5.47 N_{ratio} VS f_{ratio} for Power Total thrust and Blade No1 root bending moment concerning a 10%, 20%, 30% tip swept rotor at rated operation (V=11.4m/s) and sweep angle variation according to Λ=10sin(ωt) for ω = pi/4, pi/2, pi

159
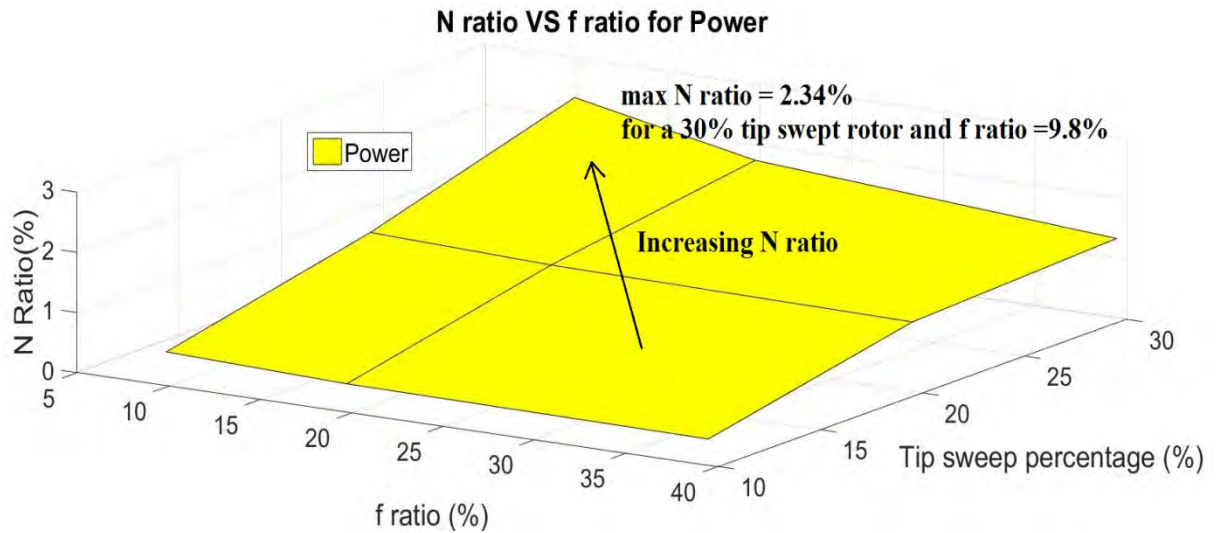
Figure 5.48 N_{ratio} VS f_{ratio} for Power concerning a 10%, 20%, 30% tip swept rotor at rated operation (V=11.4m/s) and sweep angle variation according to $\Lambda=10\sin(\omega t)$ for ω = pi/4, pi/2, pi

Figure 5.49 N_{ratio} VS f_{ratio} for Total thrust concerning a 10%, 20%, 30% tip swept rotor at rated operation (V=11.4m/s) and sweep angle variation according to $\Lambda=10\sin(\omega t)$ for ω = pi/4, pi/2, pi

160

N ratio VS f ratio for Blade No1 Root Bending Moment
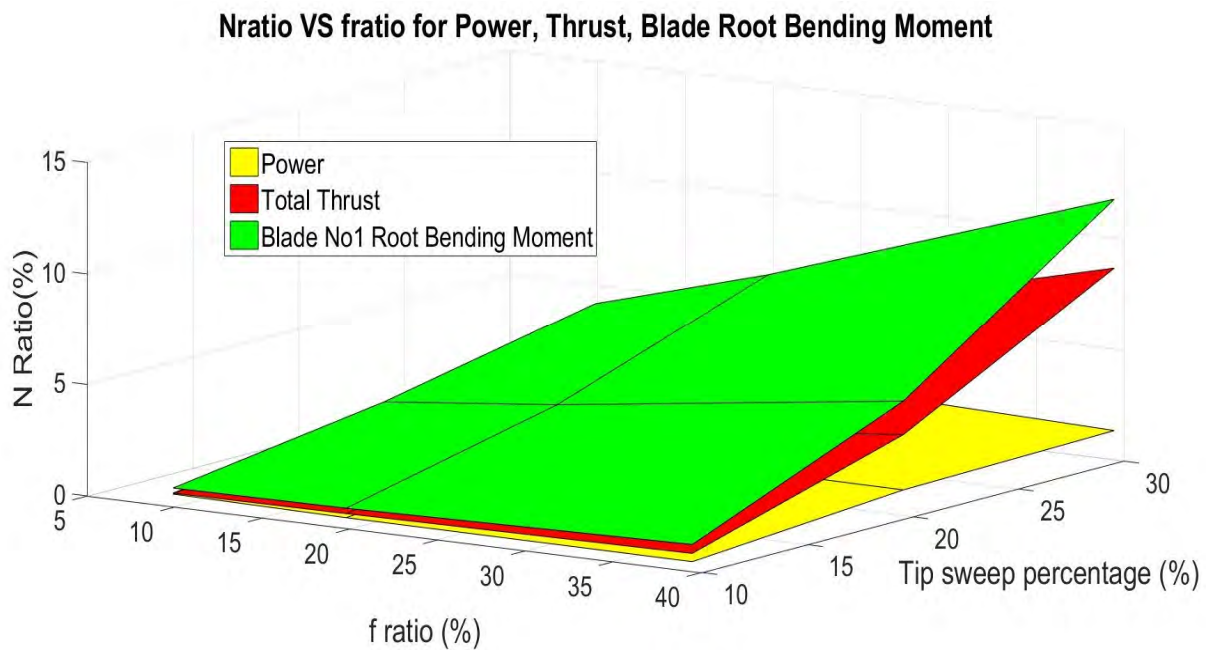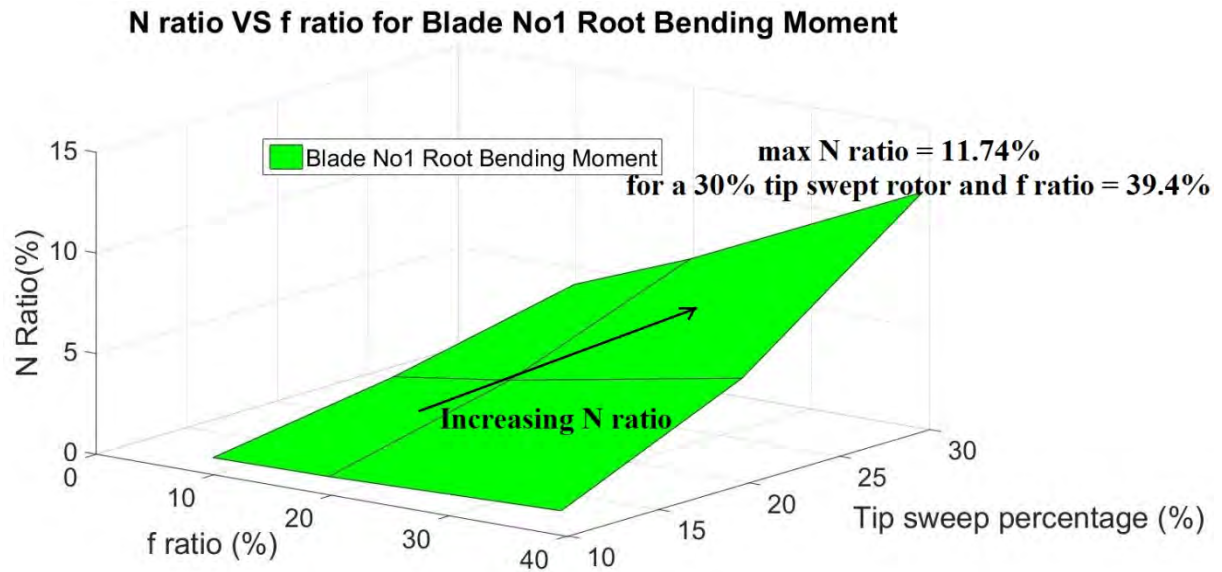
Figure 5.50 N_{ratio} VS f_{ratio} for Blade No1 root bending moment concerning a 10%, 20%, 30%

tip swept rotor at rated operation (V=11.4m/s) and sweep angle variation according to

$\Lambda=10\sin(\omega t)$ for ω = pi/4, pi/2, pi

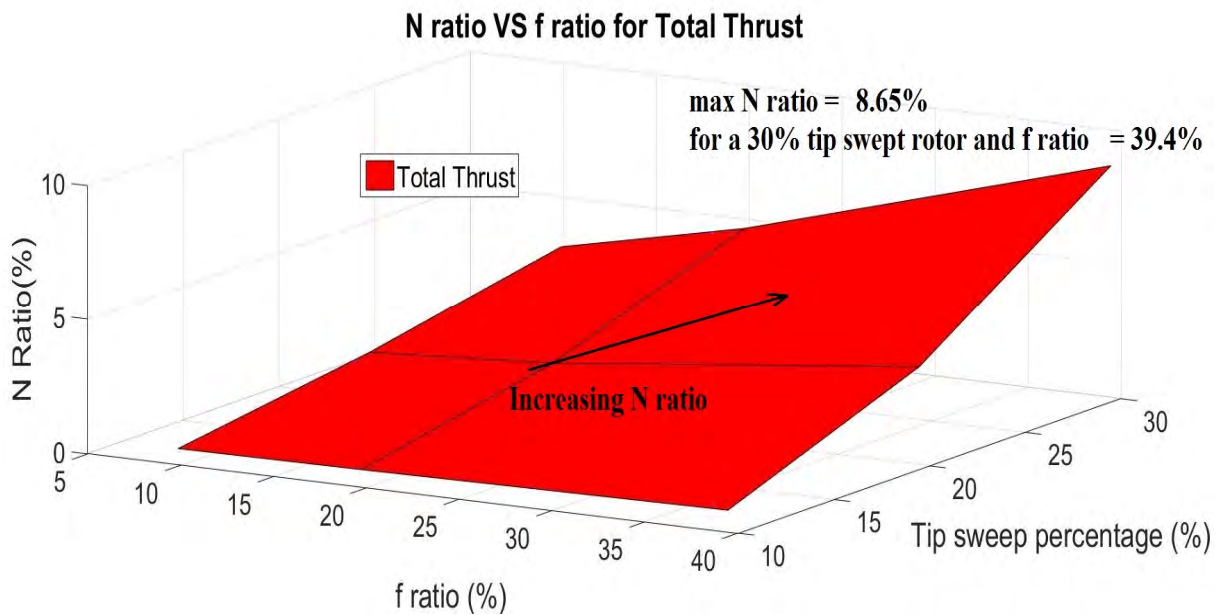As expected, every parameter is affected from the sweeping motion, with Blade No1

root bending moment being the most affected one. The same conclusion was obtained in

paragraph 5.4.3 concerning the step changes in sweep angle. In addition, power seems to have

a different behavior compared to Total thrust and Blade root bending moment in terms having

N_{ratio} increase direction. In particular as sweeping motion increases in frequency, the

amplitude of power decreases. However, all parameters increase with higher tip sweep

percentage of the rotor blades. The maximum N_{ratio} value for every parameter is accordingly

2.34%, 8.65% and 11.74% for a 30% tip swept rotor and f_{ratio} 39.4% - namely for a sweeping

motion frequency about half the rotational frequency of the rotor.

Thus, it is concluded that tip swept rotors have a higher impact on out of plane loads

(namely Thrust and blade root bending moment which is directly connected to thrust –

equation 2.45) rather than in plane loads (namely power 2.46). So, if variable blade tip sweep

161

is to be developed as a control feature it is presumed that it would be more suitable for load reduction rather than power improvement.

5.6 Conclusions

In this Chapter the implementation of Unsteady Lifting Line Theory on the reference Wind Turbine NREL 5MW which incorporates tip swept blades is performed. The basic goal is to uncover the influence of variable blade tip sweep angle on the wind turbine's loads and performance. However, only the aerodynamic impact of this geometric feature is examined. The results can be used as reference in developing an active control device with the ability to compensate for fatigue loads on blades during unsteady conditions or to maximize energy capture. In addition, useful conclusions can be drawn for conventional wind turbines whose flexible blades undertake edgewise oscillations during operation and result in tip sweep - like variations.

The geometric feature of tip - sweep is modeled through a blade whose tip has the ability to pivot backwards or forward about a vertical axis that passes through the quarter chord. The effect of this feature on the wind turbine performance is expressed as a reduction in lift generated by the swept blade sections and governed by equation 4.1 ,as a modification in the resultant velocities of the swept blade sections expressed with equation 5.1 and as a reduction in rotor diameter.

Results of the model are obtained through an inviscid code written in Matlab, in two configurations. Both are based on the Unsteady Lifting Line Theory however the wake can be either prescribed or free to develop and reveal a physical result expressed as wake roll - up, distortion and expansion. It is proven though that in this type of oscillation the prescribed wake configuration generates very similar results to the free wake configuration while

162

maintaining considerably low demands on computational resources. So, the prescribed wake code is an efficient choice to study the dynamic response of the reference wind turbine concerning blades with variable tip sweep.

The dynamic behavior is separated into two cases: The introduction of a small (5 deg) and a large (12deg) sweep angle step change with forward / backward direction at the blade tips and the harmonic variation of sweep angles there with three different frequencies. Starting from the step case, the parameters under study are power, thrust, Lift of blade 1, root bending moment of blade 1 and the distributions of induction and circulation of blade 1 20 seconds after the step. It is shown that in the beginning of the step power drops regardless of the direction of sweep but for different reason. Then, power converges to a new value - which is lower of that before the step - and in a manner which depends upon the direction and magnitude of the step. Furthermore, the converged value is practically equal for the forward and backward sweep. As for the other parameters (thrust - Blade Lift - Blade Root bending moment) opposite direction of sweep causes opposite peaks and larger sweep angles cause larger peaks which converge quickly to a new value. In fact wind turbine thrust and root bending moment are directly related to blade lift. The root bending moment is found to be the most affected parameter (in percent) by the sweep step. As for the induction and circulation distributions, it is seen that mainly the swept part of the blade and only a few meters of the un-swept blade are affected. Again opposite direction of sweep step generates opposite distribution in that area which is more altered as the step becomes larger. Of course, in wind turbine applications these distributions gain a more important role especially when the tip is included in the affected area.

The same parameters are studied, in the case of a harmonic sweep angle variation (of 5 degrees amplitude) at the blade tips in three different frequencies (ω=pi/4, pi/2, pi). The

power curve which converges slower than wind turbine Thrust, Lift and root bending moment of blade 1 is studied first. It is seen that at lower frequencies the predominant factor is the position of the blade and power has valleys when sweep angle value reaches maximum (forward or backward) and peaks when tip passes through the neutral position (sweep angle =0). As frequency becomes larger additional velocity gains more strength which causes the second peak (neutral position with backward direction) to reduce. In the fastest case examined (T=2 sec) lead-lag phenomenon is also observed. Lag refers to the most forward sweep angle and lead to the most aft. The rest three parameters (Total Thrust - Lift of blade No1 - Root Bending moment of blade No1) which generally converge faster than power present a more straightforward picture. The curves indicate a definite phase lag in respect to the tip sweep angle and in the order of 88 degrees which increases with increasing oscillating frequency.

Finally, a parametric study for three blade configurations (10%, 20% and 30% tip sweep percentage) is performed utilizing the same ULL based model with the suitable modifications for a harmonic sweeping motion of the blade tip and useful conclusions are obtained. The variable blade tip sweep feature has a higher impact on out of plane loads rather than in plane loads and thus it is more suitable for load reduction (fatigue or peak loads) rather than power improvement.

The originality that this chapter incorporates is the development of a robust ULL theory based model for a three bladed HAWT capable of modeling the effects of variable tip swept rotor blades on wind turbine parameters.

Chapter 6. Application Of BEM Method To Swept Bladed Rotors

In this chapter, a modified Blade Element Momentum (BEM) theory based model is presented for a three bladed HAWT (Appendix A.2). The innovation that this model incorporates is variable blade tip sweep capability. Firstly, the modeling of tip sweep in a BEM code is introduced. Thereafter, a comparison with a more accurate method in that case, an Unsteady Lifting Line (ULL) theory based model, uncovers the inherent inability of BEM to model correctly this blade geometric feature. In the end, the modification to the BEM code is presented along with results of representative cases which depict the improvement. The correction is obtained through a new Prandtl & Glauert based tip - loss correction adapted to tip swept blades and as such extends the applicability of BEM based models.

6.1 Introduction into the problem of correcting a BEM code according to tip swept rotor blades

Blade Element Momentum (BEM) theory is the basis of the most common engineering codes used by industries. The implementation of the theory in aeroelastic design codes constitute an integrated tool with very good accuracy and speed. However, since the development of the method many corrections have been implemented that take effectively into account trailing vorticity from the blades modeled by a tip loss factor, unsteady rotor wake dynamics modeled by a dynamic inflow model and unsteady airfoil aerodynamics modeled by Theodorsen theory [64], [119]. A recent work [110] based on the Near Wake

165

model originally proposed by Beddoes is a representative example of the current state of the art of high fidelity BEM codes. Every modification incorporated in BEM codes is derived either from experiments, simulations based on alternative methods or theoretical approaches. All of them contributed to the overcoming of BEM theory limitations.

One of the basic assumptions of BEM theory is that there is no radial flow interaction between the discretized annular regions of the rotor disk. In addition unsteady effects are often modeled independently for each region such as dynamic inflow and unsteady airfoil aerodynamics [110]. This implies that turbulent flows are not modeled correctly. It also implies that geometric features like tip sweeping of rotor blades cannot be modeled correctly because of the large radial changes in lift and velocity triangles that are induced due to partial movement of the blade. As an alternative vortex methods like ULL theory create a more physical result because of their embedded ability to account for wake structure phenomena [25]. The wake calculated by this theory is a vortex lattice (figure 2.1) which consists of shed and trailing vortices. The shed vortices include the history of the blade loads as parameters change (such as inflow velocity, blade pitch angle) and their effects are mainly local [36]. On the other hand trailing vortices account for the span-wise bound circulation distribution and play a more important role to the calculation of the blade loads. Among the trailing vortices that are produced from the discretized wing, the tip vortex has the greatest effect and this is accounted for by a tip loss factor correction.

Thus a suitable way to study the effect of tip swept blades and then incorporate the tip sweep capability in a BEM-based code for a three bladed wind turbine is through a Lifting Line theory based model. Of course, there are also other more analytical vortex methods such as the Vortex Lattice Method (paragraph 2.2) and even the more analytical Computational

166

Fluid Dynamics (CFD) method [21] however their high demands in computational time render them less suitable for this approach.

In this chapter, the idea of tip sweeping the rotor blades of a wind turbine is applied simultaneously to the three blades. Again the simulations refer to the 5MW NREL wind turbine of the previous chapter and the sweep configurations examined here are limited to engineering applications. In particular, one part of every blade tip (max 10% of the blade span) is able to pivot aft by the same degree of sweep angle (max 2 degrees) resulting in an in-plane movement which is depicted in figure 6.1 . The axis of rotation is located in the quarter chord (c/4) of the blade and the case of the forward sweeping is not examined at all because it is proven to generally increase the wind turbine loads [120] so, renders it impractical for engineering applications.

Figure 6.1 : Wind Turbine sweeping aft

6.2   Comparison of ULL Vs BEM - sweep uncorrected code

As mentioned before, the effect of variable tip sweep is examined through a ULL code with prescribed wake configuration that was presented in Chapter 5. This code was further improved in order to reduce the simulation time by utilizing CUDA platform [108] and its integrated support in Matlab. The process was accelerated up to 60 times and the part with

167

the largest volume of calculations (calculation of induced velocities on the control points) was executed by the Graphic Processor Unit (GPU). The reasons that render this method suitable for this investigation are that wind turbine blades are of high aspect ratio that allows the transfer of bound vorticity of the lifting surface on a single line and that wing geometric features like sweep (or dihedral) can be modeled quite accurately with this method. It is also proven in Chapter 5 that the prescribed wake code models at least, the basic physics and dynamics of the sweeping wing tip so it is used as reference for the design of the necessary correction to the BEM - based model.

As for the BEM based model (which is based on the aerodynamic part of DUSWAMP model [72] (Appendix A.2)) the following necessary improvements were implemented. The Prandtl - Glaeurt tip loss factor [51] to account for the trailing vorticity from the blades and a dynamic inflow model which considers an individual time constant for every radial distance were presented in [121] to model the unsteady rotor wake dynamics. However, unsteady airfoil aerodynamics analyzed in Theodorsen's theory [64], [119] are not considered because of the low reduced frequencies (equation 2.58) that are encountered in the cases studied in the current work.

The cases are separated into two groups - the first refers to a smooth sweep angle change of 10 and 20 degrees with a duration of 2 seconds and the second to the oscillating case of the sweep angle with a 0.25Hz motion frequency and amplitude of 20 degrees. In addition, the results are for the typical cases of 10% and 5% tip swept blades of the reference 5MW wind turbine operating at rated speed (12.1 rpm and wind of 11.4 m/s – Table 5.1) [117].

6.2.1 Comparison of ULL VS Uncorrected for sweep BEM code - Sweep Angle Change in 2 secs

At figures 6.2 ,6.3 and Figure 6.4 of rotor power, rotor thrust and total in-plane rotor force (raw parameters) are presented for the 10% and 5% respectively and then diagrams of induction distribution (blade parameter). The total simulation time in every case is 70 seconds with the first 60 seconds referring to the transient phase and only the seconds during sweep angle change are shown.
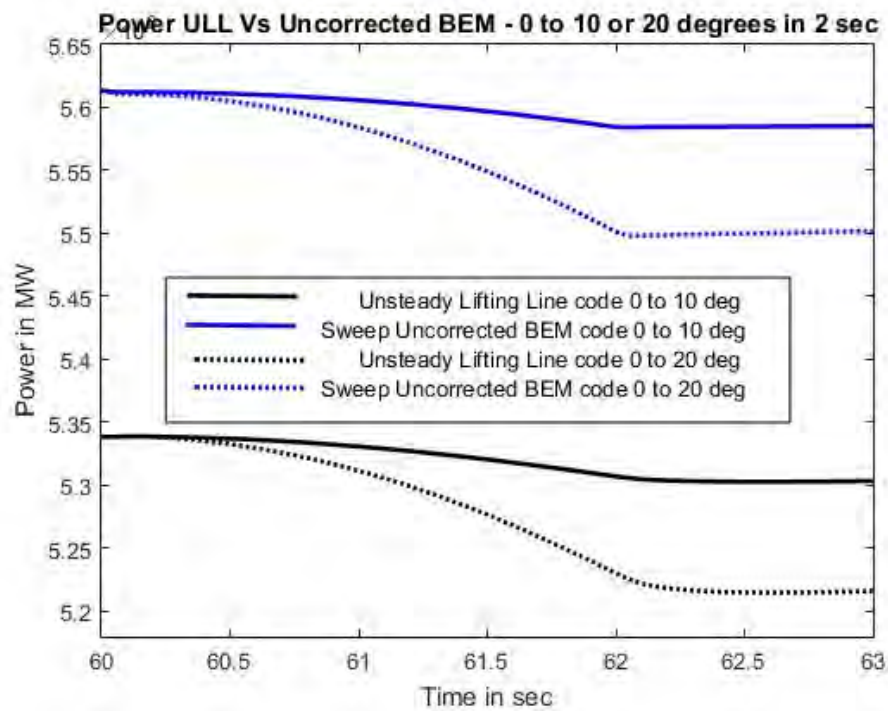

Figure 6.2: Power for ULL and sweep uncorrected BEM code 10 and 20 deg aft sweep 10% tip sweep
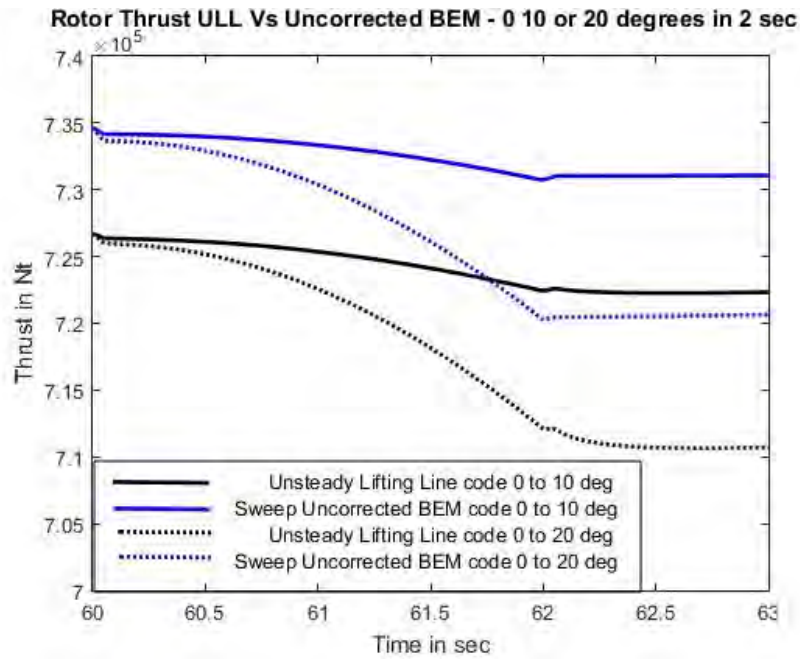
169

Figure 6.3: Thrust for ULL and sweep uncorrected BEM code 10 and 20 deg aft sweep 10% tip sweep
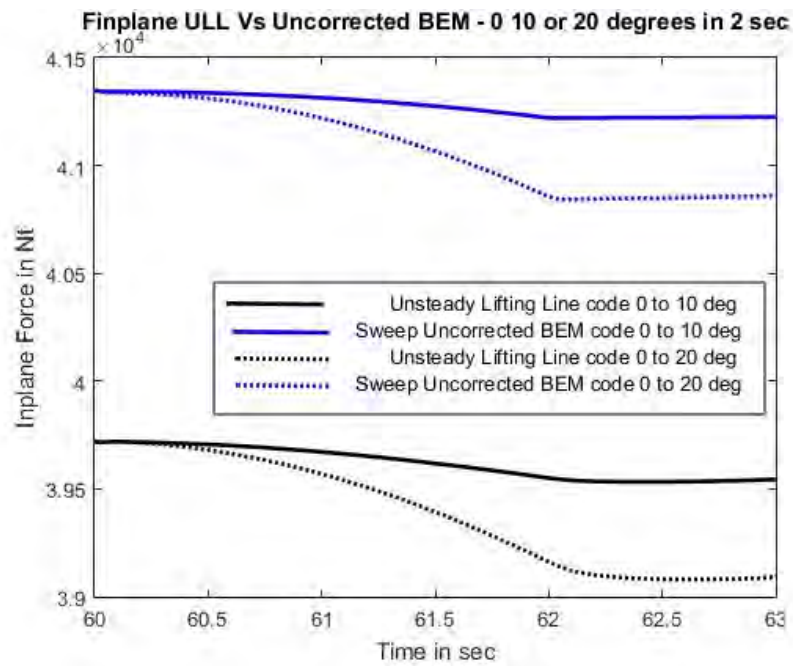

Figure 6.4 : In-plane Rotor Force for ULL and sweep uncorrected BEM code 10 and 20 deg aft sweep 10% tip sweep
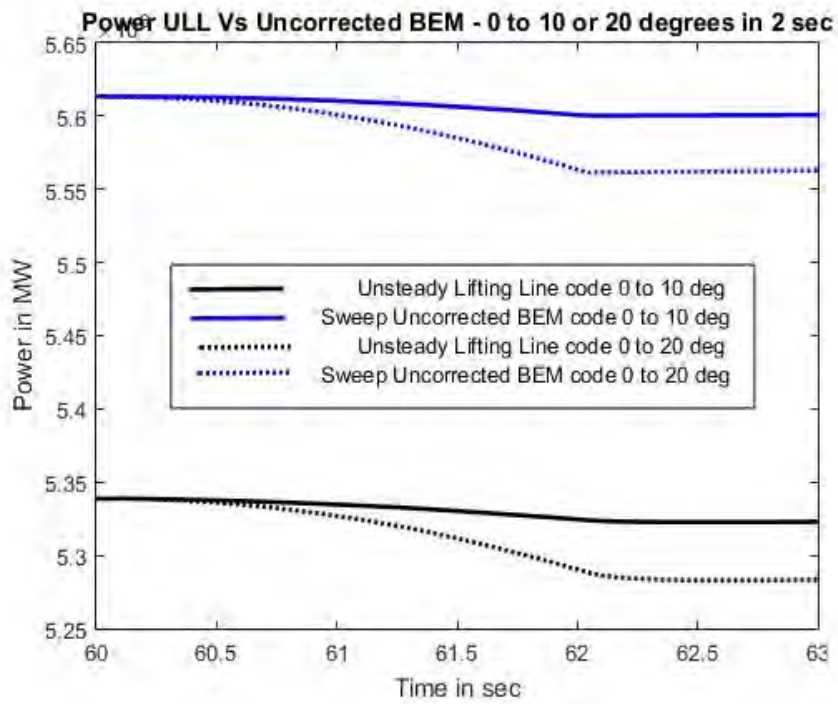
170

Figure 6.5 : Power for ULL and sweep uncorrected BEM code 10 and 20 deg aft sweep 5%
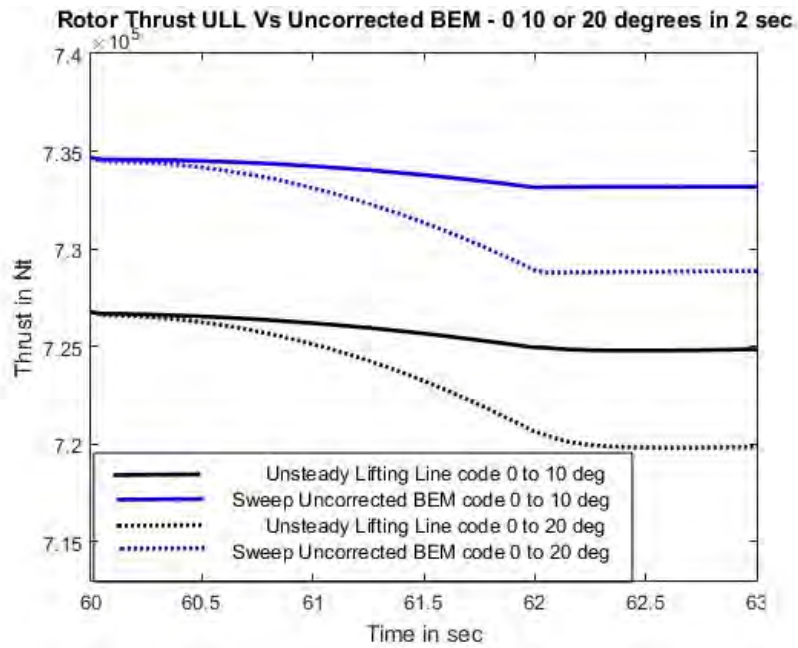
tip sweep

Figure 6.6: Thrust for ULL and sweep uncorrected BEM code 10 and 20 deg aft sweep 5% tip

sweep

171
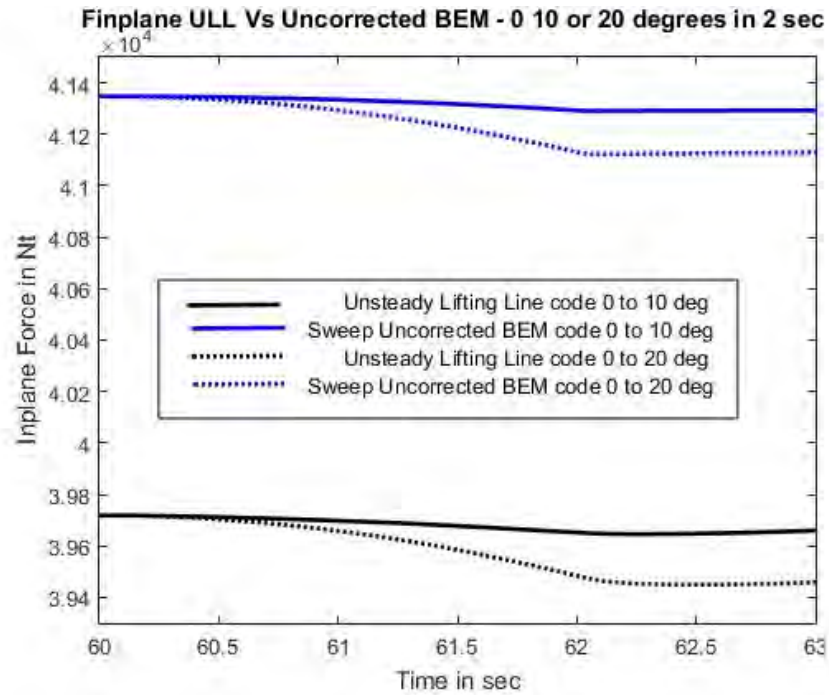
Figure 6.7 : In-plane Rotor Force for ULL and sweep uncorrected BEM code 10 and 20 deg

aft sweep 5% tip sweep

From the above diagrams it is seen that a good agreement is achieved between the two methods (BEM and ULL) despite the fact that they are based on different theoretical background. The basic difference is the offset which seems to be maintained during and after the sweep angle step proving that the BEM code performs also well in dynamic phenomena of this kind. Table 6.1 shows the percentage loss after a stabilization period of 8 seconds for the raw wind turbine parameters.

172

Loss %	Tip sweep percentage							
	5%				10%			
	Degrees aft sweep							
	10		20		10		20	
	Code							
	BEM	ULL	BEM	ULL	BEM	ULL	BEM	ULL
Power	0,195	0,25	0,78	0,82	0,43	0,54	1,69	1,78
Thrust	0,19	0,21	0,74	0,83	0,46	0,52	1,79	1,97
Finplane	0,113	0,03	0,45	0,43	0,25	0,28	1,00	1,17

Table 6.1: Power -Thrust -In plane Force loss (%) after a sweep angle step for two different

tip sweep percentages

The following diagrams provide a more detailed picture about the differences of BEM and ULL by showing the blade induction distribution curve 10 seconds after sweep angle change.

Figure 6.8 : Induction Distribution for ULL and sweep uncorrected BEM code 10 deg aft

sweep 10% tip sweep

Figure 6.9 : Induction Distribution for ULL and sweep uncorrected BEM code 20 deg aft
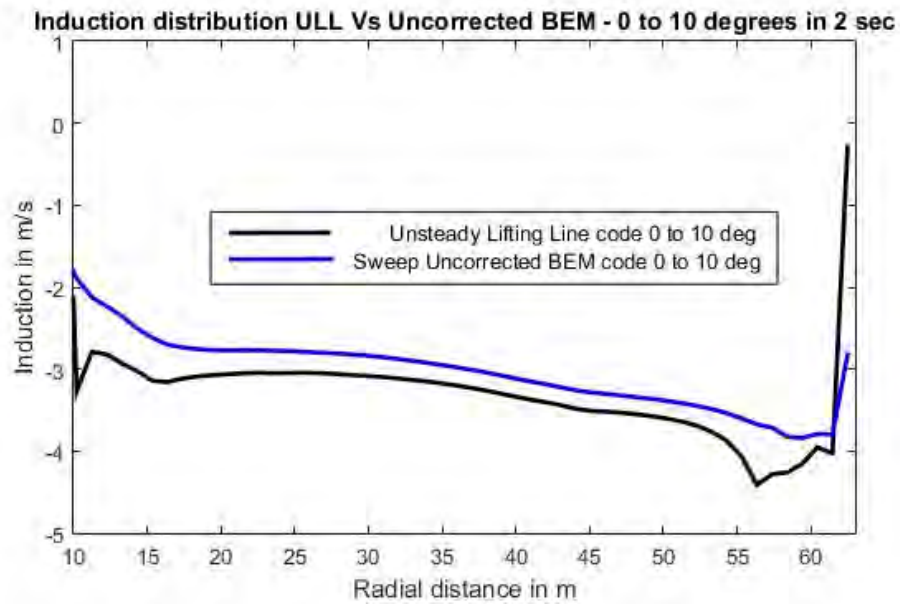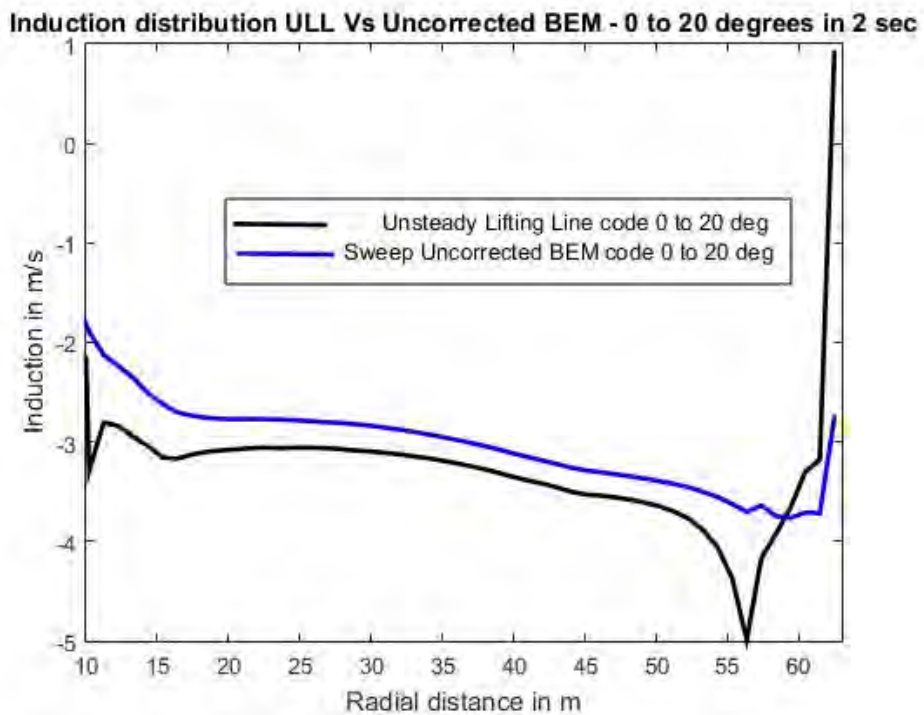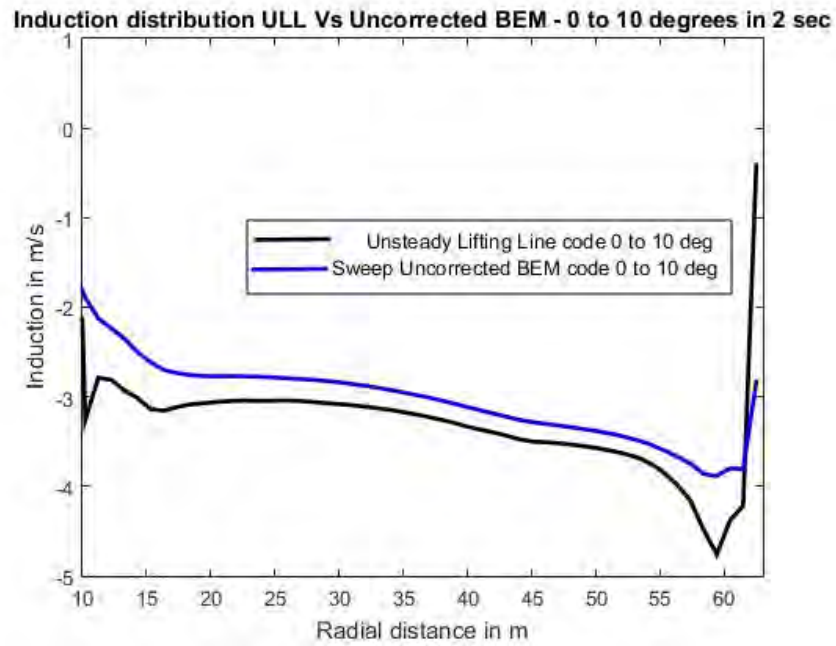
sweep 10% tip sweep

174

Figure 6.10 : Induction Distribution for ULL and sweep uncorrected BEM code 10 deg aft
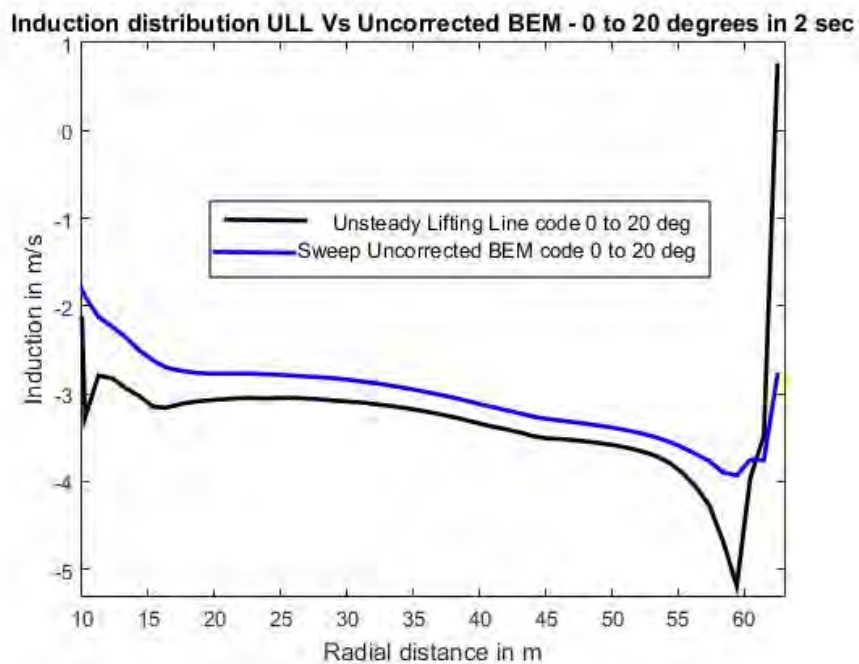
sweep 5% tip sweep

Figure 6.11 Induction Distribution for ULL and sweep uncorrected BEM code 20 deg aft

sweep 5% tip sweep

175

It is seen that in the blade level the differences after the sweep angle change are noteworthy. In particular the characteristic "kink" is not seen in the BEM code and additionally the tip area is not affected at all when sweep angle change doubles, as happens in the ULL model. The correct prediction of induction distribution is of high importance as the angle of attack in every blade section is calculated from this, then the aerodynamic loads and lastly the wind turbine parameters such as power, thrust, in-plane blade force. The fact that the discrepancy is located at the tip area where the distances from the hub are the largest heightens the need to implement an additional correction to the already calculated tip - losses and take into account more accurately the effect of tip swept blades for the BEM code. The calculated forces of the tip area are a large fraction of the total forces and an agreement there is valuable.

6.2.2 Comparison of ULL VS Uncorrected for sweep BEM code - Oscillating blade tip

Complementary to the smooth sweep angle change cases where agreement in 'weak' dynamic phenomena was discovered, in this section agreement between ULL and BEM is also sought in more aggressive changes of sweep angle. The tip is forced to oscillate with a frequency of 0.25Hz, amplitude of 20 degrees and only one direction of movement is allowed, so sweep angle values are between 0 and 20 degrees. Diagrams of power, thrust and in-plane total rotor force are presented for the two tip sweep percentages (10% and 5%) along with the corresponding ones of the un-swept rotor case.

176

Figure 6.12 : Power for ULL and sweep uncorrected BEM code 20 degrees Amplitude

0.25Hz for 10% tip swept rotor

Figure 6.13: Thrust ULL and sweep uncorrected BEM code 20 degrees Amplitude 0.25Hz for

10% tip swept rotor

177

Figure 6.14 : Total In-plane Rotor Force for ULL and sweep uncorrected BEM code 20

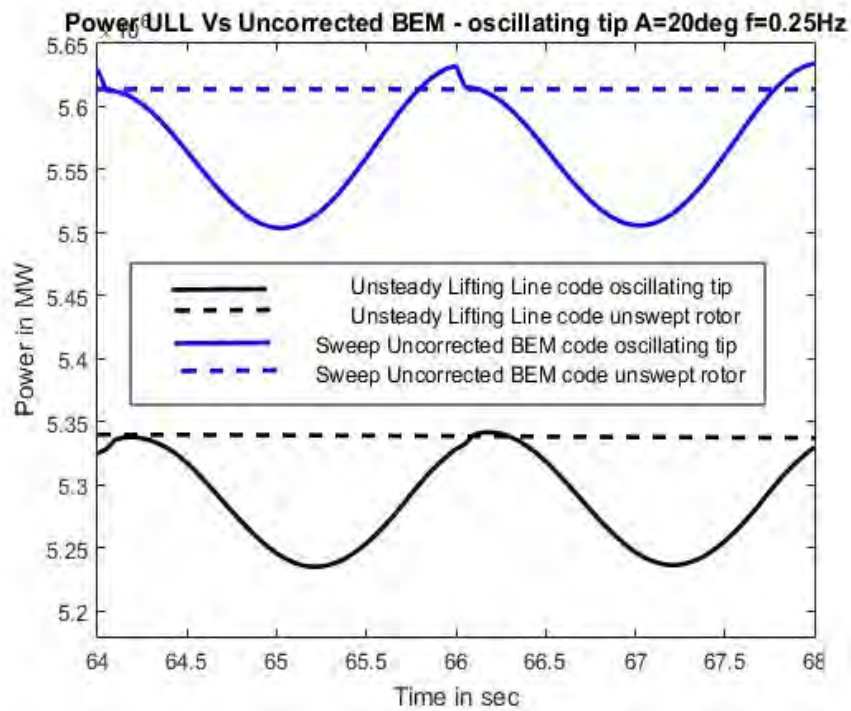degrees Amplitude 0.25Hz for 10% tip swept rotor

Figure 6.15: Power for ULL and sweep uncorrected BEM code 20 degrees Amplitude

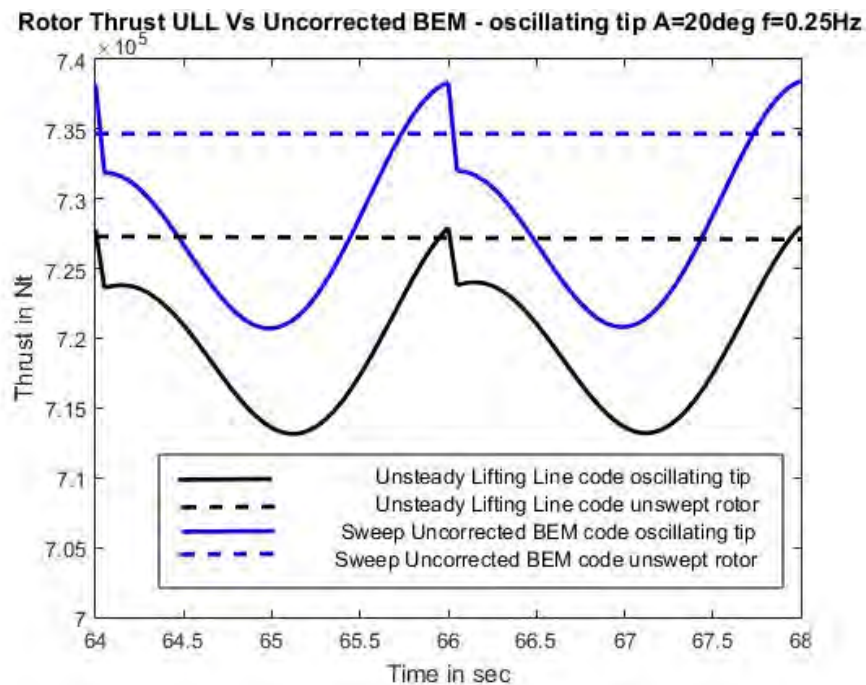0.25Hz for 5% tip swept rotor

178

Figure 6.16: Thrust for ULL and sweep uncorrected BEM code 20 degrees Amplitude
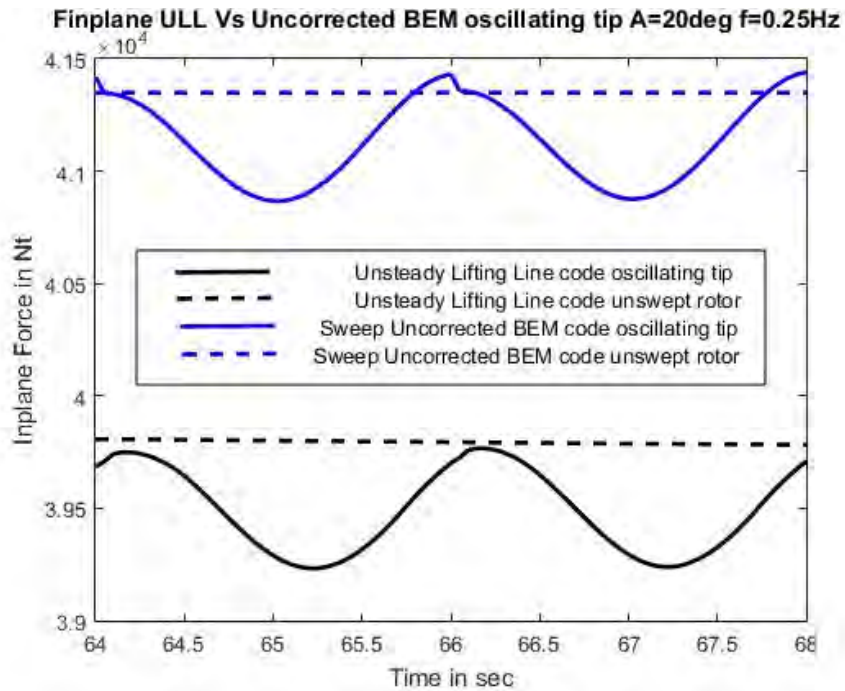
0.25Hz for 5% tip swept rotor

Figure 6.17 : Total In-plane Rotor Force for ULL and sweep uncorrected BEM code

20 degrees Amplitude 0.25Hz for 5% tip swept rotor
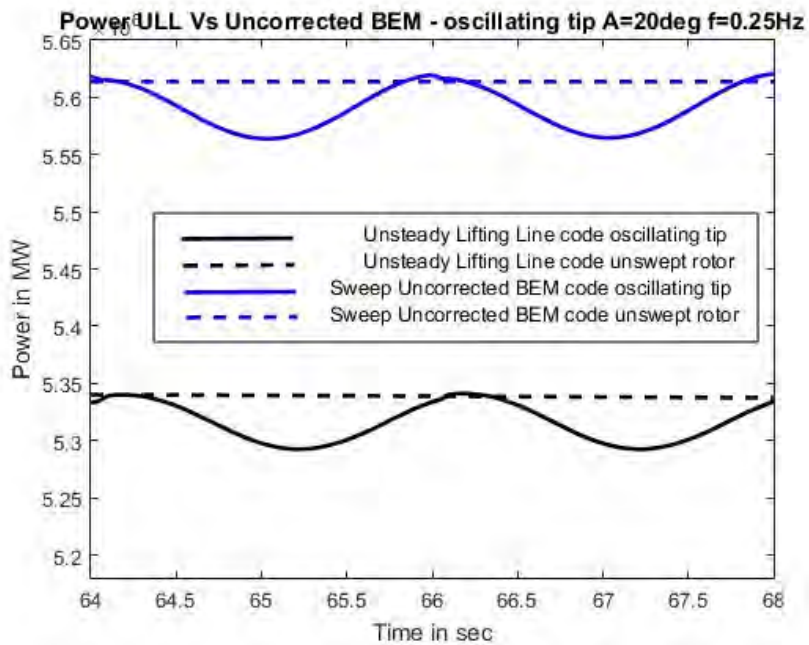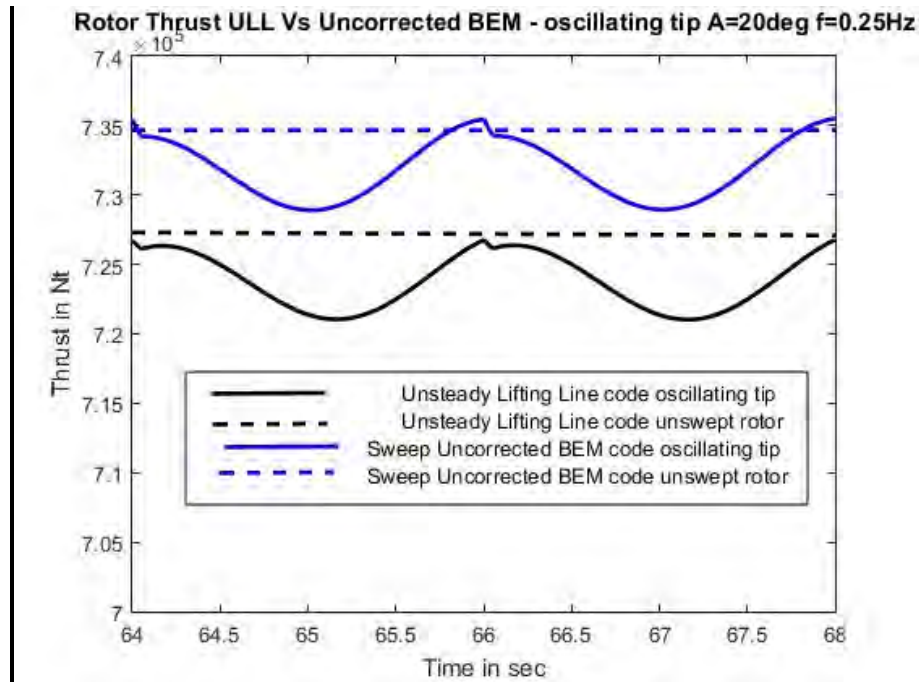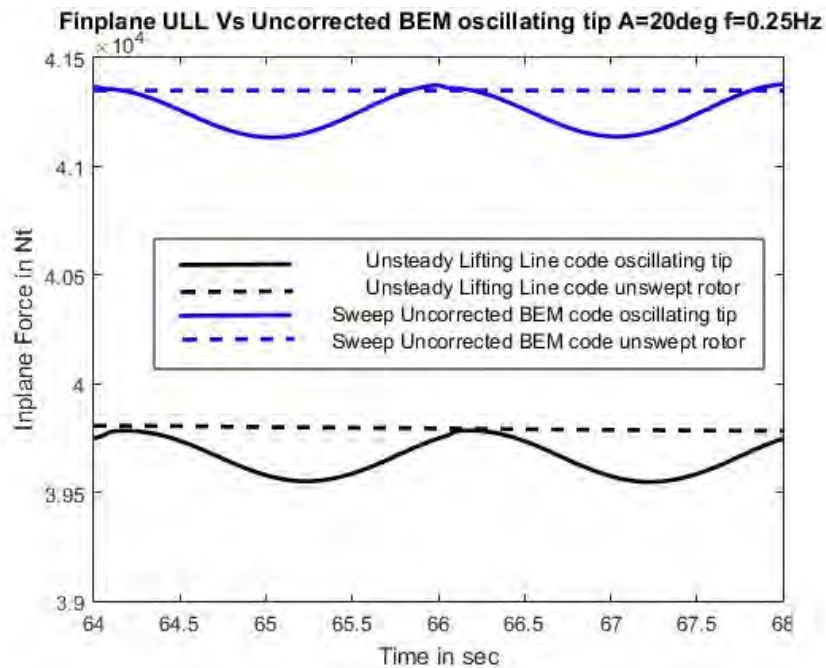
179

The above diagrams indicate that the agreement of the two codes is maintained during dynamic phenomena. Besides the offset which is of the same order compared to the smooth sweep angle change, the behavior is almost the same. Discrepancies are expressed as negligible differences in the overshoots of the moving tip case at the un-swept positions (highest values) and a small phase lag between the two codes. Unsteady aerodynamics do not need to be modeled because in the 10% tip swept rotor case (which has the longest fraction of moving blade) the additional velocity of the outer section is not higher than 3.1 m/s and the corresponding reduced frequency equation 2.58 is below 0.05.

6.3 Correction of the BEM code

From the results of paragraph 6.2 it is clear that BEM performs fairly well with relatively few modifications (paragraph 5.2). But there is also room for improvement in the blade level and specifically the induction distribution which is a crucial factor as it affects any other calculated parameter of the wind turbine. It was already mentioned that mainly the tip area needs correction and this is rational because BEM codes do not take effectively into account trailing vorticity which is altered significantly by the aft sweeping blade tip. Thus, it is important to discover a parameter that is already calculated in the BEM code and changes according to sweep angle. A suitable parameter for the sweep correction is the radial bound circulation difference distribution ($d\Gamma(r+1) - d\Gamma(r)$) and this is depicted below in Figures 6.18 and 6.19 : . Actually this difference causes the trailed vorticity which is not considered at all in the BEM code although it is calculated internally.

An alternative choice for correction could be an establishment of a new theoretical model which is based on the new position of the stemming trailing vorticities as the blade tip sweeps aft and develop new factors or new time constants that affect the induction

180

distribution of the blade. A representative example is the further development of the near wake model originally proposed by Beddoes and the coupling of it with a far wake model [110] in order to provide a better tip loss correction. However, in this work the aim is to develop an engineering model which is fast, effective and collaborates well with the current BEM code configuration.
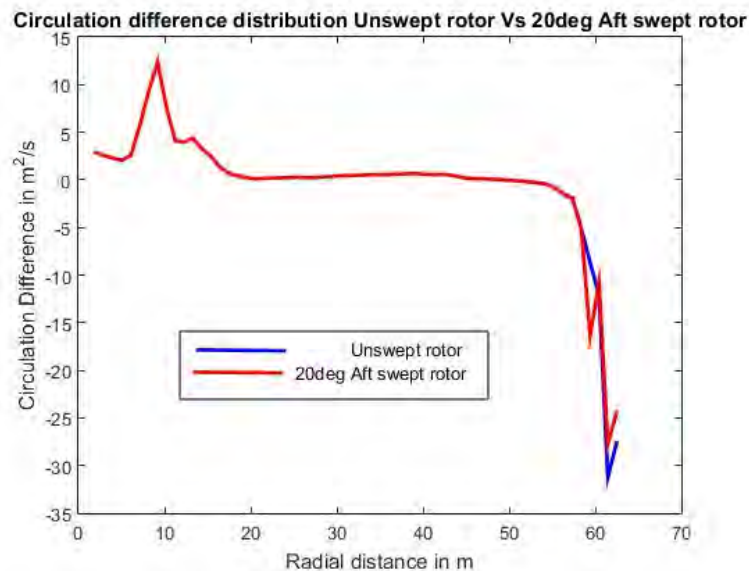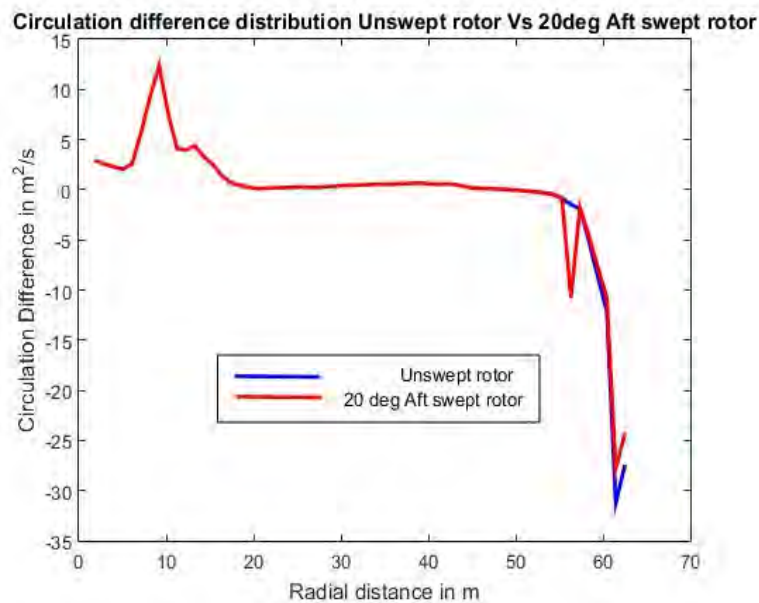
Figures 6.18 & 6.19 : Radial bound circulation difference for Un-swept and 20deg Aft swept rotor - 10% (up) and 5% (down) sweep percentage

181

The above figures indicate that a "kink" is formed in the distributions of circulation difference as the blade tip sweeps aft and it is located at the hinge area. The same "kink" is discovered in figures 6.8 , 6.9 , 6.10 and 6.11 and thus, the induction distribution of the BEM code can be corrected utilizing this fact. However it seems that improvement can be pursued mainly on this small part of the blade because changes in circulation difference are not extended to the rest of the tip. So, an additional consideration for the rest of the blade tip should be made. A suitable parameter that changes noticeably as the tip sweeps aft is the distance travelled by the swept part of the blade in the plane of rotation. This distance is proportional to the distance of the blade element from the hinge and expresses the potential of the tip vortex as it changes stemming position.

The philosophy of the correction in the induction distribution could be based on the Biot Savart formula (equation 2.10) that is already used to calculate the induction in the ULL model.

In this work the proposed correction consists of two parts - the first focuses on the hinge area and the second on the rest of the blade tip. The following equation presents the general form of the proposed correction:

$$G = -ag_1 Circ_{diff} / (V_{inf\,low} 4\pi dr^2) - bg_2 X_{CpG}{}^2 Circ_{diff} / ((V_{inf\,low} 4\pi dr^4))$$

(non-dimensional)

(**6.1**)

where:

- α , b   : factors that accrue from tests and adjust the correction

- g_1 , g_2 : factors that maximize the correction at the hinge area (g1) and also amplify the correction at the blade tip area (g2). The values of this factors accrue from the

182

normal distribution curves of the blades' elements radial distances. G1 factor results from this normal distribution shifted to the hinge area and g2 shifted to the tip area accordingly. The following figures corresponds to the typical cases of 10 percent and 5 percent tip swept blades.
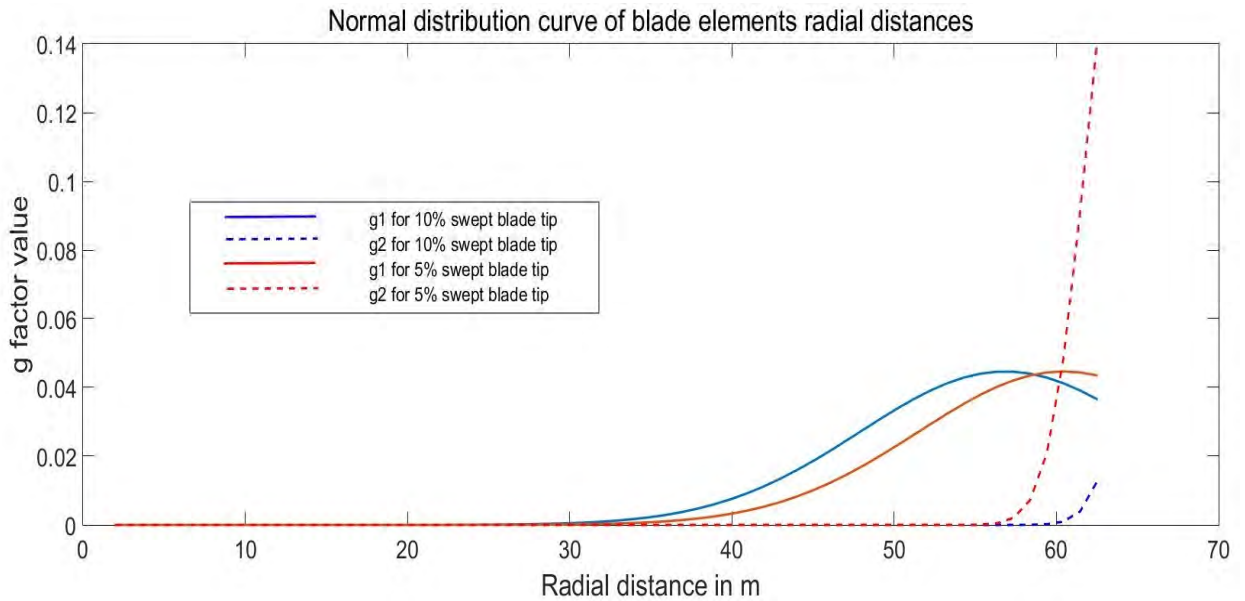
Figure 6.20 : g factor calculation utilizing the normal distribution curve

- Circ $_{diff}$ **:** the bound circulation difference between adjacent blade elements in other words the trailed vorticity. (the value of the outermost circulation difference is the subtraction of the tip element bound circulation with zero)

- X_{CpG} **:** is the vertical distance travelled in - plane by the blade elements according to the sweep angle of the blade tip (in relation to the unswept blade)

- dr   **:** the blade element length

The G factor of equation 6.1 is calculated for every blade element of all rotor blades and is applied directly to the already calculated and corrected for the tip loss phenomena axial induction factor in the form of:

183

$$a_{if} = a_{if}(1+G)$$

<div align="right">(6.2)</div>

However, in order to establish a correction that accounts only for the blade tip sweeping and thus would not interfere in the axial induction factor calculation when the blades remain un-swept factor k is subtracted from G (equation 6.3). i.e.

$$a_{if} = a_{if}(1+G-k)$$

<div align="right">(6.3)</div>

The k factor is calculated from equation 6.1 with the only difference that "*Circ_diff*" is the bound circulation difference between adjacent blade elements as if the blades are un-swept. So on one hand, there is no correction when the blades are un-swept (for example during the stabilization phase of the wind turbine parameters) because G=k and on the other hand correction is applied to the aif only when the blades sweep. In this case the correction results from the difference in the trailed vorticity of the current blade configuration in relation to the trailed vorticity for the un-swept configuration G≠k.

6.3.1 Corrected BEM VS Uncorrected for sweep BEM code - Sweep Angle Change in 2 secs

In this paragraph diagrams of the same parameters and blade configurations of paragraph 3.1 are shown (rotor power, rotor thrust and total in-plane rotor force for 10% and 5% tip swept blades) for the modified BEM code (red color) and the un-modified BEM code (blue color) in order to quantify the correction.

<div align="center">184</div>

Figure 6.21 : Power for sweep modified and unmodified BEM code 10 and 20 deg aft

sweep 10% tip sweep

Figure 6.22: Thrust for sweep modified and unmodified BEM code 10 and 20 deg aft sweep

10% tip sweep

185
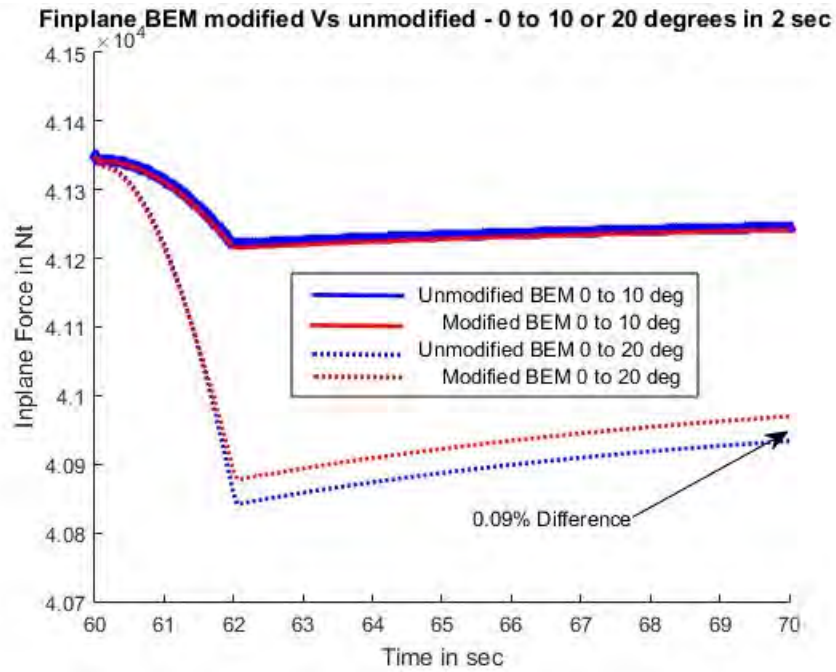
Figure 6.23 : In-plane force for sweep modified and unmodified BEM code 10 and 20 deg aft
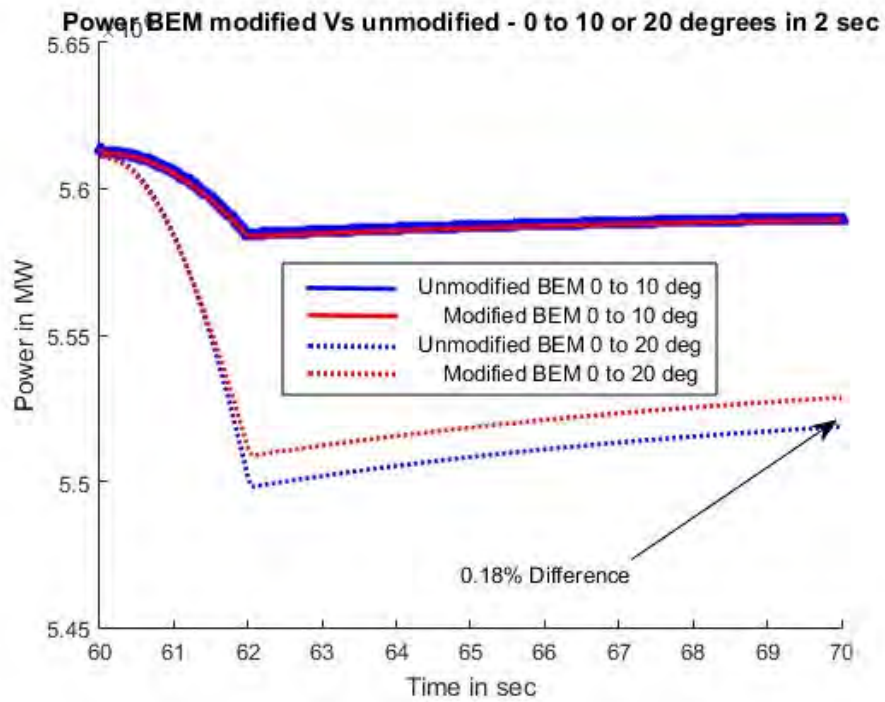
sweep 10% tip sweep
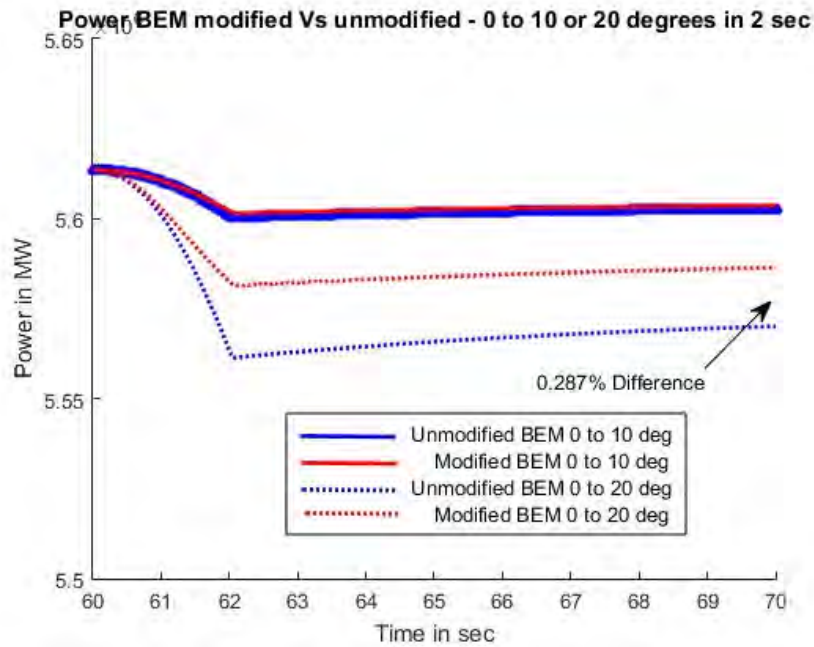
Figure 6.24 : Power for sweep modified and unmodified BEM code 10 and 20 deg aft sweep

5% tip sweep

186

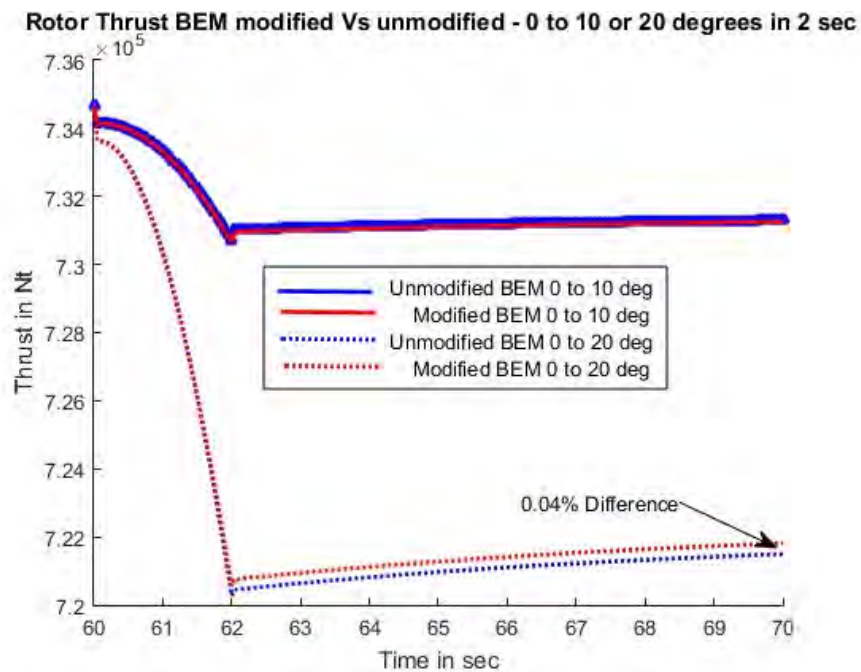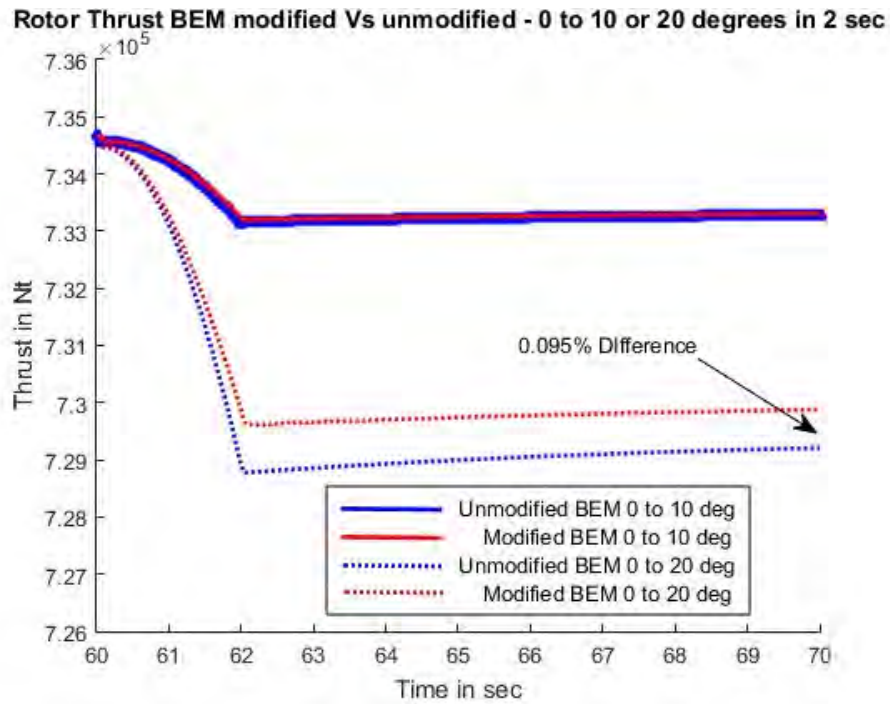Figure 6.25: Thrust for sweep modified and unmodified BEM code 10 and 20 deg aft
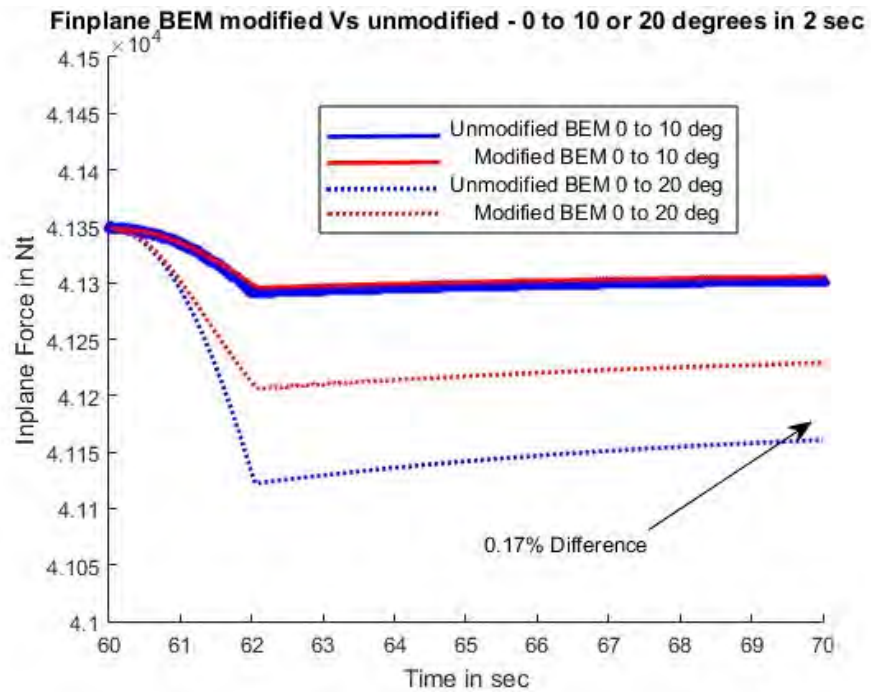
sweep 5% tip sweep

Figure 6.26: In-plane force for sweep modified and unmodified BEM code 10 and 20 deg aft

sweep 5% tip sweep

187

From the above diagrams it is seen that the applied modification to the BEM code results only in an offset change of the examined parameters while keeping the dynamics unaffected. Additionally the correction is only significant for sweep angle changes of the order of 20 degrees and nearly twice as much for 5% blade tips compared to the corresponding 10% blade tip case. This is due to larger differences that are created in the bound circulation distribution (which is the main parameter of the characteristic correction equation [equation 6.1]) as sweep angle increases and the swept blade tip length decreases. Moreover, the correction concerns mostly the in plane rotor forces and subsequently the rotor power and quaintly is not in the direction of reducing the offset between ULL model and BEM code. However, the following diagrams show the effect of the applied modification to the BEM code concerning the axial induction factor (aif) which is a crucial parameter in the calculation of the above parameters. The aif distributions in red color refer to the modified BEM code and beneath every distribution diagram the corresponding difference of the aif resulting differences following sweep angle changes between BEM and ULL code is shown. The cases once again refer to 10% and 5% swept blade tips and sweep angles of 10 and 20 degrees.
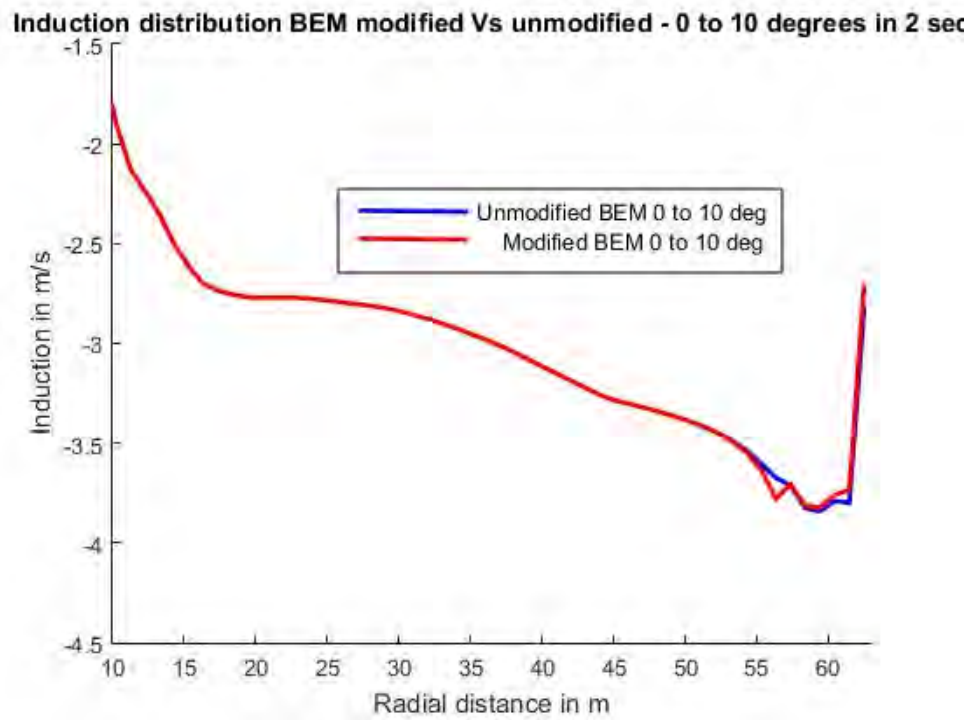
Figure 6.27: Induction distribution curves for sweep modified and unmodified BEM

code 10 deg aft sweep 10% tip sweep
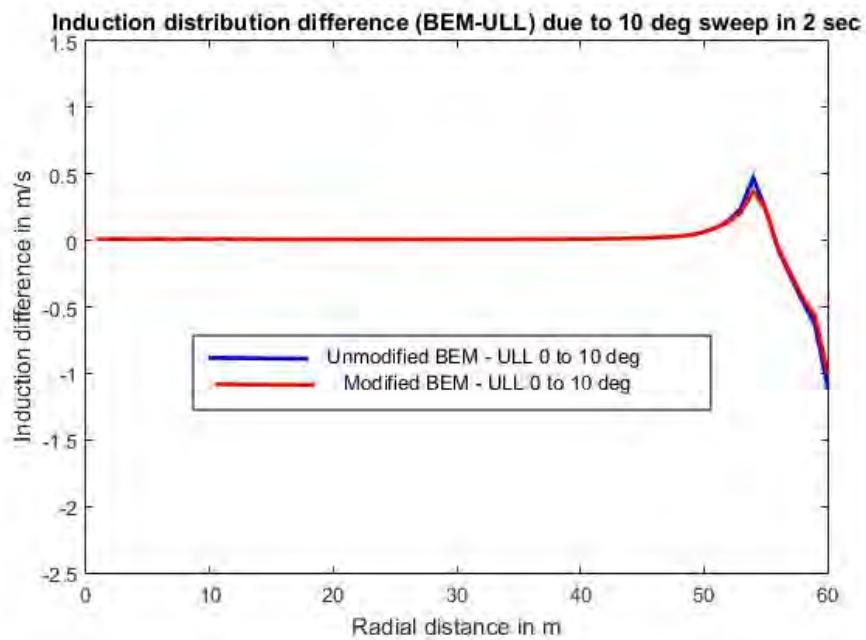
Figure 6.28 : Induction difference (BEM-ULL) distribution curves for sweep

modified and unmodified BEM code 10 deg aft sweep 10% tip sweep

189
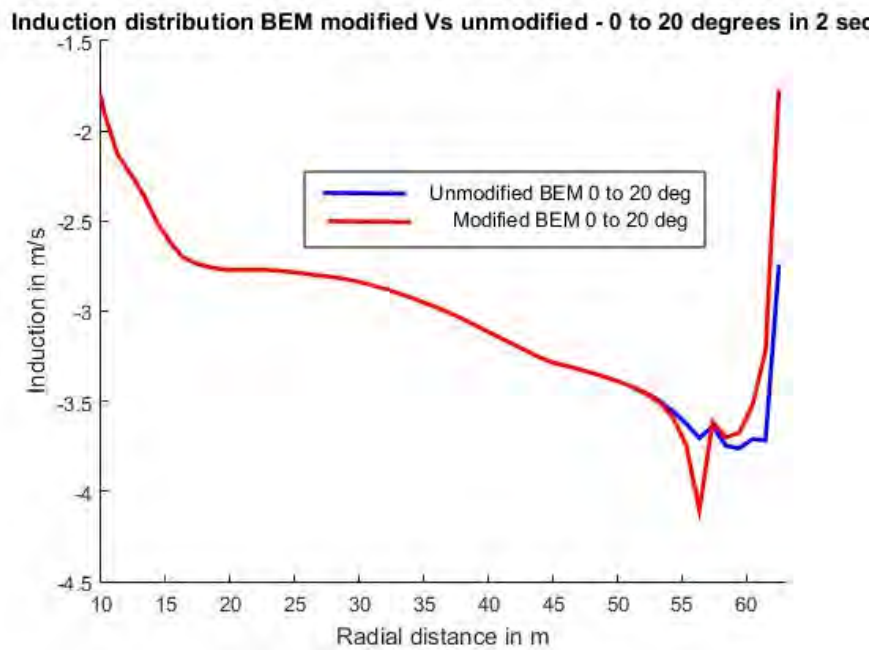
Figure 6.29 : Induction distribution curves for sweep modified and unmodified BEM code 20

deg aft sweep 10% tip sweep
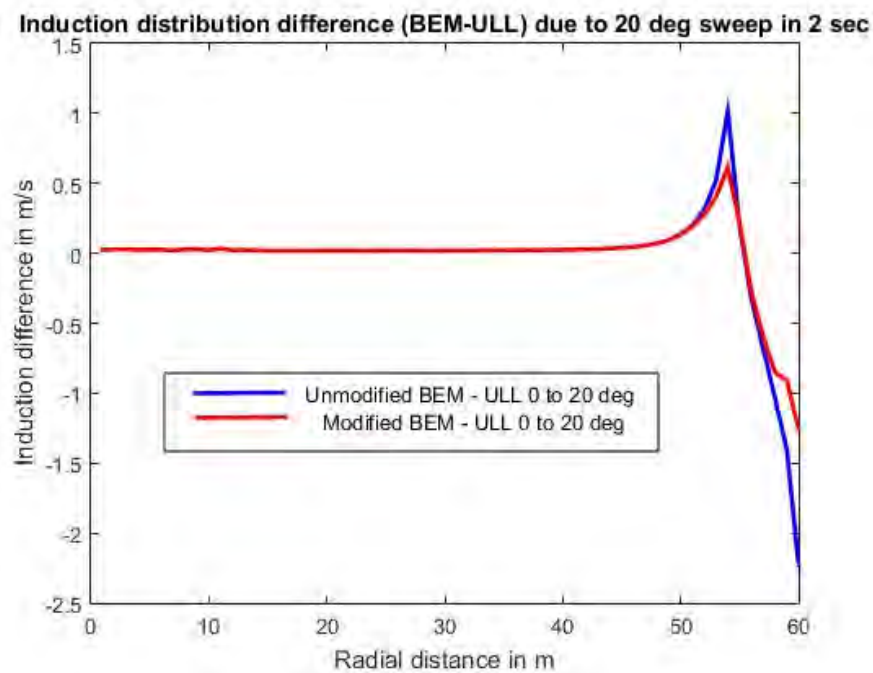
Figure 6.30 : Induction difference (BEM-ULL) distribution curves for sweep modified and

unmodified BEM code 20 deg aft sweep 10% tip sweep

190
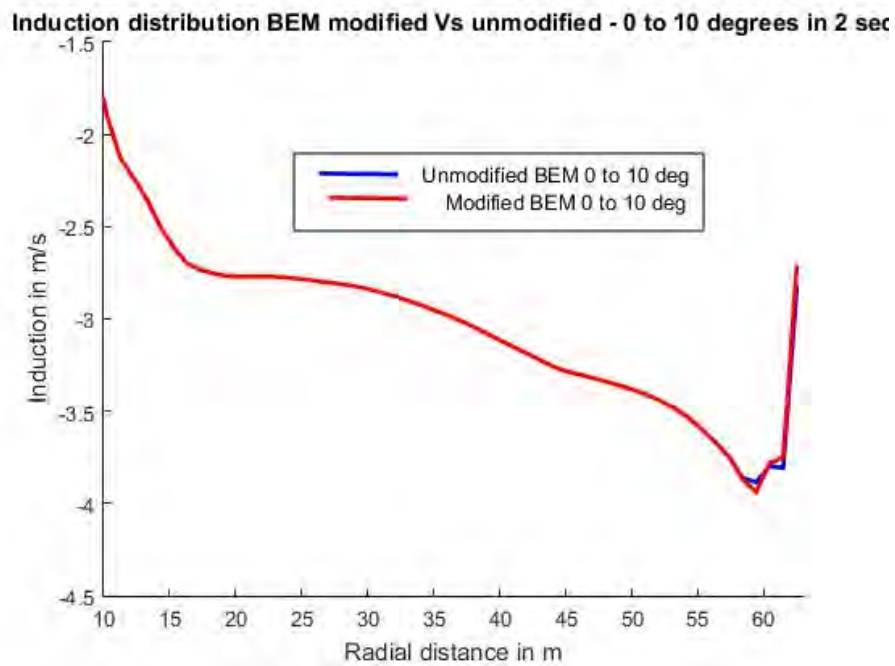
Figure 6.31: Induction distribution curves for sweep modified and unmodified BEM code 10

deg aft sweep 5% tip sweep
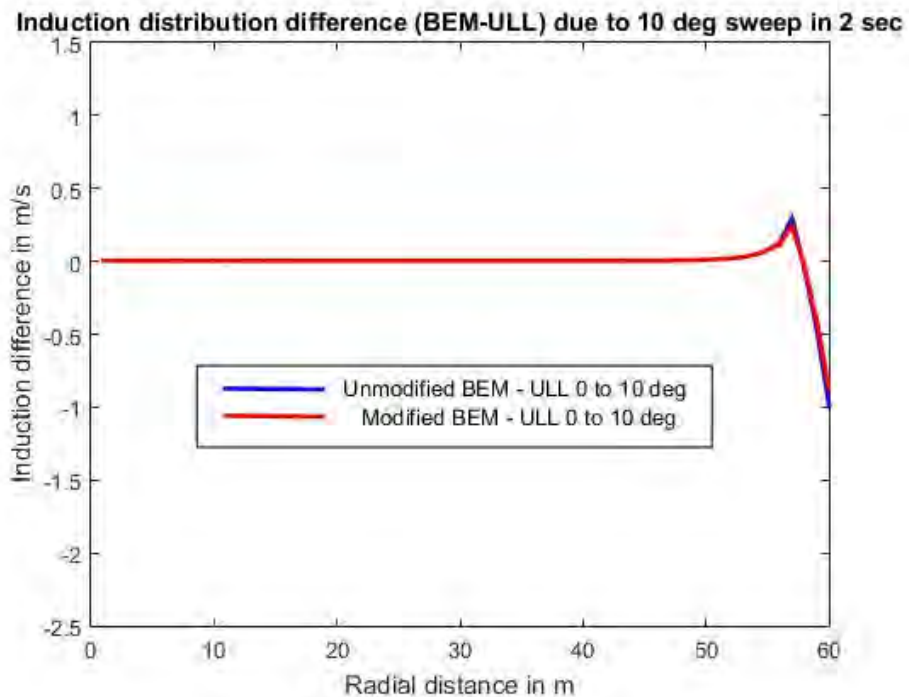
Figure 6.32 : Induction difference (BEM-ULL) distribution curves for sweep modified and

unmodified BEM code 10 deg aft sweep 5% tip sweep

191
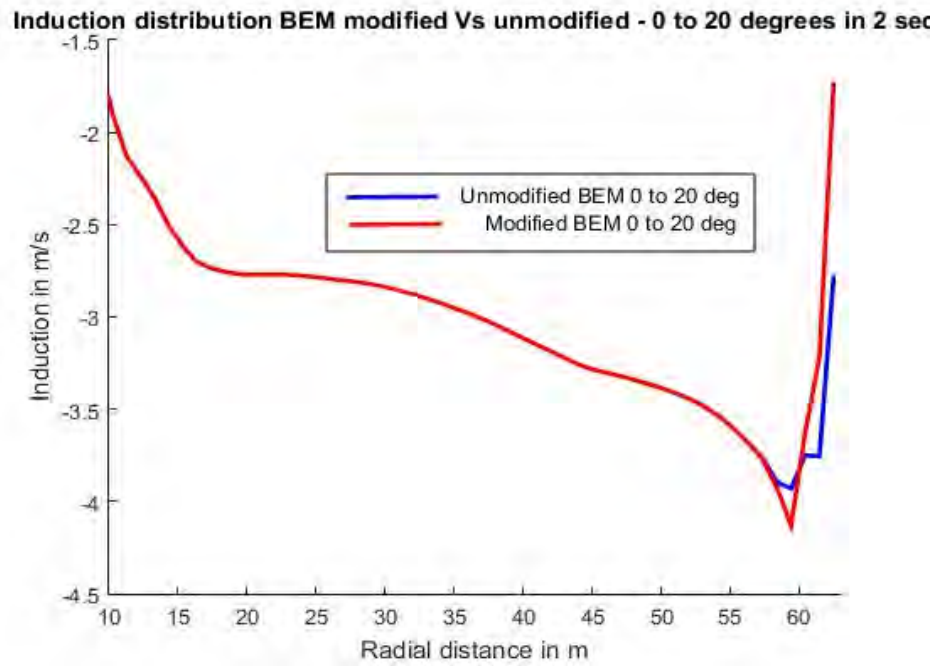
Figure 6.33: Induction distribution curves for sweep modified and unmodified BEM code 20

deg aft sweep 5% tip sweep
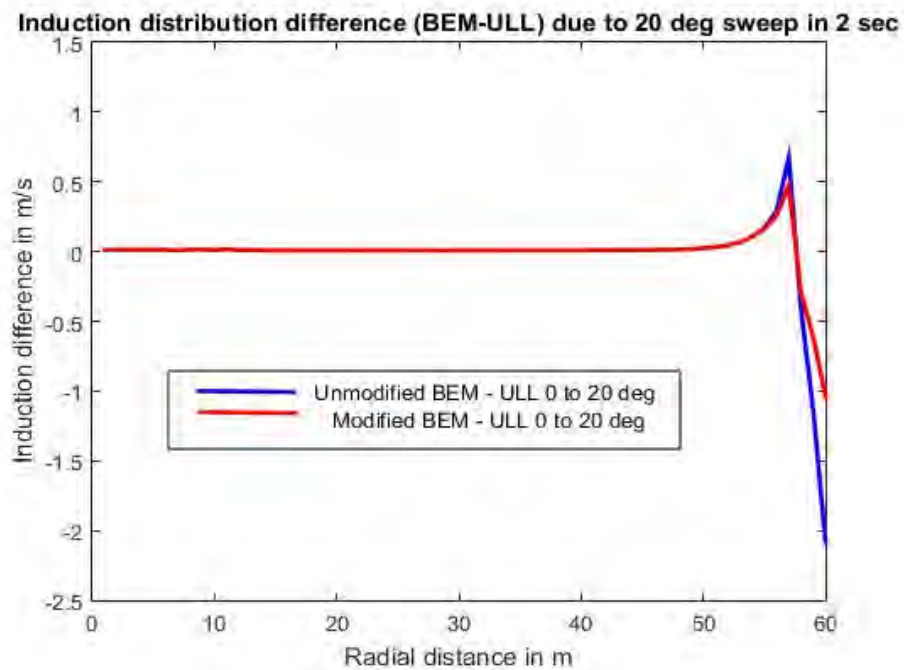
Figure 6.34 : Induction difference (BEM-ULL) distribution curves for sweep modified and

unmodified BEM code 20 deg aft sweep 5% tip sweep

192

In the ideal case of total agreement in the calculation of the aif distribution between BEM and ULL code the right diagrams should show a straight zero line and the applied modification to the BEM code points to this direction. This is obvious in the aif distributions (figures 6.27 , 6.29 , 6.31 & 6.33) which have the characteristic kink in the hinge area and increased aif values in the tip area (figures 6.8 - 6.11). As expected the correction is significant for the 20 degrees sweep angle change and stronger for the 5% blade tip.

6.3.2 Comparison of ULL VS corrected for sweep BEM - sweep corrected code oscillating blade tip

The diagrams below refer to the same case of paragraph 6.2.2 (20 degrees amplitude and 0.25Hz frequency) and represent more aggressive sweep angle changes while maintaining the reduced frequency value low in order to exclude unsteady aerodynamics.
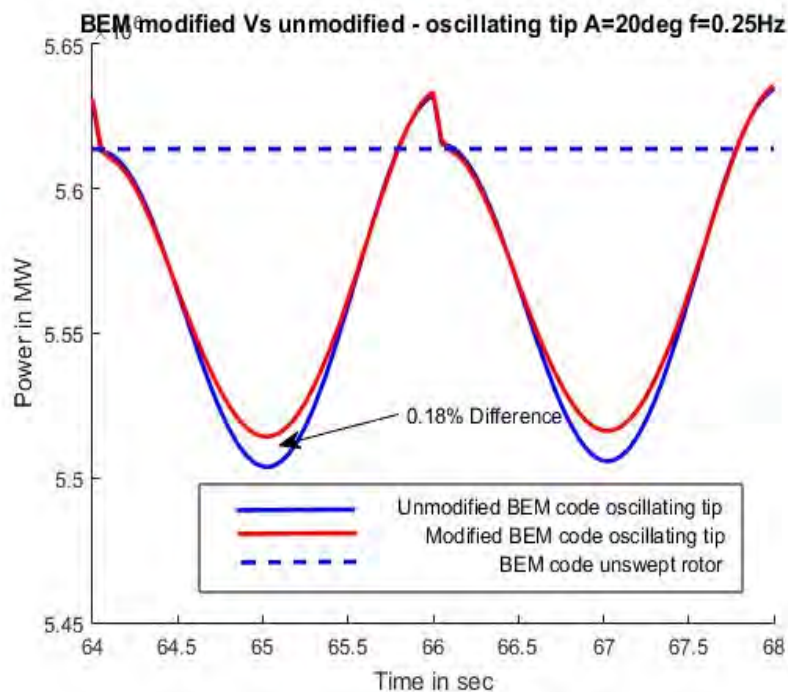
Figure 6.35: Power for BEM modified and unmodified code 20 degrees Amplitude 0.25Hz for 10% tip swept rotor

193
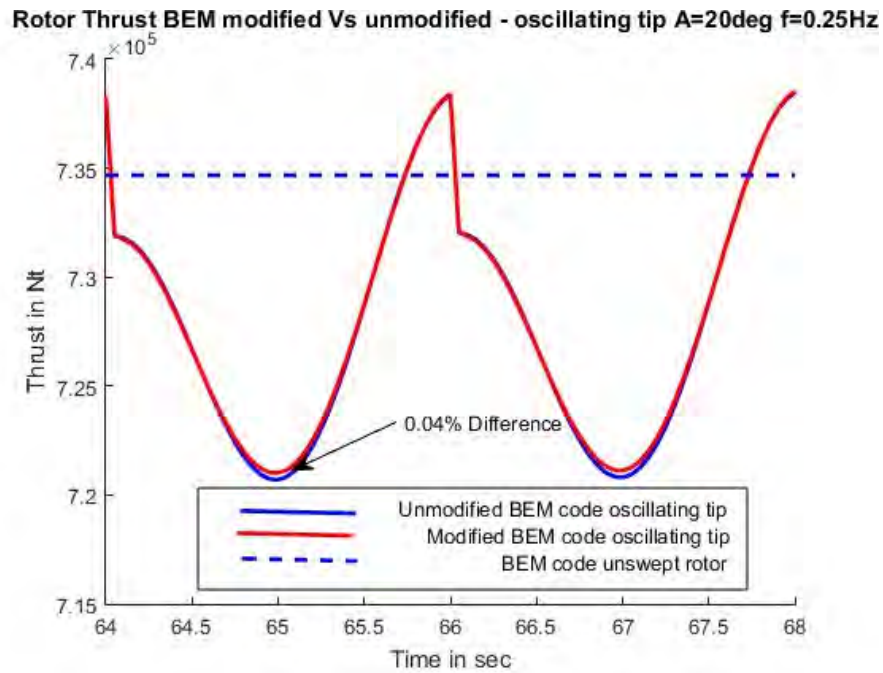
Figure 6.36: Thrust for BEM modified and unmodified code 20 degrees Amplitude 0.25Hz

for 10% tip swept rotor
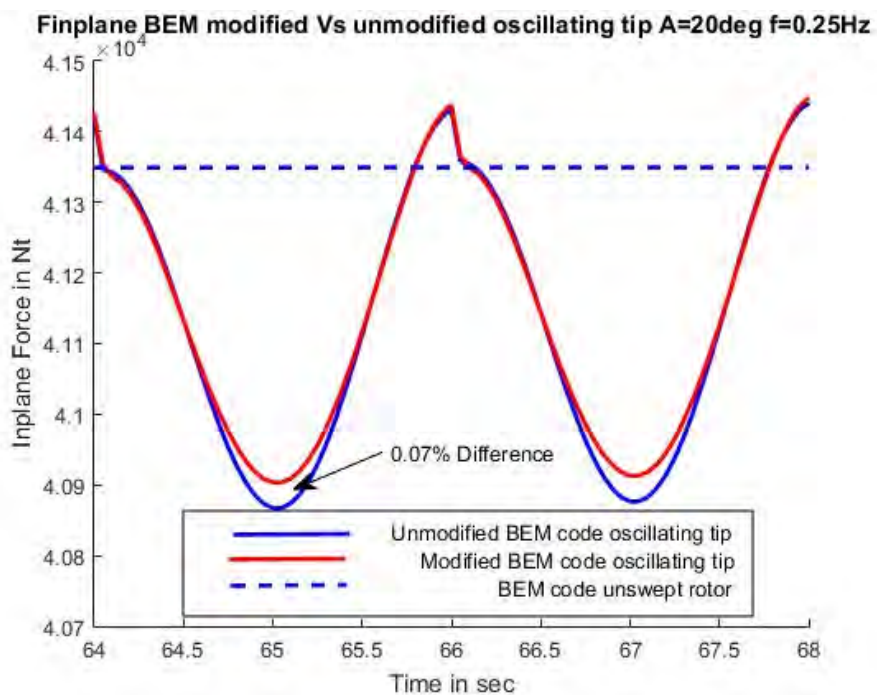
Figure 6.37: In-plane force for BEM modified and unmodified code 20 degrees Amplitude

0.25Hz for 10% tip swept rotor

194
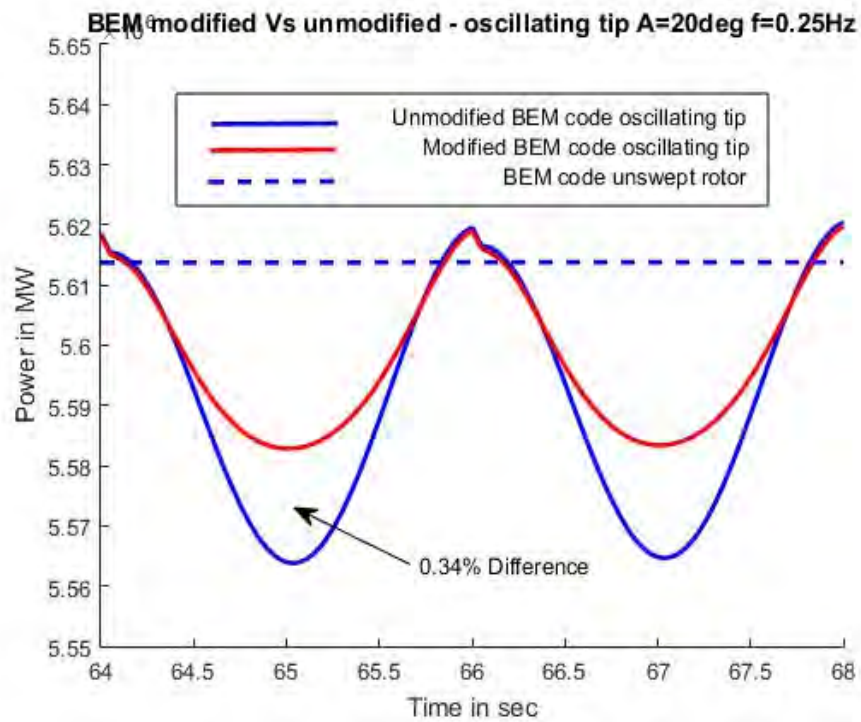
Figure 6.38 : Power for BEM modified and unmodified code 20 degrees Amplitude 0.25Hz

for 5% tip swept rotor
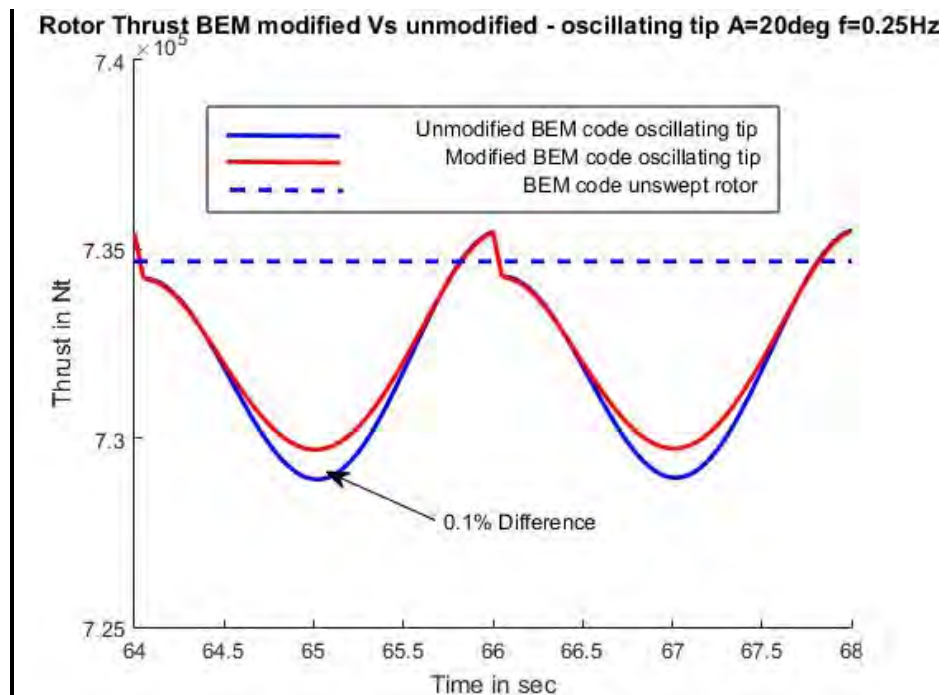
Figure 6.39 Thrust for BEM modified and unmodified code 20 degrees Amplitude 0.25Hz for
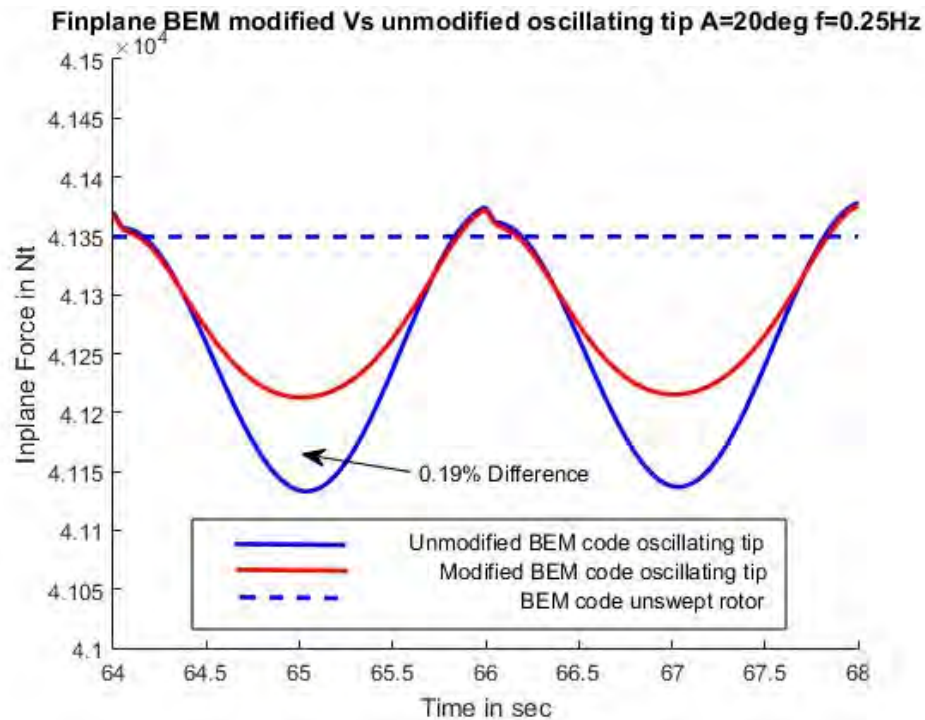
5% tip swept rotor

Figure 6.40: In-plane force for BEM modified and unmodified code 20 degrees Amplitude

0.25Hz for 5% tip swept rotor

Differences between modified and un-modified BEM code (red line and blue line respectively) are only obvious for sweep angles greater than 10 degrees and of the same order compared to the corresponding smooth sweep angle change cases (paragraph 6.3.1). In addition the dynamic response does not seem to be affected at all.

6.4 Conclusions

In this chapter the incorporation of a three bladed rotor (in particular the 5MW NREL wind turbine) with tip sweep capability in a BEM based code is presented. The corresponding results of a more physically correct model based on the ULL theory were used as a guideline. The latter code is based on the ULL model of Chapter 5 but it was modified and accelerated up to 60 times utilizing CUDA platform of *Matlab*. The incorporation of this feature is

196

modeled according to the three considerations of paragraph 5.2 and are implemented in both codes.

The results that are produced indicate a good agreement between the two codes in stabilized and dynamic conditions except for an offset which is possibly due to the different theory that are based on that leads to different converged values of rotor power, total thrust and total in-plane force. Nevertheless, a discrepancy in the calculation of axial induction factor distribution by the BEM based code is discovered which is focused at the tip region where the expected change is not seen as the blade tip sweeps aft. Thus, a modification is applied to the BEM code utilizing parameters that are already calculated, such as Circulation distribution, and improve this distribution. This correction is stable within the BEM code (aerodynamic part of DU SWAMP [72]) and it is noteworthy for sweep angle changes over 10 degrees and for swept blade tips of smaller blade span percentage. The correction is basically seen in the prediction of the in-plane forces and thus the rotor power and its value is in the order of 0.25% (for power) which is relatively small but can become significant in the calculation of AEP of rotors with variable tip sweep capability.

The originality that this chapter incorporates is the development of a BEM theory based model for a three bladed HAWT capable of modeling the effects of variable tip swept rotor blades on wind turbine parameters and the introduction of a corresponding correction that leads to better estimations of the axial induction factor.

Chapter 7. Optimization Of Annual Energy Production And Load Reduction

In this chapter, the benefits that can be acquired from a typical wind turbine configured with variable tip sweep capability are demonstrated. The results refer to the 5MW NREL wind turbine and the simulations are performed within the modified - for tip sweep - BEM model which was analyzed in the previous chapter. However, the benefits are examined only from the aerodynamic point of view which is the first step for making a reliable assessment about the order of magnitude of the benefits. Improvement is sought to the following three key parameters: power production, fatigue loads and gust loads. These parameters play an important role to the efficiency of a wind turbine and contribute to the reduction of the energy.

7.1 Annual Energy Production (AEP) Improvement

The majority of either the implemented control methods or those which are currently under investigation at the Research and Development (R&D) laboratories of the industries aim to increase the wind turbine's energy production. Of course the introduction of a control method to a wind turbine has to be designed carefully in order not to raise extensively the cost of energy. The production cost of the device has the largest share of the overall cost and the maintenance cost the second largest share. AEP improvement is a more complicated task than the other two tasks examined later in the chapter. The increase is highly dependent upon the

Institutional Repository - Library & Information Centre - University of Thessaly
19/05/2024 19:53:00 EEST - 18.119.112.4

wind characteristics of the site where the device is installed. This means that a control method may be more efficient for one site where there are larger periods of below – rated operation than another site with shorter periods over the year.

Nevertheless, power increase may be pursued from three different directions:

- Increase of the Power coefficient (C_p) which is translated to more efficient operation. According to figure 2.8 C_p is maximized when axial induction factor equals 0.3. So, the target of the controller could be the improvement of the axial induction factor of the wind turbine.

- Increase of the swept area A of the rotor. According to equation 2.29 this would increase the available power. However, this inevitably leads to higher loads experienced by the structure.

- Selection of the best site. According to equation 2.29 the site with the best wind characteristics which means wind velocities close to the rated operation for the most period of time throughout the year increases the AEP.

AEP is calculated with the use of the wind's probability density function (PDF) which depends on the location of the site. PDF is usually given by a Rayleigh or a Weibull distribution and represents the probability that wind velocity is between V_i and V_{i+1} . So, after calculating the Power (in MW) for wind velocity between V_i and V_{i+1} and multiplying this with the corresponding probability (that wind velocity lies between V_i and V_{i+1}) and 8760 hrs / year, yields the power production in MWH for this wind margin. Total AEP results from the summation of all individual margins of the operational envelope of the wind turbine (V_{cut-in}– $V_{cut-out}$) and is given by equation 7.1 [4].

$$AEP = (\int_0^\infty P_{PDF}(V)P(V)dV)8760$$

or

$$AEP = \sum_{i=1}^{N-1} \frac{1}{2}(P(V_{i+1}) + P(V_i))f(V_i < V < V_{i+1})8760$$

(**7.1**)

where:

- $P(V)$ is the power produced by the wind turbine in MW

- P_{PDF} is the probability density function of wind velocity V, given from a Rayleigh or a Weibull distribution

- $f(V_i < V < V_{i+1})$ is the probability that wind velocity lies between V_i and V_{i+1} and it is given from a Rayleigh or a Weibull distribution

It is already obvious from Chapter 6 that loads and power are reduced when the blade tips are swept aft (figures 6.21 - 6.26). In addition, from figures 6.29 and 6.33 (looking at the red lines) it is deduced that the axial induction factor does not have a unidirectional change along the span of the swept part). There is an opposite behavior in the hinge area and the rest of the blade tip, when the blade tip sweeps. Thus, the only solution is to increase the swept area A while maintaining the same loads on the blades. This was also the case for the STAR development program explained earlier in paragraph 2.6 of this thesis. So, two different blade design recommendations are made next both of which increase the blade span 5%.

7.1.1 Blade design 1 – 5% blade span extension with 5% tip swept part

The extension of the wind turbine blades is a task that requires a small scale parametric study in order to achieve the maximum AEP increase while keeping the loads close to the design values, at the same time. In addition, it is preferable to introduce as less as possible changes to the geometry of the baseline blade (5MW NREL wind turbine) so that the adoption of the geometric feature of tip sweep would be an attractive project for further research and development tasked by the industries. Figures 7.1 and 7.2 present the recommended design in terms of chord and twist angle spanwise distribution in contrast to the baseline blade and table (7.1) contains the exact values. In addition, figure (7.3) is provided for better understanding of the new design. Specifically, the blade geometry is modified after point "C" (at rotor radius 58,9m), with the chord length following a linear reduction and the twist angle remaining constant to the designed value. The blade modification results in a rotor radius of 66,075m instead of 63m of the baseline rotor.

NREL			NEW DESIGN		
R (m)	THETA (deg)	CHORD (m)	R (m)	THETA (deg)	CHORD (m)
2,8667	13,3082	3,5416	2,8667	13,3082	3,5416
5,6	13,3082	3,854	5,6	13,3082	3,854
8,3333	13,3082	4,1666	8,3333	13,3082	4,1666
11,75	13,3082	4,5573	11,75	13,3082	4,5573
15,85	11,4798	4,6519	15,85	11,4798	4,6519
19,95	10,1625	4,4584	19,95	10,1625	4,4584
24,05	9,0113	4,2492	24,05	9,0113	4,2492
28,15	7,7949	4,0069	28,15	7,7949	4,0069
32,25	6,544	3,7481	32,25	6,544	3,7481
36,35	5,3613	3,5021	36,35	5,3613	3,5021
40,45	4,1878	3,2561	40,45	4,1878	3,2561
44,55	3,1251	3,0101	44,55	3,1251	3,0101
48,65	2,3194	2,7641	48,65	2,3194	2,7641
52,75	1,5259	2,5181	52,75	1,5259	2,5181
56,1667	0,8631	2,3131	56,1667	0,8631	2,3131
58,9	0,3704	2,0858	58,9	0,3704	2,0858
61,6333	0,1064	1,419	62,5	0,3704	1,1
62,3	0	1	64,8	0,3704	0,4
63	0	0,01	65,5	0,3704	0,2
			66,075	0,3704	0,01

Table 7.1: NREL Vs Blade design 1 chord and twist angle distribution
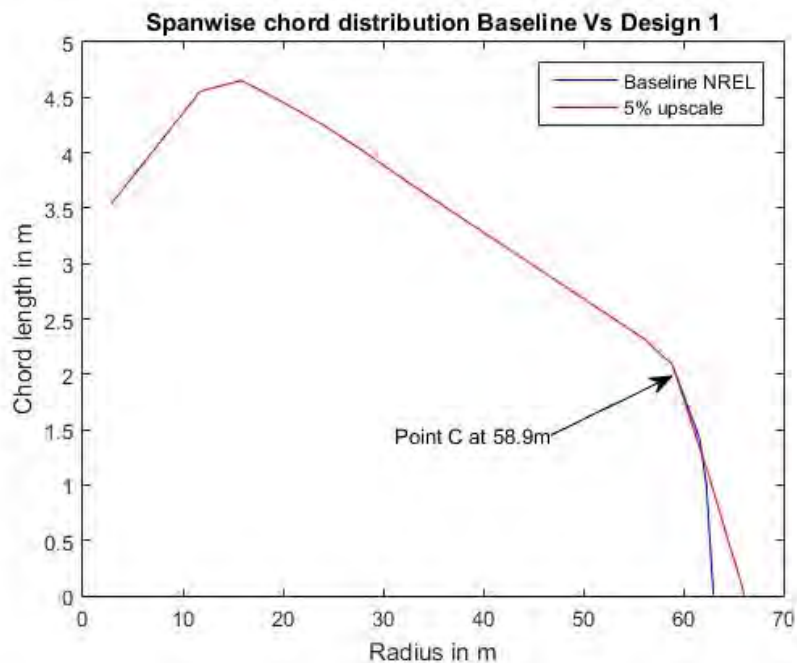
Figure 7.1 : NREL Vs Blade design 1 chord length distribution

202
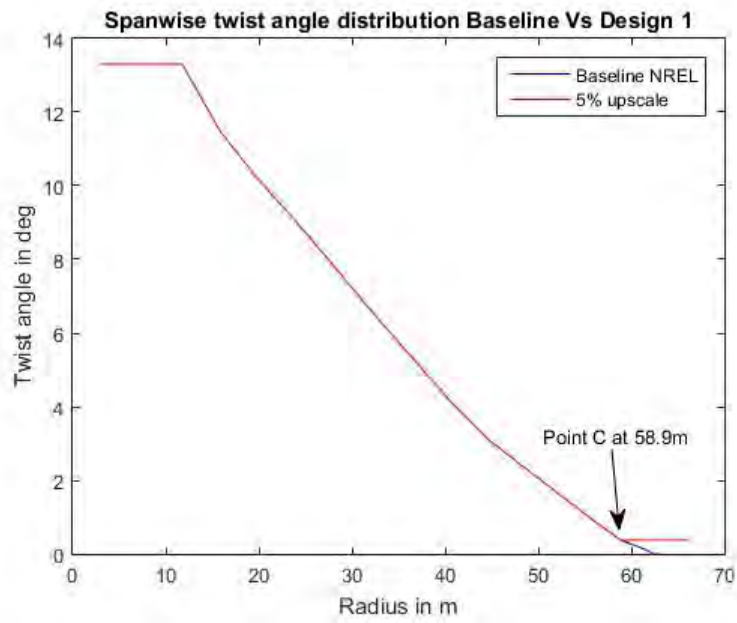
Figure 7.2 : NREL Vs Blade design 1 twist angle distribution
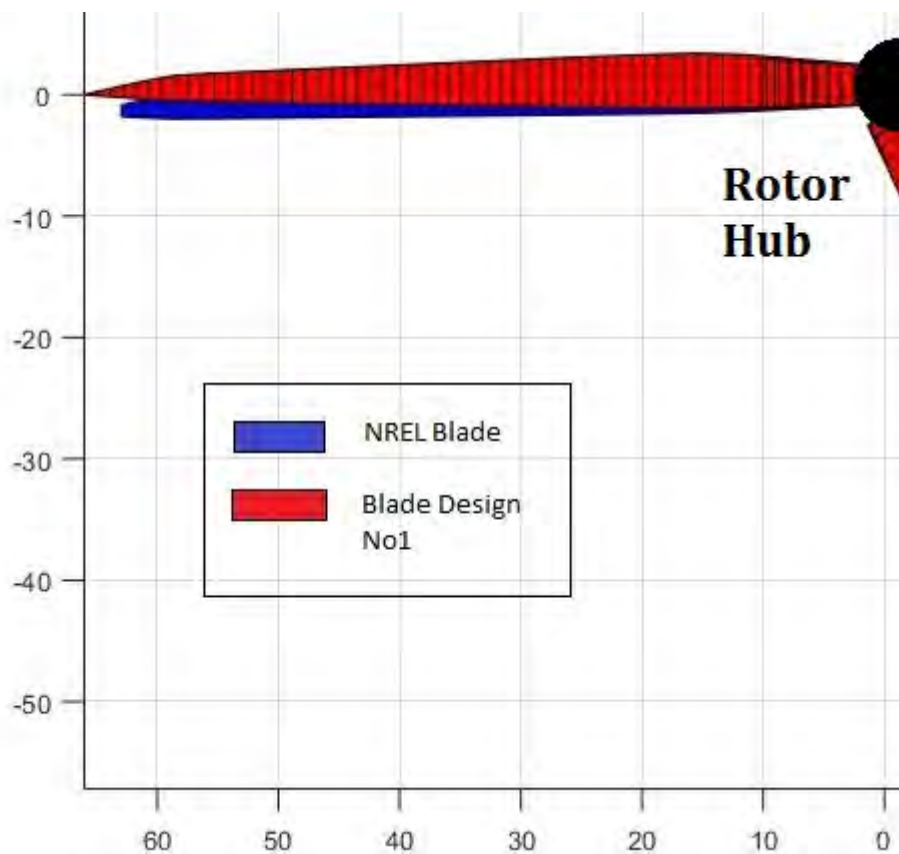
Figure 7.3 : Visualization of the blade design No1 Vs NREL blade design

203

As it was already mentioned earlier in the paragraph the increase of rotor radius, leads inevitably to higher loads (expressed as out of plane root bending moment). So, tip sweeping of the blades could be the solution to this side effect and with relatively small sweep angles considering the arm of the tip area from the rotor hub. The chord and twist angle distribution of blade design 1 was proven to be the best among 9 other designs examined, in terms of increasing the percentage of power more than the percentage of out of blade root bending moment. From this parametric study it is also concluded that higher sweep angles result in higher differences between power increase and load increase for every examined wind velocity (between cut – in and rated) . Thus, the concept of active control of tip sweep would not provide more benefits compared to the passively controlled tip swept wind turbine. The required mechanism does not have any use if the blade has to be swept as much as possible. The value of 30 degrees aft sweep for the modified blade tips, is considered a feasible idea and according to the following table leads to slighly higher power increase than load increase for the rated wind speed 11.4 m/s and the under-rated 6 m/s (steady – no shear).

Power and Root bending moment Percentage Increase						
		Sweep angle in deg				Max Difference
Vinflow (m/s)		0	20	25	30	
11,4	Power	6,30%	5,81%	5,57%	5,30%	
	Loads	6,35%	5,78%	5,48%	5,14%	0,17%
6	Power	6,84%	6,31%	6,04%	5,74%	
	Loads	6,71%	6,10%	5,79%	5,42%	0,32%

Table 7.2 : Power and Out of plane root bending moment percentage increase for blade design No 1 for two different constant wind speeds

However, calculation of AEP is a more reliable index of the expected benefit from this concept and it is calculated according to equation (7.1). The wind range is set between 4m/s (cut – in speed) and 11.4m/s (rated operation) which corresponds to the range where the pitch

204

controller of the NREL wind turbine is not activated (see also figure 2.21). Many concepts focus on this area as it represents the sub-rated operation of the wind turbine and so there is room for improvement. The probability $f(V_i < V < V_{i+1})$ is calculated from the following equation according to the Weibull distribution:

$$f(V_i < V < V_{i+1}) = \exp(-(\frac{V_i}{A})^k) - \exp(-(\frac{V_{i+1}}{A})^k)$$

(**7.2**)

where:

- k is the shape parameter of the Weibull function and can be evaluated from local meteorological data, obstacles and landscape [4], [76]. It is set to 2 and according to [76] in this case the Rayleigh function is identical to Weibull function.

- A is the scale parameter of the Weibull function and can be evaluated from local meteorological data, obstacles and landscape [4], [76]. It is equal to $2*V_{ave}/\sqrt{\pi}$, where V_{ave} (annual average wind speed at hub height) equals 0.2*Vref [76] for standard wind turbine classes and Vref = 42.5m/s (reference wind speed average over 10 min) according to Table 1 of the [76] for a Class II wind turbine.

Figure (7.4) shows the energy capture improvement in steady conditions for the aforementioned wind speed range and according to equation (7.1) the percentage AEP increase is calculated at **5.68%**. However, the maximum percentage load increase for this design is calculated at **5.44%** and thus, new calculations and possibly structural modifications will be necessary not only for the blades but also for other parts, of the wind turbine. Obviously it will lead to heavier structure and the AEP increase will be considered insufffcient to cover the higher manufacturing cost.
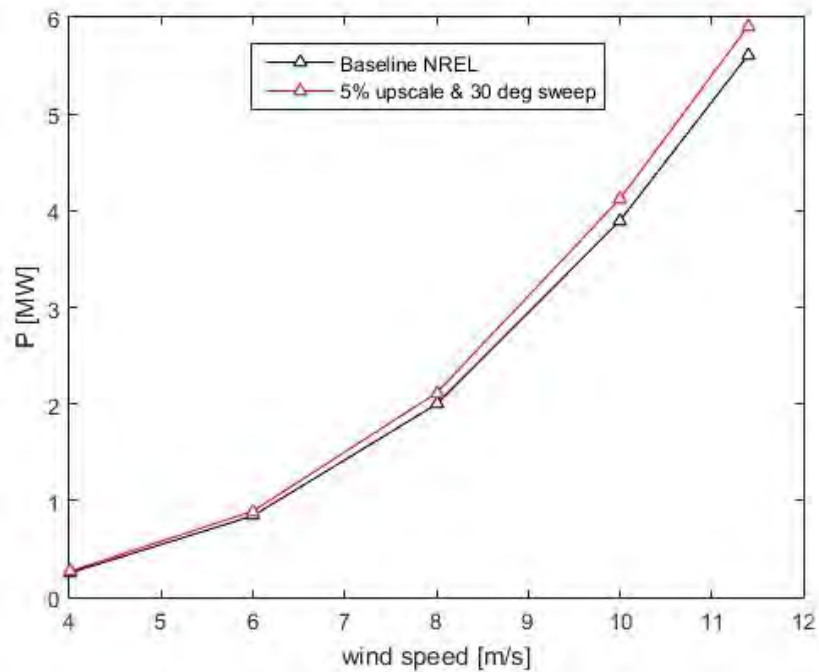
Figure 7.4 : Power production increase for Blade design No1 and steady conditions

7.1.2 Blade design No2 – 5% blade span extension with 10% tip swept part

In an effort to achieve AEP increase with a smaller "penalty" in loads the recommended design is modified only in terms of blade tip sweep percentage. In particular 10% (and not 5%) of the extended blade is allowed to sweep 30 degrees in aft direction. This results in a 6.6m swept tip of an overall 66.075m rotor that has the chord and twist angle distribution of Table 7.1 .

206
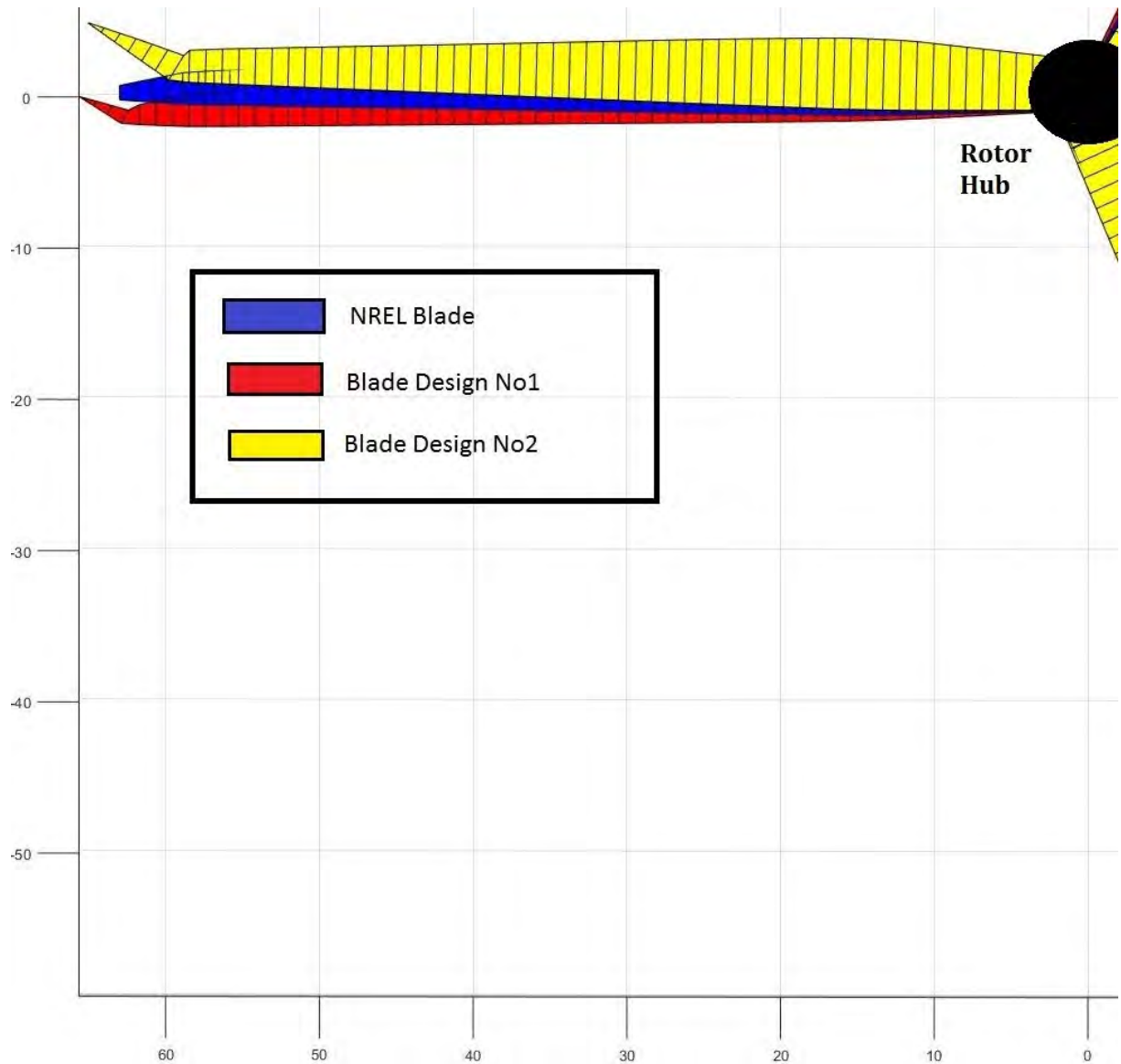
Figure 7.5 : Visualization of the blade design No1 Vs NREL blade design Vs blade design

No2

Preliminary tests at rated and sub – rated constant wind speeds indicate more promising results and are presented in Table 7.3 .

207

Power and Root bending moment Percentage Increase						
		Sweep angle in deg				Max Difference
Vinflow (m/s)		0	10	20	30	
11,4	Power	6,29%	5,93%	5,04%	3,91%	
	Loads	6,34%	5,85%	4,51%	2,52%	1,39%
6	Power	6,84%	6,46%	5,53%	4,38%	
	Loads	6,71%	6,20%	4,81%	2,76%	1,62%

Table 7.3 : Power and Out of plane root bending moment percentage increase for blade design

No 2 for two different constant wind speeds

Thus, after applying equation 7.1 for blade design No2, in the same way as in blade design No1, the percentage AEP increase is calcuated at **4.28%**. Meanwhile, the maximum percentage load increase for this design is calculated at **2.77%**, rendering this design a more conservative recommendation but also, a more feasible concept. Figure 7.6 shows the energy capture improvement in steady conditions for the same wind speed range of blade design No1.
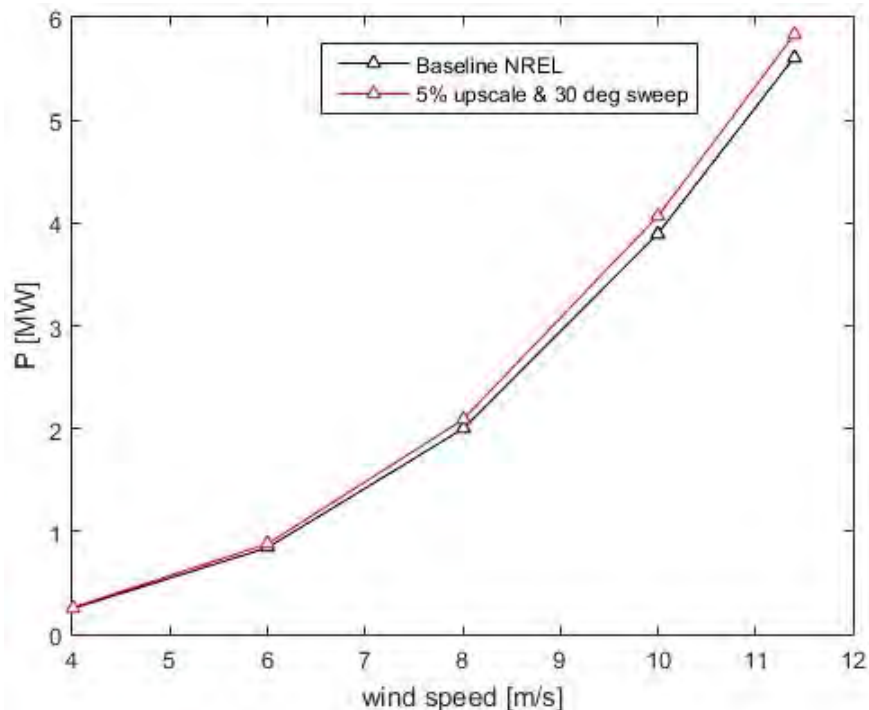
Figure 7.6 : Power production increase for Blade design No2 and steady conditions

7.2 Fatigue load reduction

In Chapter 2 the unsteady operating environment of HAWTs was analyzed and most of the investigated control concepts were reviewed. Fatigue load reduction is the main motivation for every concept as they are intended for use in large wind turbine rotors where unsteady load reduction is something more than necessary. The benefits from this achievement are translated either to extended service life of the wind turbine or lower production cost through lighter components. In this paragraph, fatigue load reduction is investigated through a variable tip swept wind turbine rotor with the recommended design geometry No2 of the previous paragraph. The purpose of this investigation is to disclose the capabilities of this control concept to wind turbine rotors of this class (NREL 5MW 63m rotor). But first, the proposed control method for fatigue load reduction is presented.

The proposed controller is based on a closed loop feedback system that monitors the numeric average root bending moment (M_x) of the 3 blades which then passes to a high pass filter (HPF) where only the dynamic effects are included. The average root bending moment (MeanM_x) is the input to the controller. The high pass filter transfer function is shown in equation (7.3) and represents a simple Proportional high pass controller. Then this value is multiplied with a suitable gain K which commands an actuator to make a collective change to the blades' sweep angle values.

$$G(s) = \frac{s}{tau * s + 1}$$

(**7.3**)

where:

- G(s) is the transfer function of the HPF

209

- s is the Laplace operator

- tau is the time constant of the HPF

The sweep commands, as an output to the sweep actuator, are filtered by a low pass filter (1/τ) with a time constant τ, of 0.5 sec, in order to simulate a realistic response of a mechanical tip sweep system during a step response. Of course, a careful study on the structural and dynamic characteristics of an actuator that should pivot the blade tips to the desired sweep angle will specify this parameter. In addition, a separate module maintains a stable operation during the start up phase in which the controller behaves aggressively because of the large gradients that appear and the "**abs** " module is used to prevent fore sweep commands. The following figure illustrates the proposed control scheme:
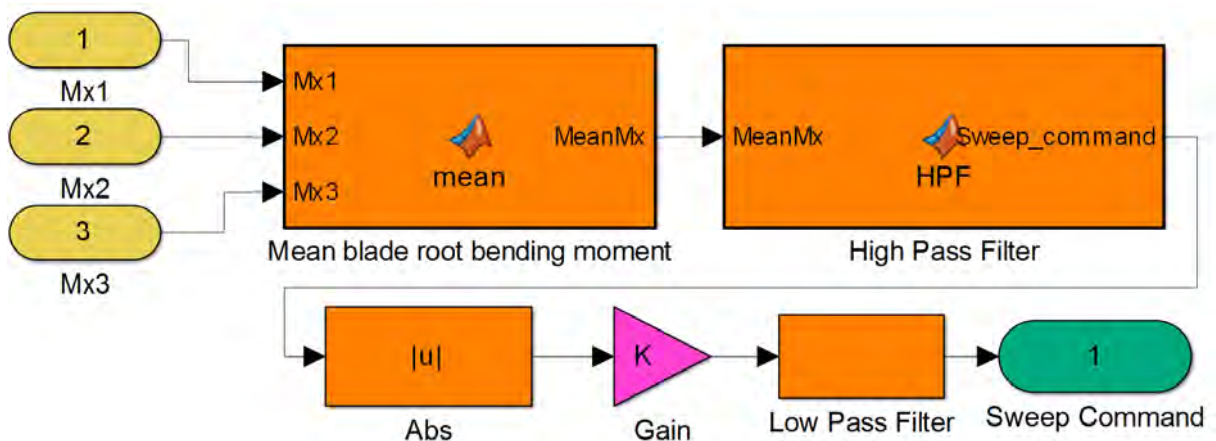
Figure 7.7 The control method for fatigue and extreme load reduction.

The control system performance in load reduction is tested first for an extreme operating gust (figure 7.12). During this test case, the optimum values of the controller's HPF time constant **tau** and controller gain **K** that maximize blade load reduction, are determined. This process is performed with the aid of the response optimization toolbox in *Matlab-Simulink* and the values of **tau** and **K** are used for the fatigue and the extreme load reduction (next paragraph) test cases.

For the fatigue load test case of this thesis, a 3-D turbulent wind input field of 10% turbulent intensity according to Kaimal spectrum (Appendix A.4), is considered for the modified NREL wind turbine equipped with blade design No2 blades. The average wind speed is equal to the rated speed (11.4 m/s), for which the wind turbine loads are maximum. So, the potential for fatigue load reduction of the proposed controller is investigated in a high load operational environment.

The wind field is generated in TurbSim software [109] which uses *a statistical model to create time series of three components velocity vectors at points in a two-dimensional vertical rectangular grid that is fixed in space* [figure (7.8)]. *Spectra of velocity components and spatial coherence are defined in the frequency domain, and an inverse Fourier transform produces time series* [109].
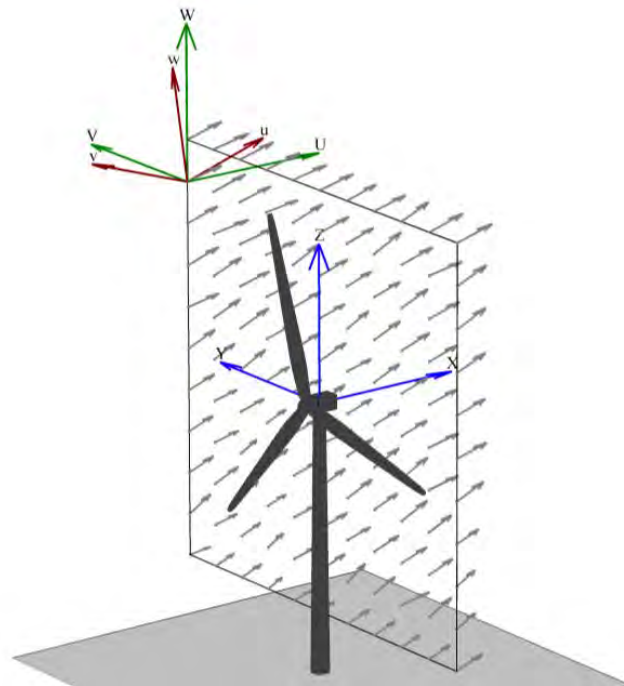
Figure 7.8 Turbulent 3-D wind field created in TurbSim, source: [109]

Figure 7.9 refers to the three wind velocity components at the wind turbine's hub height, during a 650 second period, generated in TurbSim for the examined test case. The

211

modified BEM code of this thesis finds the closest to the blades grid points, in every time step, and through interpolation determines the actual wind speed seen by the blades.
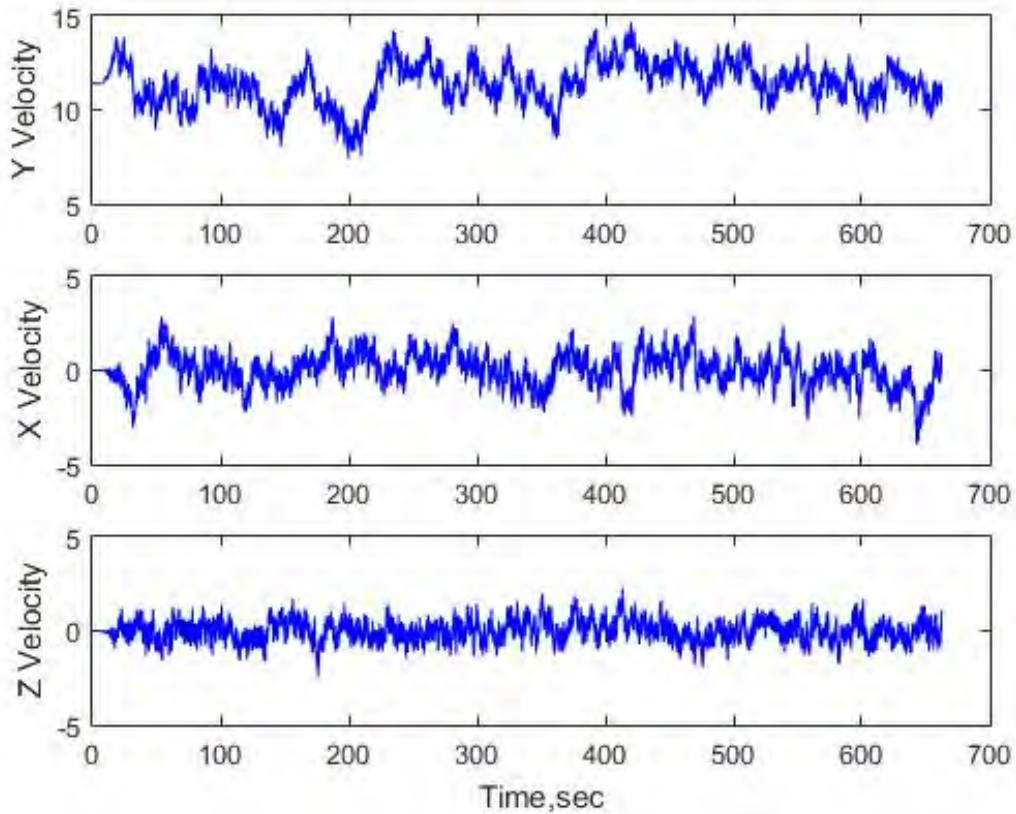
Figure 7.9 The three wind velocity components at hub height for the examined test case

In figure 7.10 it is seen in practice, how the controller responds to the unsteady wind environment of figure 7.9 . The controller operates constantly as a response to the unsteady wind input with a maximum tip sweep angle command of 18 degrees. In addition, the maximum additional tip speed (outmost blade element) due to the controller commands, is 2m/s which means that there are not any abrupt changes that are translated to high inertia loading of the control mechanism.

In figure 7.11 the root bending moment of blade 1 is shown with and without the controller and it is seen that it operates in a way that lowers the peak loads during the

212

turbulent wind input but it is not as effective during the load "valleys". This is explained by the controller settings (responds when loads increase) and generally by the operating principle of the tip sweeping concept; aft tip sweeping concept decreases the loads for every sweep angle and thus, it is not so efficient in raising the loads when they tend to decrease due to wind speed drops.
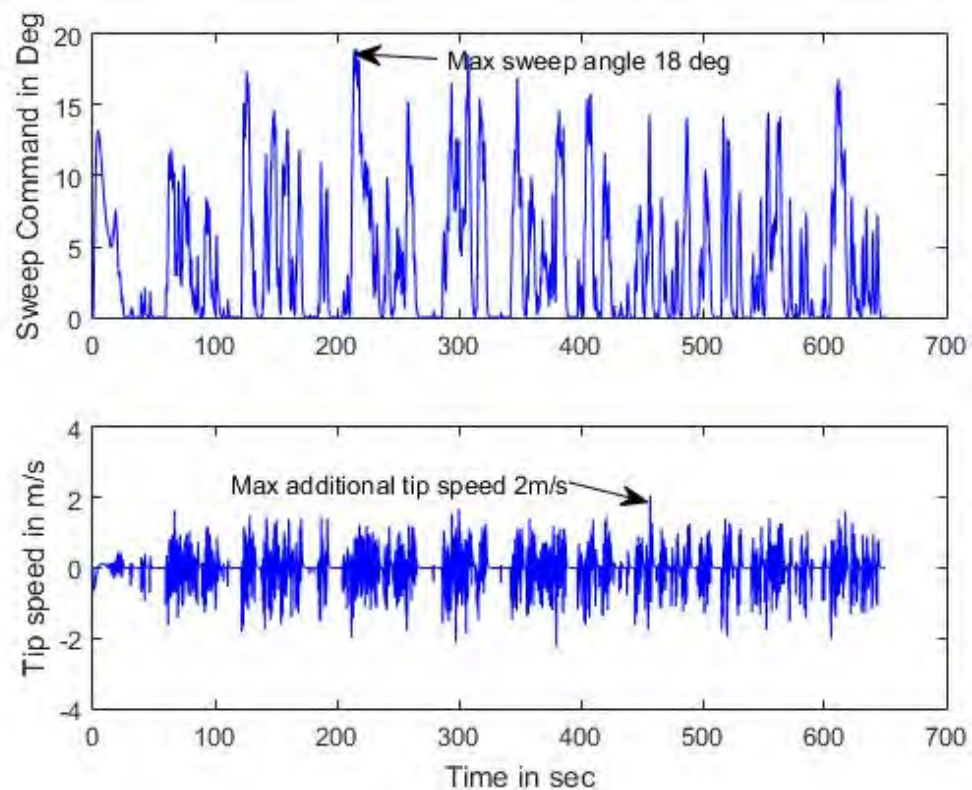
Figure 7.10 Tip sweep angle response during a turbulent wind input for the modified NREL wind turbine.
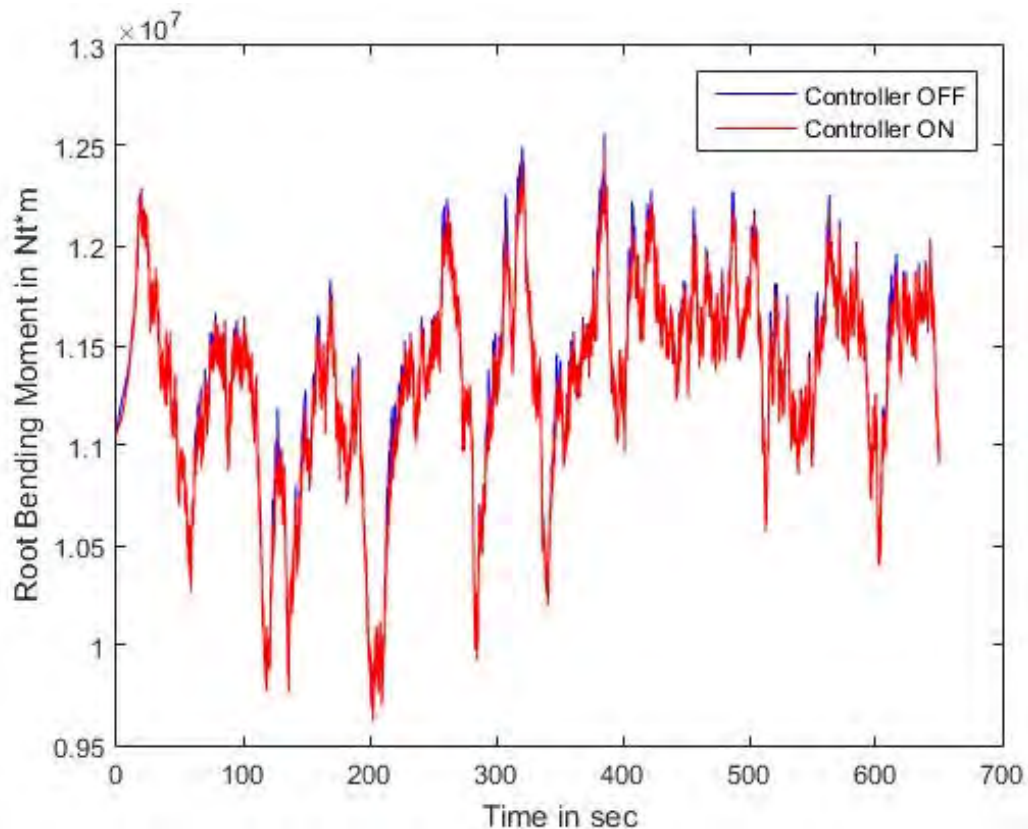
Figure 7.11 Fatigue load reduction during a turbulent wind input for the modified NREL wind turbine.

The fatigue load reduction is estimated with the use of the MCrunch engineering tool, developed by NREL [122]. MCrunch is a set of scripts initially developed for processing wind turbine test and simulation data, but it can be used for other applications, too. In this case, the blade root bending moment, is rainflow counted (using MCrunch) for the 650sec simulation test of the modified wind turbine, with and without the controller operating at the 3-D turbulent wind field of figure 7.9. From the rainflow counting process the signal of the root bending moment is discretized into cycle amplitudes and the corresponding number of them. Then, the Damage Equivalent Load (DEL) is calculated for this two cases and the percent decrease in fatigue loading, yields.

214

The calculation of DEL is not always a simple process especially for the wind turbines as different materials are met in the blades. The cylindrical part near the root is made out of steel and the rest of the blade skin is made out of fiberglass, which means different Miner S-N slopes (Stress – Number of cycle). Miner's rule [123] gives the damage fraction of a material that is subjected to a set of cyclic loads with a specific load range. An expression for the DEL is given in [72]:

$$D_{eq} = \left(\frac{\sum_i n_i * D_i^m}{f * T} \right)^{\frac{1}{m}}$$

(**7.4**)

where:

- n_i is the number of cycles for each stress amplitude

- D_i is the stress amplitudes

- m is the inverse S-N slope of the material

- f is the frequency of the reference signal , usually 1Hz

- T is the time period of the reference signal (same as stress time duration).

In this work, the calculated DELs for the controller off and on cases, do not represent the actual equivalent loads, as the reference signal contains the root bending moments. However, the calculated number is directly connected to the damage equivalent load (as the stress is load divided by the cross section area which is not modified) and the corresponding percentage reduction is a reliable measure of the benefit. It should be noted that the first 50 seconds of the simulation are not taken into account because they refer to transient operation.

215

So, the calculated percentage fatigue load reduction is **3.2%** (excluding the first 50 secs of the simulation test) with the controller on and this is a noteworthy improvement considering the high loading operation of the wind turbine, at rated wind speed and turbulence intensity of 10%. A full scale fatigue analysis for the entire envelope of the wind turbine would determine the total benefit.

7.3 Gust Load Reduction

One of the design requirements of a wind turbine according to [76] is tolerance to an extreme operating gust (EOG). EOG refers to the event of an abrupt rise in wind speed value, (not direction) that lasts for some seconds. This consequently leads to peak loads that may compromise the integrity of the turbine's structure. The concept of a variable tip swept rotor could help alleviate those peak loads with a suitable control system that is capable of sweeping the blades in the case of an EOG event. So, in this paragraph the load reduction margin is calculated for the unmodified 5MW NREL wind turbine configured with a 10% and a 5% tip swept rotor that is exposed to an EOG during its rated operation at 11.4m/s uniform wind speed and 12.1rpm.

The gust is given by the following equation in accordance with paragraph 6.3.2.2 of [76]:

$$V_{gust} = Min\left\{1.35(V_{e1} - V_{hub}); 3.3\left(\frac{\sigma_1}{1+0,1\left(\frac{D}{\Lambda_1}\right)}\right)\right\}$$

(**7.5**)

where:

- V_{gust} is the velocity of the EOG

- V_{e1} is 80% of the V50 extreme wind speed with a recurrence period of 50 years

- V_{hub} is the velocity at the hub height

- σ_1 equals $0.11\,V_{hub}$ and is calculated from equation (7.6)

- D is the rotor diameter

- Λ_1 is the longitudinal turbulence scale parameter and is equals 42m for hub height over 60m (in this case hub height equals 90m)

$$\sigma_1 = I_{ref}(0.75V_{hub} + b)$$

(7.6)

where:

- σ_1 is the turbulence standard deviation

- I_{ref} is the wind turbine class according to table 1 of [76] equal to 0.14 for this case

Equation (7.7) defines the wind speed variation in relation to time for a period of T=10.5sec which is also depicted at figure 7.12 :

$$V(z,t) = V(z) - 0.37V_{gust}\sin(3\pi t / T)(1 - \cos(2\pi\tau / T)$$

(7.7)

where:

- $V(z)$ is equal to 11.4m/s assuming a uniform wind inflow

217

- V_{gust} is calculated from equation (7.5)

- T equals 10,5 sec according to [76]
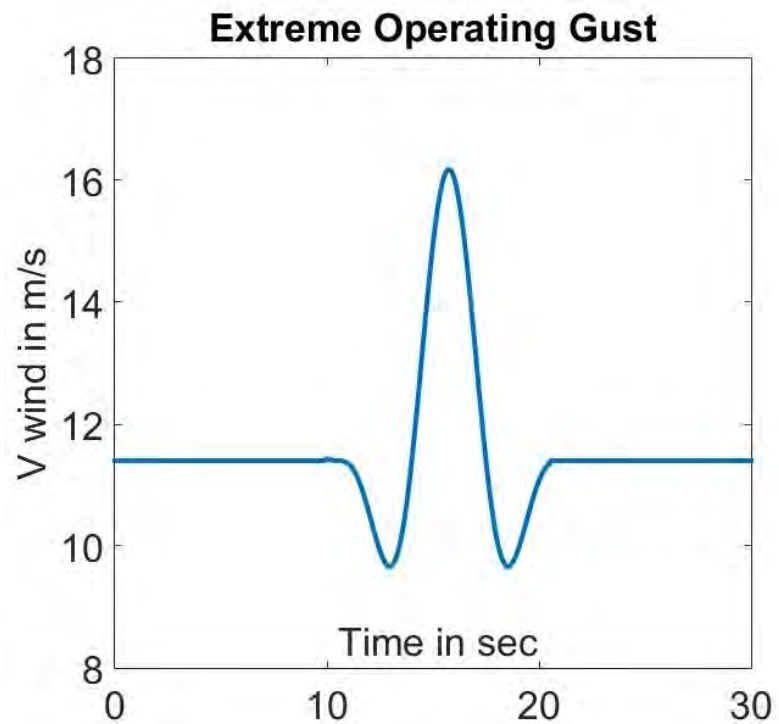
Figure 7.12 An extreme operating gust according to IEC 61400-1 [76] on the 5MW NREL

wind turbine

The following results refer to the 10% and 5% tip swept 5MW NREL wind turbine which is subjected to the extreme operating gust of figure 7.12 while operating at rated wind speed (11.4 m/s). The controller's design and characteristics was explained in the previous paragraph.

218
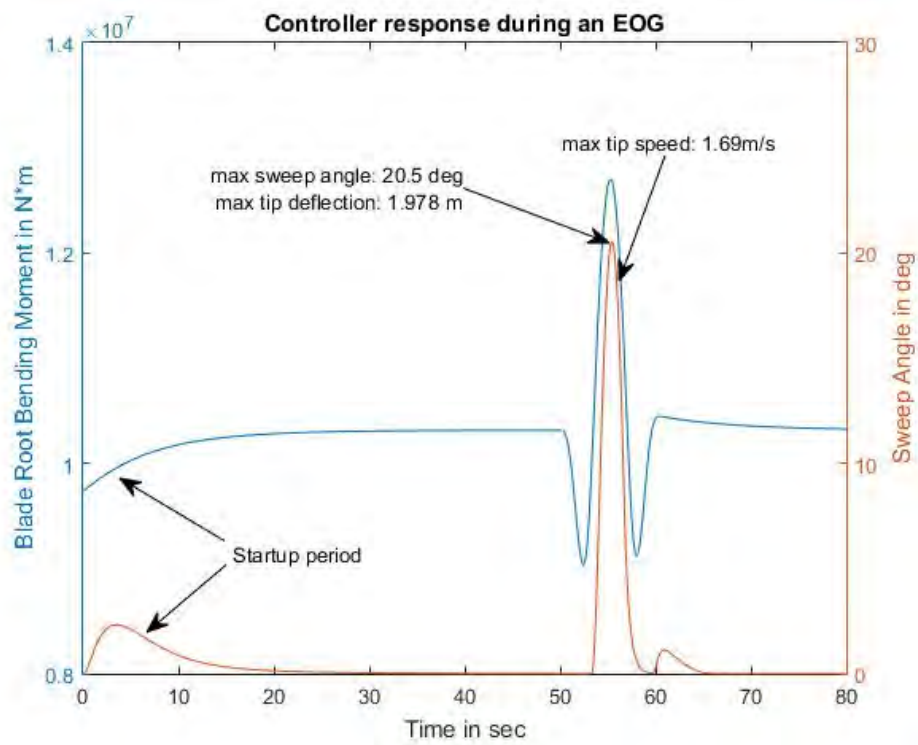
Figure 7.13 Tip sweep angle response during an EOG for 10% tip swept rotor.
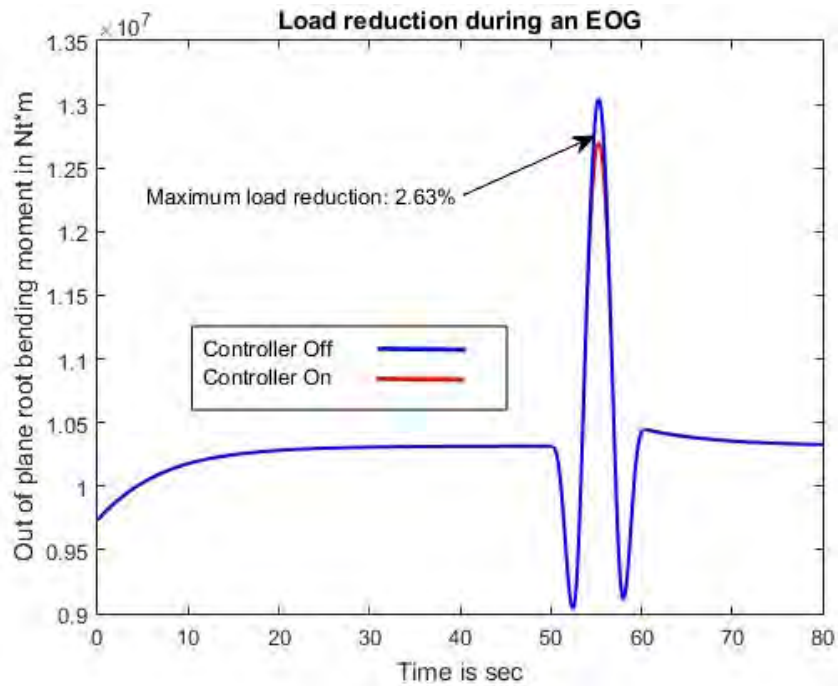
Figure 7.14 Out of plane root bending moment of Blade No1 during an EOG for 10% tip

swept rotor.

219
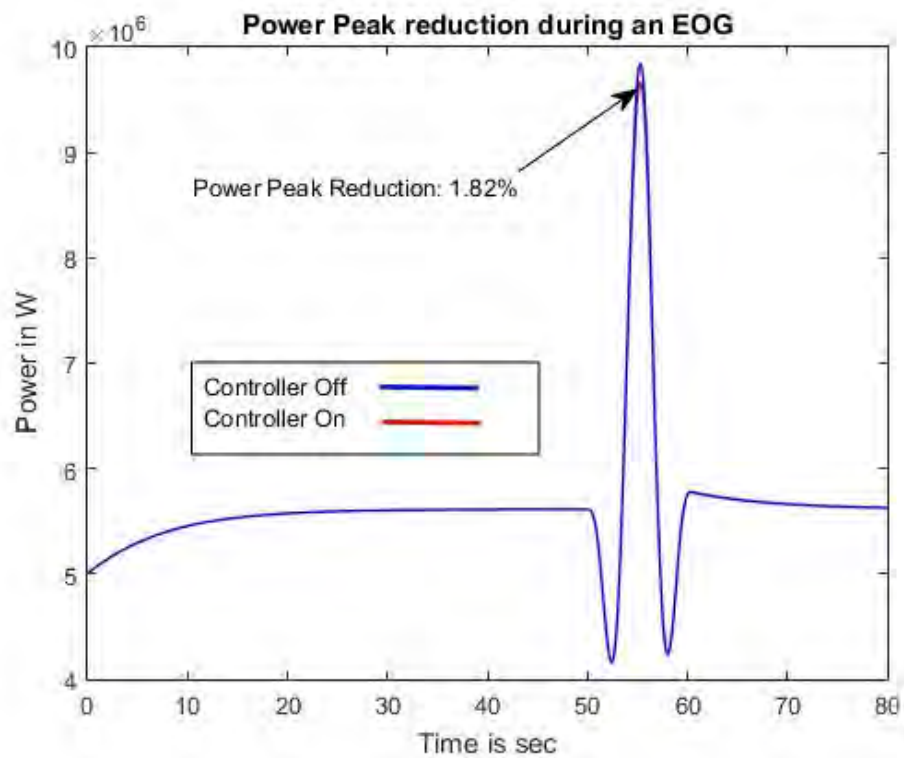
Figure 7.15 Wind Turbine Power Peak reduction during an EOG for 10% tip swept rotor.
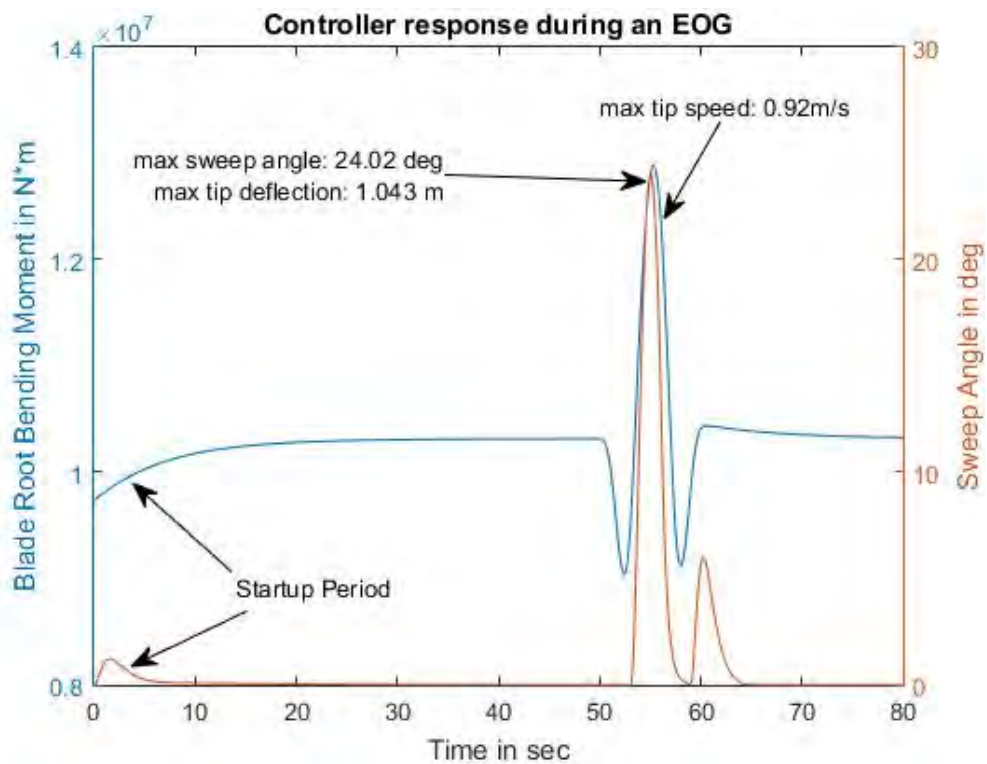
Figure 7.16 Tip sweep angle response during an EOG for 5% tip swept rotor.

220
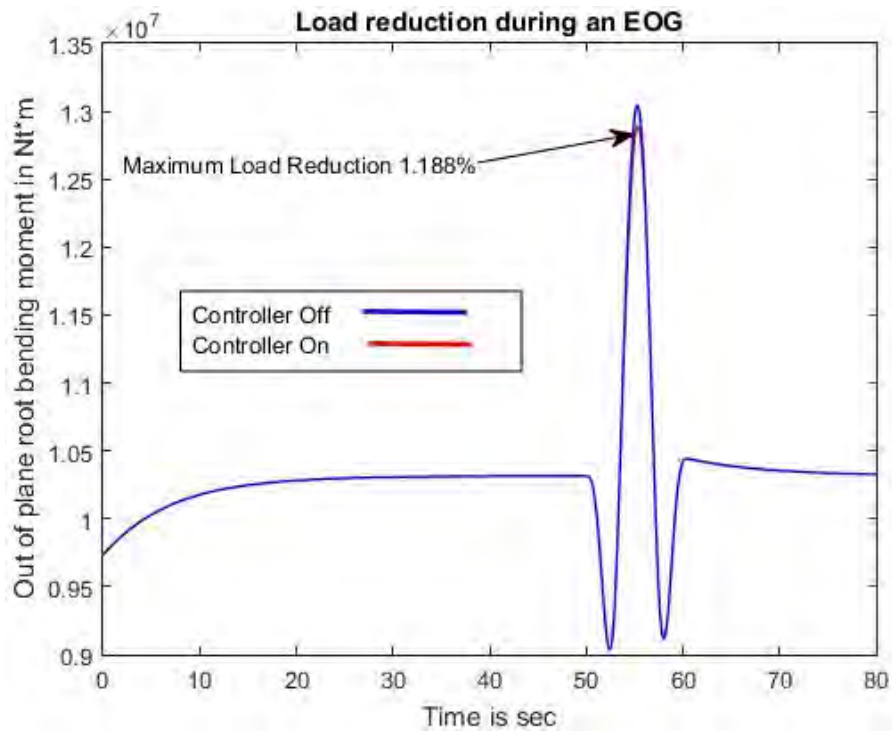
Figure 7.17 Out of plane root bending moment of Blade No1 during an EOG for 5% tip swept
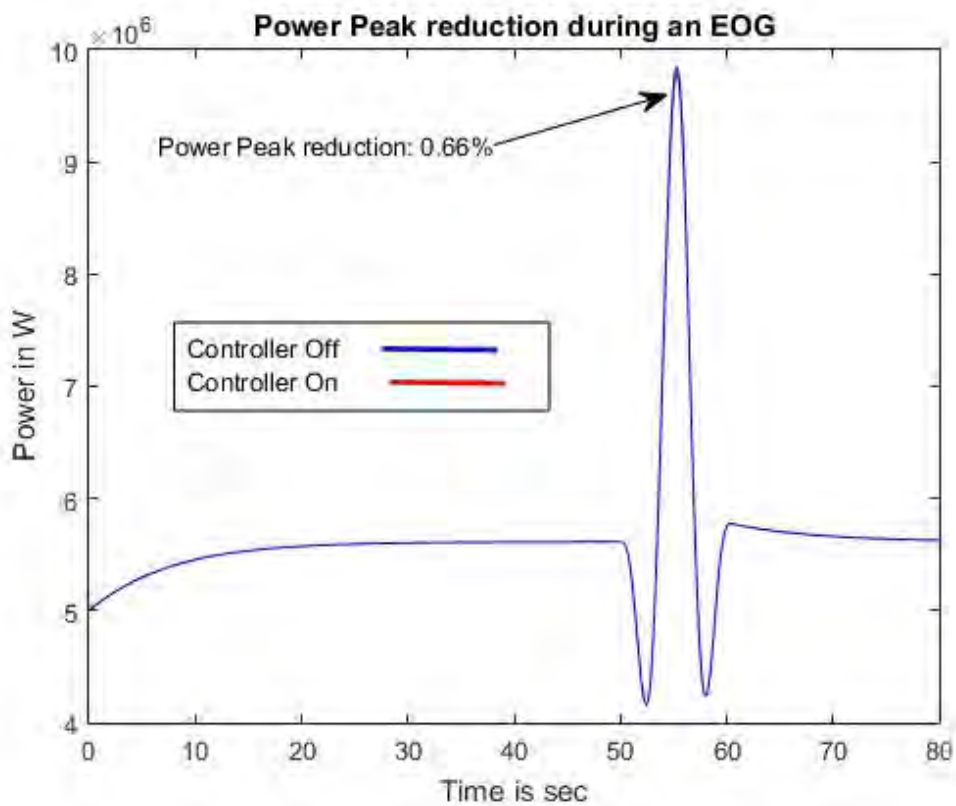
Figure 7.18 Wind Turbine Power Peak reduction during an EOG for 5% tip swept rotor.

221

Figures 7.13 and 7.16 show in practice how a wind turbine with active tip sweep control capability can lower the blade loads during an extreme operating gust of Figure 7.12 . In specific the controller doesn't react at the beginning of the gust (t=50sec) when the velocity drops and the blade loads tend to drop accordingly. However, when the opposite phenomenon sets in it successively sweeps the rotor blade tips in order to lower the blade root bending moment. Then, the acceleration of wind velocity excites once again the controller but in a more gentle way as it recovers fast to the value of 11.4m/s. The authority of the controller for both cases is set to the value of 25 degrees and the gain and time constant of the high pass filter are found from the optimization process. It is noteworthy that load reduction is achieved through smooth and small deflections of the blade tips (in the order of 2m) which implies low inertia loads experienced by the control device.

The maximum load reduction for the 10% and 5% tip swept rotor is 2.63% and 1.188% accordingly which is an important result considering the small part of the blade that is swept. The capability of the controller in reducing the extreme loads could be taken into account in the design phase and lead to lighter blade structure. In addition, a reduction in the power peak, in the order of 1%, is observed which is beneficial in terms of introducing lower energy spikes into the grid.

7.4 Summary

The capabilities of the active tip sweep concept in terms of increasing power production and reducing fatigue and extreme loads were outlined in this paragraph. The results have as reference the NREL 5MW wind turbine. It was concluded that power increase is only possible through increase of the rotor diameter, similar to the STAR project (paragraph

222

2.6). An active controller was not useful in this case as power production decreases monotonically with increasing sweep angle of the blade tips. So, after a small case study the adoption of a new rotor with 5% longer blades and 10%, of the overall blade span, swept blade tips in a 30 degrees angle results in a **4.28%** AEP increase while increasing by only **2.77%** the blade loads. The same design was tested for fatigue load reduction, in a turbulent wind field with an average wind speed of 11.4 m/s, with the use of a simple closed loop feedback controller and the damage equivalent load was decreased by **3.2%.** During this study the modified BEM code was also verified for stable operation in an unsteady wind field. Lastly, the extreme load reduction potential for the baseline NREL wind turbine equipped with 5% and 10% actively controlled (same controller) tip swept rotor blades reduction was investigated during an EOG and the maximum loads were decreased by **2.63%**. Overall, the controller achieves these results, when activated, through small collective tip deflections and in a smooth way.

The adoption of an actively controlled tip swept rotor gave promising results for a typical 120m rotor wind turbine and could potentially give more for larger rotors which encounter higher loads. The implementation of an active control mechanism of this kind is part of a complete study which is undertaken by research and development departments of the wind turbine industries. A full scale aeroelastic study and related experiments would determine the exact trade – off between the benefits and the disadvantages accompanying the modification and / or addition of a sweep control mechanism to the rotor blades.

The originality that this chapter incorporates is the investigation of active blade tip sweep concept as an innovative control method aiming to improve the performance of three bladed HAWTs.

Chapter 8. Conclusions

8.1 Summary and Concluding Remarks

The subject of controlling wind turbines in order to improve their performance is more apropos than ever, considering the current trend for offshore and bigger structures that are capable of producing rated power in the order of 10MW [124]. The rotor diameter of these prototypes have already overcome 180m and now the designers face new challenges. The blade loads increase along with the tip deflections and tower-hit issues arise. The tip speeds tend to reach 100m/s and thus compressibility effects may appear and influence the aerodynamic performance of the blades. The development and construction of these new longer blades, the reinforcement of the other components and the design of the generator properties is more demanding than ever.

Active control of wind turbines can help the designers in this effort, by increasing the power coefficient C_P in sub – rated operating range, by reducing the fatigue loads and with the introduction of safety mechanisms that will ensure the integrity of the wind turbine during extreme events that take place occasionally in offshore installations. The contribution of active control features to the industry of wind turbines is generally expressed as extended service life, lighter structures and eventually lower cost of energy.

In this work many different methods for controlling aerodynamic blade loads were reviewed and some of them have taken their final form and they are gradually get

Institutional Repository - Library & Information Centre - University of Thessaly
19/05/2024 19:53:00 EEST - 18.119.112.4

commercialized. Focusing on the blade tip area where higher loads are met is tempting, as small modifications there could have significant influence to the overall performance. Tip sweeping the rotor blades has only been investigated as a passive control concept with beneficial results in reducing the loads and increasing power production if a suitable extension to the blades is considered. This thesis is a first approach to the active control concept of wind turbines through variable blade tip sweep and fills in a knowledge gap in the research field.

The investigation was carried out with numerical and computational methods and a step by step analysis of the problem was performed. It started with the identification of the influence of tip sweeping on a fixed wing and a lifting line theory based code was developed for this reason in Matlab software. The results of this code were compared to the corresponding results obtained from CFD simulation (in ANSYS CFX software module). The test cases referred to constant tip sweep angle configurations and harmonic sweep angle variations and convergence was observed. Then the code for fixed wing was upgraded for the 5MW NREL three bladed wind turbine and was accelerated 60 times, by utilizing CUDA platform and its integrated support in Matlab. The results of this model were considered reliable due to the convergence with CFD results (only for the fixed wing case) and due to the physics that are included in Lifting Line theory.

However, one of the main targets of this thesis was to incorporate the variable tip sweep feature in a more simple engineering BEM code. The main inability of the BEM theory, is to take into account trailed vorticity, which affects the overall blade aerodynamics and in the case (tip sweeping), the shortcoming is more obvious. So, suitable modifications to the BEM code were made based on the developed Lifting Line code and a semi-empirical correction in the tip area was developed that takes into account trailed vorticity. In this way axial induction factor, which is one of most important parameters, is calculated more correctly

225

and more reliable results are acquired. It is worth to note that the correction is more efficient for sweep angle values over 10 degrees and more efficient for small tip sweep percentages. Without the correction, power production is slightly underestimated (in the order of 0.2%) but this can impose larger differences in the AEP calculations.

After the development of the customized BEM code for tip sweep, the active control concept was considered. The concept was investigated in terms of power production increase, fatigue load reduction and extreme load reduction during a wind gust, for the reference 5MW NREL wind turbine. It was concluded that active tip sweep will not be useful for power production increase and a new design of the blades was recommended after a small case study - this statement was already obvious from preliminary results of a parametric study in the ULL model (paragraph 5.5). The 5% extended blades configured with 30 deg aft swept tips measuring a length of 10% of the overall span, resulted in a 4.28% AEP increase with only 2.77% increase of the maximum blade loads.

For the other two cases, of fatigue load reduction and extreme load reduction, a suitable controller was developed that is scheduled to reduce the root bending moment of the blades through collective sweep angle commands. A fatigue load reduction of 3.2% was calculated for the reference wind turbine configured with the new blade design. The device was subjected to a 3-D turbulent wind field of 10% turbulence intensity and 11.4m/s average speed. Lastly, the unmodified reference wind turbine equipped with the same controller, was subjected to an EOG according to Design Regulations [76] and the calculated extreme load reduction was 2.63% and 1.82% for the 10% and 5% tip swept rotors accordingly. It is noteworthy that the aforementioned improvements are obtained through small and smooth tip deflections.

The results indicate that the active control concept of variable tip sweep is worth to be investigated in depth. The improvement is noticeable and could be more significant for larger wind turbines that experience higher tip speeds and deflections. The variable tip sweep concept could be considered not only as a constant load regulator but also as a safety feature, during extreme operating conditions (gusts, high turbulent wind fields). In addition, the conclusions drawn about the power increase with standard tip swept blade tips could be useful to industries in terms of improving the performance of in – service wind turbines with the addition of extended swept tips (tip sleeve) with a slight increase of the blade loads [125].

8.2 Future Work

In this work, the effort was focused on the development of a corrected BEM code that will be also used for the study of the active control concept through variable tip swept blades. Despite the fact that a reliable lifting line theory based model was already developed, a BEM code was preferred and corrected accordingly, due to its simplicity, low computational demands, and its wide acceptance and use from industries and research laboratories. The correction for tip sweep provided a noticeable improvement to the axial induction factor calculations and thus, it could be tested in similar blade tip modifications (winglets).

Also, as part of the future work, the BEM code is worth to be coupled to an elastic model and more accurate predictions about the overall benefits and drawbacks could be drawn; for example, increase of the critical speed to flutter, impact to torsion loads, impact to aeroelastic phenomena. It could be improved further with the incorporation of a dynamic stall model for better predictions of the aerodynamic loads, despite the fact that in the test cases of this study the blade tips did not enter the stall area. Moreover, more efficient controllers could

be tested for the fatigue load reduction case that could "cut" not only the peaks but also the valleys through suitable sweep angle commands.

Last but not least, the design of the sweeping mechanism will be crucial to an integral evaluation of the concept. The use of rods, gears or pneumatic actuators that will rotate the blade tips and special fairings at the hinge area of the blade tip would determine the overall characteristics of the wind turbine, the added cost of the concept and the reduction of the cost of energy.

228

References

[1] "Windmill." Wikipedia. Wikimedia Foundation, 08 Mar. 2017. Web. 09 Mar. 2017. <https://en.wikipedia.org/wiki/Windmill>.

[2] Shepherd, Dennis G. "Historical development of the windmill." (1990).

[3] "Denmark breaks its own world record in wind energy." EURACTIV.com. N.p., 15 Jan. 2016. Web. 09 Mar. 2017. http://www.euractiv.com/section/climate-environment/news/denmark-breaks-its-own-world-record-in-wind-energy/

[4] Martin, O. L. "Hansen. Aerodynamics of wind turbines [M]. Earthscan published." Inc., New York (2008): 28-63.

[5] Barlas, Thanasis K., and G. A. M. Van Kuik. "Review of state of the art in smart rotor control research for wind turbines." Progress in Aerospace Sciences 46.1 (2010): 1-27.

[6] Harlow, Francis H. "Fluid dynamics in group T-3 Los Alamos national laboratory:(LA-UR-03-3852)." Journal of Computational Physics 195.2 (2004): 414-433.

[7] White, Frank. Viscous fluid flow. McGraw-Hill series in mechanical engineering. New York: McGraw-Hill, 1991.

[8] Spalart, Philippe R., et al. "A new version of detached-eddy simulation, resistant to ambiguous grid densities." Theoretical and computational fluid dynamics 20.3 (2006): 181-195.

[9] Menter, Florian R. "Two-equation eddy-viscosity turbulence models for engineering applications." AIAA journal 32.8 (1994): 1598-1605.

[10] Wilcox, David C. "Formulation of the kw turbulence model revisited." AIAA journal 46.11 (2008): 2823-2838.

[11] Spalart, P. R., et al. "Comments on the feasibility of LES for wings, and on a hybrid RANS/LES approach." Advances in DNS/LES 1 (1997): 4-8.

[12] Di Pasquale, D., A. Rona, and S. J. Garrett. "A selective review of CFD transition models." 39th AIAA Fluid Dynamics Conference. No. 2009-3812. 2009.

[13] Arieli, R., and M. Tauber. "Computation of subsonic and transonic flow about lifting rotor blades." 5th Atmospheric Flight Mechanics Conference for Future Space Systems. 1979.

[14] Caradonna, F. X., C. Tung, and A. Desopper. "Finite difference modeling of rotor flows including wake effects." Journal of the American Helicopter Society 29.2 (1984): 26-33.

[15] Hansen, M., et al. "A global Navier-Stokes rotor prediction model." 35th Aerospace Sciences Meeting and Exhibit. 1997.

[16] Xu, Guanpeng, and Lakshmi N. Sankar. "Computational study of horizontal axis wind turbines." Transactions-American Society of Mechanical Engineers Journal of Solar Energy Engineering 122.1 (2000): 35-39.

[17] Sorensen, N. N., J. A. Michelsen, and S. Schreck. "Navier-Stokes predictions of the NREL phase VI rotor in the NASA Ames 80-by-120 wind tunnel." ASME 2002 Wind Energy Symposium. American Society of Mechanical Engineers, 2002.

[18] Hansen, Martin Otto Laver, et al. "State of the art in wind turbine aerodynamics and aeroelasticity." Progress in aerospace sciences 42.4 (2006): 285-330.

[19] Guerrero, Joel. "Numerical simulation of the unsteady aerodynamics of flapping flight." Department of Civil, Environmental, Architectural Engineering (2009).

[20] Ansys, Inc Release 14.0, December 2011, www.ansys.com

[21] Ferrer, E., and X. Munduate. "Wind turbine blade tip comparison using CFD." Journal of Physics: Conference Series. Vol. 75. No. 1. IOP Publishing, 2007.

[22] Michelsen, Jess, and N. N. Sørensen. "Current development in Navier-Stokes modelling of wind turbine rotor flow." (2001).

[23] Rasmussen, Flemming, et al. "Present status of aeroelasticity of wind turbines." Wind energy 6.3 (2003): 213-228.

[24] Prandtl, Ludwig. "Applications of modern hydrodynamics to aeronautics." (1923).

[25] Katz, Joseph, and Allen Plotkin. Low-speed aerodynamics. Vol. 13. Cambridge university press, 2001.

[26] Van Garrel, A. "Development of a wind turbine aerodynamics simulation module." (2003).

[27] Lamb, Horace. Hydrodynamics. Cambridge university press, 1932.

[28] Leishman, J. Gordon, Mahendra J. Bhagwat, and Ashish Bagai. "Free-vortex filament methods for the analysis of helicopter rotor wakes." Journal of aircraft 39.5 (2002): 759-775.

[29] Squire, H. B. "The growth of a vortex in turbulent flow." Aeronautical Quarterly 16.03 (1965): 302-306.

[30] Bhagwat, Mahendra J., and J. Gordon Leishman. "Generalized viscous vortex model for application to free-vortex wake and aeroacoustic calculations." Annual forum proceedings-American helicopter society. Vol. 58. No. 2. AMERICAN HELICOPTER SOCIETY, INC, 2002.

[31] Sørensen, Jens Nørkær, et al. Three-level, viscous-inviscid interaction technique for the prediction of separated flow past rotating wing. Diss. Technical University of DenmarkDanmarks Tekniske Universitet, AdministrationAdministration, Office for Finance and AccountingAfdelingen for Økonomi og Regnskab, 1986.

[32] Hess, John L. Calculation of potential flow about arbitrary three-dimensional lifting bodies. No. MDC-J5679-01. DOUGLAS AIRCRAFT CO LONG BEACH CA, 1972.

[33] Chorin, Alexandre Joel. "Numerical study of slightly viscous flow." Journal of fluid mechanics 57.04 (1973): 785-796.

[34] Scully, Michael P. A method of computing helicopter vortex wake distortion. No. ASRL-TR-138-1. MASSACHUSETTS INST OF TECH CAMBRIDGE AEROELASTIC AND STRUCTURES RESEARCH LAB, 1967.

[35] Landgrebe, Anton J. "The wake geometry of a hovering helicopter rotor and its influence on rotor performance." Journal of the American Helicopter Society 17.4 (1972): 3-15.

[36] Leishman, Gordon J. Principles of helicopter aerodynamics with CD extra. Cambridge university press, 2006.

[37] Miller, R. H. "A simplified approach to the free wake analysis of a hovering rotor." (1981).

[38] Bliss, D. B., T. R. Quackenbush, and A. J. Bilanin. "A new methodology for helicopter free wake analysis." 39th Annual Forum of the American Helicopter Society. 1983.

[39] Bagai, Ashish, and J. Gordon Leishman. "Rotor free-wake modeling using a pseudoimplicit relaxation algorithm." Journal of Aircraft 32.6 (1995): 1276-1285.

[40] Miller W., Bliss D., Direct Periodic Solutions of Rotor Free Wake Calculations, Journal of the American Helicopter Society (1993): 54-60.

[41] Bagai, Ashish, and J. Gordon Leishman. "Adaptive grid sequencing and interpolation schemes for helicopter rotor wake analyses." AIAA journal 36.9 (1998): 1593-1602.

[42] Coton, F. N., and T. Wang. "The prediction of horizontal axis wind turbine performance in yawed flow using an unsteady prescribed wake model." Proceedings of the Institution of Mechanical Engineers, Part A: Journal of Power and Energy 213.1 (1999): 33-43.

[43] Simoes, F. J., and J. M. R. Graham. "Application of a free vortex wake model to a horizontal axis wind turbine." Journal of Wind Engineering and Industrial Aerodynamics 39.1-3 (1992): 129-138.

[44] Voutsinas, Spyros G. "Vortex methods in aeronautics: how to make things work." International Journal of Computational Fluid Dynamics 20.1 (2006): 3-18.

[45] Gupta, Sandeep. Development of a time-accurate viscous Lagrangian vortex wake model for wind turbine applications. Diss. 2006.

[46] Kalenteridis S., "Innovative rotor design concepts for a 10 MW wind turbine, " MSc thesis, TUDelft, 2015.

[47] Templin, R. J. Aerodynamic performance theory for the NRC vertical-axis wind turbine. No. N-76-16618; LTR-LA-160. National Aeronautical Establishment, Ottawa, Ontario (Canada), 1974.

[48] Paraschivoiu, Ion. "Double-multiple streamtube model for Darrieus in turbines." (1981).

[49] Read, S., and D. J. Sharpe. "An extended multiple streamtube theory for vertical axis wind turbines." Wind Energy Workshop. Vol. 1. 1980.

[50] Goude, Anders. Fluid mechanics of vertical axis turbines: Simulations and model development. Diss. Acta Universitatis Upsaliensis, 2012.

[51] Glauert, Hermann. The elements of aerofoil and airscrew theory. Cambridge University Press, 1983.

[52] Glauert, Hermann. "Airplane Propellers, Division L of Aerodynamic Theory, Durand, WF, Editor." (1963).

[53] Betz, Albert. "Das Maximum der theoretisch möglichen Ausnützung des Windes durch Windmotoren." Zeitschrift für das gesamte Turbinenwesen 26.307-309 (1920): 8.

[54] Burton, Tony, et al. Wind energy handbook. John Wiley & Sons, 2001.

[55] Goldstein, Sydney. "On the vortex theory of screw propellers." Proceedings of the Royal Society of London. Series A, Containing Papers of a Mathematical and Physical Character 123.792 (1929): 440-465.

[56] Branlard, Emmanuel, Kristian Dixon, and Mac Gaunaa. "Vortex methods to answer the need for improved understanding and modelling of tip-loss factors." IET Renewable Power Generation 7.4 (2013): 311-320.

[57] Glauert, Hermann. The analysis of experimental results in the windmill brake and vortex ring states of an airscrew. HM Stationery Office, 1926.

[58] Glauert, Hermann. "A General Theory of the Autogyro, volume 1111 of reports and memoranda ed." British ARC, UK (1926).

[59] Pitt, Dale M., and David A. Peters. "Theoretical prediction of dynamic-inflow derivatives." (1980).

[60] Øye, S. "Unsteady wake effects caused by pitch–angle changes." IEA R&D WECS Joint Action on Aerodynamics of Wind Turbines, 1st Symposium. 1986.

[61] McCroskey, W. J. "Some current research in unsteady fluid dynamics." ASME J. Fluids Eng 99.1 (1977): 8-39.

[62] Carr, Lawrence W. "Progress in analysis and prediction of dynamic stall." Journal of aircraft 25.1 (1988): 6-17.

[63] Tolouei, Elhaum, et al. "Flow analysis around a pitching airfoil." 22nd Applied Aerodynamics Conference and Exhibit. 2004.

[64] Theodorsen, Theodore. "General Theory of Aerodynamic Instability and the Mechanism of Flutter, NACA Report 496, 1935." This paper is also included in 'A Modern View of Theodore Theodorsen'published by AIAA in (1992): 2-21.

[65] Von Karman, T., and W. R. Sears. "Airfoil theory for non-uniform motion." AIAA Journal 41.7 (2003): 5-16.

[66] Wagner, Herbert. "Über die Entstehung des dynamischen Auftriebes von Tragflügeln." ZAMM-Journal of Applied Mathematics and Mechanics/Zeitschrift für Angewandte Mathematik und Mechanik 5.1 (1925): 17-35.

[67] Küssner, Herbert G. "Zusammenfassender Bericht über den instationären Auftrieb von Flügeln." Luftfahrtforschung 13.12 (1936): 410-424.

235

[68] Leishman, J. Gordon. "Challenges in modeling the unsteady aerodynamics of wind turbines." ASME 2002 Wind Energy Symposium. American Society of Mechanical Engineers, 2002.

[69] Jonkman, Jason M., and Marshall L. Buhl Jr. "FAST user's guide." National Renewable Energy Laboratory, Golden, CO, Technical Report No. NREL/EL-500-29798 (2005).

[70] Bossanyi, E. A. "GH bladed theory manual." GH & Partners Ltd (2003).

[71] Larsen, T. J. "How 2 HAWC2, the user's manual, ver. 3-7." Copenhagen (Denmark): RisøNational Laboratory, Technical University of Denmark (2009).

[72] Barlas, Athanasios. "Active aerodynamic load control on wind turbines: Aeroservoelastic modeling and wind tunnel." (2011).

[73] Pirrung, Georg. "Fast Trailed Vorticity Modeling for Wind Turbine Aerodynamics and its Influence on Aeroelastic Stability." (2014).

[74] Beddoes, T. S. "A near wake dynamic model proc. of the AHS national specialist meeting on aerodynamics and aeroacoustics." (1987).

[75] Van der Hoven, Isaac. "Power spectrum of horizontal wind speed in the frequency range from 0.0007 to 900 cycles per hour." Journal of meteorology 14.2 (1957): 160-164.

[76] International Electrotechnical Commission IEC 61400-1 Ed.3, "Wind turbines - Part 1: Design Requirements", Tech Report 61400-1,IEC, 2005

[77] Pritchard, J. Laurence. "Aerodynamics. Selected topics in the light of their historical development. Theodore von Kármán. Cornell University Press, Ithaca, New York. Oxford University Press, Oxford, 1954. 194 pp. illustrated. 38s." Journal of the Royal Aeronautical Society 58.528 (1954): 841-842.

[78] Erich, Hau. "Wind turbines: fundamentals, technologies, application, economics." (2000): 67-80.

[79] Barlas, Thanasis K., and G. A. M. Van Kuik. "State of the art and prospectives of smart rotor control for wind turbines." Journal of Physics: Conference Series. Vol. 75. No. 1. IOP Publishing, 2007.

[80] Sánchez, Alberto. "Modern control systems, Richard C. Dorf and Robert H. Bishop, Prentice-Hall, Upper Saddle River, NJ, 2001, 831 pages, ISBN 0-13-030660-6." International Journal of Robust and Nonlinear Control 16.7 (2006): 372-373.

[81] Collis, S. Scott, et al. "Issues in active flow control: theory, control, simulation, and experiment." Progress in Aerospace Sciences 40.4 (2004): 237-289.

[82] Wilson, David, et al. "Active aerodynamic blade distributed flap control design proceedure for load reduction on the UPWIND 5MW wind turbine." 48th AIAA Aerospace Sciences Meeting Including the New Horizons Forum and Aerospace Exposition. 2010.

[83] Hulskamp, A. W., et al. "Design of a scaled wind turbine with a smart rotor for dynamic load control experiments." Wind Energy 14.3 (2011): 339-354.

[84] Castaignet, Damien, et al. "Full-scale test of trailing edge flaps on a Vestas V27 wind turbine: active load reduction and system identification." Wind Energy 17.4 (2014): 549-564.

[85] Barlas, Thanasis K., and Helge Aagaard Madsen. "Influence of actuator dynamics on the load reduction potential of wind turbines with distributed controllable rubber trailing

237

edge flaps (CRTEF)." 22nd International Conference on Adaptive Structures and Technologies. 2011.

[86] Mayda, E. A., C. P. Van Dam, and D. Nakafuji. "Computational investigation of finite width microtabs for aerodynamic load control." 43rd AIAA Aerospace Sciences Meeting and Exhibit. 2005.

[87] Yen, Dora, et al. "Active load control for wind turbine blades using MEM translational tabs." 20th 2001 ASME Wind Energy Symposium. 2001.

[88] Woods, Benjamin King Sutton, and Michael I. Friswell. "Preliminary investigation of a fishbone active camber concept." ASME 2012 Conference on Smart Materials, Adaptive Structures and Intelligent Systems. American Society of Mechanical Engineers, 2012.

[89] Gandhi, Farhan, Mary Frecker, and Andrew Nissly. "Design optimization of a controllable camber rotor airfoil." AIAA journal 46.1 (2008): 142-153.

[90] Wilbur, Matthew L., and W. Keats Wilkie. "Active-twist rotor control applications for UAVs." SELECTED TOPICS IN ELECTRONICS AND SYSTEMS 42 (2006): 185.

[91] Barrett, Ron, and Saeed Farokhi. "On the aerodynamics and performance of active vortex generators." 11th Applied Aerodynamics Conference. 1993.

[92] Hagg, F., et al. "The Results of the Dutch Flexhat Programme: The Technology for the Next Generation of Wind Turbines.'." Winpower '93 Proceedings, American Wind energy Association (1993).

[93] Joosse, P. A., and I. Kraan. "Development of a tentortube for blade tip mechanisms: part 2 fatigue test and aeroelastic stability prediction tool." EWEC-CONFERENCE-. BOOKSHOP FOR SCIENTIFIC PUBLICATIONS, 1997.

[94] Lobitz, D. W., P. S. Veers, and P. G. Migliore. Enhanced performance of HAWTs using adaptive blades. No. CONF-960154--. Sandia National Laboratory, 1996.

[95] Liebst, Bradley S. "Wind turbine gust load alleviation utilizing curved blades." Journal of Propulsion and Power 2.4 (1986): 371-377.

[96] Larwood, Scott Michael. Dynamic analysis tool development for advanced geometry wind turbine blades. Diss. UNIVERSITY OF CALIFORNIA DAVIS, 2009.

[97] "Swept wing." Wikipedia. Wikimedia Foundation, 17 Feb. 2017. Web. 09 Mar. 2017. http://en.wikipedia.org/wiki/Swept_wing

[98] "Forward-swept wing." Wikipedia. Wikimedia Foundation, 01 Feb. 2017. Web. 09 Mar. 2017. <https://en.wikipedia.org/wiki/Forward-swept_wing>.

[99] <https://commons.wikimedia.org/wiki/File:F-14_Tomcat_VF-2.jpg>

[100] "Wingtip device." Wikipedia. Wikimedia Foundation, 06 Mar. 2017. Web. 09 Mar. 2017. <https://en.wikipedia.org/wiki/Wingtip_device>.

[101] Ashwill, Thomas D. Sweep-twist adaptive rotor blade: final project report. No. SAND2009-8037. Sandia National Laboratories, 2010.

[102] Larwood, Scott M., and Mike Zutek. "Swept wind turbine blade aeroelastic modeling for loads and dynamic behavior." (2006).

[103] Griffin, Dayton A. "Windpact turbine design scaling studies technical area 1-composite blades for 80-to 120-meter rotor." National Renewable Energy Laboratory, Colorado, USA, Tech. Rep. NREL/SR-500-29492 (2001).

[104] Verelst, David Robert, and Torben J. Larsen. Load consequences when sweeping blades-A case study of a 5 MW pitch controlled wind turbine. Danmarks Tekniske Universitet, Risø Nationallaboratoriet for Bæredygtig Energi, 2010.

[105] Riziotis, V. A., D. I. Manolas, and S. G. Voutsinas. "Free-wake aeroelastic modelling of swept rotor blades." European Wind Energy Conference and Exhibition 2011, EWEC 2011. 2011.

[106] Solidworks Help, Dassault Systemes SolidWorks Corporation, 2014.

[107] Matlab Documentation, The Mathworks Inc., 2014

[108] "Parallel Programming and Computing Platform | CUDA | NVIDIA | NVIDIA." Parallel Programming and Computing Platform | CUDA | NVIDIA | NVIDIA. N.p., n.d. Web. 09 Mar. 2017. <http://www.nvidia.com/object/cuda_home_new.html>.

[109] Jonkman B.J., Kilche L., TurbSim User's Guide: Version 1.06.00, Technical Report NREL/TP, September 2012

[110] Pirrung, G. R., Morten Hartvig Hansen, and Helge Aagaard Madsen. "Improvement of a near wake model for trailing vorticity." Journal of Physics: Conference Series. Vol. 555. No. 1. IOP Publishing, 2014.

[111] Hoerner, Sighard F., and Henry V. Borst. "Fluid-dynamic lift: practical information on aerodynamic and hydrodynamic lift." (1985).

[112] NASA. NASA, n.d. Web. 09 Mar. 2017. <http://history.nasa.gov/SP-468/ch10-4.htm>.

[113] Kloosterman, M. H. M. Development of the Near Wake behind a Horizontal Axis Wind Turbine Including the development of a Free Wake Lifting Line Code. Diss. M. Sc Dissertation, TUDelft, 2009.

[114] <http://www.edr.no/blogg/ansys_bloggen/workbench_cfx_remesh>

[115] Ng, Bing Feng, et al. "Aeroservoelastic state-space vortex lattice modeling and load alleviation of wind turbine blades." Wind Energy 18.7 (2015): 1317-1331.

[116] Odgaaard, Peter Fogh, et al. "Importance of dynamic inflow in model predictive control of wind turbines." IFAC-PapersOnLine 48.30 (2015): 90-95.

[117] Jonkman, Jason, et al. "Definition of a 5-MW reference wind turbine for offshore system development." National Renewable Energy Laboratory, Golden, CO, Technical Report No. NREL/TP-500-38060 (2009).

[118] Murua, Joseba, Rafael Palacios, and J. Michael R. Graham. "Assessment of wake-tail interference effects on the dynamics of flexible aircraft." AIAA journal 50.7 (2012): 1575-1585.

[119] Fung, Yuan Cheng. An introduction to the theory of aeroelasticity. Courier Corporation, 2002.

[120] Maggio, T., F. Grasso, and D. P. Coiro. "Numerical Study on Performance of Innovative Wind Turbine Blade for Load Reduction." EWEA, EWEC2011, Bruxelles (2011): 14-17.

[121] Snel, H., and J. G. Schepers. Joint investigation of dynamic inflow effects and implementation of an engineering method. Netherlands Energy Research Foundation ECN, 1995.

[122] Marshall L. Buhl, Jr., Crunch User's guide, NREL, 2003 .

[123] Miner, M. A. "Cumulative fatigue damage." Journal of applied mechanics 12.3 (1945): A159-A164.

[124] "The world's 10 biggest wind turbines." Power Technology. N.p., n.d. Web. 09 Mar. 2017. <http://www.power-technology.com/features/featurethe-worlds-biggest-wind-turbines-4154395/>.

[125] Stege J et al, Rotor blade of a wind turbine, Patent, US20150132141A1

Appendix

A.1   NACA 64-618 Profile
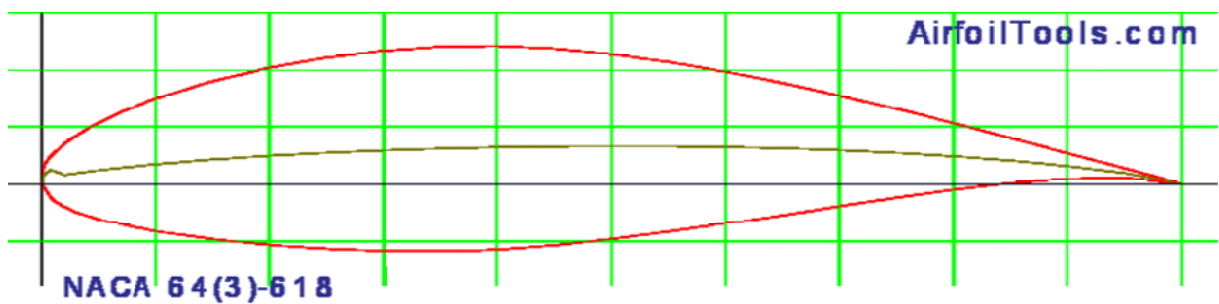
Source : <http://airfoiltools.com/images/airfoil/naca643618-il_l.png>

Aerodynamic Characteristics of NACA 64618 Airfoil			
Angle of Attack (Deg)	Lift Coefficient	Drag Coefficient	Moment Coefficient
-80	-0.299	13.181	0.3388
-75	-0.409	12.765	0.3248
-70	-0.512	12.212	0.3099
-65	-0.606	11.532	0.294
-60	-0.689	10.731	0.2772
-55	-0.759	0.9822	0.2595
-50	-0.814	0.882	0.2409
-45	-0.85	0.7742	0.2212
-40	-0.866	0.661	0.2006
-35	-0.86	0.5451	0.1789
-30	-0.829	0.4295	0.1563
-25	-0.853	0.3071	0.1156
-24	-0.87	0.2814	0.104
-23	-0.89	0.2556	0.0916
-22	-0.911	0.2297	0.0785

243

-21	-0.934	0.204	0.0649
-20	-0.958	0.1785	0.0508
-19	-0.982	0.1534	0.0364
-18	-1.005	0.1288	0.0218
-17	-1.082	0.1037	0.0129
-16	-1.113	0.0786	-0.0028
-15	-1.105	0.0535	-0.0251
-14	-1.078	0.0283	-0.0419
-13.5	-1.053	0.0158	-0.0521
-13	-1.015	0.0151	-0.061
-12	-0.904	0.0134	-0.0707
-11	-0.807	0.0121	-0.0722
-10	-0.711	0.0111	-0.0734
-9	-0.595	0.0099	-0.0772
-8	-0.478	0.0091	-0.0807
-7	-0.375	0.0086	-0.0825
-6	-0.264	0.0082	-0.0832
-5	-0.151	0.0079	-0.0841
-4	-0.017	0.0072	-0.0869
-3	0.088	0.0064	-0.0912
-2	0.213	0.0054	-0.0946
-1	0.328	0.0052	-0.0971
0	0.442	0.0052	-0.1014
1	0.556	0.0052	-0.1076
2	0.67	0.0053	-0.1126
3	0.784	0.0053	-0.1157
4	0.898	0.0054	-0.1199
5	1.011	0.0058	-0.124
6	1.103	0.0091	-0.1234
7	1.181	0.0113	-0.1184
8	1.257	0.0124	-0.1163
8.5	1.293	0.013	-0.1163
9	1.326	0.0136	-0.116
9.5	1.356	0.0143	-0.1154
10	1.382	0.015	-0.1149
10.5	1.4	0.0267	-0.1145
11	1.415	0.0383	-0.1143
11.5	1.425	0.0498	-0.1147
12	1.434	0.0613	-0.1158
12.5	1.443	0.0727	-0.1165
13	1.451	0.0841	-0.1153
13.5	1.453	0.0954	-0.1131
14	1.448	0.1065	-0.1112

244

|			
14.5	1.444	0.1176	-0.1101
15	1.445	0.1287	-0.1103
15.5	1.447	0.1398	-0.1109
16	1.448	0.1509	-0.1114
16.5	1.444	0.1619	-0.1111
17	1.438	0.1728	-0.1097
17.5	1.439	0.1837	-0.1079
18	1.448	0.1947	-0.108
18.5	1.452	0.2057	-0.109
19	1.448	0.2165	-0.1086
19.5	1.438	0.2272	-0.1077
20	1.428	0.2379	-0.1099
21	1.401	0.259	-0.1169
22	1.359	0.2799	-0.119
23	1.3	0.3004	-0.1235
24	1.22	0.3204	-0.1393
25	1.168	0.3377	-0.144
26	1.116	0.3554	-0.1486
28	1.015	0.3916	-0.1577
30	0.926	0.4294	-0.1668
32	0.855	0.469	-0.1759
35	0.8	0.5324	-0.1897
40	0.804	0.6452	-0.2126
45	0.793	0.7573	-0.2344
50	0.763	0.8664	-0.2553
55	0.717	0.9708	-0.2751
60	0.656	10.693	-0.2939
65	0.582	11.606	-0.3117
70	0.495	12.438	-0.3285
75	0.398	13.178	-0.3444
80	0.291	13.809	-0.3593

245

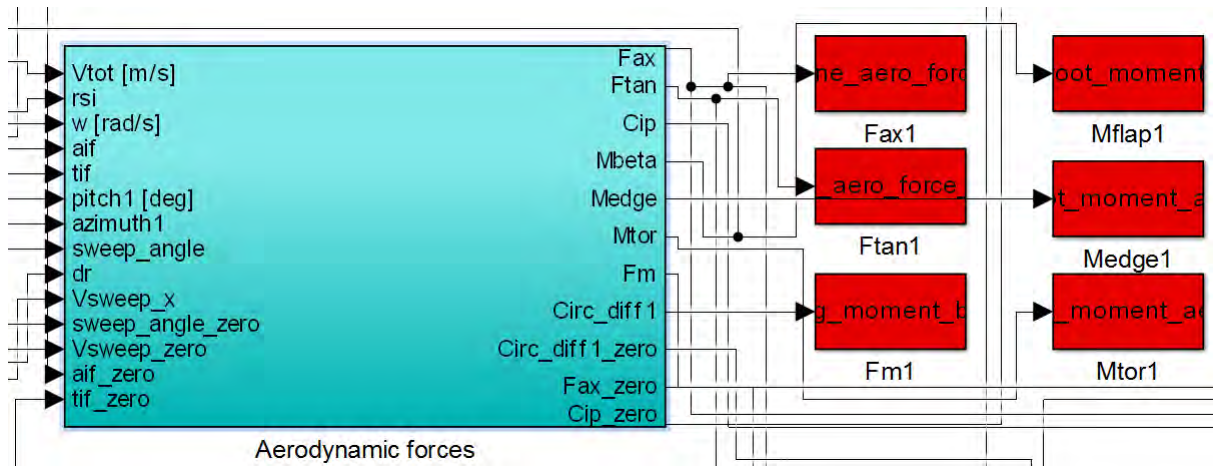## A.2 BEM code in Matlab / Simulink - representation

General View of the BEM model in Simulink

246
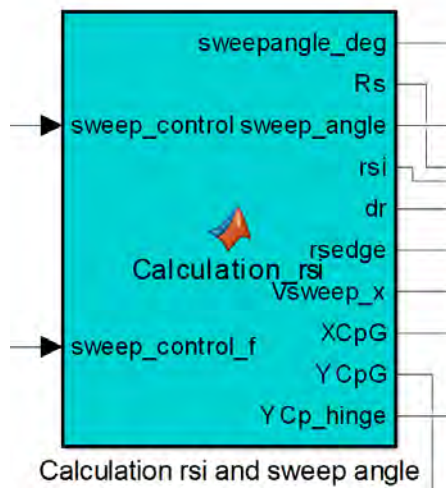
The module that calculates the position of the blade elements and the additional velocity due

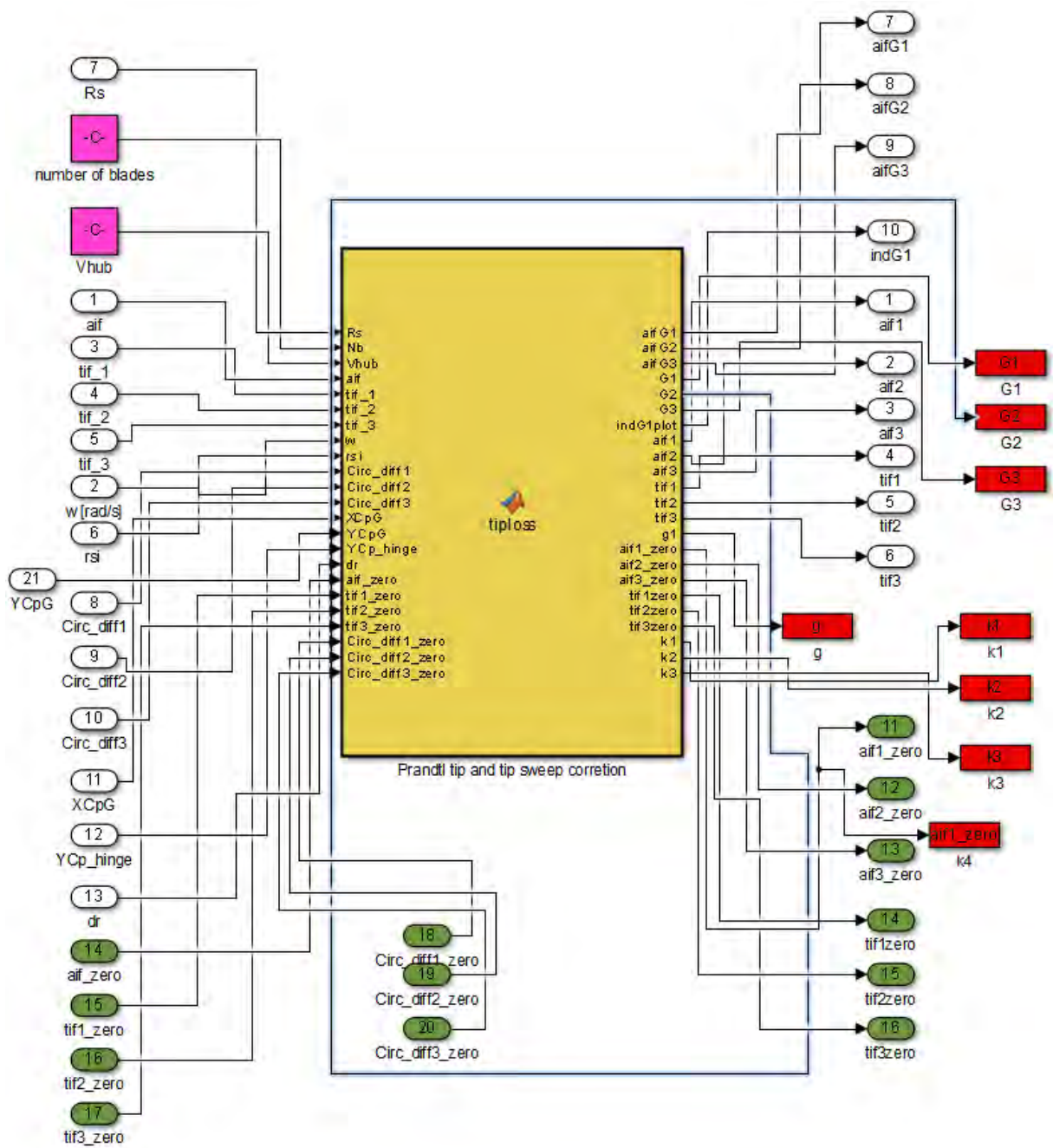to sweep angle variation for every time step
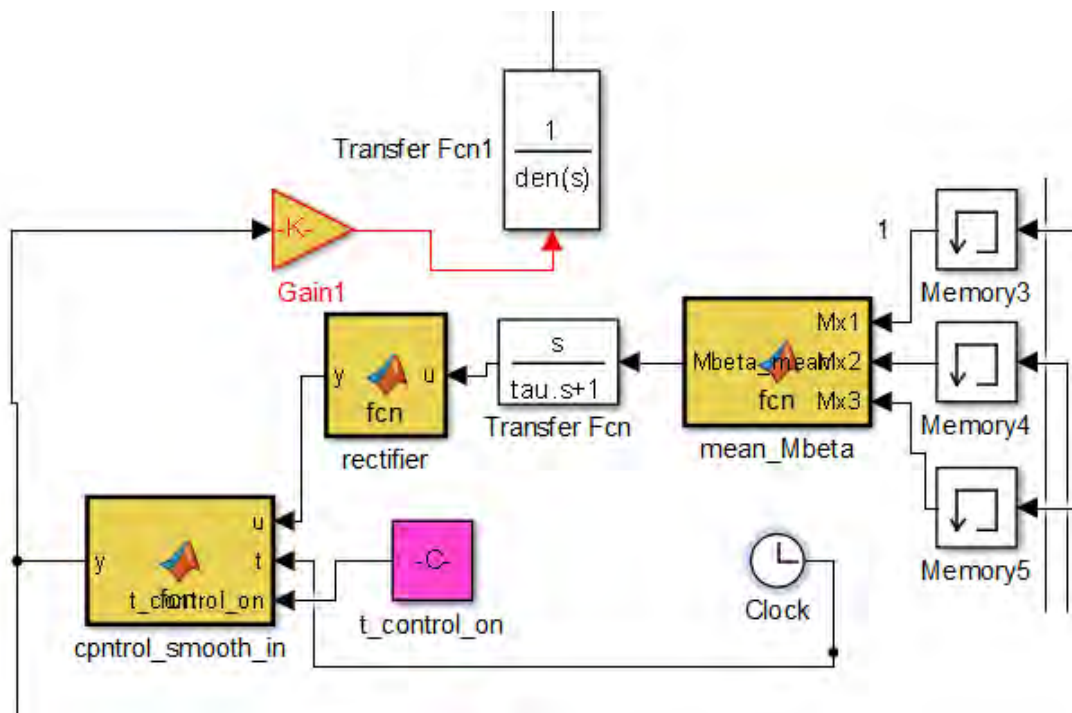
The module that controls sweep angle of the blade tips according to the mean value of

Blade No1 Root Bending Moment

247

The module that calculates the blade aerodynamic forces and moments
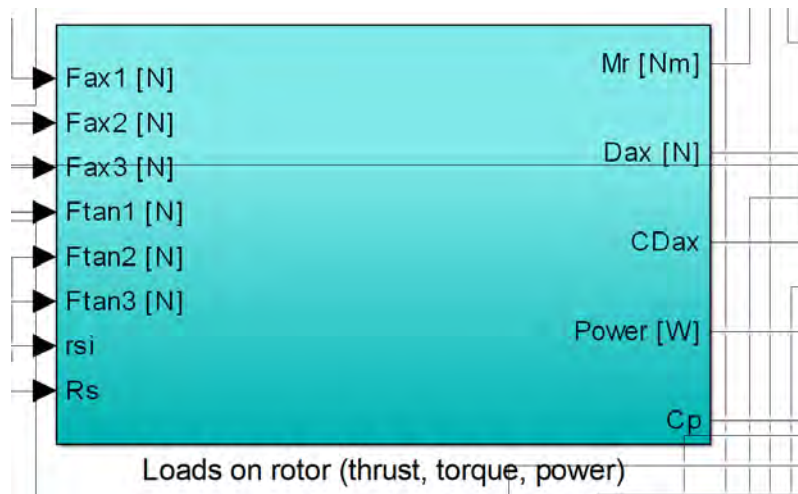
The module that calculates rotor loads and rotor power

248

The module that calculates Prandtl's correction and correction for blade tip sweep

A.3   Acceleration of ULL code written in Matlab by utilizing CUDA

```matlab
ULL_PW_rotor_s_tripleblade.m    ×    +
784 -    □ for k=1:N
785
786 -          A=gpuArray(ones(1,N).*(XCp(i,k)));
787 -          B=gpuArray(ones(1,N).*(YCp(i,k)));
788 -          C=gpuArray(ones(1,N).*(ZCp(i,k)));
789 -          A2=gpuArray(ones(1,N).*(XCp2(i,k)));
790 -          B2=gpuArray(ones(1,N).*(YCp2(i,k)));
791 -          C2=gpuArray(ones(1,N).*(ZCp2(i,k)));
792 -          A3=gpuArray(ones(1,N).*(XCp3(i,k)));
793 -          B3=gpuArray(ones(1,N).*(YCp3(i,k)));
794 -          C3=gpuArray(ones(1,N).*(ZCp3(i,k)));
795
796 -    [Ub11,Vb11,Wb11]=arrayfun(@Smooth_VORT_BOUND,A,B,C,XCp_edge_c(i,1:(end-1)),
797 -    [Ub12,Vb12,Wb12]=arrayfun(@Smooth_VORT_BOUND,A,B,C,XCp_edge_c2(i,1:(end-1))
798 -    [Ub13,Vb13,Wb13]=arrayfun(@Smooth_VORT_BOUND,A,B,C,XCp_edge_c3(i,1:(end-1))
799
```

Application of a function, in this case "Smooth_VORT_BOUND", on an array of points utilizing CUDA in order to calculate induced velocities on specific points.

A.4   The IEC Kaimal Model in TurbSim

Standard deviation σ of the three velocity components are calculated by the following equation:

$$\sigma^2 = \int_0^\infty S(f)df$$

where:

- σ is the standard deviation of the velocities

- S is the Spectra of the velocities

The Spectra for the three wind velocity components u,v,w is given by

250

$$S_K(f) = \frac{4\sigma_K{}^2 L_K / \overline{u}_{hub}}{(1 + 6fL_K / \overline{u}_{hub})^{\frac{5}{3}}}$$

where:

- f is the cyclic frequency and L_K is an integral scale parameter. According to IEC 61400-1 the integral scale parameter is given by:

- $L_K = 8.1\Lambda_u$ for K=u

- $L_K = 2.7\Lambda_u$ for K=v

- $L_K = 0.66\Lambda_u$ for K=w

where:

- Λ_u is the turbulence scale parameter

and

$\Lambda_u = 0.7 \min(60m, \text{Hub}_{height})$ where $\min(x_1, x_2)$ is the minimum of x_1 and x_2

The standard deviations of the three velocity components are related according to:

- $\sigma_v = 0.8\,\sigma_u$

- $\sigma_w = 0.5\,\sigma_u$

The velocity spectra are assumed to be invariant across the grid. Only a small variation in u component occurs due to the spatial coherence model.